


Winter 12-14-2018

Intra- and Inter-Molecular Signaling in a Cardiac Connexin: Role of Cytoplasmic Domain Dimerization and Phosphorylation

Andrew J. Trease
University of Nebraska Medical Center

Follow this and additional works at: <https://digitalcommons.unmc.edu/etd>

 Part of the [Cell Biology Commons](#), [Molecular Biology Commons](#), and the [Other Biochemistry, Biophysics, and Structural Biology Commons](#)

Recommended Citation

Trease, Andrew J., "Intra- and Inter-Molecular Signaling in a Cardiac Connexin: Role of Cytoplasmic Domain Dimerization and Phosphorylation" (2018). *Theses & Dissertations*. 322.
<https://digitalcommons.unmc.edu/etd/322>

This Dissertation is brought to you for free and open access by the Graduate Studies at DigitalCommons@UNMC. It has been accepted for inclusion in Theses & Dissertations by an authorized administrator of DigitalCommons@UNMC. For more information, please contact digitalcommons@unmc.edu.

**INTRA- AND INTER-MOLECULAR SIGNALING IN A CARDIAC CONNEXIN: ROLE OF
CYTOPLASMIC DOMAIN DIMERIZATION AND PHOSPHORYLATION**

BY

ANDREW J. TREASE

A DISSERTATION

Presented to the Faculty of

The Graduate College in the University of Nebraska

In Partial Fulfillment of the Requirements

For the Degree of Doctor of Philosophy

Department of Biochemistry and Molecular Biology

Under the Supervision of Professor Paul L. Sorgen

University of Nebraska Medical Center

Omaha, Nebraska

November, 2018

Supervisory Committee

Paul L. Sorgen, Ph.D.

Justin L. Mott, M.D. Ph.D.

Amarnath Natarajan, Ph.D.

Tahir H. Tahirov, Ph.D.

INTRA- AND INTER-MOLECULAR SIGNALING IN A CARDIAC CONNEXIN: ROLE OF CYTOPLASMIC DOMAIN DIMERIZATION AND PHOSPHORYLATION

Andrew J. Trease, Ph.D.

University of Nebraska, 2018

Supervisor: Paul L. Sorgen, Ph.D.

ABSTRACT

As critical mediators of cell-to-cell communication, gap junctions (GJs) are comprised of membrane channels that directly link the cytoplasm of adjacent coupled cells thereby allowing for the passage of ions, small metabolites, and secondary messengers. Each channel is formed by the apposition of two connexons from adjacent cells, each composed of six connexin (Cx) proteins. Each GJ channel functions to promote signal propagation and synchronization of cells and tissues in organs. Furthermore, GJs are essential for proper propagation of cardiac action potentials from one cell to the next, leading to the coordinated contraction and relaxation of heart muscle powering circulation. In diseased human hearts, the organization and expression of Cxs in the working myocardium is remodeled leading to impaired impulse propagation and risk of lethal arrhythmias. Diverse post-translational modifications (e.g., phosphorylation) and protein partner interactions, the majority of which involve the carboxyl-terminal (CT) domain, serve to regulate Cx function.

The CxCT domain serves a critical role in the regulation of all aspects of the Cx life cycle including trafficking, assembly, channel open states, as well as internalization and degradation. Importantly, the CT domain is the site at which the greatest degree of sequence divergence is observed between family members. A number of studies have highlighted that little conservation of regulatory mechanisms contained within the CT domain exists between family members. Furthermore, a clear understanding of the molecular determinants that influence different Cx channel properties between family members is lacking. Thus, investigation into the specific

mechanisms that regulate each family member is essential to develop a complete picture of Cx biology and to develop novel therapeutics with which to modulate Cx function.

Previous work from our laboratory identified a novel feature of the Cx45CT domain, high-affinity ($K_D \sim 100$ nM) dimerization. Here using a combination of biophysical, biochemical, and cell/molecular biology approaches we demonstrate that dimerization is essential for proper Cx45 turnover, localization, phosphorylation, and function. Additionally, we demonstrate that phosphorylation by three kinases that are dysregulated in heart disease alter the function of Cx45 to promote cell coupling and consequently may contribute to the pathogenic phenotype.

ACKNOWLEDGEMENTS

First, I am eternally grateful for the opportunity provided to me by the Department of Biochemistry and Molecular Biology to pursue my doctorate here at the University of Nebraska Medical Center. I would like to offer thanks and acknowledgement to the faculty, staff, and graduate students in the Biochemistry and Molecular Biology department for the aid, support, and comradery throughout my time here. Without it, I surely would not have been successful in this endeavor. I would especially like to thank Dr. Paul L. Sorgen for opening the door to his lab for me and providing excellent training, feedback, and support on both a professional and personal level. I would also like to thank him for constantly being upbeat, excited, and approachable, I could not have asked for a better graduate mentor.

I would also like to thank my supervisory committee members: Dr. Justin Mott, Dr. Amarnath Natarajan, and Dr. Tahir Tahirov for their encouragement, support, and direction throughout this process. The suggestions of the committee have proved to be invaluable lessons in doing research. I would also like to thank the lab of Dr. Steve Caplan, and Dr. Naava Naslavsky for sharing their cell culture space and experience as well as providing the HeLa cells used herein, Dr. Myron Toews for providing HEK293T cells, and Dr. Paul Lampe at the Fred Hutchinson Cancer Research Center for providing the MDCK cells used throughout my project. I would like to thank our collaborators at Rutgers University, Drs. Andrew Harris and Jorge Contreras, and Juan M.V. Capuccino for their assistance in collecting the macroscopic hemichannel currents presented in Chapter Two as part of our collaborative publication.

I would like to thank both current and past members of the Sorgen Laboratory: Dr. Gaelle Spagnol, Li Zheng, Dr. Hanjun Li, Dr. Jennifer Kopanic, Dr. Mona Al-Mugotir, and Sydney Zach for their daily support and assistance in my training. I would especially like to thank Dr. Spagnol, Dr. Hanjun Li, and Li Zheng, for their assistance with my projects, their willingness to listen and bounce ideas around as well as their social support. You have all helped to make this time much more than another stage of education and I cannot thank you enough.

Thanks to all who have been a part of my time here at the University of Nebraska Medical Center. I will always look back on this time fondly and miss you all greatly.

DEDICATION

I would like to dedicate this dissertation to my family. First, my mother, Sharrie Trease, who lost her battle with cancer when I was a child. It was she, who taught me to be tenacious, dedicated, and to pursue my dreams. To my father, Jerald Trease, who graduated from the Department of Biochemistry here at the University of Nebraska Medical Center and really inspired my love of science. To my wife, Morgan Wetterstrom, who has stood by me through the roller coaster that is graduate school and supported me in ways she may never understand. I love and thank you every day. Finally, I dedicate this work to my two amazing and beautiful daughters Olive, and Rennie. It is my hope that this will one day serve as motivation and inspiration for you to pursue your own dreams whatever they may be. I love you more than you may ever know!

TABLE OF CONTENTS

ABSTRACT	ii
ACKNOWLEDGEMENTS	iv
DEDICATION	v
TABLE OF CONTENTS	vi
LIST OF FIGURES	xiii
LIST OF TABLES	xvi
LIST OF ABBREVIATIONS	xvii
CHAPTER ONE	1
1. Gap Junction Overview	2
2. Gap Junction Regulation	6
2.1 Transcriptional Regulation of Cxs	7
2.2 Connexin Life Cycle	11
2.2.1 Connexin Biosynthesis	11
2.2.2 Trafficking and Assembly of Gap Junctions	12
2.2.3 Internalization and Gap Junction Turnover	15
2.3 Channel Gating	16
2.3.1 Voltage Gating	17
2.3.2 pH Gating	18
2.3.3 Ca ²⁺ Gating	19
2.4 Importance of the CT Domain	20

2.4.1 Intrinsically Disordered Proteins	20
2.4.2 Connexin Cytoplasmic Domains	21
2.4.3 Connexin CT Dimerization	24
3. Post-Translational Regulation of Connexins	26
3.1 Connexin Phosphorylation	26
3.1.1 Introduction to Connexin Phosphorylation	26
3.1.2 Methods for Studying Connexin Phosphorylation	27
3.1.3 Serine/Threonine Phosphorylation	31
3.1.4 Tyrosine Phosphorylation	37
3.1.5 Phosphorylation of Cx45	43
3.2 Other Connexin Post-translational Modifications	44
3.2.1 Connexin Carbon-based Modifications	44
3.2.2 Connexin Ubiquitination	46
3.2.3 Connexin SUMOylation	46
3.2.4 Connexin S-nitrosylation	48
4. Objective	48
CHAPTER TWO	50
5. Introduction	51
6. Materials and Methods	54
6.1 Cell Culture and Transient Transfections	54
6.2 Stable Cell Line Generation	54
6.3 Antibodies and Immunostaining	54
6.4 Live Imaging	55
6.5 Cell Lysis for Direct Western blot	55

6.6 Co-IP and Western blot	55
6.7 RT-PCR	57
6.8 Cycloheximide Chase	58
6.9 Scrape Loading Dye Transfer Assay	58
6.10 Triton X-100 Solubility Assays	59
6.11 siRNA Knock-down of Cx43	59
6.12 Bimolecular Fluorescence Complementation	60
6.13 Blue-Native PAGE	60
6.14 Sucrose Density Gradient Fractionation	60
6.15 Calmodulin Binding Assay	61
6.16 Hemichannel Dye Uptake Assay	62
6.17 Statistical Analysis	62
7. Results	63
7.1 Cx45CT WT Dimerizes at the Plasma Membrane	63
7.2 Inhibiting CT Dimerization of Cx45 Alters Protein Localization	68
7.3 Cx45 6E Has Altered Protein Expression	75
7.4 Cx45CT Dimerization is Essential for Proper GJIC	77
7.5 Inhibition of Cx45 CT Dimerization Impairs GJ Plaque Formation	77
7.6 Inhibiting Dimerization Does Not Alter Oligomerization	82
7.7 Increased Membrane Cx45 6E Mediates Increased Hemichannel Activity	84
7.8 Cx45CT Dimerization Reduces Hemichannel Currents	87
7.9 Cx45CT Dimerization Enhances Tyrosine but Not Serine Phosphorylation	89
7.10 Cx45CT Dimerization Affects Cytoskeletal Adapter Protein Partner Interactions	91

7.11 Inhibiting Cx45CT Dimerization Disrupts Nedd4 but Not TSG101 Interactions	93
7.12 The Cx45CT A333-N361 Contains a Potential CaM IQ Motif	95
8. Discussion	99
CHAPTER THREE	105
9. Introduction	106
10. Materials and Methods	108
10.1 Expression and Purification of Recombinant GST-tagged Proteins	108
10.2 Analytical Ultracentrifugation (AUC): Sedimentation Equilibrium	108
10.3 Circular Dichroism (CD): Secondary Structural Analysis	108
10.4 Cell Culture and Stable Cell Line Generation	110
10.5 Antibodies and Immunostaining	110
10.6 Cell Lysis for Direct Western blot	110
10.7 Western blot	111
10.8 Triton X-100 Solubility Assay	111
10.9 Scrape Loading Dye Transfer Assay	112
10.10 Hemichannel Dye Uptake Assay	112
10.11 Statistical Analysis	113
11. Results	114
11.1 Design of Cx45CT Chimeric Constructs	114
11.2 Biophysical Characterization of Cx45CT Mutants	114
11.3 Similar to Cx45 6E dimerization incompetent Cx45 mutants display increased plasma membrane localization	120
11.4 Loss of CT Dimerization Results in Decreased TX-100 Solubility	120
11.5 Dimer Incompetent Cx45 Mutants Display Increased Hemichannel Dye Uptake	122

11.6 Inhibiting Dimerization Correlates with Impaired GJIC	124
11.7 Homologous Mutations of A333-N361 from Cx40 or Cx43 Alter Trafficking	126
11.8 Cx45 40 _{MD} and Cx45 43 _{MD} Show Increased Hemichannel Dye Uptake	129
11.9 Homologous A333-N361 Mutations Preserve or Enhance GJIC	129
12. Discussion	132
CHAPTER FOUR	135
13. Introduction	136
14. Materials and Methods	141
14.1 Antibodies and Reagents	141
14.2 Expression and Purification of Cx45CT WT and Mutants	141
14.3 Kinase Screen (Eurofins KinaseProfiler)	141
14.4 <i>In vitro</i> Phosphorylation	141
14.5 Mass Spectrometry	143
14.6 Validation of Mass Spectroscopy	143
14.7 Cell Culture and Stable Cell Line Generation	144
14.8 Transient Transfections	144
14.9 Co-IP and Western blot	144
14.10 Antibodies and Immunostaining	145
14.11 Scrape Loading Dye Transfer Assay	146
14.12 TX-100 Solubility Assay	146
14.13 Circular Dichroism (CD): Secondary Structural Analysis	147
14.14 Analytical Ultracentrifugation (AUC): Sedimentation Equilibrium	147
14.15 Statistical Analysis	148

15. Results	149
15.1 Screen Identifies Kinases that Phosphorylate the Cx45CT	149
15.2 Src, Pyk2, and PKC α Interact with Cx45 in HeLa Cells.	149
15.3 Src Regulates Cx45 Phosphorylation in LA25 Cells	151
15.4 v-Src Activity Does Not Alter Cx45 Localization in LA25 Cells	153
15.5 v-Src Disrupts Cx45 GJ Plaque Formation in LA25 and HeLa Cells	155
15.6 v-Src Negatively Regulates Cx45 GJIC in HeLa Cells	157
15.7 Physiological Activation of Src by EGF Enhances Cx45 GJIC	159
15.8 Acute Exposure to Pervanadate Increases GJ Plaque Formation	161
15.9 PMA Enhances Anchoring of Cx45 to Cytoskeleton in MDCK and HeLa Cells	161
15.10 Treatment with PMA Does Not Affect Cx45 GJ Plaque Formation	167
15.11 Activation of PKC by Treatment with PMA Impairs Cx45 GJIC	169
15.12 MS Identifies Cx45 Residues Phosphorylated by Src, Pyk2, and PKC α	169
15.13 Cx45CT Mutants Confirm MS and Identify Additional Phosphorylated Tyrosines	171
15.14 Phosphorylation of Y356 Reduces Cx45CT A333-N361 Dimerization Affinity	175
15.15 Cx45 Y356 Phosphorylation Does Not Alter Structure of A333-N361	177
15.16 Phosphomimetic Cx45 Y356E Localizes Similar to Cx45 WT	179
16. Discussion	181
CHAPTER FIVE	186
17. Introduction	187
18. Materials and Methods	189
18.1 Antibodies and Reagents	189
18.2 Cell Culture and Stable Cell Line Generation	189
18.3 siRNA Knock-down of Exogenous Cx45	189

18.4 Antibodies and Immunostaining	189
18.5 Scrape Loading Dye Transfer Assay	190
18.6 TX-100 Solubility Assay	190
18.7 Statistical Analysis	191
19. Results	192
19.1 Cx45 Prevents Src Mediated Turnover of Cx43 Containing GJs	192
19.2 Knock-down of Exogenous Cx45 Results in Src Mediated Cx43 Turnover	194
19.3 Presence of Cx45 Does Not Protect Against Src Mediated Channel Closure	194
19.4 Cx43 Maintained in GJs by Cx45 Shows Altered Phosphorylation Patterns	196
20. Discussion	200
CHAPTER SIX	203
21. Introduction	204
22. Materials and Methods	206
22.1 Cell Culture and Treatments	206
22.2 Antibodies and Immunostaining	206
22.3 Co-IP and Western blot	207
22.4 GST Pull Downs	207
22.5 NMR-HSQC Experiment	208
22.6 In vitro Phosphatase Assay	208
22.7 Scrape Loading Assay	209
22.8 Statistical Analysis	210
23. Results	211
23.1 EphB1 directly interacts and phosphorylates the Cx32CT domain	211
23.2 TC-PTP interacts with and dephosphorylates Cx32CT residue pY243	213

23.3 EphB1 phosphorylates and TC-PTP dephosphorylates Cx32 in HeLa cells	215
23.4 Cx32 Y243E increases GJIC	218
23.5 EphA1 also phosphorylates Cx32 on the CT domain	220
23.6 Phosphorylation at Y243 has little-to-no effect on the Cx32CT interaction with calmodulin or synapse-associated protein 97	222
24. Discussion	227
CHAPTER SEVEN	230
25. Summary and Conclusions	231
References	240

LIST OF FIGURES

Figure 1.1. Topology and organization of connexin proteins.	3
Figure 1.2. Protein partners that directly interact with the Cx43CT domain to promote intercellular communication.	40
Figure 1.3. Protein partners that directly interact with the Cx43CT and Cx43CL domains to impede intercellular communication.	41
Figure 2.1. Schematic of Cx45CT BiFC constructs for <i>in cyto</i> dimerization assay.	64
Figure 2.2. Cx45CT WT dimerizes at the plasma membrane.	66
Figure 2.3. Localization of Cx45 WT and Cx45 6E in HeLa cells.	67
Figure 2.4. Inhibition of Cx45CT dimerization alters proteins localization.	69
Figure 2.5. Endogenous Cx43 does not alter Cx45 expression or localization.	71
Figure 2.6. Localization of Cx45 WT and 6E are not species specific.	73
Figure 2.7. Live imaging using Cx45-eGFP WT or 6E reveals diffuse localization of Cx45 6E along plasma membrane.	74
Figure 2.8. Inhibiting Cx45CT dimerization disrupts protein degradation.	76

Figure 2.9. Inhibiting Cx45CT dimerization impairs gap junction intercellular communication.	78
Figure 2.10. Inhibiting Cx45CT dimerization impairs GJ plaque formation.	80
Figure 2.11. Endogenous Cx43 does not impact Cx45 GJ plaque formation.	81
Figure 2.12. Inhibiting Cx45CT dimerization does not impact oligomerization state or cell compartment.	83
Figure 2.13. Inhibiting Cx45CT dimerization affects hemichannel dye uptake.	86
Figure 2.14. Inhibiting Cx45CT dimerization affects hemichannel currents.	88
Figure 2.15. Inhibiting Cx45CT dimerization increases Tyr but not Ser phosphorylation.	90
Figure 2.16. Loss of Cx45CT dimerization alters cytoskeletal anchoring.	92
Figure 2.17. Inhibiting Cx45CT dimerization correlates with decreased associated of Nedd4 but not TSG101.	94
Figure 2.18. <i>In silico</i> prediction of Cx45 CaM binding motifs.	96
Figure 2.19. Cx45CT A333-N361 does not bind CaM.	98
Figure 2.20. Sequence alignment of the Cx45CT dimerization domain (A333-N361) from different species.	100
Figure 3.1. Helical wheel analysis of heterologous and scrambled Cx45 mutants.	115
Figure 3.2. Purification of the CT domains of Cx45 WT and mutants.	117
Figure 3.3. Circular dichroism spectra of Cx45CT WT and dimerization domain mutants.	119
Figure 3.4. Immunofluorescence of Cx45 WT and mutants reveals altered plasma membrane localization.	121
Figure 3.5. Inhibiting Cx45CT dimerization increases TX-100 solubility.	123
Figure 3.6. Dimerization incompetent Cx45 mutants display increased neurobiotin uptake through hemichannels.	125
Figure 3.7. Inhibiting Cx45CT dimerization impairs cell coupling of neurobiotin.	127
Figure 3.8. Homologous Cx45 mutants display increased plasma membrane localization.	128
Figure 3.9. Homologous Cx45 mutants have increased hemichannel uptake of neurobiotin.	130
Figure 3.10. Homologous Cx45 mutant maintain or enhance neurobiotin transfer.	131
Figure 4.1. Kinase screen reveals several kinases phosphorylate Cx45CT <i>in vitro</i> .	150

Figure 4.2. Co-IP of Src, Pyk2, and PKC α by Cx45.	152
Figure 4.3. Cx45 Tyr phosphorylation increases with Src activity in LA25 cells.	154
Figure 4.4. Src activity does not appreciably alter the localization of Cx45 in LA25 cells.	156
Figure 4.5. Src activity disrupts Cx45 GJ plaque formation in LA25 and HeLa cells.	158
Figure 4.6. Transfection with v-Src impairs Cx45 GJIC.	160
Figure 4.7. More physiologically relevant activation of Src by stimulation of the EGFR by EGF enhances Cx45 GJIC.	163
Figure 4.8. Acute pervanadate treatment enhances Cx45 GJ plaque incorporation.	164
Figure 4.9. PMA increases Cx45 Tyr and Ser phosphorylation and enhances cytoskeletal anchoring in MDCK cells.	165
Figure 4.10. PMA increases Cx45 Ser and Tyr phosphorylation and enhances interactions with cytoskeletal anchors in HeLa cells.	166
Figure 4.11. PMA does not affect Cx45 GJ plaque stability.	168
Figure 4.12. Treatment with PMA impairs Cx45 GJIC in HeLa cells.	170
Figure 4.13. MS reveals residues of Cx45CT phosphorylated <i>in vitro</i> by Src, Pyk2, and PKC α .	172
Figure 4.14. Cx45CT single Tyr mutants reveal novel phosphorylated residues and validate <i>in vitro</i> MS results.	174
Figure 4.15. Phosphorylation of Y356 reduces the dimerization affinity of Cx45 A333-N361 by an order of seven magnitudes.	176
Figure 4.16. Phosphorylation of Y356 does not alter A333-N361 secondary structure.	178
Figure 4.17. Phosphomimetic Cx45 Y356E similarly to Cx45 WT.	180
Figure 5.1. Cx45 mutes the effect of Src on Cx43, reducing the transition of junctional to non-junctional Cx43.	193
Figure 5.2. Knock-down of exogenous Cx45 restores Cx43 lability when Src is active.	195
Figure 5.3. Cx45 does not prevent Src mediated downregulation of GJIC in LA25 cells.	197
Figure 5.4. Cx43 is maintained the GJ plaque with altered phosphorylation landscape when Cx45 is co-expressed in LA25 cells.	199
Figure 6.1. EphB1 phosphorylates the Cx32CT domain <i>in vitro</i> .	212

Figure 6.2. Cx32CT residues affected by the direct interaction with TC-PTP.	214
Figure 6.3. TC-PTP interacts with the Cx32CT domain and dephosphorylates pY243.	216
Figure 6.4. EphB1 increases and TC-PTP decreases the Tyr phosphorylation level on Cx32.	219
Figure 6.5. Cx32 Y243E increases GJIC.	221
Figure 6.6. EphA1 phosphorylation of Cx32 increases gap junction intercellular communication <i>in vitro</i> and <i>in cyto</i> .	223
Figure 6.7. Phosphorylation of Cx32 Y243 has little-to-no effect on the interaction with CaM.	225
Figure 6.8. Phosphorylation of Cx32 Y243 has no effect on the interaction with SAP97.	226

LIST OF TABLES

Table 1. Kinases that phosphorylate Cx43 Ser residues and their effect on GJIC.	34
Table 2. Antibodies and reagents.	56
Table 3. Measurements of GJ plaque length.	70
Table 4. Source of homologous and heterologous Cx45 mutants.	109
Table 5. Summary of observed mass and K_D for Cx45 mutants.	118
Table 6. Cx45CT WT and single Tyr mutants.	142
Table 7. Kinetic constants for dephosphorylation of Cx32	217

LIST OF ABBREVIATIONS

6E	Cx45 L335E, L338E, I342E, L349E, I353E, Y356E
A	Alanine (single-letter code)
aa	Amino acids
Ang II	angiotensin II
APC	Antigen presenting cells
Asp	Aspartic acid
ATP	Adenosine triphosphate
AUC	Analytical ultracentrifugation
BCA	Bicinchoninic acid
BFA	Brefeldin A
C	Cysteine (single-letter code) or Celcius or Carboxyl
CaM	Calmodulin
CaMKII	Ca ²⁺ /calmodulin-dependent kinase II
cAMP	Cyclic Adenosine monophosphate
CD	Circular dichroism
cDNA	Complimentary deoxyribonucleic acid
CHX	Cycloheximide
CL	Cytoplasmic loop
cm	Centimeter
CMTX	X-linked Charcot-Marie-Tooth Disease
Co-IP	Co-immunoprecipitation
c-Src	Cellular-sarcoma tyrosine kinase
CT	Carboxyl-terminus
Cx(s)	Connexin(s)
DAPI	4',6-Diamidino-2-Phenylindole, Dihydrochloride
DDSc	Cx45 Dimer Domain (A333-N361) Scrambled
DNA	Deoxyribonucleic acid
Drebrin	<u>Developmentally regulated brain protein</u>
DTSSP	3,3'-dithiobis[sulfosuccinimidylpropionate
DTT	Dithiothreitol
E	Glutamic Acid (single-letter code) or Extracellular loop
<i>E. Coli</i>	<i>Escherichia coli</i>
EDTA	Ethylenediaminetetraacetic acid
EGF	Epidermal growth factor
EGFP	Enhanced green fluorescent protein

EGFR	Epidermal growth factor receptor
EGTA	Ethylene glycol tetraacetic acid
Eph	erythropoietin-producing hepatocellular receptor
Ephrin	Eph family receptor interacting protein
ER	Endoplasmic reticulum
ERAD	Endoplasmic-reticulum-associated degradation
ERGIC	ER-Golgi-intermediate compartment
ERP29	<u>ER</u> resident protein 29
ET-1	Endothelin-1
F	Phenylalanine (single-letter code)
FAT	Focal adhesion targeting domain
FBS	Fetal bovine serum
FERM	Protein 4.1, ezrin, radixin and moesin homological domain
FGF	Fibroblast growth factor
G	Glycine (single-letter code) or Immunoglobulin G
<i>g</i>	Grams or Centrifugation constant (<i>italics</i>)
GCN4	General control protein 4
<i>g_j</i>	Junctional conductance
GJ	Gap junction
GJIC	Gap junction intercellular communication
Glu	Glutamic acid
GSH	Glutathione
GST	Glutathione S-transferase
H	Histidine (single-letter code)
HC	Hemichannel (connexon)
HDAC	Histone deacetylase
hr	Hour(s)
HSQC	Heteronuclear single quantum coorelation
I	Isoleucine (single-letter code)
ID	Intercalated disc
IDP	Intrinsically disordered protein
Inx	Innexin
IP	Immunoprecipitation
IP ₃	Inositol 1,4,5-triphosphate
IPTG	Isopropyl β-D-1-thiogalactopyranoside
Itk	interleukin-2-inducible T-cell kinase
Jak	Janus kinase
<i>K</i>	Equilibrium
K	Lysine (single-letter code)

K_D	Dissociation constant
kDa	Kilodaltons
K _m	Michaelis constant
L	Leucine (single-letter code)
LB	Luria Broth
Leu	Leucine
LY	Lucifer yellow
M	Methionine (single-letter code) or Molar
MAPK	Mitogen-activated protein kinase
mg	Milligrams
MHC	Major histocompatibility complex
MHz	Megahertz
min	Min
ml	Milliliters
mm	Millimeters
mM	Millimolar
mol	Mole
MonA	Monensin A
MOPS	3-(N-morpholino)propanesulfonic acid
mRNA	Messenger ribonucleic acid
MS	Mass spectrometry
MW	Molecular weight
N	Asparagine (single-letter code) or Amino or number of samples
n	Number of sites
NB	Neurobiotin
Nedd4	<u>N</u> eural precursor cell <u>e</u> xpressed <u>d</u> evelopmentally <u>d</u> own-regulated protein <u>4</u>
nM	Nanomolar
nm	Nanometers
NMR	Nuclear magnetic resonance
NRK	Normal rat kidney
NT	Amino-terminus
OD	Optical density
ODDD	Oculodentodigital dysplasia
ON	Overnight
p	Phosphorylated
PAGE	Polyacrylamide gel electrophoresis
PBS	Phosphate buffered saline
PBST	Phosphate buffered saline Tween 20%

PDGFR	Platelet-derived growth factor receptor
PDZ	PSD-95/Dlg/ZO-1
PI3K	Phosphoinositide 3-kinase
PIB	Protease inhibitor buffer
PKA	cAMP-dependent protein kinase A
PKC	protein kinase C
PKG	protein kinase G
PMA	Phorbol myristate acetate
PMSF	Phenylmethylsulfonyl fluoride
ppm	Parts per million
PPR	Poly-proline region
Pyk2	Protein tyrosine kinase 2 beta
R	Arginine (single-letter code)
RAS	Renin–angiotensin system
rpm	Revolutions per minute
RT	Room temperature
S	Serine (single-letter code) or Standard
s	Seconds
S.E.M.	Standard error of mean
SAP	Synapse-associated protein
SD	Standard deviation
SDS	Sodium dodecyl sulfate
Ser	Serine (three-letter code)
SH2	Src homology 2 domain
SH3	Src homology 3 domain
siRNA	Small interfering RNA
STAT	Signal transducer and activator of transcription
SUMO	<u>S</u> mall <u>u</u> biquitin-like <u>m</u> odifier
T	Threonine (single-letter code)
TBST	Tris-buffered saline Tween-20
TC-PTP	T-Cell Protein Tyrosine Phosphatase
TGN	Trans-Golgi network
Thr	Threonine (three-letter code)
TK	Tyrosine kinase
TM	Transmembrane
Tris	Tris-(hydroxymethyl)aminomethane
TSA	Trichostatin A
Tub	Tubulin
TX-100	Triton X-100

Tyk2	Tyrosine kinase 2
Tyr	Tyrosine (three-letter code)
UTR	Untranslated region
UV	Ultraviolet
VEGF	Vascular endothelial growth factor
V_j	Transjunctional voltage
V_m	Transmembrane voltage
W	Tryptophan (single-letter code)
WB	Western (Immuno) blot
WT	Wild-type
X	Any amino acid
Y	Tyrosine (single-letter code)
ZO-1	Zonula occludens protein 1
ZO-2	Zonular occludens protein 2
α	Alpha or anti-
β	Beta
γ	Gamma
δ	Delta or Chemical shift
ΔDD	Cx45 Dimer Domain (A333-N361) Deleted
μg	Micrograms
μL	Microliters
μM	Micromolar
ψ	Bulky hydrophobic
ζ	Zeta

CHAPTER ONE

Introduction

1. Gap Junction Overview

At the heart of physiological function within an organism is a diverse network of coordinated cellular actions. This coordination is achieved by many diverse mechanisms, from the binding of ligand to a receptor, to changes in membrane potential elicited from the release or uptake of ions. These mechanisms categorized into four groups include endocrine, paracrine, juxtacrine, and autocrine signaling; defined as long distance, short distance, juxtaposed (contact dependent), and self-acting signals, respectively. Paracrine, juxtacrine, and autocrine signaling are mediated, in part, by the activity of the connexin (Cx) family of GJ proteins.

GJs are composed of tetraspan integral membrane proteins that contain four transmembrane (TM1-4) domains, two extracellular loops (EL1 and EL2), a cytoplasmic loop (CL), amino-terminus (NT), and carboxyl-terminus (CT) [1-5]. Six Cx proteins (homomeric or heteromeric) oligomerize into connexons (hemichannels) that can further dock (homotypic or heterotypic) with connexons apposed from adjacent cells. Six conserved cysteines are present in the ELs (three in each) that are essential for proper docking and GJ formation [1-5]. GJs are semi-crystalline arrays of 100s-1000s of individual GJ channels [6, 7]. Figure 1.1 illustrates this hierarchy. GJs consisting of Cx proteins are found only in vertebrates. Invertebrates possess a homologous family of GJ proteins known as the innexins (Inxs) [8, 9]. The homology between Cxs and Inxs is limited to topological and functional homology as they contain no sequence homology [8, 9]. In humans, there are 21 Cx proteins, while in mice there are only 20 (19 can be paired as orthologues) (reviewed in [10-12]). Two major nomenclature classifications for Cxs exist. The most commonly used system names Cx proteins for their apparent molecular weight (e.g., Cx45 is a Cx protein of 45 kDa) [13]. The second system, based on evolutionary homology, names the Cx genes based on the extent of sequence similarity and the length of the CL domain [13]. This nomenclature based on homology, segregates Cxs into three major (α , β , or γ) and two minor (δ , or ϵ) classes and the names begin with Gj (for gap junction) and ends numerically for the order in which the specific family member was discovered [13]. For example, the gene for Cx43 is *Gja1* as it was the first α -Cx described.

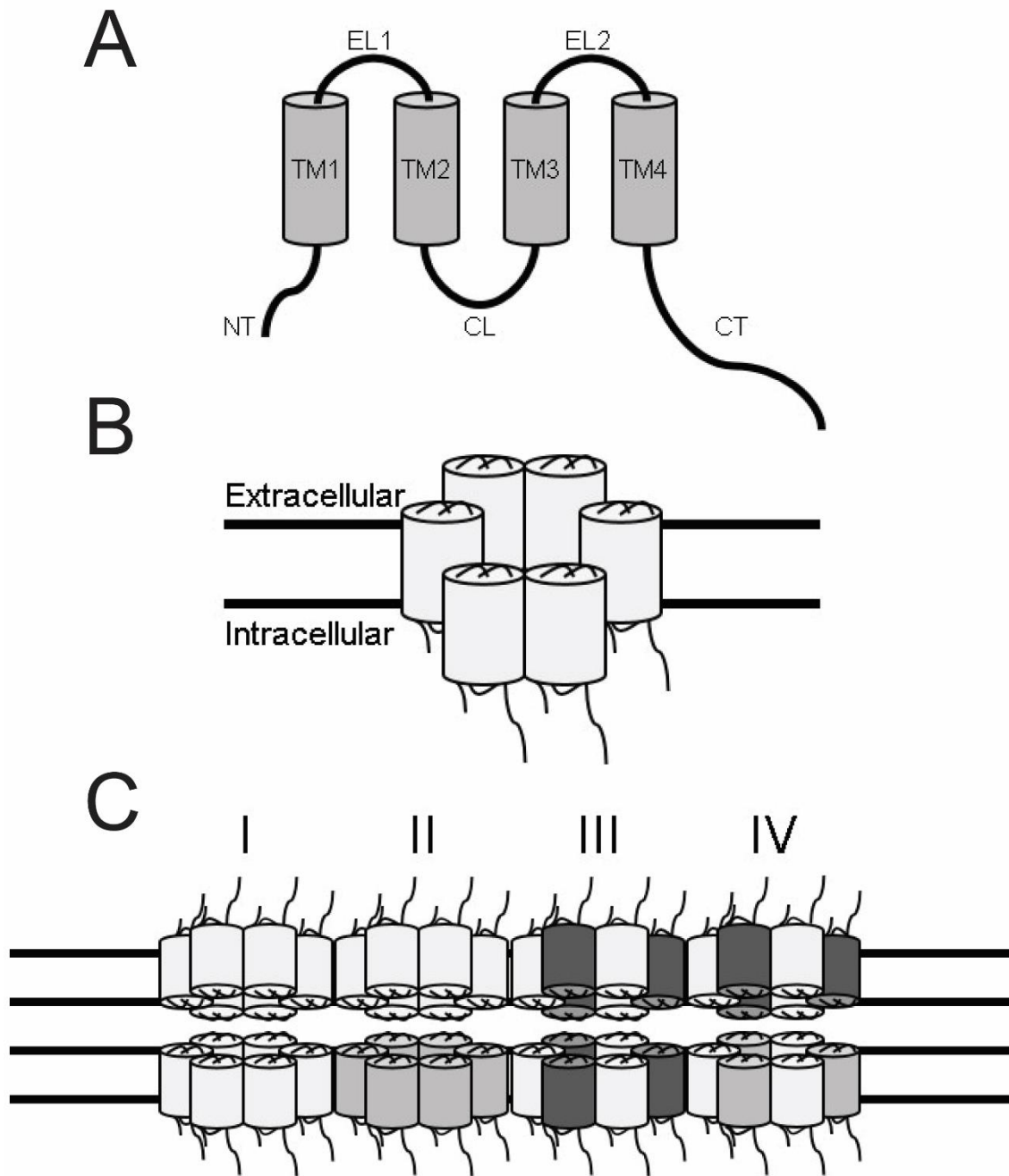


Figure 1.1. Topology and organization of connexin proteins.

A) Membrane topology of a Cx protein, having four transmembrane (TM) domains, two extracellular loops (EL1 and EL2), and a cytoplasmic loop (CL) as well as cytoplasmic amino- and carboxyl-termini (NT and CT respectively). B) Oligomerization of six Cx proteins into a connexon (hemichannel), each barrel shape represents a single Cx protein. C) Organization and docking of Cxs from two adjacent cells forms a single channel, channels cluster in semicrystalline arrays to form gap junctions, which can be of four distinct types (I-homomeric/homotypic, II-homomeric/heterotypic, III-heteromeric/homotypic, and IV-heteromeric/heterotypic). Solid black lines represent the plasma membrane.

In general, GJs serve to allow the passage of small (≤ 1000 Da) cytoplasmic constituents including ions, small metabolites, and second messengers (e.g., cAMP) between the cytoplasm of coupled cells or with the extracellular space, thereby propagating and amplifying signals transduced from various initiating events [14]. The initiating stimuli can be in the form of growth factor receptor signaling, kinase cascades, ion release, cytokine stimulation, or mechanical stretch [15-30]. Each Cx isoform contributes a unique set of channel properties when homomeric homotypic channels are considered, for heteromeric and heterotypic channels there is often the development of novel channel properties not seen in either family member when homomeric (reviewed in [31]). This high degree of variability coincides with a high degree of differential Cx family member expression among different tissues and organs [32]. Furthermore, the Cx expression patterns for a given organ or tissue are regulated spatiotemporally [32]. Cxs are found in most tissues and organ systems in the adult under normal conditions with the exception of skeletal muscle and some mobile cells (e.g., sperm and red blood cells) [32]. Importantly, a given cell type can express multiple Cx family members simultaneously creating the possibility for the formation of heteromeric and/or heterotypic GJs (Fig. 1.1). This variable diversity allows Cxs to perform a number of highly specialized roles in various tissues and cell types.

With widespread distribution and the high degree of interplay between family members, it follows that dysregulation or loss of function for a particular family member may pose deleterious for the host. Indeed, a number of pathologies have been attributed to dysregulation or loss of a particular Cx family member. For example, loss of Cx45 (genetic ablation or loss of function) results in death on approximately embryonic day 10 in mice due to a cushion defect in cardiogenesis [33]. Cx43 null mice survive throughout fetal development but suffer from perinatal lethality due to pulmonary outflow defects in the heart, and also exhibit anomalous lens development and germ line deficiency in both sexes [34-37]. Additionally, mutations within the Cx43 protein sequence cause oculodentodigital dysplasia (ODDD) [38-45]. Other Cxs have also been attributed to human maladies including Cx32 which is shown to be causal to X-Linked Charcot-Marie-Tooth disease (CMTX), or Cx26 for which a subset of mutations lead to non-syndromic hearing loss in humans

while homozygous null mice die around embryonic day 11 [46-55]. Furthermore, mutations in Cx46 and Cx50, the dominant lens Cxs, have been associated with cataracts (reviewed in [56]).

In the heart, GJs play a critical role in the propagation and amplification of impulses originating in the sinoatrial (SA) node [57]. There are specifically four Cxs known to function in the heart. In decreasing order of relative expression level, the four cardiac Cxs are: Cx43, Cx40, Cx45, and Cx30.2 [57-60]. The bulk of impulse propagation in the working myocardium is handled by Cx43 (atria and ventricles) and Cx40 (atria) [60-64]. Although Cx40 is of significant interest in the atria, it will not be discussed in detail. In the human heart Cx45 is the first Cx expressed during embryogenesis, but by the time of birth has been limited to the cells of the specialized conductance and pace making system [65]. Here the unique properties of Cx45 channels serve to prevent re-entrant arrhythmia by slowing conduction velocity between the ventricles and atria thereby ensuring sequential contraction [66, 67]. Cx30.2 is expressed in the mouse heart in a similar localization pattern to Cx45, and its expression is stabilized by Cx45, however, in humans the orthologue Cx31.9 has not been detected in the heart [68-70]. Cx30.2 therefore likely plays a mouse specific role in the fine-tuning of impulse propagation in the special conductance system and for the purposes of this dissertation will not be discussed further [68, 69]. In diseased hearts Cx expression is altered. A number of studies have demonstrated a primary effect of cardiac remodeling subsequent to ischemic events or during end stage heart failure is loss of Cx43 expression at the intercalated disc (ID) (reviewed in [67, 71]). This loss of Cx43 is preceded by lateralization of Cx43 away from the ID where internalization processes have been suggested to reduce overall Cx43 expression and limit cell connectivity [72]. In addition to remodeling of Cx43, Cx40 and Cx45 are also remodeled [67, 71, 73-78]. Ischemic heart disease was shown to increase overall Cx40 expression in the ventricles, where under healthy conditions its expression is absent, specifically localizing in a band of working myocytes adjacent to the conduction system [71, 79, 80]. It has been suggested that this may be a compensatory mechanism to the loss of Cx43 coupling in the ventricle [79, 80]. In the atria where Cx40 is the primary Cx, its expression was shown to increase in heart disease, leading to increased incidence of atrial fibrillation [81]. Cx45 similar to Cx40 is not appreciably expressed in the healthy adult ventricular myocardium and has been demonstrated to

be upregulated in various heart disease states [65, 82, 83]. In end stage heart failure, work from Yamada et al. have demonstrated upregulation of Cx45 localizing to the ID in ventricular myocytes [82]. This was observed in conjunction with the typical lateralization and downregulation of Cx43 [82, 84]. Importantly, Yamada et al. also demonstrated Cx45 and Cx43 colocalized at the ID, suggesting the possibility for heteromeric channels to form [82, 83]. Channel properties of the primary cardiac Cxs differ such that they serve specific functions with little overlap. It therefore stands to reason that remodeling (alterations in localization, size, or composition of the GJ plaques) can have significant effects on conduction properties of the heart. This is especially the case for the formation of heteromeric channels (e.g., Cx43/Cx45) because the properties of these channels can be dominated by the properties of one of the family members, or they can take on new properties either intermediate or novel to either homomeric counterpart [83, 85, 86]. Indeed, using cell and molecular biology techniques a number of groups have substantiated the existence of Cx43/Cx45 heteromeric channels [86, 87]. Furthermore, studies have also shown Cx45 exerts a dominant negative effect on Cx43/Cx45 heteromeric channels such that channel properties are more similar to homomeric Cx45 channels than those of homomeric Cx43 channels; altering dye permeability, conductance, open probability, and plaque size [83, 86, 88]. In the heart, this is thought to be a potential substrate for lethal arrhythmias [82, 83, 86, 88]. Therefore, the formation and regulation of heteromeric channels is of significant clinical interest to the therapeutic and GJ community alike.

2. Gap Junction Regulation

With the diverse set of physiological functions carried out by GJs (e.g., cell-to-cell communication, hemichannel functions, etc.) it is essential that they are tightly regulated. The regulation of GJs occurs at a number of hierarchical levels. First, Cxs are regulated spatiotemporally. Not every Cx family member is expressed by all cell types, and in cell types where multiple family members are expressed they are not always expressed simultaneously. Several layers of regulatory mechanisms exist to ensure proper spatial (tissue type or subcellular localization) and temporal (developmental stage, cell cycle stage, or stimulus response) regulation of GJs including transcriptional, translational, trafficking, post-translational, assembly, or turnover

mechanisms. This is especially true for functional regulation of GJ intercellular communication (GJIC). GJ functions are regulated at the plaque by various factors including but not limited to: phosphorylation, voltage, Ca^{2+} , pH, and association with binding partners. Here, we will discuss the various regulators of Cx proteins and GJs.

2.1 Transcriptional Regulation of Cxs

Typical Cx gene structure involves two (or more) exons. The first exon normally includes a 5'-untranslated region (UTR) which is separated from the second exon by an intron of variable length [89, 90]. The second exon for most Cxs includes the entire protein coding sequence and the 3'-UTR (reviewed in [91, 92]). Deviations from this scheme have been described, including alternative/consecutive splicing of the 5'-UTR thought to function in alternate promoter usage, leading to changes in mRNA stability, or altered translation efficacy (reviewed in [91, 92]). Furthermore, the protein coding region of the second exon can be punctuated with one or more introns (e.g., mCx36, hCx36, mCx39, hCx40.1) leading to alternative splice variants.

The gene structure for Cx43 (*Gja1*) in mice was originally thought to only contain the two canonical Cx exons, however, it was more recently shown that the gene for *Gja1* contains four additional exons totaling six overall [93, 94]. Five of the six *Gja1* exons are dedicated 5'-UTR regions (Exons 1A-1E) and the sixth (Exon 2) includes the remaining portion of the 5'-UTR, all of the Cx43 coding sequence, and the 3'-UTR [93, 94]. Additionally, the *Gja1* gene in mice has been shown to have three promoters, two of which are downstream of the originally discovered *Gja1* promoter (P1). The first, P2, is located in Exon 1A, and P3 is located in the intron that precedes Exon 1C. Through combinations of differential promoter usage and intron splicing this leads to nine different Cx43 transcripts in mice [93].

Similar to Cx43 in mice, Cx45 (*Gja7*; *Gjc1*), exceeds the traditional two exons with five total exons (1A-C, 2, and 3) [90, 95]. Contrary to Cx43, however, Exons 1A-C and 2 include only 5'-UTR, while Exon 3 contains the remaining 5'-UTR, the Cx45 protein coding sequence, and the 3'-UTR [90]. Cx45 transcripts observed in mice suggest that Exons 1A-C splice independently to E2-E3, or alternatively a second transcription start site exists in Exon 2, resulting in four total mouse Cx45 transcripts [90, 95]. The transcripts produced have been found to be tissue specific.

Transcripts containing Exon 1A are present in nearly all cell types where Cx45 is expressed, however, expression of Exon 1B and 1C transcripts are less widespread. Exon 1B transcripts are found only in trace amounts in the colon, and Exon 1C transcripts are found in the heart, skeletal muscle, lung, bladder, colon, and ovary [90, 95]. Conservation of Exon 2 and 3 sequences was shown between mouse and human for *Gja7* [96].

Promoter analysis for many Cxs has revealed the presence of multiple promoters (reviewed in [91]). For most Cx proteins P1 (the basal level promoter) is contained approximately 300 base pairs upstream of the transcription start site contained in Exon 1 and includes the binding site for numerous ubiquitous and cell/stimulus dependent transcription factors (reviewed in [91]). In the following paragraphs, we will highlight a number of the transcription factors and the conditions (if applicable) that lead to the activation of the gene.

Transcription factor specificity protein 1 (Sp1) is a zinc-finger transcription factor that binds GC rich regions of promoters. Sp1 drives basal transcription for several Cxs including Cx26, Cx32, Cx40, and Cx43 (reviewed in [91]). Specifically, for Cx43 analysis revealed four potential Sp1 binding sites that contributed to Cx43 promoter activity [96]. Another study found that disruption of histone deacetylases by trichostatin A (TSA) induced expression of Cx43 in a Creb binding protein dependent manner [97]. For Cx40, ablation of the Sp1 binding sites in the promoter region by mutation severely impaired promoter activity [96]. Another basal transcription factor found to activate Cx transcription is the AP-1 complex (reviewed in [91]). The AP-1 complex consists of heterodimers of the c-Fos, c-Jun, activating transcription factor (ATF), and Jun dimerization protein (JDP) protein families and binds to the consensus sequence [TGAC (T/G) TCA] [98]. In the proximal promoter for Cx43 there have been two identified AP-1 binding sites in rat while only one site has been identified in human and mouse [99]. Activation of AP-1 mediated transcription of Cx43 was stimulated by transforming growth factor β (TGF- β), mitogen activated kinase 4 (MKK4), and Erk1/2 signaling [100] [101] [102]. In addition to Sp1 and AP-1, Wnt signaling and cAMP mediated transcription have also been shown to regulate at least Cx43 transcription (reviewed in [91]).

More critical to expression of GJs in the heart and cardiac pathology are the cell/stimulus dependent transcription factors. Tissue specific promoter usage occurs in virtually all organs and tissues of the body [103]. Despite the occurrence of GJs in the majority of organ systems and tissues, this section will focus solely on the cardiac specific transcription factors and some of the functions they serve. Regular development of the cardiac tissues requires the symphonious function of several transcription factors including Nkx2.5, Shox2, Homeodomain-only protein (Hop), Iroquois homeobox 3 (Irx3), T-box transcription factors (Tbx), and GATA family transcription factors (reviewed in [91]). Nkx2.5 is a transcription factor that is essential for proper cardiac development [104]. Indeed, mutations in Nkx2.5 interfering with its DNA binding function promote cardiac maladies such as conduction block [105]. Importantly, binding sites for Nkx2.5 have been detected in the promoters of Cx40, Cx43, and Cx45 [99, 106, 107]. Interestingly, while several studies have concluded that Nkx2.5 acts as a transcriptional activator for both Cx43 and Cx40, at least one study has identified a repressive role of Nkx2.5 for Cx43 expression [108, 109]. Specifically, exogenous expression of a constitutively active version of Nkx2.5 showed downregulation of Cx43 expression within 16 hr of transduction, suggesting that subsequent heart failure was not a contributing factor [109]. Dupays et al. demonstrated that day E9.2 Nkx2.5 null mouse embryos lacked significant expression of Cx43 in the heart as the result of poorly developed ventricular trabeculae as well as substantially reduced gene expression of Cx45 [106]. The same study concluded that mouse embryos heterozygous for Nkx2.5 developed normally [106]. Furthermore, ventricular loss of Nkx2.5 in mice resulted in no overt structural cardiac abnormality, however, slowed progressive atrioventricular conduction was observed [110]. The same study also showed that while mutant mice perinatally expressed Cx40 in the conduction system, its expression was essentially absent in the adult mutants, suggesting a Nkx2.5 was not essential for perinatal expression of Cx40 but was required for age related continuity [110].

Shox2, another homeobox type transcription factor is also essential for cardiac development. Mice null for Shox2 display lethality at embryonic days E11.5-13.5 and die from heart defects such as abnormally slow beating rhythm, and underdeveloped sino-atrial node and valves [111, 112]. Interestingly, Shox2 functions upstream of a number of the important cardiac

transcription factors including Nkx2.5 and Tbx factors [112]. For Nkx2.5, Shox2 appears to be a transcriptional repressor ensuring genes activated by Nkx2.5 (Cx43 and Cx40) remain repressed in the area of the sino-atrial node [112]. Conversely, and consistent with known expression patterns of Cx45, Shox2 appears to activate Cx45 gene expression to facilitate differentiation of the pace-making system [67, 71, 75, 113].

Similar to Nkx2.5 and Shox2, the Hop, Irx, Tbx, and GATA families of transcription factors function to regulate the expression of the cardiac Cxs. Hop for example, which is expressed in the developing heart, is essential to development of the mature conduction system (reviewed in [91]). Homozygous loss of Hop results in loss of Cx40 expression throughout the heart when homozygous, while heterozygous knock-out of Hop reduces Cx40 expression in the atrio-ventricular node and associated conduction system [114]. Furthermore, overexpression of Hop reduced expression of Cx40 in the atria in models of ventricular hypertrophy that was restored by the addition of the HDAC inhibitor TSA [115]. The Irx family transcription factor Irx3 functions to repress Cx43 and induce expression of Cx40 [116]. The Tbx family of transcription factors, namely Tbx2, Tbx3, Tbx5, Tbx18 also function to regulate the expression of Cxs in the heart (reviewed in [91]). Cx43 and Cx40, for example, are repressed transcriptionally by both Tbx2 and Tbx3 [117, 118]. Interestingly, the expression of Cx45 does not seem to be affected by either Tbx2 or Tbx3 [117]. Similar to Tbx2 and Tbx3, Tbx18 suppressed the expression of Cx43, however, unlike Tbx2 and Tbx3 it does not appear to downregulate Cx40 or Cx45 [119]. In contrast to the other Tbx transcription factors noted here, Tbx5 appears to be the only transcriptional activator, activating the expression of Cx40 in a dose dependent manner [120]. Finally, of the GATA family of transcription factors, GATA4 has been observed to regulate both Cx40 and Cx30.2 in mice [107, 121].

In addition to regulation by transcription factors, Cx gene expression can be regulated epigenetically. Similar to all genes, histone modification (and modulation thereof) affects the expression of Cx transcripts (reviewed in [122]). Two other mechanisms described also fine tune the expression of Cxs: DNA methylation and the expression of microRNAs that target Cx transcripts (reviewed in [122]). Although these mechanisms are important for the regulation of Cxs, discussion of their specific nature (beyond noting they occur) is beyond the scope of this dissertation.

2.2 Connexin Life Cycle

Temporally, all functional Cx family members follow a similar expression scheme that can be referred to as the Cx life cycle. The Cx life cycle is closely tied to both cell cycle as well as extracellular stimuli (e.g., cell surface receptor activation) and begins with transcription and ends with turnover/recycling. A number of factors contribute to the regulation of the Cx life cycle including transcription factors, the interactions with protein partners, and post-translational modifications ((PTMs); e.g., phosphorylation). This section provides an overview of the Cx life cycle and explores some of the factors that regulate it. Since the control of Cx expression by transcription was addressed in Section 2.1 it will not be addressed in detail in this section. Additionally, since the vast majority of studies illustrating stages of the Cx life cycle focus on Cx43, the discussion in this section will have a similar primary focus.

2.2.1 Connexin Biosynthesis

Biosynthesis of Cxs begins in the nucleus of the cell with transcription of a Cx gene by transcription factors. The degree to which the gene is transcribed is a function of the combinations of various transcription factors present. For example, one mechanism by which Cx43 transcription is initiated in cell culture is activation of Wnt signaling from cell-cell contact. This leads to the inhibition of GSK-3 β , leading to stabilization of β -catenin which translocates to the nucleus where it promotes transcription of a number of genes including *Gja1* (Cx43; [123-125]). There are a number of general and tissue specific conditions and transcription factors (e.g., general - SP1, cardiac specific - Nkx2.5) that regulate the transcription of GJ genes (reviewed in [91, 92]). To further increase the diversity of Cx family member expression as well as tissue specific levels of expression, not all Cx genes contain the same promoters (reviewed in [91, 92]). Once transcribed Cx mRNAs are exported from the nucleus to the endoplasmic reticulum (ER) for protein translation.

Cx protein translation, like that of all integral membrane proteins, occurs on ribosomes studding the surface of the rough ER. However, in contrast to most proteins, the mRNA structure of Cx transcripts (abnormally long 5'-UTR) favors cap-independent translation [90, 126]. In cap-independent translation, specific sequences contained in the 5'-UTR promote ribosomal entry and translation initiation [127, 128]. This is important for the Cx family proteins because it allows their

expression to bypass cellular stress responses that impact cap-dependent translation thereby maintaining cell coupling [127, 128]. As integral membrane proteins Cx polypeptide chains are co-translationally inserted into the membrane of the rough ER. This is accomplished by the translation of hydrophobic domains (likely the TM1) which are recognized and bound by the signal recognition particle (SRP), halting translation. The Cx peptide/ribosome/SRP complex then docks with ER translocons where translation proceeds [129]. The nascent polypeptide chain is retained in the lumen of the translocon until translation completes and the complete protein is inserted into the ER membrane (secretory proteins are released into the ER lumen) [130-134]. For Cx43 integration into the ER membrane and folding of the general topological features (i.e., four TM domains with cytoplasmic NT and CT domains) occurs simultaneously [135]. Additionally, studies have begun to demonstrate the importance of ER resident protein partners (chaperone proteins) in Cx synthesis (reviewed in [136]). One example is ER resident protein 29 (Erp29) which was shown to stabilize Cx43 as a monomer in the ER to prevent early oligomerization of Cx43 connexons [137]. An important caveat revealed by the Das et al. study was the saturable nature Erp29 and thus extreme overexpression systems may drive early channel oligomerization [137]. In addition to Erp29, the ER-associated cytosolic protein—Connexin interacting protein of 75 kDa (CIP75)—regulates expression and trafficking of Cxs [138-142]. For Cx43, CIP75 binds Cx43 over a large region of the CT domain (K264-Q317) where it mediates ejection from the ER lumen and transport of misfolded Cx43 to the proteasome via ER associated degradation (ERAD) [139-142]. It has been suggested that this is a mechanism of both quality control and fine tuning of expression levels [141]. Supporting CIP75's role in Cx quality control, treatment of cells with denaturing compounds increases the association of CIP75 with Cx43, and suggests that only Cx43 that is not bound by CIP75 escapes the ER and continues into the secretory pathway [141].

2.2.2 Trafficking and Assembly of Gap Junctions

Following successful translation of monomeric Cx protein, oligomerization of six Cx proteins into a connexon (hemichannel) and trafficking to the plasma membrane is essential for proper Cx function. The oligomerization of Cx channels has been described for Cx43, Cx46, Cx32, and Cx26 by several studies [129, 143-146]. In the studies characterizing Cx32 and Cx26,

oligomerization of both family members was observed to occur in ER membranes; however, an important caveat to the studies was the use of cell-free expression systems [129, 145, 146]. In contrast, Cx43 and Cx46 were demonstrated to oligomerize in the *trans*-Golgi network (TGN) using numerous methods [137, 143, 144]. In one study, a large panel of secretory pathway inhibitors were used to demonstrate that Cx43 requires export from the ER to successfully form connexons [144]. Another study examining the oligomerization of Cx43 and Cx46 in rat osteosarcoma (ROS) cells also used secretory pathway inhibitors and sucrose gradient density centrifugation to determine that Cx43 and Cx46 were both retained in the ER as well as *cis*-Golgi in a monomeric form [143]. A follow up study then used Cxs (Cx43 and Cx32) expressed with C-terminal retention tags for either ER and ER-Golgi intermediate compartment (ERGIC) retention (HKKSL or AKKFF, respectively) [147]. The results of that study confirmed that Cx43 indeed oligomerizes in the TGN, while it offered support to the work of Falk et al., as Cx32 was observed to oligomerize even when retained in the ER [129, 145-147]. Importantly, the study also demonstrated that Cx43 and Cx46 could form heteromeric channels and this occurred in the TGN, as co-expression of tagged Cx43 and untagged Cx46 led to Cx43 immunoreactivity present at the plasma membrane in structures consistent with GJ plaques [147].

In addition to connexon oligomerization a critical step in the Cx life cycle is trafficking from the ER and/or Golgi to the plasma membrane. Interestingly, a study demonstrated an early phosphorylation event closely following translation for Cx43 using Brefeldin A ((BFA); blocks ER to Golgi transport in the ERGIC) and is likely essential for subsequent maturation steps [148]. Upon exiting the TGN Cx43 is contained in vesicles that are trafficked along the microtubule network to be delivered to the plasma membrane [149-152]. A number of phosphorylation events occur during trafficking that regulate the vast number and types of protein interactions that are critical for efficient transport to the plasma membrane and subsequent membrane insertion (reviewed in [153]). These phosphorylation events will be discussed in greater detail in a later section dedicated to regulation of Cxs by phosphorylation. Of note, delivery (and insertion) of connexon containing vesicles to the plasma membrane appears to be random (i.e., not targeted) [135, 154]. Although, further characterization is required to clearly define the mechanism by which Cxs are incorporated into the

plasma membrane, recent studies have begun to implicate roles for the cAMP-dependent protein kinase A (PKA)- and actin-binding protein Ezrin as well as 14-3-3 protein in the capture and insertion of Cx43 containing vesicles into the plasma membrane [155-164]. Once in the plasma membrane, lateral diffusion processes seem to direct the connexons to the periphery of the GJ plaque (perinexus) [154, 165, 166]. Conversely, an alternative mechanism has been suggested in cardiomyocytes where trafficking via microtubules target Cx43 containing vesicles directly to the adherens junctions in the ID [152, 167].

The final step of GJ assembly is the docking of connexons (via the ELs) and incorporation into the GJ proper. As Cx43 connexons from apposed cells are retained in the perinexus, they are generally bound by interactions with ZO-1, and release from ZO-1 coincides with docking [166]. In addition to ZO-1, Ca²⁺-dependent cell adhesion proteins such as E- and N-cadherin are important for GJ formation, however, further investigation is required to clearly delineate the role as studies have produced conflicting results [168, 169]. In one study knock-down of N-cadherin was shown to reduce GJ formation in NIH3T3 cells and thereby impaired GJIC [170]. Conversely, another study using mouse L cells concluded that loss of cadherin increased GJ formation when stimulated with forskolin, while cells expressing cadherins showed decreased overall Cx43 expression [171]. A third study investigating the role of cadherins on Cx43 expression in hepatocytes demonstrated that expression of E-cadherin correlated with increased GJ assembly, while N-cadherin expression resulted in GJ disassembly [172]. Although, the exact roles for cadherins in GJ assembly remain unclear, it is clear that cadherins influence GJ assembly. Additionally, catenins (cadherin-associated intracellular proteins) also influence GJ formation. Colocalization of α -catenin with Cx32 and Cx26 in hepatocytes as well as Cx43 in cardiomyocytes has been demonstrated [173, 174]. This was also observed for β -catenin in cardiomyocytes, and authors subsequently demonstrated the association of β -catenin with Cx43 was essential to GJ formation [174]. Additionally, recently our laboratory took an NMR approach and demonstrated a direct interaction between the CT domain of Cx43 and β -catenin that can be modulated by phosphorylation of Cx43 residues (Y265 and Y313) via Src [175]

2.2.3 Internalization and Gap Junction Turnover

Completion of the Cx life cycle requires internalization and subsequent turnover (or alternatively recycling) of GJs. A process that is mediated by a number of normal and pathological cellular stimuli, including but not limited to cell division, response to growth factors, differentiation, apoptosis, wound healing, depletion of cellular metabolites, and preventing the spread of toxic factors (preventing the by-stander effect) (reviewed in [176, 177]). Similar to the diverse stimuli that promote GJ turnover, a diverse set of protein interactions are required for proper turnover of GJ channels.

Although Cxs are membrane proteins they uniquely have relatively short half-lives (1-5 hr) [178, 179]. This is somewhat variable depending on the tissue and cell type, for example in the lens of the eye the predominant Cxs (Cx45.6 and Cx56) seem to be more static with half-lives approaching 90 hr under organ culture conditions [31]. However, in the same study when primary cells were isolated and cultured *in vitro* the stability was lost, and half-lives were more consistent with studies of other family members [31]. Although the molecular determinants resulting in this stability were not identified, the authors did observe differential phosphorylation of Cx56 between the organ and primary cultures [31]. Consistent with observations of relatively short half-lives, Cx26, Cx32, Cx37, Cx43, and Cx45 have all been shown to have half-lives ranging from 1-5 hr [148, 180-197]. This was even true for Cx43 in isolated perfused hearts suggesting the difference seen with lens Cxs is likely tissue specific or as the authors suggested may have been the consequence of large non-synchronized pools of Cx45.6 and Cx56 in the lens [31, 188].

Degradation of GJs has been shown to occur by multiple mechanisms. The primarily described mechanism is through the generation of annular GJs, which are double membrane vesicles containing intact GJ plaques that are internalized by one of the adjoined cells [198]. It is generally accepted that the EL interactions between docked connexons are of sufficient strength that separating them into connexons is not possible [66, 86, 199, 200]. This is supported by evidence from immunogold labeled electron microscopy studies [66, 86, 199, 200]. Despite the general acceptance of this model of internalization, other groups have suggested mechanisms by which the GJ are disassembled into pools of connexons and then internalized by endocytic

mechanisms. In one study, hepatic GJs immunogold labeled appeared to disaggregate and the authors speculated this may represent undocking and internalization, however, were unable to provide concrete evidence [173]. More recent studies have provided evidence that Cx43 GJs partially turnover by through internalization of central connexons as new connexons are integrated into the GJ at the periphery [154, 201]. Exactly how this occurs remains to be determined.

Degradation of Cx43 has been shown to involve both proteasomal and lysosomal pathways. In their study of perfused rat hearts Beardslee et al. used inhibitors of proteasomal and lysosomal degradation and determined that in both circumstances Cx43 expression levels were increased [188]. Interestingly, they showed that phosphorylation of Cx43 may be a critical determinant of which pathway was utilized. They observed increased Cx43 phosphorylation when lysosomal degradation was inhibited and conversely accumulation of non-phosphorylated Cx43 when the proteasomal pathway was inhibited [188]. This was in contrast to a previous study demonstrating both increased Cx43 phosphorylation and GJIC following blockade of proteasomal degradation, suggesting the existence of cell type specific mechanisms [202].

Additionally, Cx ubiquitination has been suggested as a contributor to GJ turnover. For Cx43, specific phosphorylation events have been linked to increased ubiquitination and turnover. Specifically, phosphorylation of key Ser residues (addressed in detail in the section on phosphorylation) creates a high affinity binding site for the E3 ubiquitin ligase neuronal expressed developmentally downregulated protein 4 (Nedd4) [203, 204]. Ubiquitination of Cx43 by Nedd4 recruits adapter protein 2 (AP2) and clathrin to mediate internalization and transport to the lysosome (reviewed in [205]). In addition to AP2 and clathrin, 14-3-3 has been shown to play a role in the internalization and degradation of Cx43 [164, 206].

2.3 Channel Gating

Cell-cell communication via GJs is controlled by various mechanisms in the cell. A primary control mechanism for coupling is expression and turnover as described in the previous section. Additional mechanisms include phosphorylation and channel gating, the latter being an important control of when and to what degree channels are open. This is important as communication must

be regulated for proper tissue synchronization and to control the spread of ions and metabolites. In this section, the three major types of channel gating will be discussed in detail.

2.3.1 Voltage Gating

One of the three major types of GJ channel gating is voltage gating. Voltage gating works to modulate channel openness by translating changes in electrical potential surrounding the GJ channel into a conformational change which leads to channel closure [207]. Similar to other voltage regulated channel proteins, GJ proteins contain a series of charged amino acid residues that constitute a “voltage sensor” [208-210]. In vertebrate GJs, voltage gating can be derived from either the transjunctional voltage (V_j ; ubiquitous, albeit to variable degrees) or transmembrane voltage (V_m ; less common) [211].

In vertebrates, all GJ family members to a degree are gated by changes in V_j indicated by the ability of generating junctional conductance (g_j) by either hyperpolarizing or depolarizing one cell of the coupled pair [207]. Furthermore, early studies indicating the presence of two types of V_j dependent gating, fast-gating and slow-gating [212]. All three of the intracellular domains are involved to some degree in voltage gating. The NT domain was shown to contribute to V_j dependence using mutational approaches abolishing key charged residues on Cx26 and Cx32 channels [208-210]. Studies on Cx43 and Cx32 revealed a role for the CT domain in fast V_j -gating. Where truncation of Cx32 at residue 222, or Cx43 at residue 257 resulted in a disruption of fast conductance, and led to voltage gating mostly of the slow-gating type [213]. Based on the studies investigating the mechanisms of fast-gating the current model (“ball-and-chain”) posits the CT domain physically moves into proximity of the channel pore sterically blocking the conductance [207].

In contrast to V_j dependent gating, V_m dependent gating is much less common amongst Cx family members. Three Cxs that are gated in a V_m dependent manner are Cx43, Cx45, and Cx57 [214-216]. Interestingly, for Cx45 channels it was shown that V_m dependence was the result of two separate gates, one in each hemichannel [214]. It is suggested that V_m dependence is likely cell type or species specific, as Cx43 channels exhibit strong V_m dependence in oocyte expression systems, but rather limited V_m dependence in HeLa cells [216, 217]. It has been speculated that

V_m dependent gating may serve to prevent the spread of excess charge from damaged cells to healthy neighboring cells.

2.3.2 pH Gating

In addition to voltage gating, GJ channels are also gated by changes in pH. Specifically, intracellular acidification, such as what occurs during ischemia, has been identified as a mechanism by which GJ channels close [218-221]. Similar to voltage gating during membrane depolarization this may be a protective mechanism by which cells suppress the by-stander affect [222]. Additionally, like the “ball-and-chain” model proposed for voltage gating one proposed model describing how intracellular acidification leads to channel closure is a “particle receptor” model, again involving CT-CL interactions [223, 224]. Several electrophysiological studies support the notion that a CT-CL interaction mediates pH gating [225-228]. For pH gating in Cx43 there is a clear dependence of the CT domain, as truncation of the CT domain rendered Cx43 channels pH insensitive and co-expression of a soluble Cx43CT domain restored pH sensitivity of the truncated Cx43 channels [223]. Furthermore, soluble Cx43CT increased the pH sensitivity Cx32 channels when co-expressed [223]. Although a similar effect was also shown for Cx40, the model may not apply to all Cx family members as similar truncations of Cx26 and Cx45 failed to prevent pH mediated channel closure suggesting alternative mechanisms may also be involved [229]. Interestingly, for Cx45 homotypic and Cx45/Cx43-enhanced green fluorescent protein (eGFP) heterotypic channels a relationship between voltage gating and pH gating has been observed [230]. Specifically, it was observed that as pH increased, open probability and the g_j - V_j dependence increased, while acidification conversely had the opposite effect resulting in more channel closure and a decreased g_j - V_j dependence [230]. In addition to the “particle receptor” interactions, a number of studies have shown that pH dependent changes in Cx CT domain structure occur, which may lead to altered affinity for the CL or other protein partners [204, 231]. For Cx43, a decrease in pH from 7.5 to 5.8, as would occur in ischemia, results in an increase in helical content from essentially 0% at pH 7.5 to 7% at pH 5.8 [231]. Increasing helical content was also detected for the CT domains of Cx32 and Cx45 under acidic conditions [204]. Cx hemichannels also appear to be pH gated as reported by a number of studies [232-235]. Trexler et al. suggested that the pH sensor

for Cxs is likely contained on a domain near the pore as a result of two observations [234]. First, intracellular application of acidic solution led to rapid long-term channel closure, while extracellular application resulted in closure that rapidly returned to the open state [234]. Second, extracellular application of weak membrane permeable acids prevented hemichannel openings under positive membrane potentials, while strong acids (membrane impermeable) had little effect on opening, but rapidly closed open hemichannels [234].

2.3.3 Ca²⁺ Gating

Another form of GJ channel gating is Ca²⁺ dependent gating. Ca²⁺ dependent gating is an important effect of cellular Ca²⁺ signaling, and likely plays an important role in cardiac tissue where Ca²⁺ signaling is critical for proper myocyte function [236]. Ca²⁺ dependent gating has been suggested to occur via two primary mechanisms, directly via Ca²⁺ ion binding to Cx hemichannels and indirectly through the action of the Ca²⁺ binding protein Calmodulin (CaM) [237, 238]. The direct mechanism of Ca²⁺ ion binding is a mediator of Cx hemichannel closure [237]. In this mechanism Ca²⁺ ions bind to charged residues disrupting a salt bridge between the hemichannel subunits in the extracellular portion of the pore resulting in a conformational change [237]. CaM mediated Ca²⁺ gating serves to close GJ channels through Ca²⁺ dependent interaction of CaM with the cytoplasmic domains of Cx family members [238]. Ca²⁺ regulation has been reported for several Cxs including Cx32, Cx36, Cx43, Cx44, Cx45, and Cx50 [239-245]. In this mechanism increased levels of intracellular Ca²⁺ enhance the affinity of CaM for the cytoplasmic domains and the binding of CaM has been observed to alter secondary structure [243]. Specifically, for Cx43 CaM has been shown to interact with both the CL and CT domains, and induces significant helical structure in the Cx43CL domain [246, 247]. The induction of secondary structure may occlude the pore to ions [243, 246]. A similar increase in helical content was observed for the Cx32CT, however, unlike Cx43, Cx32 also has a CaM binding domain present on the NT where W3 has been shown to be critical for the interaction [248-250]. CaM was recently shown to interact directly with Cx45 via the CL domain, mediating channel closure [251]. Interestingly, when interacting with the Cx45CL, CaM was not observed to adopt a more compact structure in contrast to what was observed for Cx50 [245, 251]. This was noted to be similar to the binding of CaM to non-Ca²⁺ dependent targets like

myosin, however, similar to other Cxs the binding of CaM to the Cx45CL was greatly enhanced by Ca^{2+} [251, 252]. In addition to the CL, CaM was also recently shown to interact with the CT domain of Cx45, albeit the functional implications were not explored [247]. This significance of this observation remains to be determined.

2.4 Importance of the CT Domain

The CT domain of Cx proteins has long been understood as an important regulatory domain. It is a hub for protein-protein interactions, and a plethora of PTMs. Importantly, although significant homology of the extracellular and transmembrane domains of Cxs exist, the cytoplasmic domains have a large degree of divergence between family members. The CT domain containing the highest degree of divergence amongst the three cytoplasmic domains, and thus has long been hypothesized to be a determinant of differences in channel properties and regulation between Cx family members. In this section, we will highlight the importance of the CT to Cx function and regulation.

2.4.1 Intrinsically Disordered Proteins

The majority of expressed proteins are folded into well-structured arrangements to carry out specific functions and can often be categorized by their folding. Kinases for example contain a conserved kinase fold domain where the side chains of specific key residues are oriented in a manner which supports the catalytic activity required to attach a phosphate to a target (reviewed in [253, 254]). For many biochemical reactions or protein interactions, a specific 3D conformation is essential, and often loss of 3D structure correlates with decreased or abolished function (reviewed in [253, 254]). For proteins that contain stretches of contiguous residues (30 or more) that do not adopt structure, known as intrinsically disordered proteins, the regions of disorder are often essential to function (reviewed in [255]). Intrinsically disordered regions of proteins are now well understood to be good substrates for promiscuous protein-protein interactions. Intrinsically disordered regions of proteins tend to adopt secondary structure as a function of protein partner binding or PTM, allow for overlapping protein partner binding motifs, and provide large surface area for interactions to occur (reviewed in [255]). Combined these features allow intrinsically disordered

proteins to be highly dynamic. For Cxs, the cytoplasmic domains often adopt an intrinsically disordered arrangement (reviewed in [256]).

2.4.2 Connexin Cytoplasmic Domains

The cytoplasmic domains of Cxs consist of the NT, CL, and CT domains and are important for channel gating, channel formation, and regulating channel function. These domains contain sites for the interactions with protein partners as well as PTMs. While the cytoplasmic domains are less homologous between family members than the transmembrane and extracellular domains, the degree of divergence between family members is greatest for the CT domain.

The NT domain of Cxs is the most well conserved intracellular domain between family members in size (reviewed in [257, 258]). For the α -type Cxs the NT is 22 residues in length, while for the β -type Cxs the NT is 23 residues long (reviewed in [1, 258]). Two exceptions to this are Cx36 and Cx47, which have 24 and 25 NT residues, respectively [259]. Despite similarity in length, the NT domains of different family members have been shown to adopt differing secondary structure [258]. The structure of the NT domains of Cx32 and Cx26 were solved by solution NMR, and Cx32NT was determined to be disordered, however, the Cx26NT was observed as helical in structure [260, 261]. Importantly, for the Cx26NT a critical bend was detected at residues 11 and 12 which allow the first 10 residues to swing into the pore [210]. Indeed, crystallographic studies modeling Cx26 similarly observed the NT domain lining the vestibule of the pore where it contributes to ion selectivity and voltage gating [262]. Furthermore, the high-resolution crystal structure presented by the Maeda et al. study was that of the open Cx26 channel, and it provided evidence for the notion that interactions between the NT and the transmembrane helices maintain the open pore [262]. Specifically, a ring of hydrogen bonds formed between residues D2 and T5 of adjacent protomers at the narrowest point of the pore, and hydrophobic contact between W3 and a hydrophobic patch of TM1 on the adjacent protomer [262]. Importantly, studies investigating mutations in the NT domain have illustrated its importance in plaque formation, and proper channel function (reviewed in [258]). Furthermore, NT domain mutations of many family members have been linked to diseases (Cx26, Cx30, Cx30.2/Cx31.3, Cx31, Cx32, Cx43, Cx46, and Cx50) (reviewed in [258]). Interestingly, the effects of these mutations are diverse with some mutations

causing impaired trafficking and plaque assembly, others rendered channels nonfunctional, while still others induced cell death when exogenously expressed [168, 263-273]. Using mass spectrometry (MS), PTMs of the NT domain have been detected; among those are phosphorylation, acetylation, and hydroxylation, the functional effects of which will be addressed in more detail in Section 3.2 [274, 275].

In contrast to the NT domain, the CL domain of Cxs has a larger degree of size variability. Family members can be clustered into 3 groups by the length of the CL domain (and total sequence homology): small (30-35 residues; α ; e.g., Cx43, Cx40), medium (50-55 residues; β ; e.g., Cx26, Cx32), and large (80-105 residues; γ ; e.g., Cx45, Cx47) [12]. Similar to the NT domain, the CL also plays a role channel formation and gating [212]. Unfortunately, due to the dynamic and disordered nature of the CL domain, crystallographic studies have been unable to resolve the CL domain [262, 276]. Meaningful structural studies have therefore been limited to the use of solution NMR and circular dichroism (CD) and suggest the domain is primarily disordered with a tendency to adopt helical character [277]. For the Cx43CL, the structure was solved in solution by NMR and revealed the presence of two small α -helical regions that are induced by acidification or the interaction with CaM [246, 277]. Analysis of CL domain peptides of Cx43, Cx32, and Cx36 using CD spectroscopy revealed the CL of all three family members had a tendency to form α -helices when samples were supplemented with the secondary structure stabilizer trifluoroethanol (TFE) [278]. Notably, this was attributed to the distal half of the loop (where CaM binds), the proximal portion of the loop yielded complex results that were difficult to interpret [278]. Despite the lack of a crystal structure of the CL domain, truncation studies have demonstrated the importance of the CL domain in Cx trafficking and channel formation [279, 280]. Cx43 synthetic mutants harboring deletion of CL residues were shown to be non-functional suggesting a critical role for the CL in channel function [279, 280]. Interestingly, while both the Cx43 Δ 130-134 and Cx43 Δ 130-137 were non-functional, only the Cx43 Δ 130-134 properly trafficked to the plasma membrane [279, 280]. This finding suggested that a portion of the CL domain may also be critical for trafficking [279, 280]. Deletion of a similar region of the Cx32CL impaired GJIC measured by dye transfer suggesting the importance of the CL to channel function is a general feature of Cxs [281]. The CL domain is an important factor of gating

in both the “ball-and-chain” and “particle receptor” models of voltage and pH gating respectively, as well as Ca^{2+} gating. Critical to the function of the CL in gating, is interactions with other proteins (or domains; see section 2.3). The Cx43CL for example functions as the receptor in the “ball-and-chain” and “particle receptor” models of channel gating [207, 223, 224]. Similarly, the CL of several Cx family members serve as a target for CaM in Ca^{2+} gating (reviewed in [282]). The CL domain, like the NT, has been detected to be post-translationally modified by phosphorylation and carboxylation [274, 275, 283]. The importance of these modifications will be discussed in greater detail in Sections 3.1 and 3.2.

The CT domain of Cxs is the most variable domain between family members in both length and primary sequence [1]. Cx26 for example has a CT containing only 10 residues while the CT of Cx62 is 310 residues in length [1]. Like the NT and CL domains, the CT domain is important for trafficking, channel gating, and regulation, and similarly to the CL domain the CT is dynamic and unstructured, thus not amenable to crystallographic studies [1, 262, 276]. Solution NMR and CD studies have revealed the CT domain of several Cxs as primarily disordered [231, 247, 284-286]. While they are primarily disordered, structural studies of the CT domains of Cx43 and Cx45 revealed they contain α -helical regions [247, 286]. The helical domains of the Cx43CT are involved in the dimerization of Cx43CT domains and are important for the CT-CL interaction in pH dependent gating [277, 286]. Interestingly, the NMR structure of transmembrane tethered Cx43CT protein (TM4-Cx43CT) suggested that a total of 7 helical domains were present [287]. Of the 7 helical domains, the two detected when the CT domain is expressed without TM4 were contained within slightly longer helical domains when tethered [287]. For the Cx45CT, the helical region (A331-N361) mediates high affinity ($K_D \sim 100$ nM) homodimerization and will be covered in greater detail in the next section [247]. The functional implications of the Cx45CT α -helical domain are a key portion of this dissertation and will be discussed in Chapter Two. In addition to Cx43 and Cx45, helical propensity was also reported for the CT domains of Cx32 and Cx36 [278]. Worth noting in the case of Cx32 and Cx36, the secondary structure had to be stabilized by the addition of TFE [278].

2.4.3 Connexin CT Dimerization

An additional feature that has been attributed to the CT domains of Cxs is homo- and heterodimerization [231, 247, 286]. To date, the phenomenon has been reported for Cx43 and Cx45 [247, 286]. For Cx43, dimerization between the two CT domains was revealed by a combination of NMR, *in vitro* crosslinking, and analytical ultracentrifugation (AUC) sedimentation equilibrium experiments [286]. Crosslinking of recombinant Cx43CT at various pH values suggested formation of a pH-dependent dimer when analyzed by sodium dodecyl sulfate polyacrylamide gel electrophoresis (SDS-PAGE) [286]. Western blot of the same SDS-PAGE gel suggested the presence of even higher order oligomers [286]. Further analysis of the recombinant protein by AUC sedimentation equilibrium suggested that at physiological pH only 12% of the total Cx43CT was in dimer conformation, however, acidification to pH 6.5 and 5.8 yielded 84% and 86% dimer conformations, confirming the pH dependence suggested by the crosslinking experiments [286]. Use of NMR revealed the residues likely involved in the dimerization to be M281–N295, R299–Q304, S314–I327, and Q342–A348 [286]. Although dimerization of the Cx43CT was revealed, the affinity of the interaction was not determined [286]. Based on previous reports, our laboratory examined the ability of the CT domain of other primary cardiac Cxs (Cx40 and Cx45) to dimerize [231, 247, 286]. For the Cx40CT AUC sedimentation equilibrium suggested that very little Cx40CT was present as a dimer conformation regardless of pH (pH 6.0 – 5.2% and pH 7.4 – 2.3%) [231]. Interestingly, for the Cx45CT dimerization was detected at both physiological and ischemic pH [247]. Furthermore, the calculated affinity of the interaction (K_D) at both physiological and ischemic pH were comparable, albeit slightly weaker at ischemic pH (141 nM at pH 5.8 and 97 nM at pH 7.5) [247]. Interestingly, this observation is in contrast to the effect of pH on the dimerization of the Cx43CT [247, 286]. NMR analysis revealed a number of resonance peaks that broadened beyond detection when ^{15}N -labeled Cx45CT was titrated with unlabeled Cx45CT suggesting a self-interaction [247]. Assignment of the Cx45CT resonances, identified the peaks that broadened beyond detection as residues A333–N361 [247]. Subsequently, residues A333–N361 were expressed alone and characterized by AUC sedimentation equilibrium and CD spectroscopy to 1) confirm these residues mediate Cx45CT dimerization and 2) determine if a structural component

was present [247]. AUC analysis of the A333-N361 peptide indicated it sedimented with a mass of approximately 13 kDa, suggesting a tetrameric complex and the calculated K_D for the dimer species was 74 pM confirming the identity of A333-N361 as the dimerization domain of the Cx45CT [247]. Structural analysis of both the full length Cx45CT and Cx45CT A333-N361 were done using CD spectroscopy. For the full length Cx45CT the spectra revealed, similar to several other Cxs, a predominance of disorder, however, a small contribution of helical character was also detected [247]. Interestingly, the CD spectra of Cx45CT A333-N361 suggested the peptide was nearly entirely helical in structure, indicating it was the region contributing the helical character to full length Cx45CT [247]. The study also suggested that the Cx45CT dimerization was mediated by hydrophobic contacts between the two helices [247]. Several lines of evidence supported this: first molecular modeling of the energy conformers predicted the greatest number of intermolecular contacts to be between key hydrophobic residues along one of the α -helical faces [247]; second, a large buffer screen was conducted to test buffer conditions that would either disrupt hydrophobic or electrostatic interactions, and only buffer conditions that disrupted hydrophobic interactions also inhibited dimerization [247]. Confirming the hydrophobic nature of the interaction, replacement of the predicted key hydrophobic residues with charged residues resulted in a Cx45CT mutant that was dimerization incompetent [247].

In addition to homodimerization between CxCT domains, the propensity to form heteromeric channels suggests an opportunity for heterodimerization between CT domains of different Cxs. Indeed, these interactions have been described for Cx40CT-Cx43CT as well as for Cx43CT-Cx45CT [231, 247]. Although these interactions have been detected *in vitro*, whether or not they occur in the context of a GJ as well as their functional significance remain to be determined. Furthermore, recent unpublished work in our laboratory has suggested the detected interaction between the Cx45CT and Cx43CT was the result of pH differences between samples, and not likely a true representation of heterodimerization. However, this does not preclude the possibility the interaction occurs in the context of a GJ and will require further investigation.

3. Post-Translational Regulation of Connexins

Like many proteins, GJ proteins are regulated post-translationally by a number of detected modifications. Those described in the literature to date include phosphorylation, acetylation, hydroxylation, γ -carboxylation, palmitoylation, ubiquitination, SUMOylation, and nitrosylation. The effects of the PTMs are diverse and complex, and often specific to not only the modification but also the Cx family member. In this section, currently known PTMs of Cx proteins and their functional impacts are reviewed.

3.1 Connexin Phosphorylation

The most common and well-studied PTM of Cx proteins is phosphorylation. To date phosphorylation has been detected on the majority of the Cx family members including Cxs 26, 32, 36, 37, 43, 45, 46, 50, and 56 (reviewed in [288]). The Cx domain most commonly reported to be modified by phosphorylation has been the CT domain; however, for Cx36 and Cx56 CL phosphorylation has been detected, and Cx26 expressed in HeLa cells NT phosphorylation was also detected [274, 283, 289, 290]. Notably, Cx26NT phosphorylation has not yet been detected from endogenous expression systems [182, 274, 289]. The lack of detectable phosphorylation of Cx26 and the short nature of its CT domain has been suggested as evidence that phosphorylation of Cxs is not essential for channel formation (reviewed in [291]). Therefore, it is suggested that phosphorylation of Cxs serves to modify Cx function, either by enhancing or impairing some aspect of Cx regulation. Indeed, phosphorylation of Cx proteins has been linked to the regulation of virtually every stage of the Cx life cycle, as well as altering channel properties such as selectivity or conductance states (reviewed in [288, 292]).

3.1.1 Introduction to Connexin Phosphorylation

Landmark studies identifying Cxs as phosphoproteins were carried out in the 1980's and have laid the foundation for countless studies [293, 294]. Since those early studies, many Cx phosphorylation sites have been identified and characterized (e.g., 23 sites for Cx43 alone (reviewed in [288, 295]). A predominance of identified phosphorylation sites for Cxs are Ser/Thr residues. Congruent with this observation many Ser/Thr kinases have been identified that

phosphorylate Cx proteins (see Section 3.1.3). In addition to Ser/Thr residues phosphorylation of Tyr residues has also been detected for Cx proteins (reviewed in [288]). Although, a number of phosphorylated Tyr residues have been identified for Cxs, the number of kinases identified is rather low (reviewed in [288]). To date the only confirmed Tyr kinases that phosphorylate Cxs are Src, Fps, and epidermal growth factor receptor (EGFR) [296-298]. In the following subsections, we will review the methods that have been used to study phosphorylation of Cxs, the functional impacts of phosphorylation and identified kinases, the relationship of Src and Cx43, the significance of phosphorylation sites that overlap binding motifs, and finally phosphorylation of other Cx45.

3.1.2 Methods for Studying Connexin Phosphorylation

Early studies investigating phosphorylation of Cxs relied on the use of radiolabeled [³²P] orthophosphate to label proteins. Since the standard 20 amino acids do not contain phosphorus atoms, any protein labeled with [³²P] orthophosphate, consequently must be phosphorylated. A drawback to this approach for identifying phosphoproteins is the requirement for highly specific (preferentially monoclonal) antibodies that were competent for immunoprecipitation (IP). Successful IP of Cx proteins from [³²P] labeled cells can then be resolved by SDS-PAGE and detected by autoradiography [299]. While this method is useful for identifying phosphoproteins, it does not identify the number of phosphorylated residues nor their identity (type [pSer vs. pThr vs. pTyr] or specific residue). A similar approach has been used to approximate the number of phosphorylated residues and detect changes in phosphorylation of a Cx protein between basal conditions and some stimulus yielding a “phosphorylation fingerprint” for the condition, called phosphopeptide analysis. The major difference between this approach and the previous is use of tryptic digests of the [³²P] labeled proteins captured by IP, followed by 2D electrophoresis on thin layer cellulose [299]. A caveat of this method, is the potential for partial digests, and thus interpretation of the data should be conservative [299]. Finally, the classical method for determining the identity (pSer vs. pThr vs. pTyr) and the relative percentages of phosphorylated residues is phosphoamino analysis and follows a similar scheme as phosphopeptide analysis [299]. The main difference in these two techniques is the method of fragmentation and size of fragments, for phosphopeptide analysis tryptic digests are used to produce peptides of variable size, while for

phosphoamino analysis acid hydrolysis is utilized to generate free amino acids [299]. Following acid hydrolysis, the sample is resolved by 2D electrophoresis, and detected by autoradiography. Another difference between the phosphopeptide analysis and phosphoamino analysis are the conditions used in the 2D electrophoresis [299]. Major drawbacks to all of the classical methods of detecting Cx phosphorylation are the need for large amounts of starting material and the inability to identify residue specific phosphorylation and then associate that site with a specific functional outcome. Initial methods to identify site specific phosphorylation of Cxs were site-directed mutagenesis and Edman degradation (e.g., Cx43 pS368 and pS255/279/282) [300-302]. A drawback to Edman degradation is the limitation of “read length”. One benefit of the classical methods of detecting phosphorylation is the assays are amenable to using recombinant CxCT domains that are *in vitro* phosphorylated to ensure enough starting material is available. This has also reduced the need for excessive amounts of radioactive waste.

Some Cx proteins show patterns of banding consistent with slower electrophoretic mobility that collapse (or disappear) upon phosphatase treatment [291]. Multiple migratory bands have been observed for Cx32, Cx40, Cx43, Cx45, Cx46, and Cx50 [248, 303-307]. For Cx32, this consisted of a doublet of bands that were reactive to both general pTyr and pSer antibodies that collapsed into a single band of immunoreactivity only to antibodies against Cx32 [248]. Cx40 and Cx45 were similarly observed as a doublet when extracted from atrial tissue and HeLa cells, respectively [304, 306]. Cx50 was also shown to migrate as a doublet, with a phosphatase sensitive slower migrating band extracted from mouse or mink seminiferous tubules [305]. A second study which used *in vitro* phosphorylation of GST-Cx50CT by PKA similarly observed the appearance of a slower migrating band after incubation with PKA, however, activation of PKA in cells did not result in the appearance of a second slower migrating band [307]. The study by Pelletier et al. also showed Cx46 was detectable as a pair of migratory bands, however, upon phosphatase treatment both bands decreased in intensity [305]. The authors speculated this was an indicator that Cx46, when non-phosphorylated, was rapidly degraded although they did not explore this further [305]. Unlike the previous examples, Cx43 resolves into several electrophoretic bands ranging in number from three to five depending on the study and conditions of phosphorylation, however three are most often

observed (reviewed in ([308, 309]). These bands are referred to as the P0 (slow migrating; ~42kDa), P1 (slow migrating; ~44kDa), and P2 (slower migrating; ~46kDa) bands [310]. Notably, Musil and Goodenough demonstrated the P2 form was present in communication competent normal rat kidney (NRK) cells, primarily in a detergent insoluble fraction corresponding to GJ plaques [144]. Furthermore, in two communication deficient cell lines (S180 and L929) neither insoluble Cx43 nor the P2 isoform were detected [144]. This study was the first to connect a potential functional role to one of the Cx43 migratory forms. Subsequently, work from our group and others focused on determining the identities of the Cx43 contained within each migratory band [311, 312]. The work of Cooper et al. demonstrated that phosphorylation of Cx43 by Casein kinase 1 (CK1) corresponds to the P2 isoform and requires residues S325/328/330 [311]. Grosely et al. used a biophysical *in vitro* approach with phosphomimetic mutants of several known kinase phosphorylation sites of the Cx43CT [312]. Confirming the work of Cooper et al., the soluble and TM-tethered CK1 phosphomimetic (S325,328,330D) Cx43CT mutants both resulted in slowed electrophoretic mobility similar to what was observed for the P2 isoform [311, 312]. Phosphomimetic mutants corresponding to PKA, PKC, Mitogen activated protein kinase (MAPK), Src, and cyclin-dependent kinase 1 (CDK1, also cdc2) phosphorylated Cx43CT were also analyzed and only PKA and MAPK were found to result in the P1 slower migrating form [312]. Importantly, single substitution of only one of the residues targeted (regardless of which) for kinases that phosphorylate multiple sites, failed to induce an electrophoretic mobility shift [312]. The slower migration of phosphorylated proteins compared to their non-phosphorylated counterparts has been attributed to disruption of the sodium dodecyl sulfate (SDS) to protein binding ratio from the negatively charged phosphate as well as structural changes (kinks) induced by phosphorylation sites adjacent to proline residues [313, 314].

To begin to unravel the functional effects of phosphorylation, site specific methods of identification are essential. Two modern methods have begun to help discern the effects of site specific phosphorylation of Cxs: MS and the development of quality phosphorylation specific antibodies. The current gold standard for the identification of site specific phosphorylation of proteins is MS. The benefits of which are the ability to reliably detect quantities of phosphoprotein

in the femtomole range, as well as the lack of need for radiolabeled samples [315]. Furthermore, MS samples can be processed and analyzed rapidly with relatively low cost. Studies using MS to pinpoint the locations of site specific phosphorylations have relied on instruments capable of tandem MS/MS (reviewed in [316]). Although this has been relatively successful, several factors complicate analysis. These are the relative abundance of phosphorylated protein compared to the non-phosphorylated form, phosphopeptides generally produce lower signal than the non-phosphorylated peptides, observed MS/MS properties of phosphopeptides generated by collision induced decay can be difficult to analyze (reviewed in [316]). As a result, enrichment of the phosphospecies is usually to the advantage of the investigator. Several recent technological and chemical advancements have been aimed at doing just this. The simplest method of enrichment has proven to be IP of phosphopeptides using general pTyr, pSer, or pThr antibodies [317]. While a number of good antibodies exist for the enrichment of pTyr containing peptides, quality IP competent pSer and pThr antibodies are lacking [317]. A more reliable form of enrichment commonly used is immobilized metal affinity chromatography (IMAC) [318]. In IMAC, a solid phase utilizing various immobilized metal ions separates proteins to variable degree based on affinity for the metal ions, a classical example being the use of Ni^{2+} to bind His-Tag containing proteins [318, 319]. Specifically, phosphopeptides have noted affinity for Fe^{3+} , and thus columns with chelated Fe^{3+} are most commonly used for enrichment of phosphopeptides [318]. Notably, acidic residues have also been noted to bind to Fe^{3+} leading to some non-phosphorylated background, however, this can be overcome with the conversion of the carboxylic acid moieties to their corresponding methyl esters (reviewed in [316]). In addition to column based enrichment, chemical alteration of the phosphate group to stable thiol by β -elimination and Michael addition allows for the capture of the thiol by column chromatography (reviewed in [316]). A final method of enrichment follows a similar workflow, where, after β -elimination, the resulting residue is converted to an aminoethylcysteine that can be recognized by Lys targeting proteases such as trypsin (reviewed in [316]). The latter method improves analysis of the peptides because it places the phosphorylated residue at the CT, creating a unique y_1 ion (reviewed in [316]). Technological advances in instrumentation such as the employment of matrix-assisted laser desorption ionization time-of-flight (MALDI-TOF) have

improved the detection limit of phosphopeptides and helped to simplify analysis and offer a quantitative method of detecting phosphorylation [320]. The high sensitivity and overall reliability of the technique have yielded dividends in the identification of specific phosphoresidues of Cxs (reviewed in [288, 316]). Indeed, a number of studies on Cx proteins have successfully used MS to pinpoint site specific phosphorylations from both *in vitro* and *in vivo* samples [274, 321-323].

In addition to MS, the development and use of phosphospecific antibodies has been crucial in the identification of site specific functions of phosphorylation (reviewed in [308, 309]). A number of studies since the mid-2000s have described the development of phosphospecific Cx antibodies and used them to characterize site specific functions both *in vitro* and *in vivo* [312, 324, 325]. Use of phosphospecific Cx43 antibodies have helped reveal (partially) the identity of the multiple electrophoretic bands, specifically phosphorylation of residues S325/328/330 (understood to be phosphorylated by CK1) contributes to the P2 form [311, 324]. Although the use of phosphospecific antibodies has helped to define the source of the multiple electrophoretic bands observed for Cx43, the picture is not as clear as one would expect. Tyr phosphorylation of Cx43 (pY265 and pY247), for example, was observed in the P0, P1, and P2 bands of Cx43, suggesting the nature of the altered mobility by phosphorylation is complex [325]. A current drawback to the use of phosphospecific antibodies is the lack of commercial availability for family members other than Cx43. Although, labs have developed phosphospecific antibodies to other family members (e.g., Cx37, Burt laboratory unpublished data) the efficacy and applications of use have yet to be determined. Important to the studies contained herein, no phosphospecific Cx45 antibodies have been developed to date.

3.1.3 Serine/Threonine Phosphorylation

Phosphorylation of Cx proteins is an important regulatory feature. Currently, the Cx protein that is most well characterized in terms of the regulation by phosphorylation is Cx43, although phosphorylation of other family members is beginning to be unraveled (reviewed in [288, 308, 309]). As mentioned in the introduction for this section to date Cx31, Cx32, Cx36, Cx37, Cx40, Cx43, Cx45, Cx46, Cx50, and Cx56 have all been demonstrated to be phosphoproteins, through direct

[³²P] incorporation, MS, or phosphatase sensitive electrophoretic mobility shifts (reviewed in [288, 309]). However, since Cx43 is the best characterized it will be the primary focus of this section.

The primary sequence of Cx43 contains a total of 39 residues that can be phosphorylated (intracellular, 23 Ser/7 Thr/9 Tyr). Of those 39 sites, at least 22 of the residues have been detected as phosphorylated by one or another detection method, including 19 Ser residues, Thr residues, and 3 Tyr residues [295, 308, 326-328]. Although, Thr phosphorylation of several residues has been detected in a human, rat, and mouse Cx43, the studies were not focused on Cx43 specifically, utilized shotgun approach MS, and the functional effects were not explored [329-336]. Therefore, Thr phosphorylation will not be discussed in further detail, and the importance of Tyr phosphorylation will be discussed in Section 3.1.4.

Ser phosphorylation of Cx43 has been well described with respect to the phosphorylated residues, the functional effect of phosphorylation, and in many cases the kinase for the site(s) has been identified (reviewed in [288, 309]). Functional outcomes of Ser phosphorylation ranges from channel forward trafficking, channel opening and closure, and priming for internalization; ultimately leading to changes in cell-cell coupling [288, 308, 309]. A current list of Ser phosphorylation sites and their functional effects on GJIC, and the kinase (if known) are summarized in Table 1. Generally speaking, early phosphorylation by kinases such as PKA, Protein Kinase B (PKB/Akt), and CK1 are associated with forward trafficking, GJ assembly, and channel opening [153, 311, 337, 338]. While mid- and late-stage phosphorylation by kinases including MAPK, PKC, Akt, Ca²⁺/Calmodulin-dependent kinase II (CaMKII), and CDK1 promote GJ channel closure and prime Cx43 for internalization [153, 288, 301, 323, 339, 340]. A study by Laird et al. detected phosphorylation on newly synthesized Cx43 when it was blocked in the ERGIC by BFA, however the specific site and kinase involved were not identified [148]. The authors did note that a number of casein proteins are phosphorylated in the Golgi, which may suggest CK1 as the potential kinase involved [148]. Indeed, work from Cooper and Lampe, characterized CK1 phosphorylation of Cx43 and demonstrated phosphorylation of three key Ser residues (S325/328/330) regulated GJ assembly and were associated with fully open channels [311]. Two other Ser residues that promote forward trafficking of Cx43 are S373 and S364/365, phosphorylated by Akt and PKA, respectively [157, 160, 341,

342]. Specifically, in the perimembrane region an interaction of Cx43 with Ezrin promotes the phosphorylation of Cx43 S365 and S364 (and S369) by PKA, and likely primes Cx43 to interact with ZO-1 [343]. The interaction with ZO-1 is thought to hold Cx43 at the perinexus of the GJ where it can be quickly incorporated into the GJ proper when needed [166]. Interestingly, phosphorylation of S365 and S369 does not affect the binding of either Ezrin or ZO-1 to Cx43 [160, 343]. Importantly, phosphorylation of S365 is reported as a “gate keeper” site, when phosphorylated it maintains channels in the open state by preventing PKC phosphorylation of S368 [344]. Capture of Cx43 containing vesicles at the plasma membrane has been reported to be facilitated by 14-3-3 [161]. Notably, phosphorylation of Cx43 S373 by Akt modulates the affinity of 14-3-3 and ZO-1 for Cx43. Specifically, it promotes dissociation of ZO-1 and association of 14-3-3, which likely coordinates incorporation into the GJ proper [158, 159, 164]. Once incorporated into the GJ, several protein interactions serve to stabilize GJs, these will be covered in detail in Section 3.1.4 focusing on Tyr phosphorylation. Finally, another set of Ser phosphorylation events regulate the closure and priming for internalization of Cx43.

Priming of Cx43 GJ junctions for internalization begins with activation of Src kinase (will be addressed in Section 3.1.4.1) and downstream effectors [153]. Mid stage activation of MAPK (downstream of Src) leads to increasing phosphorylation of S255/262/279/282 [292, 309, 312, 345-348]. Phosphorylation of S279/282 results in partial channel closure and the recruitment of Nedd4, the E3 ubiquitin ligase for Cx43, which ultimately leads to recruitment of the clathrin machinery [203, 349, 350]. Around the same time, loss of phosphorylation at S365 allows PKC access to S368, and phosphorylation of S368 leads to subconductance states of Cx43 and contributes to channel closure [344, 351]. From a structural standpoint, the study by Solan et al. suggested that phosphorylation of S365 by PKA, induced a structural change in the Cx43CT that restricted the access of PKC to the S368 site using a S365D phosphomimetic [344]. Complete channel closure requires S262 phosphorylation by MAPK and likely occurs simultaneously to PKC phosphorylation of S368 [153]. In one study, phosphorylation of Cx43 S255/262/279/282 were observed to occur at the same time as S368 phosphorylation when cells were treated with vascular endothelial growth

Ser Phosphorylation of Cx43		
Kinase	Effect on GJIC	Residue(s) Phosphorylated
PKA	Promote (forward trafficking)	S364/365/369/373
PKB (AKT)	Promote (forward trafficking)/Impair (Internalization)	S369/S373
PKC	Impair (Channel closure/sub-conductance)	S368
CaMKII	S306 Promote	S244/255/257/296/306/314/325/328/330/364/365/369/372/373
CK1	Promote	S325/328/330
CDK1	Impair (Closure/Internalization)	S255/262/279/282
MAPK	Impair (Closure/Internalization)	S255/262/279/282

Table 1. Kinases that phosphorylate Cx43 Ser residues and their effect on GJIC.
Table derived from Sorgen et al. (2018)[153].

factor (VEGF) [345]. Surprisingly, when cells were treated with a PKC inhibitor, decreased phosphorylation was observed for the MAPK sites (S255/262/279/282) and the PKC site (S368) suggesting that PKC phosphorylation may precede MAPK phosphorylation, at least in the context of VEGF stimulated cells [345]. A number of other studies reported similar results in other kinase programs [352-354]. Similar to forward trafficking and assembly, phosphorylation of Cx43 by Akt and an interaction with 14-3-3 also occurs during turnover to promote ubiquitination and internalization [164]. Two other kinases also phosphorylate Cx43 during the late stage of its life cycle, these are CDK1 and CaMKII [355-357]. CDK1 is likely a mediator of GJ turnover in response to cell cycle, and like MAPK phosphorylates S255/262 [355, 356]. The role of CaMKII in the regulation of Cx43 is unclear and the sites phosphorylated slightly ambiguous (15 Ser detected as phosphorylated) [357]. Prediction software only identifies four canonical CaMKII consensus sequences [153, 358]. Interestingly, experimental evidence of one CaMKII site (S306) has been shown, however, S306 phosphorylation correlated with increased cell-cell coupling [359].

To this point our description of Cx43 phosphorylation has been over simplified as an all-or-none type situation to focus on the functional outcome of a specific site. In cell and tissues, however, the situation is much more complex as both the kinases involved and the Cxs are regulated spatiotemporally [338, 349]. Furthermore, it is unlikely that single phosphorylation events exist in isolation, almost certainly the functional outcome is a combinatorial effect of several phosphorylation events [338, 349]. An important caveat to this notion is that until we are able to follow a single connexon and resolve the contributions of each Cx subunit we must derive our observations from a pool of Cx proteins that may be in different stages of the life cycle or accomplishing different tasks. In the study by Solan and Lampe, a chronological approach to detecting phosphorylation events was taken. Using the PKC activating phorbol ester phorbol myristate acetate (also 12-tetra-decanoyl phorbol acetate; PMA) to stimulate cells they observed phosphorylation by Akt (S373) ranging from 5-30 min, which peaked at 5 min following addition of PMA and then tapered off. Phosphorylation by MAPK (S279/282) was the next phosphorylation site to be detected, and began to rise after 10 min and peaked around 30 min, but was detectable out to 60 min. Phosphorylation of S368 (PKC) began to rise gradually at around 10 min and had

not begun to taper off by the 60 min. They also monitored phosphorylation of the well described Src site Y247 which followed a trend similar to S368 [338]. Since Akt phosphorylation has been attributed to increased GJ plaque size stemming from enhanced forward trafficking, it seems counterintuitive that phosphorylation of S373 has been observed as a precursor to GJ turnover via internalization of annular GJs, however, the authors suggest this may be the result of two mechanisms (that are not likely mutually exclusive). First the enhanced forward trafficking may deplete the cells of intracellular Cx43 pools, and second the rapidly increasing GJ size may result in lower energetic requirements of internalization of the annular GJ due to reduced need for membrane invagination [338]. Although treatment of cells with PMA offers a good model for observing the effects of a specific kinase program on Cx43 turnover, the question is: How reflective of a physiological process is it? As it turns out, treatment with PMA closely reflects the process of Cx43 GJ shutdown and turnover as occurs in wound healing [338, 360]. Notably, in studies investigating wound healing, Cx43 phosphorylation was observed to follow the same trends; S373 (Akt) at 5-30 min, S279/282 (MAPK) and S368 (PKC) at 15-60 min, and Y247 (Src) 30 min to 24 hr [158, 361-363].

Despite the breadth of knowledge we have obtained regarding the regulation of Cx43 by Ser phosphorylation, we have only begun to scratch the surface and a number of questions remain to be answered. First, and perhaps most important: How are other Cx family members regulated by Ser phosphorylation? It is tempting to use Cx43 as the model Cx due to its near ubiquitous expression and the degree to which it is characterized with respect to phosphorylation, however, as noted in the coming section on Cx45 phosphorylation a number of opposite effects have been observed between Cx43 and Cx45 (see Section 3.1.5 on Cx45 phosphorylation). Furthermore, several notable differences have been seen between Cx43 and other family members also, including Cx32 (see chapter 6), Cx37 [364], and Cx36 [290]. This leads to a second important question: When multiple Cxs are expressed and heteromeric channels are present what happens to the regulation of these channels by phosphorylation? An example is in the working myocytes of the ventricle when Cx45 is expressed in the failing heart [82]. Since both Cx43 and Cx45 are expressed in the same cell and exposed to the same kinase programs, what determinants maintain

Cx45 containing (homomeric and Cx45/Cx43 heteromeric) connexons at the ID? The latter question is one of the focuses of this dissertation.

3.1.4 Tyrosine Phosphorylation

Tyr phosphorylation of Cxs is of significant current interest. While Ser phosphorylation has been very well characterized for Cx43, Tyr phosphorylation has not. Interestingly, Tyr phosphorylation appears to have a more dominant effect on channel function than Ser [288, 309]. Only a small number of Tyr kinases have been identified that modulate Cx43 function (Src, EGFR, Tyk2, Ephrin receptors B1 and B4) [296-298, 323, 365, 366]. In this subsection, we will discuss the importance of Tyr phosphorylation to Cx43 highlighting the special case of Src kinase.

3.1.4.1 Role of Src with Cx43

One of the most notable (and well-described mechanistically) kinases that phosphorylates Cx43 is pp60-Src (Src) [293, 367, 368]. The Src family of kinases, are segregated into 3 subfamilies: SrcA (Src, Yes, Fyn, and Fgr), SrcB (Lck, Hck, Blk, and Lyn), and Frk in its own subfamily [369]. Structurally the Src family of kinases consist of a highly conserved NT region that contains residues which are modified by lipid moieties (myristoylation - all members; palmitoylation - subset) which confer plasma membrane anchoring [369]. Additionally, they all contain SH2, SH3, Tyr kinase, and C-terminal domains [370]. For the canonical member, c-Src, activation of the kinase requires phosphorylation of a key Tyr residue (Y416) and loss of autoinhibitory phosphorylation of another Tyr residue (Y527) [370]. Constitutively active Src (v-Src) lacks the autoinhibitory Y527 and thus does not require dephosphorylation for activity and consequently has been a tool frequently used to study the regulation of Cx43 by Src [325, 371]. To date phosphorylation of three key Tyr residues of Cx43 by Src have been identified (Y247, Y265, and Y313) [295, 325]. The mechanism by which Src phosphorylates Cx43 has been well described [72, 372-374]. The general scheme is once active, Src associates with the Cx43CT on its proline rich region (P274-P284, containing a PXXP motif), through the Src SH3 domain facilitating phosphorylation of Cx43 Y265, this in turn creates an SH2 binding site [372-374]. Subsequent binding of the Src SH2 domain to pY265 then allows for the phosphorylation of Y247 and Y313 [295, 373, 374]. Notably, a Cx43 mutant (Y265F) drastically reduced Y247 phosphorylation and failed to co-immunoprecipitate (co-

IP) v-Src when cotransfected into HEK293 cells, experimentally demonstrating the importance of Y265 phosphorylation to phosphorylation of Y247 [372]. Recent work from our laboratory confirmed these results using co-transfection of v-Src and Cx43 (Y265F) into HeLa cells, and additionally demonstrated a similar effect on Y313 phosphorylation [295].

Several studies investigating the relationship of Src and Cx43 (in numerous systems) have come to the same conclusion: Src phosphorylation of Cx43 disrupts GJIC by promoting GJ turnover [295, 325, 340, 375]. Recent studies have demonstrated indirect effects on GJIC mediated by activation of Src including increased phosphorylation by MAPK and PKC, as well as decreased phosphorylation by PKA [325, 373, 374]. When Lin et al. studied the effect of site specific mutations of Cx43 on GJIC in a Cx43-KO mouse cell line, they observed Cx43 mutants Y247F, Y265F, and Y247F/Y265F to be resistant to effects of v-Src co-transfection [373, 374]. Similarly, work from our laboratory noted resistance to v-Src mediated GJ disassembly in HeLa cells expressing mutants of Cx43 (Y247F, Y265F, Y313F, Y247F/Y265F, and Y247F/Y265F/Y313F), however contrary to the Lin study, only the triple mutant was completely resistant to the effects of Src [295, 373, 374]. Contrary to both of these studies, in oocytes, injection of v-Src was still capable of downregulating g_j for the Cx43 Y247F, Y265F, and Y247F/Y265F mutants [376]. Whether this reflects the effect of Src on activating the MAPK and PKC pathways, or the requirement of phosphorylation on Y313 was not determined. Based on the studies by Zheng et al. and Solan and Lampe it is likely a combination of these [295, 325].

The phosphorylation of Cx43 by Src has both direct and indirect effects on GJIC. The indirect effects as mentioned above, include the activation of parallel pathways (MAPK and PKC) that lead to GJ closure and turnover [328]. The direct effects of Src are mediated specifically by the phosphorylation of Y247, Y265, and Y313 (reviewed in [153]). Although, this will be covered in detail in the following section a brief synopsis is: Src phosphorylation sites (Y247, Y265, and Y313) occur in the binding motifs for proteins understood to stabilize GJ plaques (β -Tubulin and Developmentally regulated brain protein 1 (Drebrin)) [295, 377, 378]. Furthermore, Src directly titrates ZO-1 binding away from Cx43 [72, 286].

3.1.4.2 Phosphorylation in Binding Motifs

Regulation of Cx43 by phosphorylation can be the result of a number of mechanisms: the addition of the negative charge can alter secondary structure, influence pore size and selectivity, or alter the affinity of protein partners. In this section, our focus is on describing the role of phosphorylation in various binding motifs on the Cx43CT. A number of phosphorylation sites on the Cx43CT overlap with the binding motifs of protein partners and thus could be expected to (at least in part) influence the binding of the protein partner (see Figs. 1.2 and 1.3) [153]. This section will be broken up into two primary focuses where phosphorylation sites overlap binding motif: 1) interactions involved in forward trafficking and GJ assembly, and 2) interactions involved in disassembly, internalization, and turnover of GJs.

During forward trafficking phosphorylation influences a number of key interactions. First phosphorylation of S373 by Akt (or PKA) disrupts the binding of ZO-1 to the far CT of Cx43 and promotes the binding of 14-3-3 [158, 159, 341, 343]. In a nearby region of Cx43, the minimal binding motif for Ezrin (enhances PKA mediated phosphorylation of S373) was identified by using a peptide scanning approach (³⁶⁶RASSR³⁷⁰), notably this contains S368 (PKC) and S369 (PKA) and S365 (PKA) directly precedes the sequence [160, 309, 341]. Surprisingly, however, phosphorylation of these sites did not affect the binding of Ezrin to Cx43 [160]. Similarly to Ezrin, ZO-1 which binds over S364-I382 was not affected by the phosphorylation of either S364 or S369 [341]. Whether S368 affects the binding of ZO-1 remains to be determined.

In GJ disassembly and turnover, the influence of both Ser phosphorylation and Tyr phosphorylation has been noted [153]. A number of important interactions with cytoskeletal anchoring proteins (β -Tubulin, Drebrin, and ZO-1) are all required to stabilize GJ plaques [153]. A commonality between these interactions is the ability of all three to be modulated by the activity of Src. For β -Tubulin, which interacts with Cx43 in a region covering Y247, use of non- and phosphorylated (Y247) Cx43 peptide (K234–D259) via NMR demonstrated that phosphorylation of this site directly inhibited the binding of β -Tubulin to Cx43 [377]. Similarly, Drebrin which interacts with three regions of the Cx43CT (K264-T275; S282-T290; and R299-G321; over Y265 and Y313)

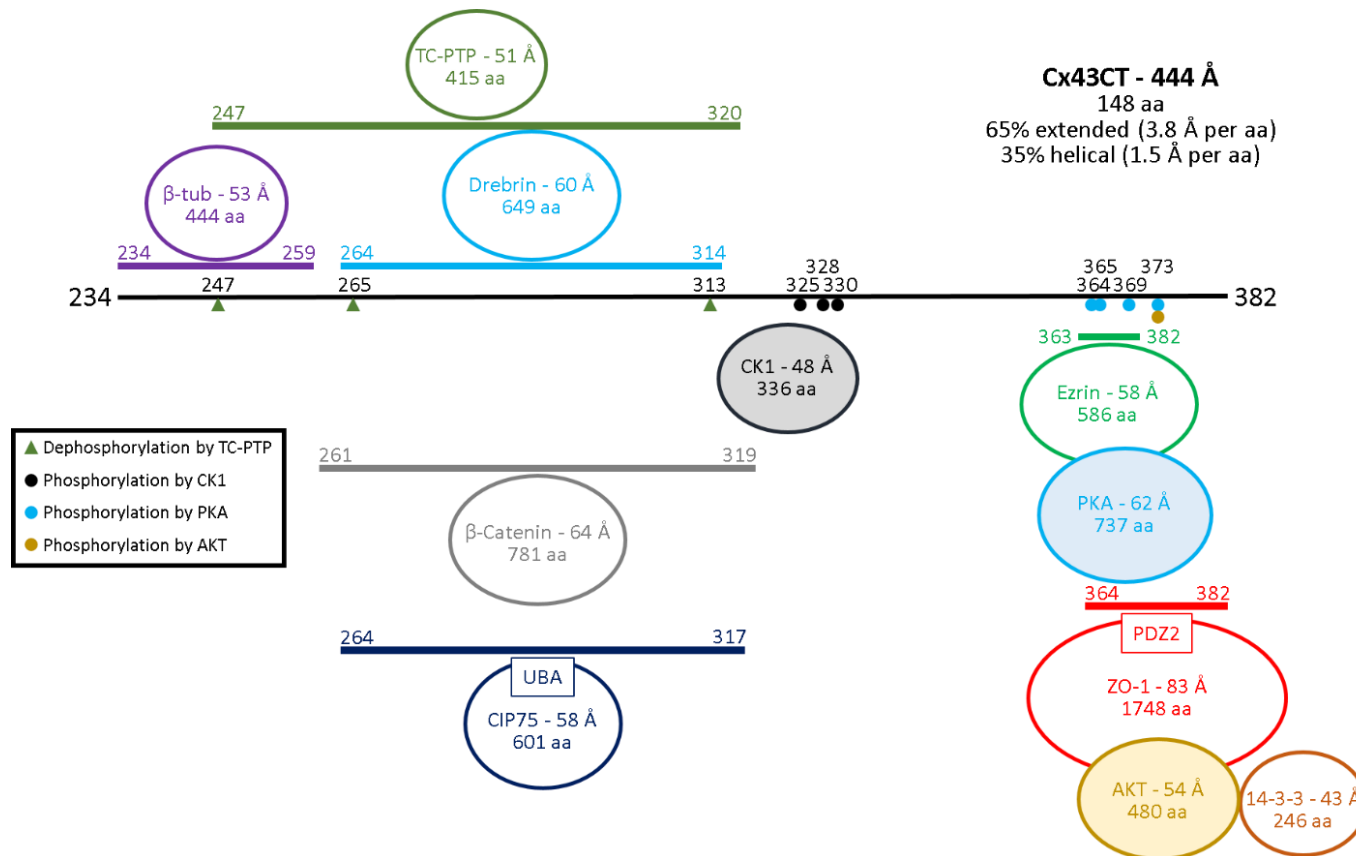


Figure 1.2. Protein partners that directly interact with the Cx43CT domain to promote intercellular communication.

The black line represents Cx43CT domain residues 234-382. Provided for each Cx43CT protein partner (circle) is its diameter (in Å) as estimated from their molecular weight, and number of amino acids (aa), and the Cx43CT residues affected as a result of the interaction (lines). If the protein partner is a kinase or phosphatase, the Cx43CT residues affected are labeled on the Cx43CT (circle or triangle). Abbreviations are as follows: β-tubulin (β-tub), T-cell protein Tyr phosphatase (TC-PTP), Connexin interacting protein 75 kDa (CIP75), Ubiquitin-associating domain (UBA), Casein kinase 1 (CK1), Protein kinase A (PKA), Zonula Occludens 1 (ZO-1), and Protein kinase B (AKT). Kinases have been highlighted (shaded circle). Reprinted from Sorgen et al., (2018).

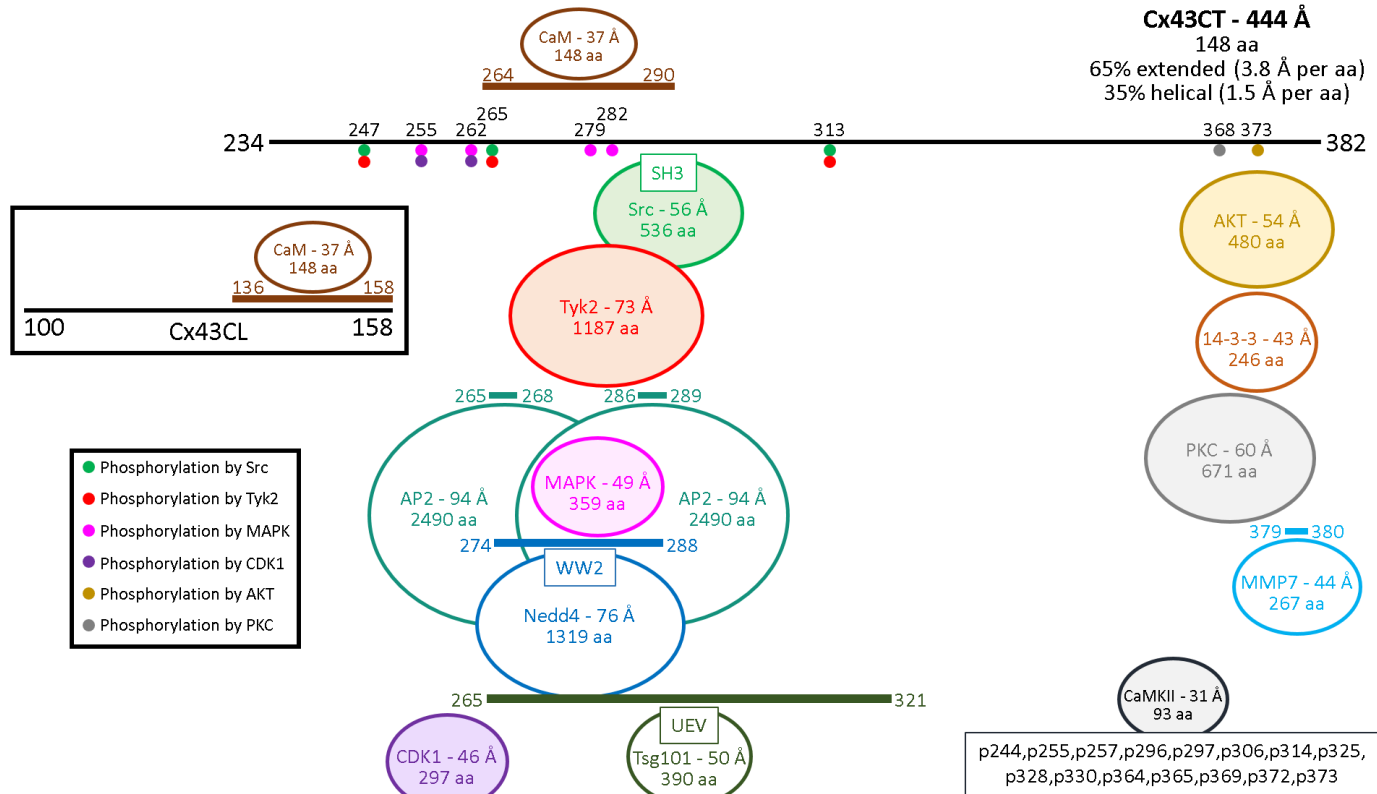


Figure 1.3. Protein partners that directly interact with the Cx43CT and Cx43CL domains to impede intercellular communication.

The black lines represent Cx43CT domain residues 234–382 and Cx43CL domain residues 100–158. Provided for each Cx43 CT and CL protein partner (circle) is its diameter (in Å) as estimated from their molecular weight, and number of amino acids (aa), and the Cx43CT residues affected as a result of the interaction (lines). If the protein partner is a kinase, the Cx43CT residues affected are labeled on the Cx43CT (circle). Abbreviations are as follows: Calmodulin (CaM), Src homology 3 domain (SH3), Tyr kinase 2 (Tyk2), Mitogen-activated protein kinase (MAPK), Neural precursor cell expressed developmentally down-regulated protein 4 (Nedd4), Cyclin-dependent kinase 1 (CDK1), Tumor susceptibility gene 101 protein (Tsg101), Ubiquitin E2 variant domain (UEV), Protein kinase B (AKT), Protein kinase C (PKC), matrix metalloproteinase-7 (MMP7), and Ca²⁺/calmodulin-dependent protein kinase II (CaMKII). Kinases have been highlighted (shaded circle). Reprinted from Sorgen et al., (2018)

is inhibited by phosphorylation of these residues [295, 378]. The initial study by Ambrosi et al. reported phosphorylation of Y265 (through the use of a Y265D mutant) was sufficient to disrupt Drebrin binding, however, recent work from our laboratory suggests complementary phosphorylation of Y313 is also required [295, 378]. Notably, when Drebrin is depleted in cells, Cx43 is internalized and degraded resulting in impaired cell-cell coupling [379]. In addition to phosphorylation by Src, MAPK phosphorylation of S279/S282 occurs in the binding motifs for both AP2 (of the clathrin complex) and the E3 ligase Nedd4 [153]. Nedd4 primarily interacts with Cx43 residues P283-Y286 (PPXY motif) via its WW2 domain and phosphorylation of the nearby MAPK sites (S279/S282) was demonstrated to increase the affinity of Nedd4 for the Cx43CT by approximately two-fold (K_D pS279/S282 = 585 μ M vs. npS279/S282 = 1064 μ M) in two independent studies [203, 204]. In addition to Nedd4, both AP2 and Tumor-susceptibility gene 101 (TSG101) interact with the Cx43CT nearby the PPXY motif and are important for the internalization of Cx43 [380, 381]. Interestingly, the Cx43 PPXY motif includes Y286, a site that has been identified to be phosphorylated by both MS and low through-put methods (Sorgen Laboratory, unpublished data; [382, 383]). Although a connection to the binding of protein partners was not investigated, the possibility exists that phosphorylation of this site may modulate the affinities of one or more protein partners. Another noted outcome of phosphorylation by MAPK is the priming for phosphorylation of S368 by PKC although an exact mechanism was not determined [325]. Speculatively, the phosphorylation of S279/S282 (or other sites by Src) may recruit a phosphatase which dephosphorylates S365, to allow PKC to phosphorylate S368. Finally, the association of AP2 with Cx43 is mediated by Tyr-based sorting motifs, of which Cx43 contains three (S1-²³⁰YVFF²³³, S2-²⁶⁵YAYF²⁶⁸, and S3-²⁸⁶YKLV²⁸⁹) [196, 381]. The proximity of S1 to the plasma membrane makes this site unfavorable for protein interactions. Notably, S2 overlaps the PPXY motif recognized by the WW2 domain of Nedd4, suggesting that both Nedd4 and AP2 likely cannot interact at the same time, suggesting that clathrin mediated endocytosis and ubiquitin mediated degradation may be alternate pathways for Cx43 internalization [196]. Whether S2 and S3 both function as AP2 binding sites remains unclear, however, a recent study demonstrated using the yeast two-hybrid system, that a Cx43CT mutant with a Y \rightarrow A mutation in S3 (Y286A) no longer functioned as bait for AP2

[354]. Similar to the speculative note above, it is likely that phosphorylation of either Cx43 Y265 or Y286 would inhibit the interaction with AP2, as Tyr phosphorylation of other proteins within Yxx ψ tyrosine-based sorting motifs inhibits the binding of AP2 [384]. Since Src phosphorylates Cx43 on Y265 it is likely, Src modulates the association of Cx43 and AP2.

3.1.5 Phosphorylation of Cx45

Despite how well phosphorylation of Cx43 is described, information regarding the phosphorylation of Cx45 is quite limited. Early phosphoamino analysis of Cx45 revealed phosphorylation of Ser, Thr, and Tyr residues, although the bulk of the phosphorylation was attributed to Ser residues [189]. It was suspected that Ser phosphorylation was contributed heavily by the enrichment of Ser residues in the far Cx45CT domain, experimentally this was supported by the observation that either deletion of the last 26 residues or mutation of the 9 most C-terminal Ser residues reduced the detectable phosphorylation by 90% [189]. The remaining phosphorylation, however, was independent of the presence of the 9 Ser residues in the last 26 residues of the CT [189]. This was supported by an earlier study, which identified several phosphorylation sites for chicken Cx45 present in both the CL and CT domains [385]. While mutation of the Ser residues did not impair GJ assembly or dye transfer by neurobiotin (NB) injection, deletion of the last 26 residues impaired both [189]. Furthermore, loss of the Ser residues correlated with decreased stability as indicated by pulse chase experiments measuring the half-life of Cx45 and mutants, however, the truncation mutant did not have significant decreases in its half-life [189]. Interestingly, mutation of certain Ser residues (e.g., Cx45 3Ser mutant; Cx45 S374A/S376A/S378P, Cx45 Ser381,382 mutant; Cx45 S381G/S382A) reduced the overall Ser phosphorylation to a greater degree than would be expected (3Ser - 33% remaining; S381,382 – 22% remaining), suggesting that these sites are prerequisites for other phosphorylation sites [189].

Another study focusing on the effect of Cx45 phosphorylation on the electric properties of the channel noted conductance was modulated by phosphorylation [306]. Activation of PKC by the addition of PMA resulted in an increase in the g_j of Cx45 HeLa cell pairs from 2.0 to 4.9 nS while the biologically inactive analogue 4 α -Phorbol 12,13-didecanoate (4 α -PDD) had no effect on g_j [306]. Conversely, activation of the cAMP dependent kinase, PKA, by addition of cAMP reduced g_j

from 27.3 nS to 18.2 nS, while addition of cGMP had no effect [306]. Similarly, treatment with pervanadate, which increases Tyr phosphorylation indirectly by inhibiting Tyr phosphatases, reduced g_j from 10.5 nS to 4.5 nS [306]. Interestingly, none of the treatments significantly altered single channel conductance states, suggesting that phosphorylation was impacting open probability [306]. Contrary to the results of the van Veen et al. study, a study by Martinez et al. reported treatment of HeLa cells expressing Cx45 by PMA reduced g_j to approximately 30% of control [86, 306]. However, in the same study the authors observed no change in the transfer of microinjected NB dye after PMA, suggesting activation of PKC alters the permselectivity of Cx45 channels, although this remains to be determined [86]. Finally, a recent study from our laboratory using NMR observed a direct interaction between the Cx45CT and the SH3 domain of c-Src, suggesting that c-Src may regulate Cx45, although this was not validated nor were the functional effects explored [247]. Investigating these aspects is the focus of Chapter Four.

3.2 Other Connexin Post-translational Modifications

In addition to phosphorylation, a number of other PTMs modulate Cx protein function through a number of mechanisms. These modifications include the addition of carbon moieties, ubiquitin, small ubiquitin modifier (SUMO) protein, and reactive nitrogen species. In the current section, these PTMs and their effect on Cx proteins are summarized.

3.2.1 Connexin Carbon-based Modifications

Primary PTMs involving carbon-based moieties include methylation, acetylation, and glycosylation among others. For Cxs, the primary relevant carbon based modifications are methylation, acetylation, and γ -carboxylation [326]. While methylation and acetylation of histones (and DNA methylation) play critical roles in the epigenetic control of gene expression they also can directly modify proteins besides histones [326].

Cxs have been shown to be modified post-translationally by methylation, acetylation, γ -carboxylation, and in one case palmitoylation [326]. Cx26 and Cx32 were among the first identified by MS to be modified post-translationally by carbon-based moieties [274, 289]. For Cx26 methylation was found on five sites. Of note one of the five methylation sites R75 when mutated (R75W or R75Q) results in non-syndromic deafness suggesting the methylation of this site may be

important to Cx26 function [289]. Other studies characterizing the R75W mutant have indicated that although it suffers no trafficking problems, the channels are non-functional and exert a dominant negative effect on wild type Cx26 and the co-expressed Cx30 [49, 52, 265, 386-388].

Acetylation of Cx26 was identified on six residues, two of which, K15 and K102, are deafness mutations (K15T, K102del). Each of these two mutations abolishes a positive charge from the lysine side chain. K15 is in the hinge region of the NT where it flips into the pore to aide in formation of the voltage gate [262, 389]. In Cx32 this residue is an Arg and a R15Q mutation—also abolishing positive charge—causes peripheral neuropathy, and although functional, the channels have altered voltage sensitivity [268, 390]. It is possible that a similar mechanism leads to the deafness seen in Cx26 K15T mutants. K102 in Cx26 is present in the CL which functions in pH gating and is a site for protein partner interactions [391, 392]. Similarly, to K15, the residue corresponding to Cx26 K102 in Cx32 is also charged (Glu in this case) that when mutated to Gly, abolishing the charge, results in changes in Cx32 pH sensitivity and mild neuropathy [391]. Colussi et al. described a functional role for Cx43 acetylation [393]. In the Duchenne muscular dystrophy mdx mouse model it was demonstrated that Cx43 was acetylated and improperly localized and mutants mimicking acetylation at the three predicted sites (K9, K234, and K264) phenocopied the improper localization seen in mdx mice [393].

Glutamate γ -carboxylation is a vitamin K dependent PTM carried out by γ -glutamyl carboxylase and was originally discovered in coagulation proteins and converts the sidechain of Glu residues to a dicarboxylic acid [394-397]. Importantly, γ -carboxylation creates a high affinity Ca^{2+} coordination site [396, 398]. To date, γ -carboxylation has been demonstrated on Cx26 and Cx32 by MS [274, 289]. Glutamate γ -carboxylation was identified on E42 and E47 in the EL1 of Cx26 as well as E114 of the CL [289]. Both of the EL1 Glu residues when mutated cause deafness and E114 is a site involved in the Ca^{2+} dependent loop gating mechanism which maintains undocked connexons in the closed state [387, 399-402]. Interestingly, E114 in the CL of Cx26 is conserved in Cx32 where it was also determined to be γ -carboxylated [274]. With the Ca^{2+} coordinating function of γ -carboxylglutamate it is possible that γ -carboxylation of E114 of Cx26 and E110 of Cx32 is involved in imparting Ca^{2+} sensitivity [274, 289]. Furthermore, with potential roles

in Ca²⁺ sensitivity it is likely that other Cx family members (e.g., Cx43) regulated by intracellular Ca²⁺ may also be γ -carboxylated.

3.2.2 Connexin Ubiquitination

Ubiquitin, a 76-residue polypeptide that is found ubiquitously, is a key PTM for protein degradation and turnover [326]. Ubiquitination is an enzymatic process that requires the transfer of ubiquitin in a cascade manner. Ubiquitin is initially bound to the ubiquitin activating enzyme (E1 family of ubiquitin ligases) then shuttled to a ubiquitin carrier (E2 family of ubiquitin ligases) which associates with a final ubiquitin ligase (E3 family of ubiquitin ligases). The E3 family of ubiquitin ligases provide substrate specificity and transfer the ubiquitin covalently via an isopeptide bond from G76 of the ubiquitin to Lys residues on the target protein [403]. Further ubiquitination of the target can occur via ubiquitin-to-ubiquitin linkages. These linkages can be on any Lys residue in the ubiquitin, however, K48 polyubiquitination chains destine the target for proteasomal degradation [403]. Cxs are substrates for ubiquitination [404].

Ubiquitination is an important quality control mechanism that couples with ERAD (with the assistance of CIP75). For Cx43 and Cx32 as much as 40% of newly synthesized protein undergoes ERAD, a feature that is correlated with levels of cellular stress. Interestingly, a mutation in Cx32 conferring CMTX results in nearly 100% of Cx32 being destined for ERAD. Cellular stress counteracts the ERAD, reducing the degree of polyubiquitination allowing improperly folded Cx32 to accumulate in the ER and oligomerizes with the remaining wild type Cx32 altering function and contributing to the disease phenotype [194, 405]. Once incorporated into the GJ plaque, Cxs are ubiquitinated by Nedd4, promoting internalization through endocytosis and trafficking to the lysosome for degradation [406].

3.2.3 Connexin SUMOylation

In addition to ubiquitin a small family of structurally and functional similar proteins known as SUMO proteins exist. In humans, the family is made up of three members (SUMO1-3) [407]. Despite structural similarity to ubiquitin little sequence conservation between the two exist. Like ubiquitin, SUMO proteins are conjugated to Lys residues in ψ KX(D/E) motifs, where ψ is a bulky hydrophobic residue (F, L, I, W) and X is any residue [408]. Similar to ubiquitin, the conjugation of

SUMO moieties to targets is achieved in a cascade manner [409]. First cleavage of a C-terminal peptide from SUMO results in the exposure of a di-glycine motif. SUMO then associates with the E1 (SUMO activating enzyme) and is passed to the E2 which can directly conjugate the SUMO to proteins with a canonical SUMO acceptor motif. For a subset of targets without the canonical motif SUMO can be shuttled to one of several E3 that, similar to ubiquitin, serve the role of target ligase [409]. Additionally, SUMO conjugates are removed, similar to the process of dephosphorylation and deubiquitination, by sentrin-specific proteases [409]. Differing from ubiquitination SUMOylation does not lead to target degradation, but is involved in various housekeeping processes such as regulation of transcription, stabilizing targets, stress response, and cell cycle progression [410].

Cx43 is the only Cx to date demonstrated to be SUMOylated [411]. However, the SUMOylated Lys residues detected, K144 and K237, are evolutionarily conserved among many mammalian species, and K144 is conserved among several of the Cx family members including Cx26 and Cx32 [411]. This suggests other Cx family members may be SUMOylated as well. SUMOylation of Cx43 is by any of the three human SUMO proteins. SUMO1 and SUMO2 were found on Cx43 only as mono-SUMOylation modifications, while SUMO3 was found as both mono- and poly-SUMOylation (both multisite mono-SUMOylation and chains of poly-SUMOylation). SUMOylation of Cx43 appears to regulate Cx43 expression levels, as when SUMO1 or SUMO2 were cotransfected into HeLa cells with Cx43, the Cx43 levels doubled. Additionally, co-expression of SUMO3 with Cx43 in HeLa cells resulted in increased GJIC, suggesting that SUMOylation plays a role in modifying Cx43 function as well [411]. Interestingly, the bulk of SUMOylated Cx43 was found in the Triton X-100 (TX-100) soluble fraction, suggesting it was not incorporated into functional plaques [411, 412]. However, it has been shown that plaques become soluble just prior to internalization, and inhibition of degradation pathways (both lysosomal and proteasomal) in myocytes resulted in both an increase in soluble Cx43 and communication [413, 414]. Additionally, K144R, K237R mutations in Cx43 reduced expression levels and plaque formation, suggesting that SUMOylation may play a vital role for proper GJ maintenance [411].

3.2.4 Connexin S-nitrosylation

S-Nitrosylation is a reversible covalent modification to Cys residues of proteins where nitric oxide (NO) is added to the thiol group [415, 416]. Nitrosylation is carried out and regulated by the activity of nitrosylases and denitrosylases [417]. Despite most targets of nitrosylation containing multiple accessible Cys residues, only a subset are detected as nitrosylated suggesting there is likely a recognition motif [417]. Nitrosylation of proteins alone can alter protein function, or alternatively can influence other PTMs on the target thereby indirectly affecting function [417]. Nitrosylation is an important regulator of vascular functions [418].

Studies providing clear evidence of a functional effect of nitrosylation on Cxs are limited. However, Cx43 was found to be constitutively nitrosylated in the myoendothelial junctions where endothelial cells are coupled to vascular smooth muscle cells [419]. Additionally, it was determined that when treated with phenylephrine, which activates denitrosylases, Cx43 GJ permeability to IP3 was reduced and correlated with a reduced degree of nitrosylation on Cx43 residue C271 [419]. Addition of NO donors resulted in decreased permeability to small molecules in vascular endothelial cells and reduced coupling of Cx37 channels [420, 421]. Nitrosylation also likely plays a regulatory role for Cx hemichannels. In astrocytes hypoxia and ischemia, which are associated with increased NO generation, also increased hemichannel permeability of the astrocytic GJ proteins, Cx43 and Cx46 [422]. This effect was reproduced by addition of S-nitrosoglutathione and reversed by subsequent treatment with reducing agents. Additionally, mutants of Cx46 abolishing the Cys residues in the CT domain prevented increased hemichannel permeability by NO donors [423].

4. Objective

Regulation of GJ function is achieved through alterations in phosphorylation and modulation of protein partner interactions within the CT domain of individual Cx proteins. Although a significant body of work exists characterizing these features for Cx43, little information exists about other Cx family members.

The objective of this dissertation is to identify the functional significance of protein interactions and phosphorylation of the Cx45CT domain. Chapter Two includes studies focused on determining how Cx45CT domain dimerization affects channel properties including expression,

localization, plaque formation, channel function (GJIC and hemichannel), basal phosphorylation, and interactions with protein partners. In Chapter Three, we use chimeric Cx45 proteins to further support our studies in Chapter Two, namely the importance of sequence specific regulatory roles of the Cx45CT dimerization domain (A333-N361). For Chapter Four, we change focus to delineate the regulation of Cx45 function by three kinases (PKC, Pyk2, and Src) that are active downstream of the Angiotensin II (AngII) type 1 receptor (AT1R) and identify key Cx45 residues phosphorylated by these kinases. Chapter Five, follows up on Chapter Four by investigating cross-regulation of Cx43 and Cx45 in both acute and chronic activation of the kinases from Chapter Four. Chapter Six contains a study on another Cx family member (Cx32) and its regulation by Ephrin receptor kinases and TC-PTP. Finally, Chapter Seven is a summary all of my projects and I propose future directions for the continuation of these studies.

The importance of GJs and intercellular communication to the homeostasis of humans makes Cxs attractive potential therapeutic targets. A clear understanding of the molecular determinants (protein partners, PTMs, etc.) that make each family member unique is essential for a solid foundation from which to develop novel therapeutic interventions.

CHAPTER TWO

Identifying the Physiological Role of Cx45 CT Domain Dimerization

The bulk of data presented in this Chapter is published Trease et al.

(2017), Journal of Molecular and Cellular Cardiology [424]

5. Introduction

GJs are plaques comprised of tens of 1,000s of passive membrane channels that directly adjoin the cytoplasm of neighboring cells. The channels allow for the direct exchange of ions, metabolites, and second messengers (cAMP, ATP, IP₃, etc.) [14]. The resulting electrical and metabolic coupling is essential to several physiological processes including: organization and synchronization of cells in organs and tissues, development, and impulse propagation in some excitable tissues [14]. Each channel is formed from the apposition of two connexon hemichannels, one contributed from each coupled cell. The connexon contributed from each cell is composed of six Cx proteins. Cx nomenclature is derived based on the molecular weight of the given family member (e.g., 45 kDa isoform is Cx45; Cx45), of which there are 21 human family members. Cxs family members share common structure from primary to tertiary. In terms of membrane topology, all Cx proteins contain four transmembrane domains, two extracellular loops (EL), a cytoplasmic loop (CL), and cytoplasmic N- and C-terminal domains (NT and CT respectively). Between Cx family members the transmembrane and extracellular domains retain the highest degree of conservation, including six critical Cys residues in the extracellular domains (three in each loop) that are essential for proper channel formation and subsequent docking. The intracellular domains, however, show sequence divergence, the greatest of which occurs in the CL and CT domains. The CT domain is of particular significance because it serves a regulatory role in all stages of the GJ life cycle including trafficking, localization and turnover. Furthermore, the CT domain has been shown to regulate intercellular communication via a number of PTMs and protein partner interactions [14, 425]. Additionally, the CT domain is an important regulator of channel properties such as junctional conductance, open probability, and voltage sensitivity [223, 426, 427]. The importance of the CT domain to Cx function lends itself to being a potentially useful therapeutic target that could differentiate between Cx family members [428-430].

Cxs have been found in nearly all cell types and organs, where their expression is often regulated spatiotemporally [32]. One example is in the heart, where the primary family members expressed are Cx43, Cx40, and Cx45. Cx43 is expressed throughout most of the working myocardium. While Cx45 expression in the adult is restricted to cells of the specialized conductance

and pace making system, however, this is altered compared to embryonic expression where Cx45 is found throughout the heart and loss of its expression is lethal [32, 66, 67]. In the specialized conductance system, channel properties of Cx45 make it ideal for propagating impulses from the atria to the ventricles, preventing reentrant arrhythmias [32, 66, 67]. In the ventricles of healthy adult hearts, GJs are made up primarily of Cx43, however, in failing hearts Cx45 is upregulated. Cx45 has also been implicated in coupling of Cx43-null ventricular myocytes. [83, 431]. This leads to altered coupling and slower conductance, contributing to increased incidence of ventricular tachy-arrhythmias [432]. The possibility also exists that in Cx43-KO mice, residual conduction may be mediated by ephaptic signaling from the NaV1.5 channel [433, 434]. Although normal intercellular current flow mediated by Cx45 is considered near non-existent in healthy hearts, in the pathological situation Cx45 mediated coupling becomes dominant due to overexpression in the ventricles. This is further confounded by the ability of Cx45 to form heteromeric channels with residual Cx43 thereby reducing current flow and voltage sensitivity, in ways that could still be managed with simple remodeling of Cx43 alone [82, 87, 432, 435-438]. Importantly, there is a lack of clear delineation of the mechanisms which make each cardiac Cx family member unique, including what makes Cx45 channel properties so different from Cx43 or Cx40, and how its upregulation makes it a potential substrate for arrhythmogenesis. As a result of this deficit and previous observations in the field we sought to better understand the possibility that interactions between the two CT domains of Cx45 molecules (i.e., dimerization) affect GJ regulation.

Work done previously in our laboratory identified a novel feature of the Cx45CT, high affinity dimerization ($K_D \sim 100$ nM). This dimerization was mediated by the presence of six key hydrophobic residues, positioned such that they create a hydrophobic face on the α -helical region (A333-N361) [247, 439]. Replacement of all six hydrophobic residues by Glu (L335E, L338E, I324E, L349E, I353E, Y356E; Cx45CT 6E; Fig. 2.18) disrupted dimerization yet maintained α -helical conformation [247]. Dimerization of cytosolic domains has previously been demonstrated to be critical regulators for ion channels (e.g., IP3 receptor [440]), and the importance of the Cx CT domain to proper channel function through modulation of protein partner interactions is well

established [153]. Basing our study on these notions, here we study the physiological role for dimerization of the Cx45CT and how it regulates Cx45 channel function and properties.

6. Materials and Methods

6.1 Cell Culture and Transient Transfections

MDCK cells (gift from Dr. Paul Lampe, Fred Hutchinson Cancer Center), HeLa cells (gift from Dr. Steve Caplan, University of Nebraska Medical Center) and HEK293T cells (gift from Dr. Myron Toews, University of Nebraska Medical Center) were cultured in Dulbecco's modified Eagle medium (Corning) at 37°C in a humidified 5% CO₂ atmosphere. Medium was supplemented with 10% fetal bovine serum (FBS, Seradigm), 2 mM L-glutamine (HyClone), 1% pen-strep (Corning), and 0.2% Normocin (Invivogen). The selective agent puromycin (Tocris) was used, when appropriate, at empirically determined concentrations. MDCK or HeLa cells at ~70% confluence were lipofected using the MDCK Avalanche (EZ Biosystems) reagent at 2.5:3.5 (plasmid:reagent) and Lipofectamine 2000/XtremeGene 9 (LifeTech/Roche) at (1:3/1:4 ratio) respectively, diluted in OptiMem under antibiotic free conditions. MDCK cells were analyzed 24-48 hr post-transfection while HeLa were analyzed 48 hr after transfection.

6.2 Stable Cell Line Generation

70% confluent MDCK, HeLa, and HEK293T cells were lipofected with indicated Sall linearized plasmid using either MDCK Avalanche (MDCK; 2.5:3.5) or Lipofectamine 2000 (HEK293T; 1:1) in OptiMem. Transfections were carried out under antibiotic free conditions, and cells were cultured 48-72 hr prior to addition of selection media. MDCK and HEK293T were selected with 5 µg/mL and 2 µg/mL puromycin respectively. Cells were either maintained as bulk (polyclonal) or clonally (monoclonal) selected cell lines. Monoclonal lines were obtained using Whatman paper cloning disks. Western blots and immunofluorescence were used to screen clones.

6.3 Antibodies and Immunostaining

All primary and secondary antibodies, detection reagents and concentration ranges utilized are summarized in Table 2. Cells seeded on glass coverslips were rinsed 2x with 1x phosphate buffered saline (PBS) and then fixed and permeabilized with either ice cold methanol at -20°C for 15 min or buffered formalin (1x PBS, 3.7% formaldehyde, 0.3% TX-100) at 37°C for 30 min. Coverslips were washed 3x 5 min in 1x PBS with gentle agitation and then blocked for 60-90 min

at 37°C (1x PBS containing 1% bovine serum albumin (BSA) and 0.3% TX-100). Coverslips were then incubated with the indicated primary antibodies diluted in blocking buffer for either 1 hr at RT or ON at 4°C. Coverslips were washed 3x with 1x PBS and then incubated with secondary antibody (if necessary) 1 hr at RT and then washed 1x for 5 min with 1x PBS containing 100 ng/mL DAPI and then 2x 5 min with 1x PBS. Coverslips were mounted with SlowFade (LifeTech) and sealed with clear nail polish and imaged. All images acquired on either Zeiss 710 or 800 LSM microscope.

6.4 Live Imaging

Live imaging dishes (*In Vitro* Scientific) were coated with bovine plasma fibronectin (Sigma) at 10 µg/mL. MDCK clones expressing Cx45 WT-eGFP or 6E-eGFP were seeded and imaged at confluence. Images were acquired over a 1 hr period at 1 min intervals on a Zeiss 710 LSM confocal microscope with definite focus module.

6.5 Cell Lysis for Direct Western blot

Cultured cells were rinsed 2x with 1x PBS and then incubated with protease inhibitor buffer (PIB; 1x PBS containing 1x Roche Complete + ethylenediaminetetraacetic acid (EDTA), 2 mM PMSF, 2 mM Pepstatin A) on ice for 20 min and then harvested with a cell scraper. Cell suspensions were pelleted at 1500 RPM for 5 min at 4°C. PIB was removed and cell pellet resuspended in an appropriate volume of lysis buffer (PIB + 1% TX-100, unless otherwise specified), mechanically lysed and incubated on ice for 30 min. Lysates were quantified by bicinchoninic acid assay (BCA; Pierce) and normalized with lysis buffer. 30 µg of total protein lysate (unless otherwise indicated) was resolved.

6.6 Co-IP and Western blot

Co-IP: MDCK cells stably expressing either Cx45 WT or 6E were seeded in either 10 or 15 cm plates and grown to confluence. Cells were rinsed 2x with 1x tris buffered saline (TBS) + 1mM EDTA and then scraped up an either 0.5 or 1.0 mL of IP lysis buffer (25 mM Tris-(hydroxymethyl)aminomethane (Tris), 150 mM sodium chloride (NaCl), 0.25% sodium deoxycholate, 0.05% SDS, 1% TX-100 plus protease and phosphatase inhibitors).

Antibodies and Reagents			
1° Antibody	Manufacturer	Applications	Concentration
Cx45 (MAB3101)	Millipore	WB/IF/IP	1:2000/1:200/1:500
Cx45 (ACC-207)	Alomone	WB/IP	1:2000/1:500
Cx43 (C6219)	Sigma	WB/IF	1:2000/1:200
Cx43 pS272/282	Fred Hutchinson	WB	1:500
Cx43 pS368	Cell Signaling	WB	1:1000
Cx43 pY247	Fred Hutchinson	WB	1:1000
Cx43 pY265	Fred Hutchinson	WB	1:1000
Cx43 pY313 (in-house)	LifeTein	WB	1:500
β-Tubulin (T8328)	Sigma	WB	1:500
Drebrin (AB10140)	Millipore	WB	1:3000
ZO-1 (61-7300)	Zymed	WB	1:500
Nedd4 (07-049)	Millipore	WB	1:3000
pTyr (pTyr-1000)	Cell Signaling	WB	1:1000
pSer (A4A)	Millipore	WB	1:500
β-Catenin (C2206)	Sigma	IF	1:200
E-cadherin (Alexa-488; 24E10)	Cell Signaling	IF	1:100
HA-Tag (Alexa-647; 6E2)	Cell Signaling	IF	1:50
Myc-Tag (Alexa-555; 9B11)	Cell Signaling	IF	1:100
2° Antibody	Manufacturer	Applications	Concentration
Goat α-mouse (Alexa-647)	Cell Signaling	IF	1:500
Goat α-rabbit (Alexa-555)	Cell Signaling	IF	1:500
Goat α-mouse-HRP	Millipore	WB	1:100,000
Goat α-rabbit-HRP	Alpha Diagnostics	WB	1:50,000
Veriblot	Abcam	WB	1:4,000
Goat α-rabbit light-chain HRP	Jackson Immuno	WB	1:300,000
Fluorescent Dye/Protein	Manufacturer	Applications	Concentration
Neurobiotin	Vector Labs	Fluorescence	2.0 mg/mL
Lucifer Yellow CH	LifeTech	Fluorescence	0.25 mg/mL
Texas Red Dextran (10,000 Da; fixable)	LifeTech	Fluorescence	1.0 mg/mL
Streptavidin (Alexa-647 or Alexa-488)	LifeTech/Jackson Immuno	Fluorescence	1:100 (1 mg/mL stock)

Table 2. Antibodies and reagents.

Cells were mechanically lysed and then incubated for 30 min at 4°C with rotation. Lysates were precleared with normal rabbit IgG (2 µg) bound protein G agarose for 1 hr at 4°C and then clarified by centrifugation. Clarified lysates were quantified by BCA (Pierce) and normalized. Input samples were reserved and either 2 or 5 mg of lysate was subjected to IP with either 2 or 3 µg of rabbit α-Cx45 (Alomone) ON at 4°C. Immune-protein complexes were captured by 2 hr 4°C incubation with protein G agarose (Pierce), washed 5x with IP wash buffer (IP lysis buffer excluding sodium deoxycholate) captured proteins were eluted using 35-50 µL 3x SDS sample buffer. Equal volumes of each sample were analyzed by Western blot and to avoid cross reactivity with the IP antibody a light chain specific secondary antibody (Jackson) or Veriblot (Abcam) were utilized for detection.

Western blot: Protein samples were resolved by SDS-PAGE with an appropriate gel concentration, transferred to PVDF (EMD Millipore), blocked either 2 hr at RT or ON at 4°C with either 5% non-fat milk/PBS + Tween 20 (PBST) or 5% BSA/TBS + Tween 20 (TBST) and incubated with indicated primary antibody in blocking buffer either 1 hr at RT or ON at 4°C. Blots were washed 3x for 10 min with either PBST or TBST, and then incubated for 1 hr at RT with secondary antibody. Membranes were then washed 4x 10 min each with either PBST or TBST and detected using Signal West Femto kit (Thermo) per manufacturer protocol and exposed to autoradiography film. Quantifications were done using NIH ImageJ software using a minimum of three independent replicates.

6.7 RT-PCR

MDCK clones expressing mCx45 WT and 6E were seeded and cultured to confluence. Cells were rinsed 2x with 1x PBS and lysed for RNA content using the GeneJet RNA Isolation kit (Thermo) per manufacturer protocol. Equivalent masses of RNA were reverse transcribed using the MuMV-RT kit (NEB) per manufacturer protocol with OligoDT priming. Equal volumes of each RT reaction were used as template for standard PCR reactions with primers to mCx45-WT/6E (5'-ACAGTAAAAGGAGGGAAGCTTGAT-3' and 5'-TGGCTTTGTTTTGCTTGTAGG-3') and GAPDH (5'-GTAGTGAAGCAGGCATCGGA-3' and 5'-GTCGAAGGTGGAAGAGTGGG-3') using Taq Green Master Mix (Thermo). Cycling was carried out as follows: Initial denaturation 95°C for 2 min, followed by 30 cycles of 95°C denaturation for 30 s, 54.5°C annealing for 30 s, and 72°C extension

for 30 s, followed by final extension of 5 min at 72°C. Equal samples volumes were analyzed by 2% Agarose/TAE electrophoresis spiked with ethidium bromide. No reverse transcriptase reactions were used to subtract genomic background. Quantification was done using NIH ImageJ software, normalizing samples to GAPDH loading control. Quantification was done using three independent replicates.

6.8 Cycloheximide Chase

MDCK clones expressing mCx45-WT or mCx45-6E were cultured to approximately 90% confluent. Cells were rinsed 2x with 1x PBS and the incubated with fresh medium containing 80 µg/mL cycloheximide (CHX; Cell Signaling) for the indicated time points. Following the desired incubation time the cell media was spiked with 10x Roche Complete + EDTA and the cells were harvested and pelleted at 1500 RPM for 5 min at 4°C. The supernatant was removed and the cells were lysed directly in 1x sample buffer supplemented to 1x PBS, with protease inhibitors and 50 units Benzonase. Equal volumes of sample were resolved by SDS-PAGE and analyzed by Western blot. Each time point was normalized to loading control and then to the starting time point.

6.9 Scrape Loading Dye Transfer Assay

Cells were scrape loaded as previously described [340]. Briefly, all buffers were pre-warmed to 37°C prior to beginning the experiment. Stable expressing MDCK clones or transiently transfected HeLa cells were seeded on bovine plasma fibronectin (Sigma; 10 µg/mL) coated 35 mm live imaging dishes (CellStar). MDCK cells were transfected with Cx43 siRNA with Lipofectamine RNAiMAX (LifeTech) according to manufacturer protocol and then cultured for 48 hr prior to scrape loading. After transfection cells were washed 1x with 1x PBS and then overlaid with dye tracer mix (1x PBS containing Lucifer yellow, NB, and Texas Red Dextran). Scrapes were introduced using a fine edged micro-scalpel and incubated at RT for 1 min. Tracer dye was gently washed away with 1x PBS and media was added and the cells returned to the incubator to culture for 5 min to allow dye to transfer. Following the dye transfer period the cells were washed with 1x PBS containing 1 mM CaCl₂ and 1 mM MgCl₂ to stop dye spread. Coverslips were then formalin fixed and stained as described above and imaged. 15 consecutive fields of view were acquired per replicate.

6.10 Triton X-100 Solubility Assays

Biochemical: The TX-100 solubility assay was modified from a method described previously [412]. Briefly, MDCK cells grown in 10-cm plates were washed with PBS and incubated in 1 mL PIB for 20 min at 4°C, harvested in the same buffer and gently pelleted. Supernatant was aspirated, and cell pellet resuspended in 1 mL of fresh PIB supplemented with 50 units of Benzonase and mechanically lysed. Lysates were quantified by BCA and normalized. A total of 450 µL of cell lysate was brought to 1% SDS with 10% SDS and reserved as total lysate. Another 450 µL was brought to 1% TX-100 with 10% TX-100 in 1x PBS and incubated at 4°C for 30 min with agitation. The TX-100 lysate was then separated into non-junctional (supernatant; soluble) and junctional (pellet; insoluble) fractions by ultracentrifugation at 100,000 xg for 1 hr at 4°C. The supernatant was carefully removed and retained as the soluble fraction. The pellet was solubilized in 500 µL of solubilization buffer (1x PBS, 8 M urea, 2.5% SDS, 0.1 M dithiothreitol (DTT), 1x Roche complete + EDTA, 2 mM PMSF, and 2 µM Pepstatin A). Volume normalized samples of total lysate (T), TX-100 soluble (S) and TX-100 insoluble (I) portions were analyzed by Western blot. Soluble and insoluble fractions were quantified as a function of total lysate. Quantification was done using NIH ImageJ software from three independent replicates. ***In situ* TX-100 extraction:** The *in situ* detergent extraction was previously described by [340]. Briefly, MDCK cells were seeded on glass coverslips (Neuvitro) and cultured to ~90% confluence. Coverslips were rinsed 2x with 1x PBS and then incubated for 30 min at 4°C with gentle agitation with either mock extraction buffer (1x PBS containing 1x Roche complete + EDTA, 2 mM PMSF, and 2 µM Pepstatin A) or extraction buffer (mock buffer + 1% TX-100). Following extraction, the cells were fixed, immunostained, and images acquired. Extractions were performed on three independent replicates to ensure reproducibility. Quantification of remaining immunostain was done by taking the DAPI normalized MFI of the Cx signal in extracted images as a percent of signal in the mock images using ImageJ.

6.11 siRNA Knock-down of Cx43

MDCK clones stably expressing Cx45 WT or 6E at approximately 60% confluent were lipofected with stealth siRNA designed against endogenous canine Cx43 using Lipofectamine RNAiMAX according to manufacturer protocol under antibiotic free conditions, cells were cultured

48 hr prior to any analysis. Complexes were generated in OptiMem. siRNA was designed using the Invitrogen design tool against the coding region (CDS) of accession number NM_001002951.3. siRNA duplex sequence: 5'-UAA CAC UCA ACA GCC UGG UUG UGA A-3' and 5'-UUC ACA ACC AGG CUG UUG AGU GUU A-3.'

6.12 Bimolecular Fluorescence Complementation

MDCK cells seeded on coverslips were transiently co-transfected with Lyn-HA-Cx45/6E-CT-mVenusN and Lyn-Myc-Cx45/6E-CT-mVenusC. Approximately 20 hr after transfection the cells were rinsed 2x with 1x PBS and ice-cold methanol fixed and immunostained as described below, and imaged. Plasma membrane measurements were made using the Zeiss profile measurement tool of at least 90 double-transfected cells for each condition at 630X and signal calculated as area under the curve. For ER/Golgi measurements images were exported to NIH ImageJ and ROIs were used to isolate the ER/Golgi and signal was measured as mean fluorescent intensity. Quantification of mVenus signal was normalized individually to both HA and Myc signal.

6.13 Blue-Native PAGE

Post nuclear triton soluble lysates were prepared as described for the TX-100 solubility assay. Samples were resolved on Blue-Native PAGE gels prepared freshly as described in [137, 441]. Gels were run on ice or in cold room with blue cathode buffer (0.01% Coomassie Blue (G250)) until dye front migrated approximately two-thirds through the gel. The cathode buffer was then exchanged for dye free cathode buffer and run to completion. Gel was incubated with 0.1% SDS containing semi-dry transfer buffer and then transferred to PVDF and blotted as described above.

6.14 Sucrose Density Gradient Fractionation

Gradient preparation: Stock sucrose solutions were prepared by dissolving the appropriate mass of sucrose in 1x PBS containing 0.1% TX-100 and 0.02% azide. Gradients were prepared segmented from stock solutions with greater sucrose concentrations on the bottom. A 200 μ L cushion of 25% sucrose was added to the bottom of a 4 mL polyallomar tube (Beckman) and snap frozen, then 850 μ L of each 20%, 15%, 10%, and 5% sucrose was layered on the previous layer snap freezing between layers. Gradients were stored at -20°C until use. On the day of use the

gradients were removed from -20°C and allowed to thaw at room temp for 30 min, and then tilted 30° from horizontal for 90 min to linearize the gradient by diffusion. **Oligomerization assay:** To determine the location of oligomerization we modified the protocol of Koval et al. [143]. Briefly, MDCK clones expressing either Cx45 WT or 6E were seeded in 10 cm plates and cultured to confluence and then treated for 4 hr with 10 µM Monensin A ((MonA); Sigma). After treatment cells were washed 2x with 1x PBS and then incubated on ice in protease inhibitor buffer PIB for 20 min. Cells were scraped up and pelleted at 1500 RPM for 5 min at 4°C. PIB was removed and cell pellet resuspended in 0.5mL lysis buffer (PIB + 1% TX-100 and 50 units Benzoylarginine hydrochloride) and mechanically lysed. Lysates were quantified by BCA and normalized. Normalized lysates were fractionated into soluble and insoluble fractions as described above. An aliquot of the supernatant was retained as input, and the remainder was overlaid on a 5-25% sucrose gradient, prepared as described above. Gradients were centrifuged at 148,000 x g for 16 hr at 4°C. 500 µL fractions were obtained by pipetting down from the top maintaining the pipette tip at the meniscus, and then vortexed. An aliquot of each fraction was resolved by SDS-PAGE and analyzed by Western blot. **Sucrose determination:** Remaining gradient fraction volumes were vortexed and allowed to warm to room temperature. 50 µL aliquots were analyzed by a Brix refractometer (Milwaukee Instruments, MA871) in triplicate and the mean of the three reads taken as °Brix. °Brix was then converted to sucrose concentration (% w/v) by a standard curve generated using stock solutions at 2.5, 5.0, 7.5, 10.0, 12.5, 15.0, 17.5, 20.0, 22.5, and 25.0% sucrose. The equation for the trend-line generated from the standard curve shown as equation 2:

$$1) y = °Brix$$

$$2) y = 0.7743x + 2.26$$

$$3) °Brix - 2.26 / .7743 = [sucrose]$$

6.15 Calmodulin Binding Assay

The LCK-GCaMP2 construct was shuttled from the pN1 vector purchased from AddGene (#24794) to the pD2529 mammalian expression vector by PCR and Gibson assembly. The A333-N361 region of Cx45 WT or 6E were QuikChanged to replace the M13 domain of myosin light chain kinase using megaprimers derived by PCR in the new LCK-GCaMP2 pD2529 vector, called WT-

and 6E-LCK-GCxaMP2 respectively. Newly developed vectors were sent for Sanger sequencing to ensure correct sequence, midi-prepped, and stably transfected into MDCK cells. Stable clones of parental LCK-GCaMP2, WT- and 6E-LCK-GCxaMP2 were chosen based on similar levels of protein expression. Clones were seeded in triplicate in live imaging dishes and cultured to confluence in phenol free DMEM. At confluence cells were rinsed 2x with 1x PBS and the medium was replenished. Images were acquired every 5 s using definite focus module on a Zeiss 800 LSM with 5% CO₂ infusion and 37°C incubation. After 3 min of baseline (36 images) image acquisition dishes were spiked with Ionomycin to a final concentration of 15 μM and images were acquired for an additional 5 min. Mean fluorescent intensity was taken for the total field of view for each image.

6.16 Hemichannel Dye Uptake Assay

To assess hemichannel activity we modified the protocol described by [442]. Briefly, all buffers were pre-warmed to 37°C prior to beginning the experiment. MDCK clones expressing either Cx45 WT or 6E were seeded on glass coverslips were cultured to approximately ~90% confluent. Some wells were pretreated with either 100 μM La³⁺ (Sigma) or freshly prepared 100 μM pervanadate or both for 15 min prior to Ca²⁺ washout and dye uptake. The presence of La³⁺ was maintained during dye uptake. Cells were rinsed 1x with HBSS + Ca²⁺/Mg²⁺ (LifeTech) and then 2x with HBSS – Ca²⁺/Mg²⁺ (LifeTech). Cells were then incubated at 37°C with HBSS – Ca²⁺/Mg²⁺ containing NB (0.1 mg/mL; Vector labs) for 10 min. Cells were then washed 2x with HBSS + Ca²⁺/Mg²⁺ to close hemichannels and GJs. Cells were formalin fixed and stained with streptavidin 647 conjugate (LifeTech) and imaged. Control cells were treated identically except all incubations were done in HBSS + Ca²⁺/Mg²⁺. Three independent replicates were used for quantification calculated by DAPI normalized mean fluorescent intensity in Zen Blue (2012) where 15 fields of view were acquired per replicate. Results presented as mean + s.e.m. of all replicates.

6.17 Statistical Analysis

All data were analyzed by using GraphPad Prism 5.0 and were presented as the mean + s.e.m. Statistical analysis performed in GraphPad Prism 5.0 was either one-way ANOVA with a Newman-Keuls post-hoc analysis or Student's T-Test (one or two-tailed as appropriate) where appropriate. P-values <0.05 were considered statistically significant.

7. Results

7.1 Cx45CT WT Dimerizes at the Plasma Membrane

Dimerization of the Cx45CT was initially identified by Kopanic *et al.* using a recombinantly expressed Cx45CT peptide *in vitro* [247]. We hypothesized that the salient features of the peptide (structure and oligomeric state) would be present in the context of the cytosol of the cell in proximity to the plasma membrane. To address this, we sought to determine if the CT domains expressed at the plasma membrane would in fact dimerize if expressed exogenously *in cyto*. We implemented a bimolecular fluorescence complementation (BiFC) approach to investigate this [443]. In this assay, the use of a fluorescent protein tag (mVenus) that has been expressed as separate N- and C-termini on the same protein (either Cx45CT WT or Cx45CT 6E) yields fluorescent signal when the protein of interest interacts with itself. Design of the BiFC constructs is illustrated in Fig. 2.1. In order to target the proteins to the plasma membrane, in the absence of the transmembrane domains, the first 16 residues of Lyn kinase domain were included on the N-terminus to mediate membrane anchoring via myristoylation and palmitoylation. To differentiate N- and C-terminal mVenus constructs as well as provide a reference signal to quantify against, we included HA- or Myc-tags, respectively. When expressed in MDCK cells mVenus signal fluorescent signal should be detected only if two Cx45CT domains interact, which places the mVenus fragments in close enough proximity to properly refold and result in fluorophore maturation. mVenus signal was detected for both the Cx45CT WT and 6E constructs, however, was restricted only to cells transfected with both HA- and Myc-tagged constructs (Fig. 2.2A; single transfections not shown). Using the profile measurement tool to isolate fluorescence signal present at the plasma membrane we quantified the area under the curve from 90 WT and 92 6E cells that had immunoreactivity to both HA- and Myc-tags (collected across three independent experiments). To quantify (and control for potential differences in expression and trafficking to the plasma membrane) the mVenus signal was normalized to the Myc-tag signal for each construct (Fig. 2.2B). For the Cx45CT WT construct, the plasma membrane signal observed was 2.46-fold greater ($P < 0.0001$) than that for Cx45CT 6E.

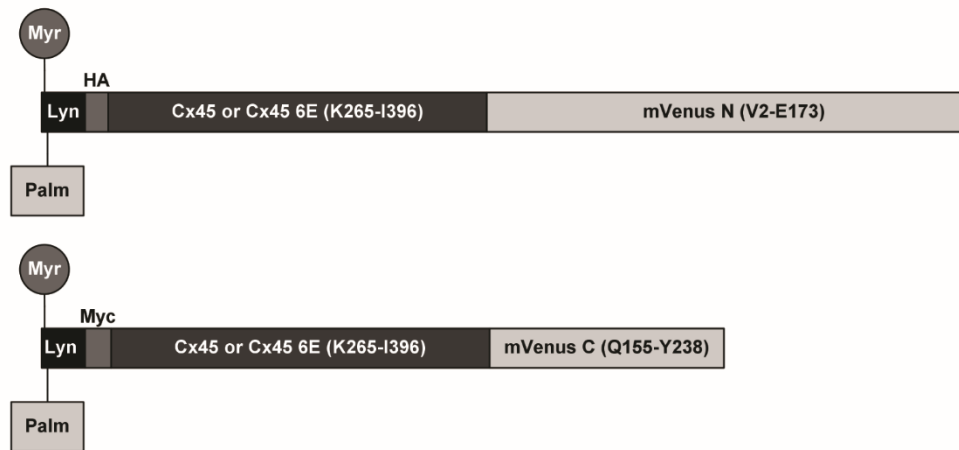


Figure 2.1. Schematic of Cx45CT BiFC constructs for *in cyto* dimerization assay.

The Cx45CT (WT or 6E) was c-terminally fused to the first 16 residues of Lyn kinase with either and HA- or Myc-tag as a linker. To the c-terminus of the Cx45CT for HA-tagged constructs the mVenus (V2-E173) were fused, similarly to the Myc-tagged constructs mVenus (Q155-Y238) was fused. Proximity of the two halves of the mVenus fragments results in refolding and measurable fluorescence. This figure is modified from Trease et al., (2017).

This data suggested that the CT domain of Cx45 was indeed dimerized when anchored to the plasma membrane, and furthermore indicated the mutations of the 6E were sufficient to inhibit dimerization. Our results are further supported by a similar trend observed when using the HA-tag to normalize the mVenus signal at the plasma membrane. Using the HA-tag we observed a 4.40-fold ($P < 0.0001$) increase in the mVenus signal of Cx45CT WT compared to that of the 6E. It is likely differences in antibody affinity for the HA and Myc tags lead to the larger difference seen with the HA-tag. Of note, significant mVenus signal was observed for both the Cx45CT WT and 6E present in the endoplasmic reticulum (ER)/Golgi apparatus. As a result, we quantified this region independently of the plasma membrane signal and determined it to be of similar albeit not identical levels (Fig. 2.2B). We believe the signal we observed in Cx45CT 6E expressing cells is the result of localized concentration, as refolding of the mVenus is dependent on proximity. Indeed, the degree of signal observed for both Cx45CT WT and 6E in the ER/Golgi supports this hypothesis. Further support of this hypothesis is a conflict in the quantification of the ER/Golgi mVenus using the HA-tag to normalize instead of the Myc-tag. Consequently, proximity leads to “background” mVenus signals that are not the result of *bona fide* dimerization. Despite this limitation, any reduction of the Myc normalized mVenus signal of Cx45CT 6E compared to Cx45CT WT indicates less dimerization and is therefore significant. We sought to test if this assay would work properly on full length Cx45 WT and 6E, however, we failed to observe a significant difference in the mVenus signal between the Cx45 WT and 6E constructs in this manner (data not shown). We speculate the since mVenus refolding is contingent upon proximity and thereby localized concentration, CT domains of adjacent Cxs in a connexon would be close enough together to allow refolding to occur independent of dimerization interactions. Indeed, when taken together with the ER/Golgi mVenus signal this hypothesis is supported, as there is an accumulation of protein in close proximity in the ER/Golgi similar to that the condition in a connexon.

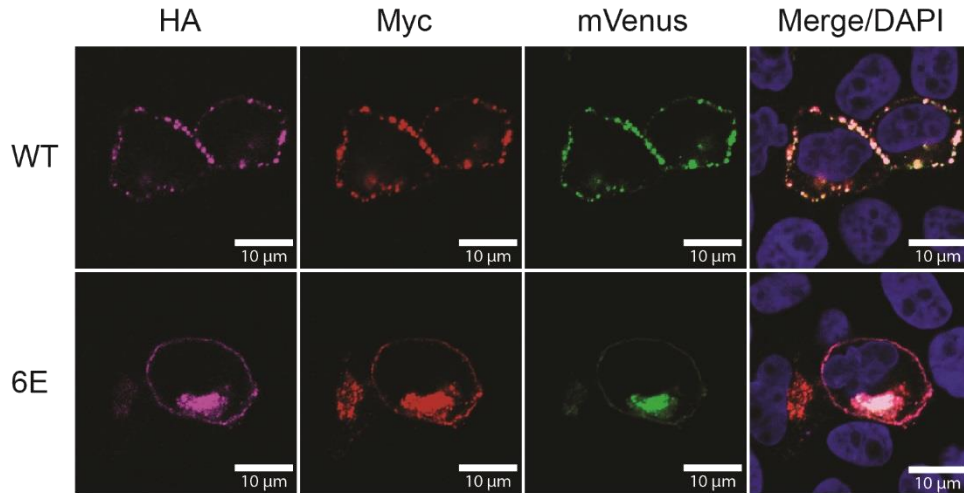
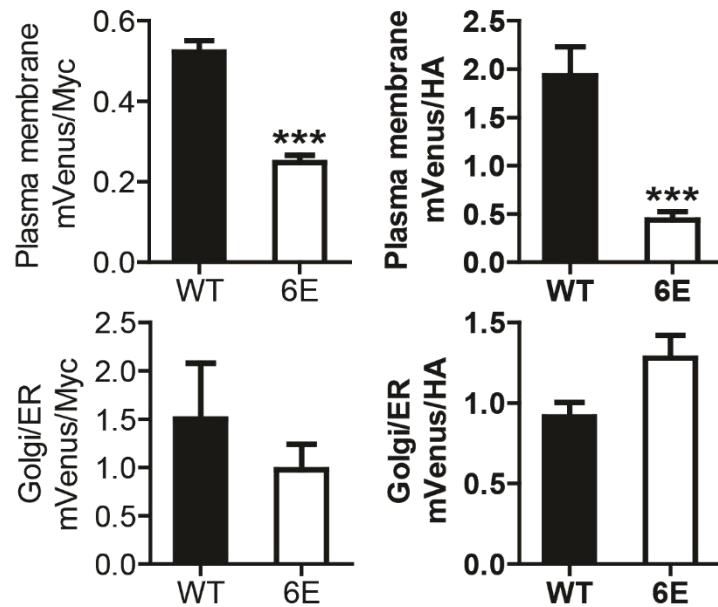
A**B**

Figure 2.2. Cx45CT WT dimerizes at the plasma membrane.

MDCK cells transiently transfected with the Cx45CT WT or 6E versions of Lyn-HA-CxCT-mVenN and Lyn-Myc-CxCT-mVenC were assessed for complemented mVenus signal. A) Representative immunofluorescence images of double transfected MDCK cells. B) Calculated area under the curve and mean fluorescent intensity of mVenus signal normalized to either the Myc- or HA-tag fluorescence at the plasma membrane (top) and Golgi/ER (bottom), respectively. Statistics are one tailed unpaired student's T-test between the Cx45CT WT and 6E groups; *** $P < 0.0001$. Scale bar = 10 μ m. This figure is modified from Trease et al., (2017).

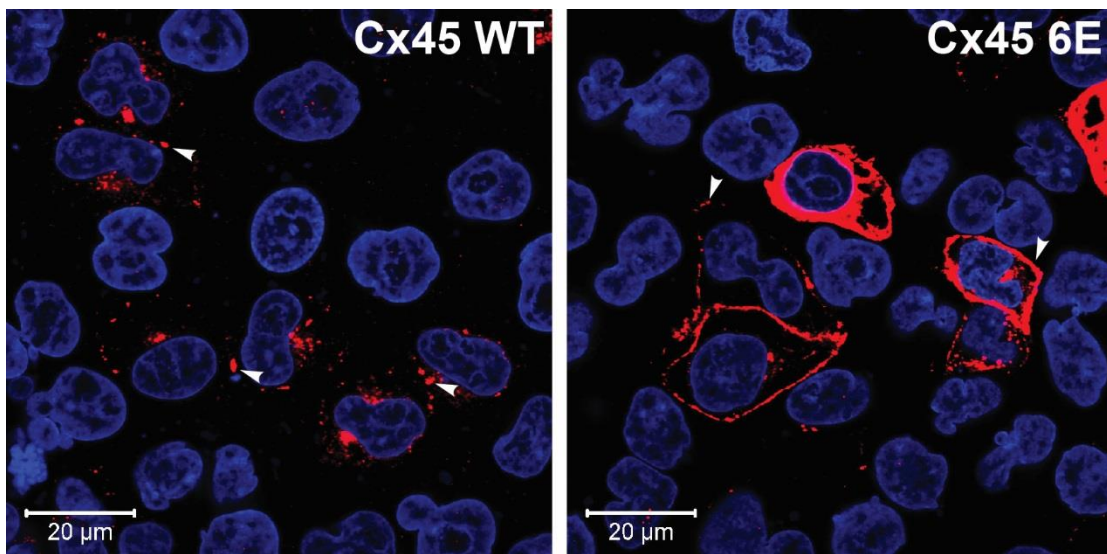


Figure 2.3. Localization of Cx45 WT and Cx45 6E in HeLa cells.

HeLa cells were transiently transfected with either Cx45 WT or Cx45 6E for approximately 20 hr, fixed and immunostained for Cx45 (red). White arrows indicate GJ plaques for Cx45 WT at cell appositions, while for Cx45 6E indicate the presence of protein at the plasma membrane in absence of apposition of another expressing cell. DAPI (blue) was used to stain the nuclei. Scale bar = 20 μm

7.2 Inhibiting CT Dimerization of Cx45 Alters Protein Localization

In order to determine if inhibiting dimerization affects proper Cx45 function our first approach was to transiently transfect Cx45 WT and 6E into Cx-deficient HeLa cells. Following transfection, the cells were cultured approximately 20 hr, fixed, and stained for Cx45. Similar to what has been shown in the literature, our immunofluorescent images demonstrate that Cx45 WT and 6E localized in the cell differently. Cx45 WT formed the expected small punctate GJs at cell to cell interfaces, while the 6E presented as a predominantly linear structure covering the bulk of the plasma membrane of each transfected cell independent of expression in apposed cells or cell-cell contact (Fig. 2.3; white arrows). To confirm this phenotype in a second cell line we also transiently transfected MDCK cells with either Cx45 WT or 6E. As we expected, immunofluorescence of the MDCK cells revealed a similar pattern as we observed in the HeLa cells for both WT and mutant Cx45 (data not shown). To further investigate the importance of Cx45 CT dimerization we then sought to create stable expressing Cx45 WT and 6E cell lines using MDCK cells as the transgene recipient. MDCK cells were chosen over HeLa cells for this portion of the study as they have been used extensively in the literature to study GJs and are capable of consistent GJ formation. Furthermore, the flattened shape of the cell line lends itself well to microscopic studies. Stable cell lines were clonally selected for clones that best represented the transiently expressed phenotype by immunofluorescence (Fig. 2.4). In addition to determining if protein localization was altered by loss of CT dimerization, we also measured the apparent GJ size for both Cx45 WT and 6E proteins using the built-in measure function of Zen software. Quantification of the length confirmed differences between the apparent length of Cx45 WT and 6E GJ plaques (Table 3). As the Cx45 WT stable cell line expressed a residual amount of Cx43, we sought to determine if the presence of Cx43 affected Cx45 localization by use of siRNA mediated knock down of endogenous Cx43. Western blot and immunofluorescent imaging indicated that the presence of Cx43 did not affect the expression levels of Cx45 or alter Cx45 localization (Fig. 2.5A and 2.5B).

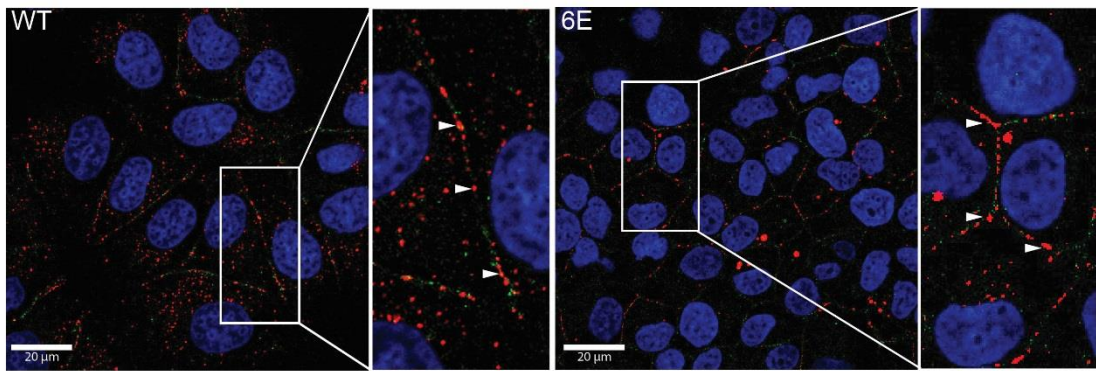


Figure 2.4. Inhibition of Cx45CT dimerization alters proteins localization.

MDCK cells were stably transfected with either Cx45 WT or Cx45 6E and were clonally selected. Representative images of the clones utilized for this study are presented here. Cx45 (red) and E-cadherin (green) were stained. DAPI (blue) was used to stain the nuclei. White arrows represent apparent GJ plaques. Scale bar = 20 μm . This figure is modified from Trease et al., (2017).

Protein	Species	Host Cell	Average Length (nm)	Plaques Measured	T-Test P value
WT	Mouse	MDCK	602 ± 141	113	<0.0001
6E	Mouse	MDCK	1330 ± 343	208	
WT	Human	MDCK	640 ± 236	311	<0.0001
6E	Human	MDCK	1756 ± 340	131	
WT	Mouse	HEK-293	749 ± 365	141	<0.0001
6E	Mouse	HEK-293	1325 ± 776	137	

Table 3. Measurements of GJ plaque length.

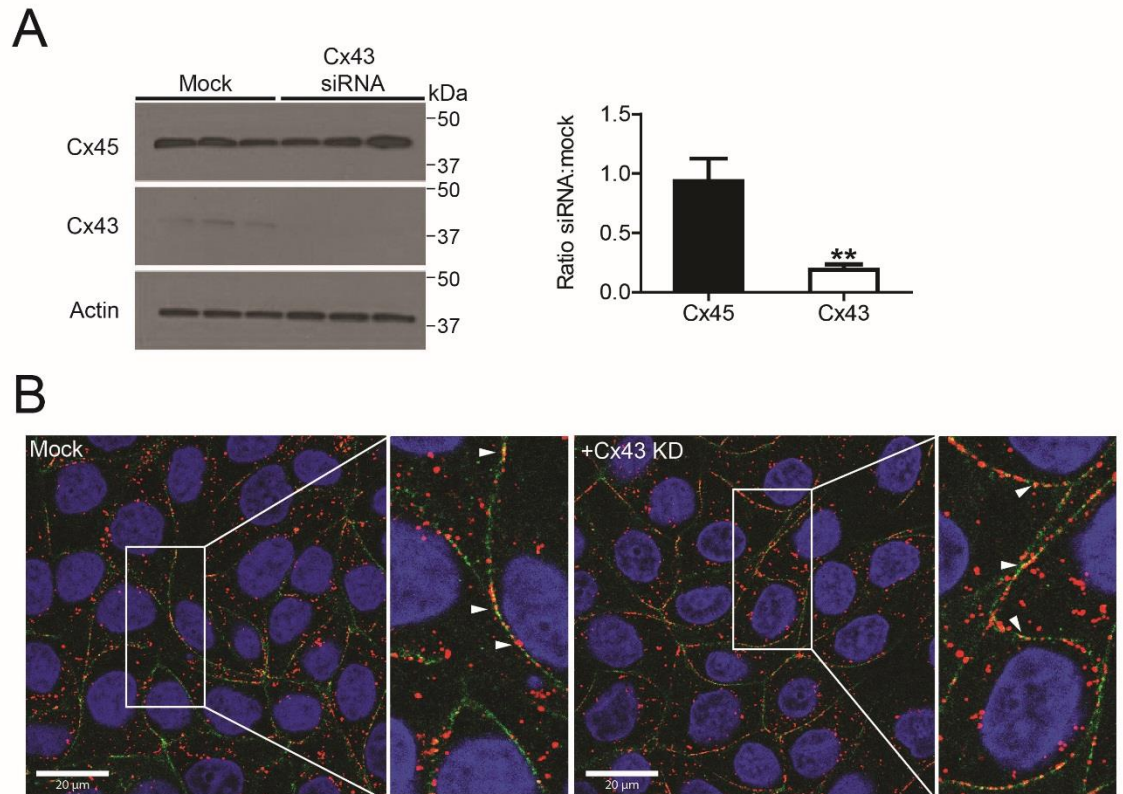


Figure 2.5. Endogenous Cx43 does not alter Cx45 expression or localization. MDCK cells expressing Cx45 were analyzed for expression of Cx45 and Cx43 and localization of Cx45 after siRNA mediated knock-down of the endogenous Cx43. A) Western blot and quantification of the expression of Cx45 and Cx43 in the stable MDCK cells. B) Representative immunofluorescent images of the localization of Cx45 (red). E-cadherin (green) was used to mark the plasma membrane, and DAPI (blue) was used to stain the nuclei. White arrows indicate GJ plaques. Scale bar = 20 μ m. This figure is modified from Trease et al., (2017).

Finally, we hypothesized that the phenotype we were observing was independent of host cell type or species of origin for the Cx45. Thus, we created humanized versions of Cx45 WT and 6E and expressed them in MDCK cells, as well as expressed mouse Cx45 WT and 6E in HEK293T cells. Similarly, we immunostained these proteins to assess cellular localization, and as we expected observed similar localization and GJ morphology to that of our stable cell lines (Fig. 2.6). We additionally, measured the GJ lengths under these conditions to compare to mouse Cx45 WT and mouse 6E. As we expected the trend for these permutations were consistent with what we observed for mouse Cx45 WT and 6E expressed in MDCK cells. The measurements are summarized in Table 3. Finally, we wanted to confirm our observations were not caused by differences in antibody affinity or an artifact of fixation. To accomplish this, we generated stable expression cell lines of C-terminal eGFP-fusions for each of our Cx45 WT and 6E constructs and used live imaging to determine protein localization (Fig. 2.7). Confirming what we observed in the fixed and stained cells Cx45 WT was restricted to puncta along the plasma membrane while the 6E was expressed as a diffuse staining all along the plasma membrane. Of note, for Cx43, the inclusion of a C-terminal eGFP-tag resulted in an increase in apparent GJ length which was determined to result from disrupted associations with the scaffolding protein ZO-1 [166]. Interestingly, when we measured the length of the Cx45-eGFP WT GJs we obtained a length of 667 ± 240 nm from a total of 12 plaques, suggesting that eGFP fusions are not altering the length of Cx45 WT GJs and consequently are unlikely to cause the diffuse membrane signal observed for the Cx45-eGFP 6E.

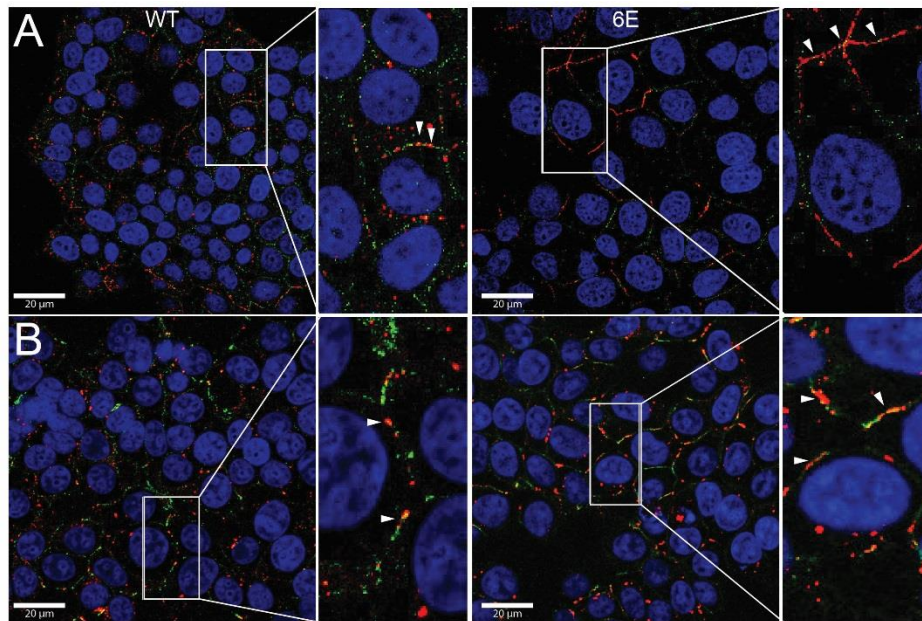


Figure 2.6. Localization of Cx45 WT and 6E are not species specific. Representative immunofluorescent images of Cx45 WT and 6E in MDCK (A) and HEK293T (B) cells. A) Human Cx45 WT and Cx45 6E were stably expressed in bulk selected MDCK cells and immunostained for Cx45 (red) and E-cadherin (green). B) Mouse Cx45 WT and 6E were stably expressed in bulk selected HEK293T and immunostained for Cx45 (red) and β -Catenin (green). DAPI (blue) was used to stain the nuclei of both. White arrows indicate apparent GJ plaques. Scale bar = 20 μ m. This figure is modified from Trease et al., (2017).

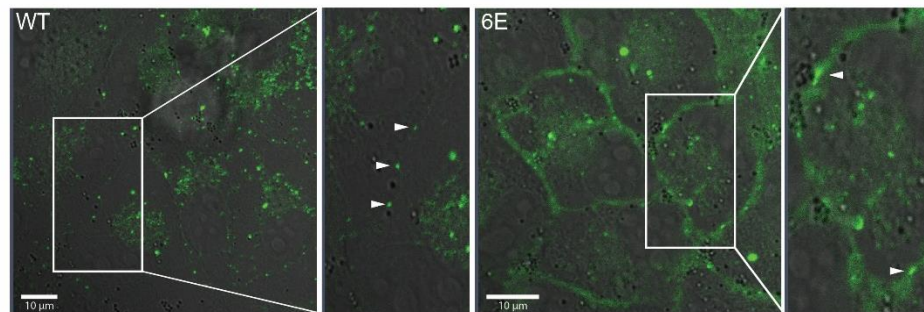


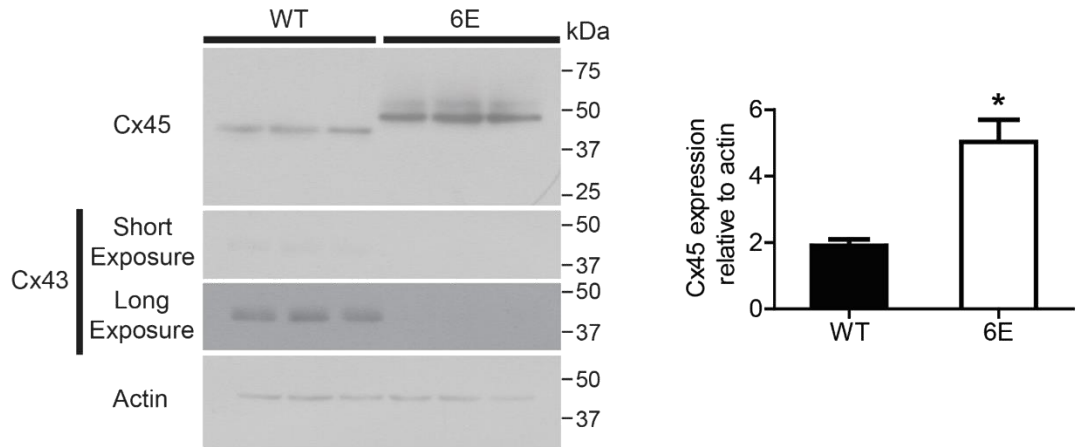
Figure 2.7. Live imaging using Cx45-eGFP WT or 6E reveals diffuse localization of Cx45 6E along plasma membrane.

Representative single time point live fluorescent images of Cx45 WT (left) or 6E (right) with c-terminal eGFP fusions. Notably the bulk of 6E-eGFP fluorescence is observed diffusely across the entire plasma membrane. White arrows indicate apparent GJ plaques. Scale bar = 10 μm . This figure is modified from Trease et al., (2017).

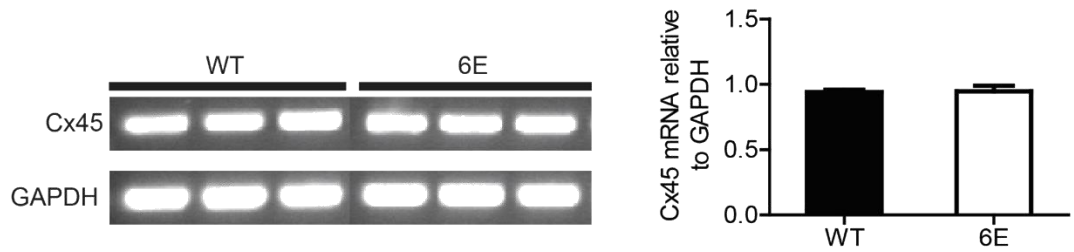
7.3 Cx45 6E Has Altered Protein Expression

Noting the increased expression of the Cx45 6E at the plasma membrane compared to that of WT, we wanted to determine if this was the result of a difference in protein expression level. To address this, we used Western blot to determine if CT dimerization was affecting protein expression levels. Our results indicated that Cx45 6E was expressing protein at approximately 1.6-fold that of WT (Fig. 2.8A). Notably, we simultaneously tested both stable lines for expression of endogenous Cx43 and our results indicate our 6E line does not express any of the endogenous Cx43 (Fig. 2.8A). We reasoned the increase in protein expression could be the result of either increased transcription (enhancing translation) or impaired turnover (enhancing stability) of the 6E mutant. We first sought to determine if increased translation was contributing to the increased protein express of the 6E mutant. To assess this, we measured the level of Cx45 WT and 6E transcripts by RT-qPCR. Relative levels of Cx45 transcript were compared to that of the housekeeping gene, GAPDH (Fig. 2.8B). We determined compared to GAPDH the levels of Cx45 WT and 6E transcript to be identical. This suggested to us that the increased 6E protein expression was likely a consequence of altered 6E turnover. To test this, we used a CHX chase assay to measure the degradation time of Cx45 WT and 6E. MDCK cells were treated over the course of 12 hr with 80 μ M CHX and samples were analyzed by Western blot (Fig. 2.8C). The Western blot results indicate that the Cx45 WT protein was degraded to near completion (~14% remaining) in 12 hr. In contrast, the 6E protein expression was relatively unchanged over the 12 hr period. Although the relative stability of the 6E protein prevented calculation of half-life, we calculated the half-life of the Cx45 WT protein to be 4.18 ± 0.90 hr; a result similar to previously published results for Cxs [189]. Taken together with the RT-qPCR data this suggests that the increase in 6E protein expression is the result of decreased turnover rather than increased synthesis.

A



B



C

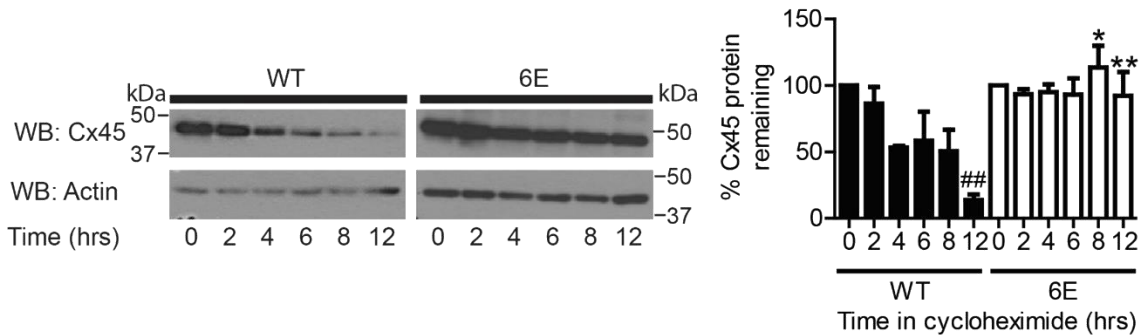


Figure 2.8. Inhibiting Cx45CT dimerization disrupts protein degradation.

Three different MDCK cells expressing either Cx45 WT or 6E were assessed for expression at the protein and transcript levels. A) Western blots and quantification of Cx45 WT, Cx45 6E, and Cx43 expression. B) RT-PCR gel images and quantification of Cx45 WT and 6E transcripts. C) Western blots and quantification of Cx45 WT or 6E subjected to a 12 hr CHX chase. Results presented as the mean + s.e.m. (n=3). Statistics are used to analyze the data were two-tailed unpaired Student's T-test (A, n=3, *P<0.05; and C, n=3, ns, *P<0.9056) and one-way ANOVA with a Newman-Keuls post hoc test (B, n=3; *P<0.05, **P<0.001 comparing Cx45 WT and 6E, and ##P<0.001 compared to time = 0). This figure is reprinted from Trease et al., (2017).

7.4 Cx45CT Dimerization is Essential for Proper GJIC

By inhibiting Cx45CT dimerization we determined an increased proportion of Cx45 6E was present at the plasma membrane relative to WT. We were curious if this increased amount of Cx protein would correlate with increase GJIC. To test this, we used scrape loading dye transfer of NB, a 322.8 Da cationic molecule that Cx45 channels have been demonstrated to be permeable to [86]. In addition to NB we utilized Lucifer Yellow CH (LY), a 457.2 Da anionic fluorescent dye as a negative control, as Cx45 channels have conversely been shown to be impermeable to LY [86]. Scrape loading takes advantage of the ability to “load” cells with membrane impermeable dyes through a cut introduced into a monolayer of cells. Stable Cx45 WT and 6E cells were cultured to confluence in live imaging dishes, scrape loaded, fixed, and stained with Streptavidin-647 conjugate to identify the NB. Confocal microscopy was used to image dishes and to determine the degree of dye transfer. As a marker of cells damaged by the scrape that take up the dye, a large (10,000 Da) fluorescently labelled dextran was utilized for its inability to pass through GJs. Similar to what has been published previously for the Cx45 WT we observed substantial dye coupling with respect to NB, in some cases dye spread reached greater than 5th order (5 rows of cells from scrape) transfer (Fig. 2.8 (top); green). Consistent with the literature we also observed little-to-no permeability of Cx45 WT channels to LY (Fig. 2.8 (top); yellow). When we repeated the assay with the 6E cells, to our surprise we observed severely impaired dye coupling with respect to NB, reaching 2nd-3rd order transfer very rarely (Fig. 2.8 (bottom); green). Furthermore, LY transfer was not altered relative to Cx45 WT remaining only in the cells immediately adjacent to the scrape (Fig. 2.8 (bottom); yellow). These data suggest a role for Cx45 CT dimerization in proper GJIC. Furthermore, the reduced coupling of NB in the 6E cells could be explained by fewer junctional channels, reduced channel open time/probability, or by reduced NB permeability.

7.5 Inhibition of Cx45 CT Dimerization Impairs GJ Plaque Formation

Our experiments on the localization of Cx45 indicated that a larger pool of Cx45 protein was present at the plasma membrane when CT dimerization was inhibited that correlated with a decreased communication of NB dye. This led us to question whether this increased plasma membrane protein was incorporated into GJ plaques. To test this, we utilized the TX-100 solubility

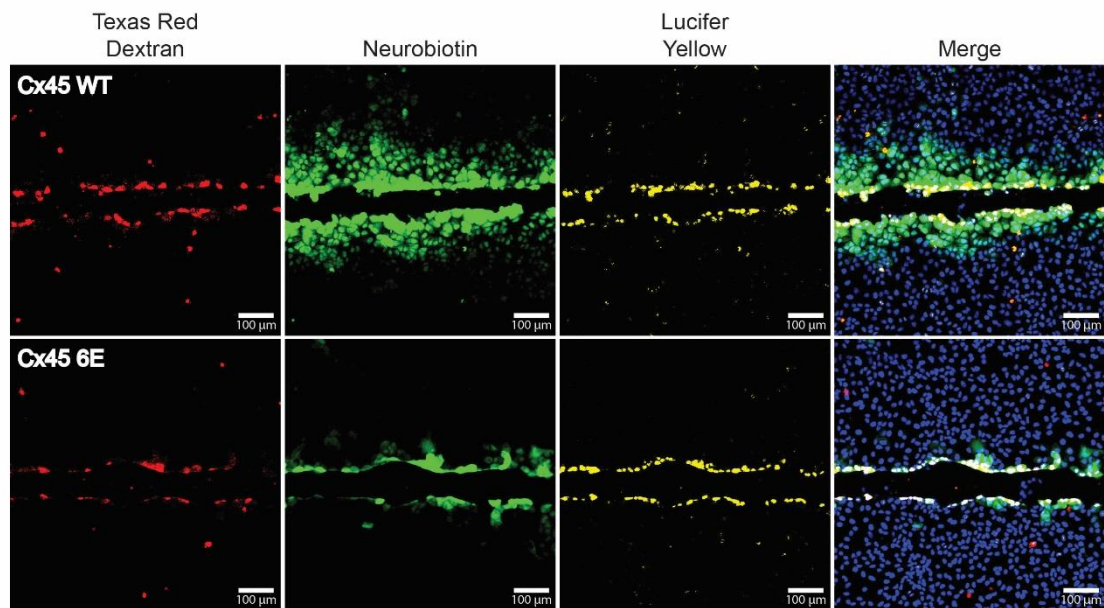


Figure 2.9. Inhibiting Cx45CT dimerization impairs gap junction intercellular communication.

MDCK cells expressing Cx45 WT (top) or 6E (bottom) were scrape loaded with tracer dyes to assess the degree of intercellular communication. Red, Texas red dextran (MW 10,000 Da); yellow, Lucifer yellow CH (MW 443 Da; -2 charge), green, NB (MW 287 Da; +1 charge); and blue, DAPI. Images are representative of greater than six independent experiments. Scale bar in = 100 μm . This figure is modified from Trease et al., (2017)

assay which allows for the separation and quantification of non-junctional (soluble; hemichannels and non-oligomerized Cx proteins in secretory pathway) from junctional (insoluble; GJ plaques) Cx protein. We found that for Cx45 WT, protein segregated reproducibly into $58.57 \pm 3.006\%$ soluble and $39.17 \pm 2.154\%$ insoluble. When we tested the 6E we determined that $86.43 \pm 4.654\%$ of the protein segregated into the soluble fraction while only $22.59 \pm 5.422\%$ of the protein was found in the junctional pool (Fig. 2.9A). We determined this to result in a 1.47-fold increase ($N=3, P < 0.0001$, one-way ANOVA) in the soluble protein pool when dimerization was inhibited. Utilizing an *in-situ* TX-100 followed by immunofluorescence we obtained results that were comparable to the Western blot data (Fig. 2.9B). Quantification of the percentage of residual Cx protein following extraction indicated 37.17% of Cx45 WT fluorescent signal remained after extraction while only 17.37% of 6E signal remained (Fig. 2.9B). Taken together this indicates that the increased protein expression at the plasma membrane seen in the 6E expressing cells is non-junctional. Furthermore, we sought to ensure co-expression of Cx43 in the Cx45 WT clone did not significantly impact segregation of Cx45 WT into GJ plaques. To determine this, we again performed the TX-100 solubility assay on Cx45 WT cells that had been treated with siRNA against the endogenous Cx43. We determined our knockdown efficiency of the endogenous Cx43 to be 91.25% (see Fig. 2.5A). With the TX-100 solubility assay we found that $39.56 \pm 4.81\%$ of the Cx45 was present in the soluble pool, while $60.44 \pm 18.46\%$ was present in the junctional pool when cells were mock transfected (Fig. 2.10). Similarly, when Cx43 was knocked down by transfection with siRNA we found $39.45 \pm 6.22\%$ and $60.55 \pm 9.95\%$ of Cx45 in the non- and junctional pools, respectively. Therefore, the presence of Cx43 did not alter Cx45 GJ formation. Taken together with the dye transfer data our results demonstrate that Cx45 CT dimerization contributes to the stability of Cx45 at the GJ plaque. Furthermore, our reduced dye transfer in the 6E expressing cells is consistent with the decreased percentage of GJ channels.

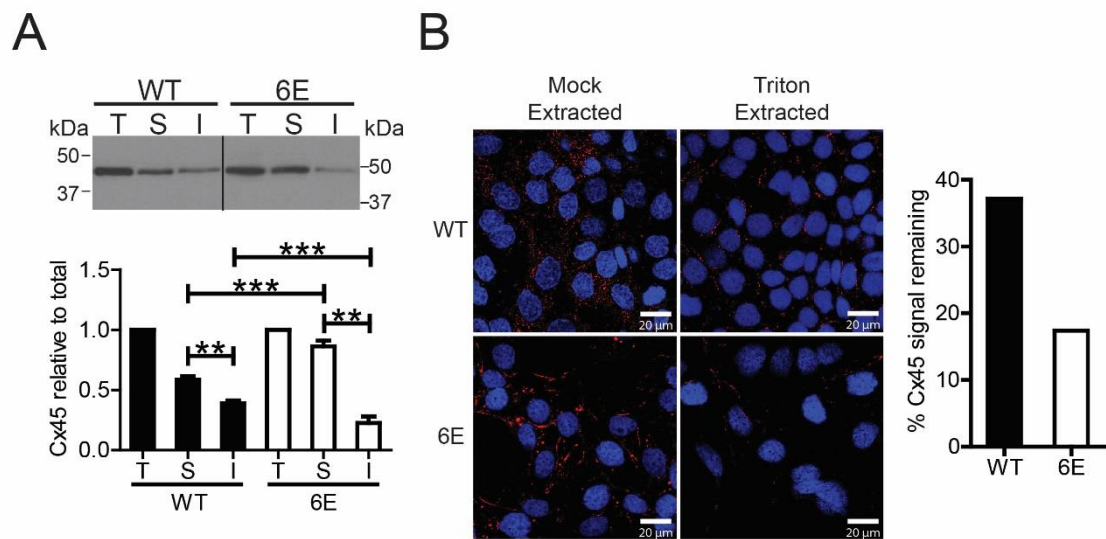


Figure 2.10. Inhibiting Cx45CT dimerization impairs GJ plaque formation.

A) TX-100 solubility was used to compare MDCK cells expressing Cx45 WT or 6E. A) Western blot image of TX-100 extracted protein; total lysate (T), soluble (S), and insoluble (I) fractions. Below is the quantification of protein in the T, S, and I fractions. Statistics represent one-way ANOVA with a Newman-Keuls post-hoc correction ($n=3$, $**P<0.001$, $***P<0.0001$). B) Representative fluorescent images (left) and quantification (right) of *in situ* TX-100 and mock (1x PBS) extracted Cx45 WT or 6E in MDCK cells (red, Cx45; blue, DAPI). This figure was modified from Trease et al., (2017).

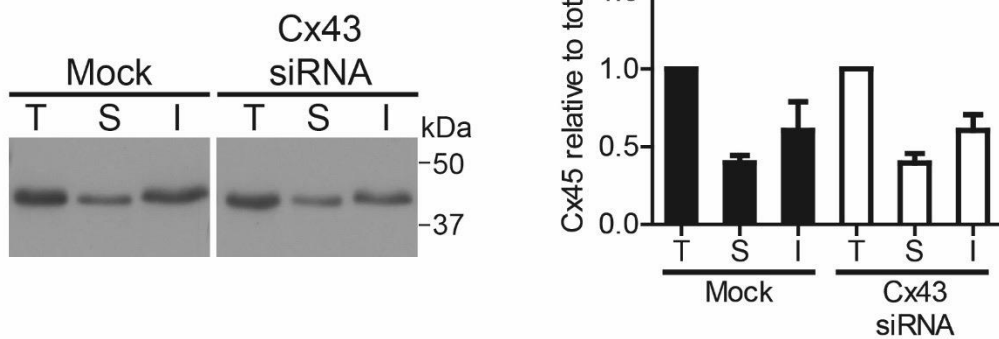


Figure 2.11. Endogenous Cx43 does not impact Cx45 GJ plaque formation. Representative Western blot and quantification of total (T), Triton soluble (S), and Triton insoluble (I) Cx45 WT after siRNA mediated knockdown of Cx43. Data presented as the mean + s.e.m. of three independent experiments. Statistics for the TX-100 solubility assay were one-way ANOVA with a Newman-Keuls post hoc test (n=3). This figure was modified from Trease et al., (2017).

7.6 Inhibiting Dimerization Does Not Alter Oligomerization

Since our previous experiments revealed inhibiting Cx45CT dimerization affected both protein localization and GJ plaque formation we hypothesized that it may alter oligomerization. As an initial test to determine if overall oligomerization was affected by inhibiting dimerization we used Blue Native PAGE to assess the oligomeric status of Cx45 WT and 6E from TX-100 soluble fractions. MDCK cells expressing either Cx45 WT or 6E were lysed in buffer containing 1% TX-100, fractionated by high speed centrifugation, and the supernatant was applied to Blue Native PAGE, resolved, and then interrogated by Western blot. Our results demonstrated that both Cx45 WT and 6E formed proper oligomers as indicated by the immunoreactivity of a species consistent in molecular weight with a connexon (Fig. 2.11A). Furthermore, and to our surprise, we found that Cx45 WT did not show any appreciable banding or immunoreactivity at a molecular weight that would be consistent with the monomeric Cx, however, showed a smear with some discrete banding present for higher order (dimer, tetramer, etc.) oligomers while 6E showed clear banding for all species from monomeric Cx to hexameric connexon. This led us to wonder if dimerization of the Cx45CT would occur prior to channel oligomerization. For Cx43 it was shown that oligomerization of Cxs into connexons occurred in the TGN [137, 147]. As such we sought to determine if oligomerization of Cx45 would occur in the TGN, as well as determine if inhibiting CT dimerization would alter this. To test this, we used linear sucrose gradient (5-25%) centrifugation to separate non- from oligomerized Cx45 WT and 6E. Work from other labs has indicated that suboligomeric Cx43 sediments below 15% sucrose [143]. Specifically, monomeric Cx43 sediments at ~8% sucrose, while hexameric Cx43 sediments at 15% sucrose. We applied Cx45 WT or 6E from 1% TX-100 soluble fractions to linear 5-25% sucrose gradients and centrifuged them overnight. We fractionated the gradients in 0.5 mL fractions in a top down manner and analyzed them for Cx content by Western blot. In order to accumulate the Cx45 in the *cis*-Golgi we treated the cells with MonA to block transport to the medial-Golgi and subsequently *TGN* compartment. MonA treated samples were compared to vehicle (EtOH) treated. In EtOH treated cells, we observed little difference between Cx45 WT and 6E. This was characterized by two peaks, one at lower sucrose

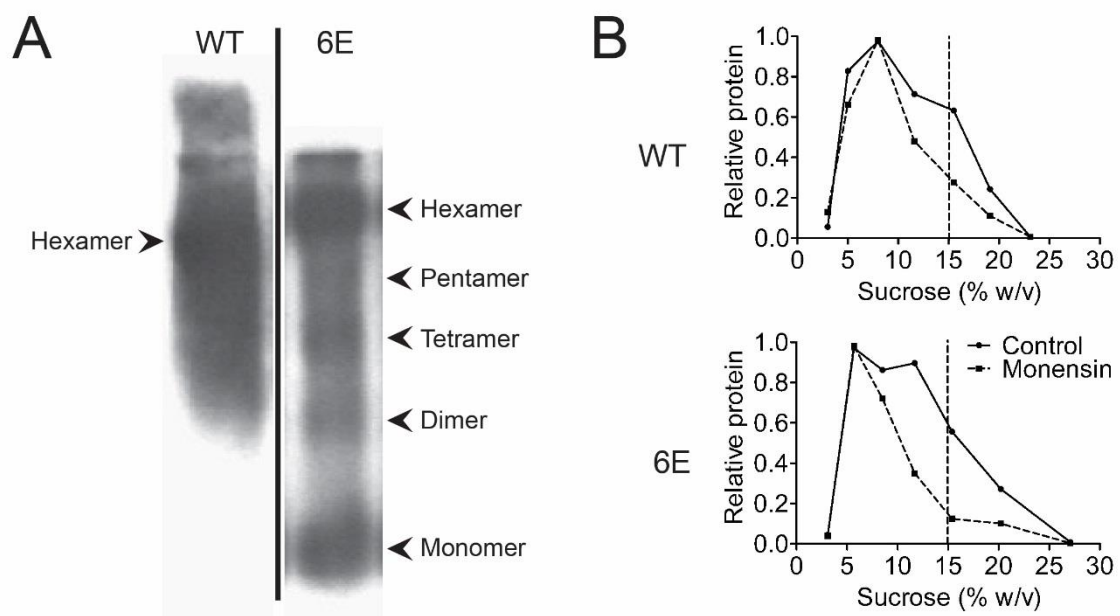


Figure 2.12. Inhibiting Cx45CT dimerization does not impact oligomerization state or cell compartment.

Post-nuclear TX-100 soluble lysates from MDCK cell stably expressing Cx45 WT or Cx45 6E were analyzed by Blue Native PAGE and sucrose density centrifugation. A) Representative Western blot of Blue Native PAGE samples. B) Plots of Western blotted fractions of Cx45 WT and Cx45 6E from sucrose density centrifugation following 4 hr treatment with MonA.

concentration, corresponding to suboligomeric Cx45 and one at ~15% corresponding to connexons (Fig. 2.11B; solid line). However, for MonA treated samples we observed a shift away from the peak corresponding to connexons and an accumulation of Cx45 in a lower sucrose density. Specifically, peak sedimentation of Cx45 WT corresponded to ~8.0% sucrose while for 6E this peak was present at ~5.7% sucrose (Fig. 2.11B; dashed line). The data suggests that oligomerization of Cx45 is not affected by inhibiting dimerization. Additionally, when taken together with the Blue Native PAGE results, this data suggests that Cx45CT dimerization occurs prior to oligomerization, consistent with a slightly larger molecular species for Cx45 WT as indicated by the slight shift to higher sucrose concentration when compared to that of 6E (Fig. 2.11B; dashed line).

7.7 Increased Membrane Cx45 6E Mediates Increased Hemichannel Activity

Having determined the excess 6E at the plasma membrane was not incorporated into GJ plaques we reasoned they may be available to mediate hemichannel activity. To test for this, we used an established hemichannel dye uptake assay [442]. Briefly, depletion of extra cellular Ca^{2+} results in a positive membrane potential that leads Cx hemichannels to open [442]. The degree of hemichannel opening can be quantified as a function of NB dye uptake. We found for the control condition ($+\text{Ca}^{2+}$) both Cx45 WT and 6E expressing MDCK cells minimally took up NB as indicated by the limited staining with Streptavidin (DAPI normalized MFI WT = 0.5873 ± 0.03083 vs. 6E = 0.4180 ± 0.02306 ; ns, Fig. 2.12A). Conversely, following extracellular Ca^{2+} depletion we determined the 6E expressing cells took up approximately 2-fold NB compared to Cx45 WT (DAPI normalized MFI WT = 0.8866 ± 0.02859 vs. 6E = 2.042 ± 0.1397 , $P < 0.0001$, $n=15$, $N=3$, Fig. 2.12A). Additionally, we wanted to test if increasing Tyr phosphorylation (a stimulus that inhibits Cx43 GJ channels) would alter Cx45 WT hemichannel activity. To test this, we pretreated the Cx45 WT expressing cells with 100 μM pervanadate for 15 min to inhibit normal dephosphorylation and again measured dye uptake [444]. Compared to untreated Cx45 WT expressing cells no difference in dye uptake was observed in normal Ca^{2+} or during Ca^{2+} depletion or (Normal Ca^{2+} : DAPI normalized MFI untreated = 0.5873 ± 0.03083 vs. pervanadate = 0.6217 ± 0.02705 , ns, $n=15$, $N=3$, Fig 2.12A; Ca^{2+} depletion: DAPI normalized MFI untreated = 0.8866 ± 0.02859 vs. pervanadate = 0.8737 ± 0.03953 , ns, $n=15$, $N=3$, Fig. 2.12A). The degree of change in Tyr phosphorylation in response to

pervanadate treatment was determined by IP of Cx45 and Western blotting with a general pTyr antibody (Fig. 2.12B). We found that treatment with pervanadate increased the amount of Cx45 total Tyr phosphorylation by 3.38-fold (pTyr: Cx45; untreated = 0.05023 ± 0.00776 vs. pervanadate = 0.1698 ± 0.0439 , $P < 0.05$, $N=3$). Our data indicate that increased Tyr phosphorylation does not alter Cx45 hemichannel mediated dye uptake. The data also demonstrates that pervanadate did not alter the requirement for Ca^{2+} depletion to open Cx45 hemichannels. Finally, we sought to confirm that our dye uptake was mediated by Cx45 hemichannels rather than some other membrane channel protein and we used the GJ hemichannel blocker La^{3+} to inhibit hemichannel channel activity. Confirming our dye uptake was mediated by Cx45 hemichannels, treatment with La^{3+} reduced dye uptake to levels similar as seen when normal Ca^{2+} bathing solution was used (DAPI normalized MFI WT = 0.6272 ± 0.0275 , WT + pervanadate = 0.7102 ± 0.0664 , 6E = 0.6462 ± 0.0440 , ns, $n=15$, $N=3$, Fig 2.12A). Taken together with the scrape loading experiments our data indicate 6E hemichannels and channels are permeable to NB, albeit channel permeability appears reduced relative to Cx45 WT. Furthermore, when correlated with the TX-100 solubility assay data the differences in NB transfer (hemichannels-higher, channels-lower) are consistent with the location of Cx45 (hemichannels vs. GJ channels; i.e., less Cx45 in the GJ correlates with increased hemichannel activity).

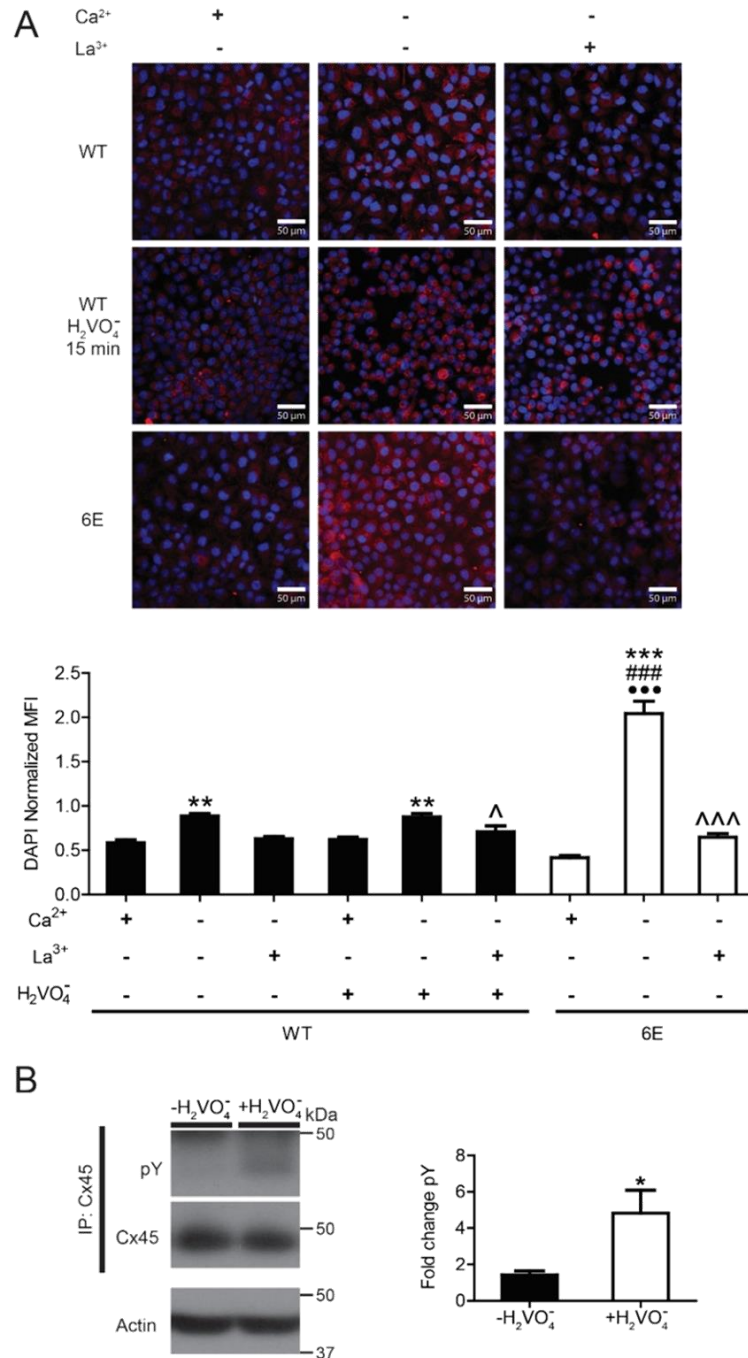


Figure 2.13. Inhibiting Cx45CT dimerization affects hemichannel dye uptake.

A) MDCK cells stably expressing Cx45 WT or 6E were subjected to conditions that activate hemichannels activity (Ca²⁺ deprivation) and the level of NB uptake was measured. Representative fluorescent micrographs of cells loaded with NB and probed with streptavidin-647 conjugate (red). Quantification of DAPI (blue) normalized mean fluorescent intensity (MFI) from 3 replicates, 15 random 100X FOVs were acquired per replicate. Statistics are one-way ANOVA with a Newman-Keuls multiple comparison test (***)P<0.0001 relative to +Ca²⁺ within same group, ^ and ^^P<0.05 and <0.0001 respectively, relative to -Ca²⁺ within same group; ###P<0.0001 between -Ca²⁺ treatment groups; ***P<0.0001 compared to WT + pervanadate). Scale bar = 50 μm. B) MDCK cells expressing Cx45 WT were treated with 100 μM pervanadate for 15 min, captured by IP with α-Cx45, analyzed by Western blot (left), and quantified using ImageJ (right). Data presented as the mean + s.e.m. of three independent experiments. Statistical analysis was done using a one-tailed unpaired Student's T-Test (P< 0.05). This figure was modified from Trease et al., (2017).

7.8 Cx45CT Dimerization Reduces Hemichannel Currents

Since we observed increased hemichannel mediated dye uptake in our stable MDCK cell lines it is important to note that dye uptake/transfer does not always correlate with current conductance due to issues with permselectivity [445]. To determine if our increase dye uptake coincided with increased hemichannel currents we measured the macroscopic conductance of Cx45 WT and 6E channels expressed in *Xenopus* oocytes by cell attached electrophysiology. Identical amounts of Cx45 WT or 6E cRNA were injected into oocytes, together with DNA antisense to the endogenous XenCx38. After voltage clamping the oocytes, hemichannel opening was induced by successive depolarizing voltage steps followed by measurement of the macroscopic conductance (Fig. 2.13). In congruence with our hemichannel dye uptake results we determined that inhibiting dimerization greatly increased hemichannel currents. Furthermore, it was determined that initial rate constants for the transition from the closed state to the open state was increased for 6E channels as compared to WT. The results illustrated are representative of data from multiple injected oocytes (WT, n=8; 6E, n=4). Importantly, these data clearly illustrate 6E channels are functional, and mediate a much greater degree of current flow than Cx45 WT channels under identical stimuli, it is unclear at this time whether this increase observed in the 6E hemichannels is the result of a single factor or several. Possible explanations include: the greater degree of “soluble” plasma membrane expression, shifted Po-V relationships, or increased unitary conductance. Although it requires further investigation, it is likely to be determined that a combination of these factors result in the greatly enhanced hemichannel currents (and dye uptake) seen with 6E channels.

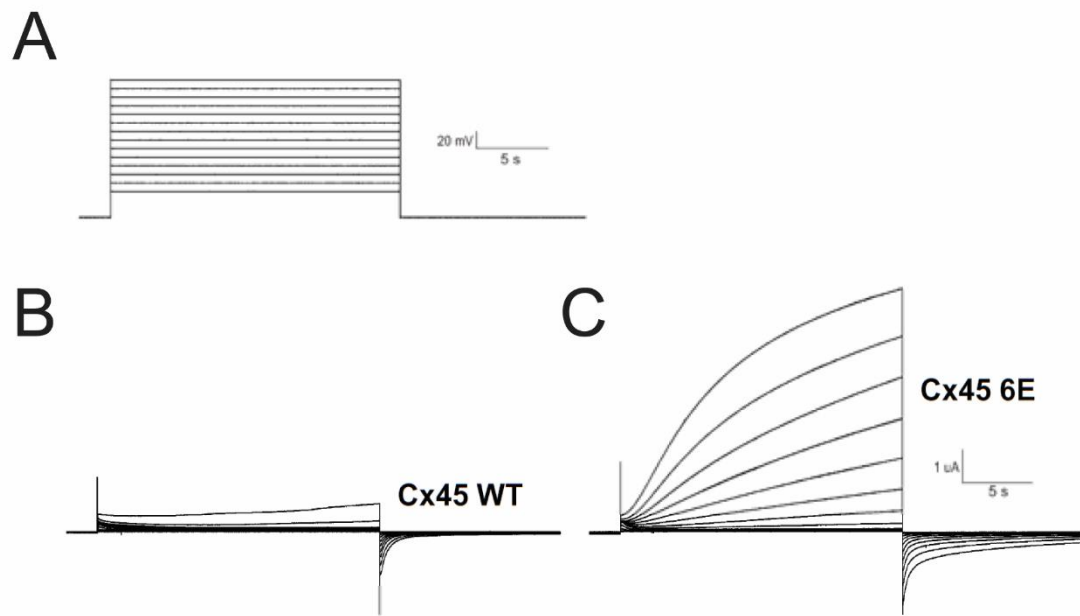


Figure 2.14. Inhibiting Cx45CT dimerization affects hemichannel currents.

Oocytes injected with equal amounts of cRNA coding for Cx45 WT or the 6E mutant were voltage clamped and hemichannel currents elicited by large depolarizing voltage steps from -50 to $+80$ mV in 10 mV increments from a holding potential of -80 mV. A) Representation of voltage protocol. Under the same voltage protocols, the WT channels mediated substantially less current than the 6E channels. Representative current plots from (B) WT and (C) 6E expressing oocytes. This figure is reprinted from Trease et al., (2017).

7.9 Cx45CT Dimerization Enhances Tyrosine but Not Serine Phosphorylation

Amongst most Cxs it has been shown consistently that changes in phosphorylation level affect GJIC [86, 306, 340, 385]. The effect has been shown via a number of mechanisms including affecting trafficking, GJ plaque stability, modulating protein partner interactions, altering turnover, or directly modulating channel properties such as open probability or conductance state [306, 309, 446]. Consequently, we hypothesized inhibiting dimerization would impact total levels of Cx45 phosphorylation and may in part influence the 6E phenotype. We therefore used IP to selectively concentrate either Cx45 WT and 6E from our stable MDCK cells and probed the eluted Cx45 by Western blot with either a general pTyr antibody (Fig. 2.14A) or pSer antibody (Fig. 2.14B). We determined that the basal level of Tyr phosphorylation of 6E was ~2.28-fold (N=3, P <0.001; WT 0.8635 ± 0.69 vs. 6E 1.971 ± 0.217) greater than that of Cx45 WT. Conversely, we did not observe a significant change in Ser phosphorylation from Cx45 6E to WT. Importantly, due to the lack of phosphospecific Cx45 antibodies we were unable to determine the locations of phosphorylated residues and therefore the possibility exists that for Tyr phosphorylation both an increase in the degree of phosphorylation as well as an alteration of the residues phosphorylated may exist, while for Ser phosphorylation only the possibility of alterations to the location of phosphorylated residues exists.

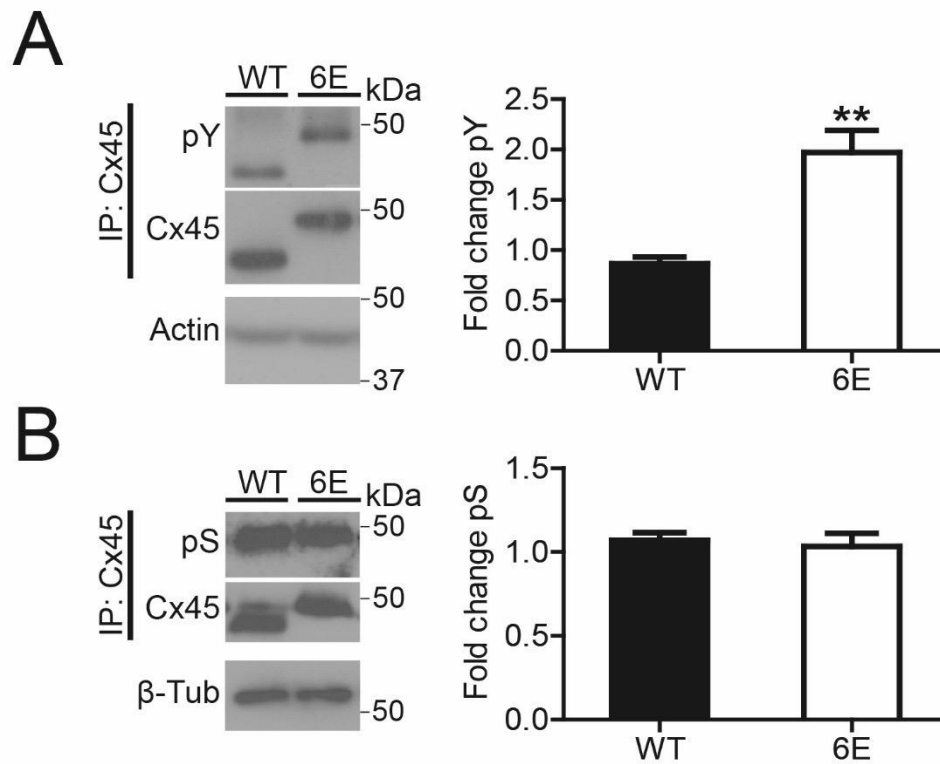


Figure 2.15. Inhibiting Cx45CT dimerization increases Tyr but not Ser phosphorylation.

IP was used to selectively concentrate Cx45 WT and 6E from MDCK cell lysate and probed for total levels of phosphorylation. A) Representative Western blot and quantification of Tyr phosphorylation using a general pTyr antibody. B) Representative Western blot and quantification of Ser phosphorylation using a general pSer antibody. Data presented as mean fold change + s.e.m. relative to the first WT replicate. Statistics are two-tailed unpaired Student's T-test. (n=3, ** P<0.01). This figure is modified from Trease et al., (2017).

7.10 Cx45CT Dimerization Affects Cytoskeletal Adapter Protein Partner Interactions

Our data indicating the 6E expressing cells contain a reduced number of docked GJ channels, increased overall plasma membrane expression and altered localization combined, strongly suggest trafficking to, at, or away from the GJ plaque is altered. Furthermore, consistent with our observation of increased Tyr phosphorylation of the 6E, trafficking of Cx43 is also affected by changes in Tyr phosphorylation. Work from our laboratory and others demonstrated that phosphorylation of Cx43 by Src kinase disrupts microtubule binding (β -tubulin) and anchoring to the actin cytoskeleton Drebrin and ZO-1 [286, 377, 378]. To determine if the increased Tyr phosphorylation observed for 6E correlated with altered cytoskeletal anchoring we used IP of Cx45 WT or 6E and Western blot to detect β -tubulin, Drebrin, and ZO-1 in the eluate (Fig. 2.15). Compared to Cx45 WT we observed a significant increase in the amount of pulled-down Drebrin (~1.97-fold $P < 0.01$; WT 0.9005 ± 0.104 vs. 6E 1.753 ± 0.138 ; Fig. 2.15B), a significant decrease for β -tubulin (~5.17-fold $P < 0.0001$; WT 0.6095 ± 0.079 vs. 6E 0.1180 ± 0.043 ; Fig. 2.15A) and non-significant albeit trending decrease in the association with ZO-1 (~1.45-fold ns; WT 1.173 ± 0.199 vs. 6E 0.8103 ± 0.184 ; Fig. 2.15C). Taken together with our phosphorylation data, these results suggest that the phenotypic difference between Cx45 WT and 6E may be in part the result of altered cytoskeletal interactions.

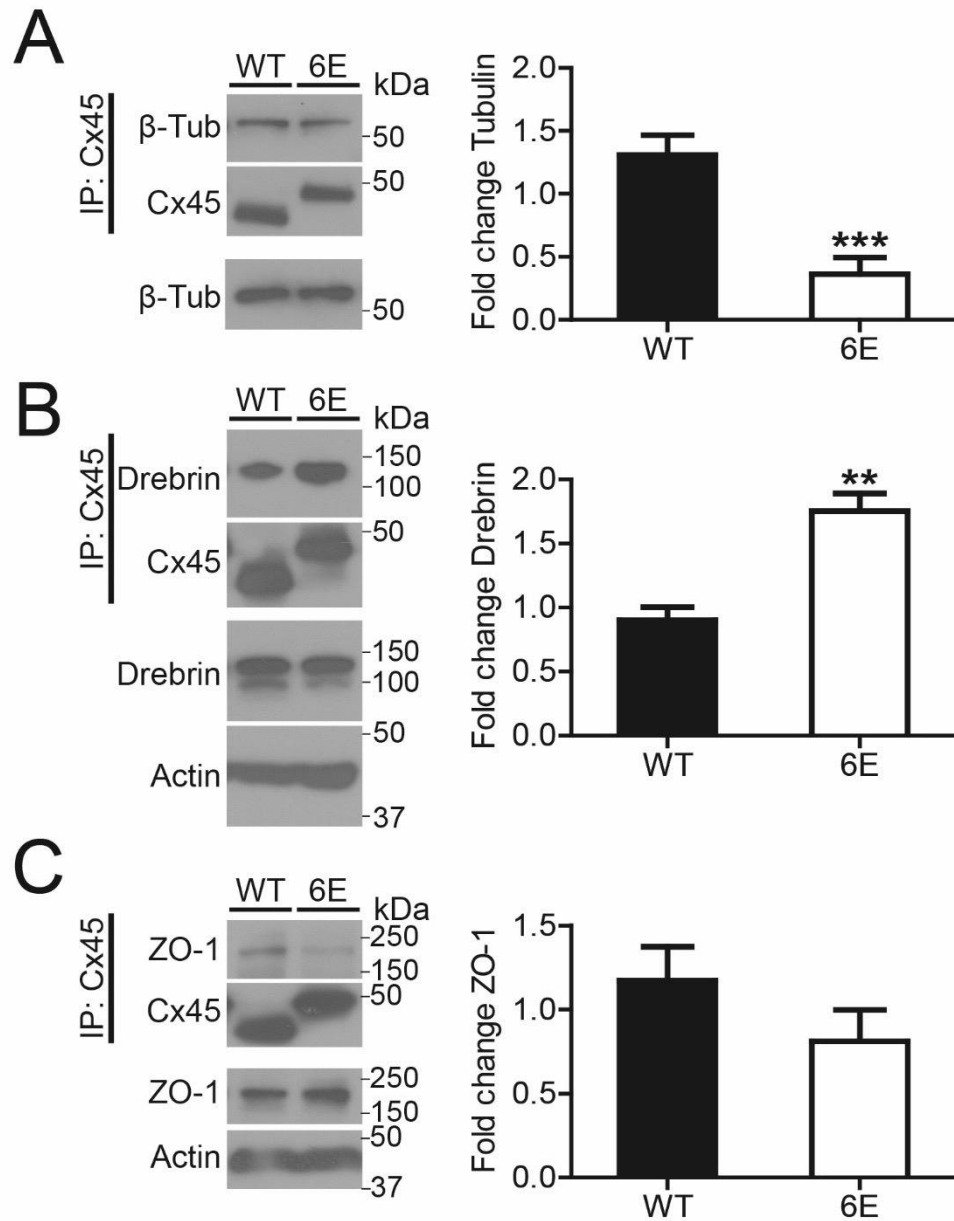


Figure 2.16. Loss of Cx45CT dimerization alters cytoskeletal anchoring.

MDCK cells stably expressing Cx45 WT or 6E were cultured, lysed, and enriched by IP to assess interactions with β -tubulin, Drebrin, and ZO-1. A) Representative Western blots of eluted Cx45 WT or 6E blotting against β -tubulin ($n=7$, *** $P<0.001$), B) Drebrin ($n=3$, ** $P<0.01$), and C) ZO-1 ($n=3$, ns) pulled-down by IP of either Cx45 WT or 6E. Data presented as mean fold change + s.e.m. relative to the first WT replicate. Statistics are two-tailed unpaired Student's T-test. This figure is modified from Trease et al., (2017).

7.11 Inhibiting Cx45CT Dimerization Disrupts Nedd4 but Not TSG101 Interactions

In addition to altered plasma membrane localization, we observed a significant increase in the total expression of Cx45 6E compared to WT that could not be explained by altered synthesis but rather impaired degradation (see Fig. 2.8). It is possible altered interactions with proteins involved in turnover and recycling of Cxs could result in the increase in 6E protein expression. For Cx43 a number of studies have highlighted the role of Nedd4, an E3 ubiquitin ligase, as an important regulator of turnover at the plasma membrane [203, 204, 447]. While intracellularly, TSG101 regulates trafficking of Cx43 to lysosomes or segregation for recycling back to the plasma membrane [448]. Additionally, previous work from our laboratory demonstrated a direct interaction via NMR between the Cx45CT domain and the WW2 domain of Nedd4 and the UEV domain of TSG101 [247]. We therefore reasoned Cx45CT dimerization may influence the interaction with these proteins. To test this, we used IP to concentrate Cx45 WT and 6E from MDCK cells and Western blotted for Nedd4 and TSG101 (Fig. 2.16). Compared to Cx45 WT, we determined 6E pulled-down significantly more Nedd4 (~2.05-fold $P < 0.01$; WT 1.088 ± 0.085 vs. 6E 0.5297 ± 0.086 ; Fig. 2.16A) and a comparable amount of TSG101 (Fig. 2.16A). The data, consistent with the CHX chase, suggests that the increase in 6E protein expression is likely the result of impaired turnover through decreased association with the E3 ligase Nedd4. Our data also suggests that altered recycling or trafficking to the lysosome is not a contributor to the phenotype.

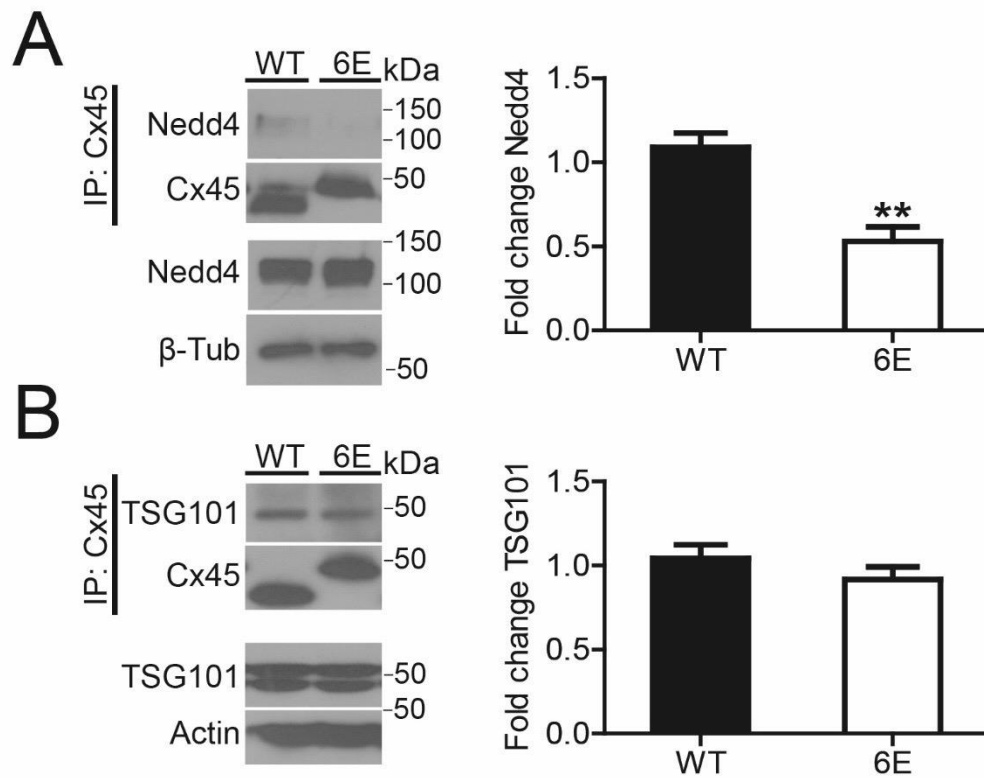


Figure 2.17. Inhibiting Cx45CT dimerization correlates with decreased associated of Nedd4 but not TSG101.

MDCK cells stably expressing Cx45 WT or 6E were cultured, lysed, and captured by IP to assess interactions with Nedd4 and TSG101. A) Representative Western blots of the IP of Cx45 WT or 6E blotting with against A) Nedd4 (n=3, **P<0.01) and B) TSG101 (n=3; ns) pulled-down by either Cx45 WT or 6E. Data presented as mean fold change + s.e.m. relative to the first WT replicate. Statistics are two-tailed unpaired Student's T-test. This figure is modified from Trease et al., (2017).

7.12 The Cx45CT A333-N361 Contains a Potential CaM IQ Motif

Another protein known to regulate channel closure for Cxs is CaM [239]. Work from a number of laboratories including our own, have identified CaM binding sites in the Cx43 CL and CT domains (Sorgen Laboratory, unpublished data; [238, 246]). Previously, we demonstrated a direct interaction of CaM with the Cx45CT domain over residues (Y275-P288 and T302-N314) [247]. We posited that CaM may serve a similar function for Cx45 and sought to determine if there were additional CaM binding sites in Cx45. Using the online bioinformatics resource Calmodulin Target Database Binding Site Search and Analysis tool (<http://calcium.uhnres.utoronto.ca/ctdb/ctdb/sequence.html>), we scanned the full-length Cx45 sequence as well as the isolated CL and CT for additional potential CaM binding sites (Fig. 2.17). The analysis suggests that potential CaM binding sites exist in both the Cx45 CL and CT. Interestingly, when analyzing our isolated CL sequence, no CaM binding motif was identified, but one was identified for the CL in the full-length sequence, suggesting that sequence information contained outside the CL was essential for prediction. Furthermore, the region identified as a direct interaction with the Cx45CT by NMR was not identified by motif prediction either. Focusing the on the CT domain we determined the predicted motif was an IQ type ([FILV]Qxxx[RK]Gxxx[RK]xx[FILVWY]; underlined in Fig. 2.17), and furthermore determined that our 6E mutations eliminated the motif by mutating the first essential bulky hydrophobic residue to Glu (L338E). As the dimerization domain of Cx45 is not amenable to NMR interaction studies as conditions that disrupt dimerization would disrupt most interactions, we decided to modify an existing calcium flux sensing tool (GCaMp2) to meet our needs. GCaMp2 is a second-generation calcium sensor that uses a fusion protein of the canonical CaM binding protein domain (M13 domain of myosin light chain kinase), CaM, and a (cyclically) modified eGFP to produce fluorescent signal in response to CaM binding to M13 in the presence of Ca²⁺ [449]. We modified this construct to replace the M13 domain with the dimerization domain region (A333-N361) of either Cx45 WT or 6E. After creating stable expressing MDCK cells we used live imaging to determine if each protein

Cx45

```

1 MSWSFLTRLL EEIHNHSTFV GKIWLTVLIV FRIVLTAVGG ESIYYDEQSK
0000000000 0000000000 0000000000 0000000000 0000000000

51 FVCNTEQPGC ENVCYDAFAP LSHVRFWVFQ IILVATPSVM YLGYAIHKIA
0000000000 0000000000 0000000000 0000000000 0000000000

101 KMEHGEADKK AARSKPYAMR WKQHRALEET EEDHEEDPMM YPEMELESEK
0000000000 0000000000 0000000000 0000000000 0000000000

151 ENKEQSQPKP KHDGRRRIRE DGLMKIYVLQ LLARTVFEVG FLIGQYFLYG
0000000000 0001357999 9999999999 9997531000 0000000000

201 FQVHPFYVCS RLPCPHKIDC FISRPTEKTI FLLIMYGVTG LCLLLNIEWM
0000000000 0000000000 0000000000 0000000000 0000000000

251 LHLGFGTIRD SLNSKRRELD DPGAYNYPFT WNTPSAPPGY NIAVKPDQIQ
0000000000 0000000000 0000000000 0000000000 0000000000

301 YTELSNAKIA YKQNKANIAQ EQQYGSHEEH LPADLETLQR EIRMAQERLD
0000000000 0000000000 0000000000 0001111111 1111111111

351 LAIQAYHHQN NPHGPREKKA KVGSKSGSNK SSISSKSGDG KTSVWI
1110000000 0000000000 0000000000 0000000000 000000

```

Cx45CL

```

99 IAKMEHGEAD KKAARSKPYA MRWKQHRALE ETEEDHEEDP MYPEMELES
0000000000 0000000000 0000000000 0000000000 0000000000

175 EKENKEQSQP KPKHDGRRRI REDGLMK
0000000000 0000000000 00000000

```

Cx45CT

```

265 KRRELDDEPGA YNYPFTWNTS SAPPYGNIAV KPDQIQYTEL SNAKIAYKQN
0000000000 0000000000 0000000000 0000000000 0000000000

315 KANIAQEQQY GSHEEHLPAD LETLOREIRM AQERLDLAIQ AYHHQNNPHG
0000000000 0000000009 9999999999 9999999990 0000000000

365 PREKKAKVGS KSGSNKSSIS SKSGDGKTSV WI
0000000000 0000000000 0000000000 00

```

Figure 2.18. *In silico* prediction of Cx45 CaM binding motifs.

Full length Cx45 (mouse) as well as the CL and CT domains in isolation were analyzed by the Calmodulin Target Database Binding Site Search and Analysis tool for putative CaM binding motifs. Areas highlighted in red are predicted CaM interaction motifs, residues within the motifs that are mutated in Cx45 6E are bold and underlined. <http://calcium.uhnres.utoronto.ca/ctdb/ctdb/sequence.html>

possessed Ca²⁺ responsiveness as a method to interpret CaM binding to the domain. We used the original GCaMp2 (M13) as positive control for the experiment. To accomplish the assay cells were seeded in live imaging dishes in phenol free DMEM and maintained at 37°C 5% CO₂ for the duration of the experiment. Images were acquired every 5 s for 3 min, the dishes were then treated with 15 μM of the Ca²⁺ ionophore, Ionomycin, and images were acquired for an additional 3-5 min in 5 s intervals. Addition of ionomycin to the control GCaMp2 expressing cell resulted in an acute sharp increase in MFI that returned to baseline rapidly (Fig. 2.18). For both Cx45 WT and 6E, addition of the ionomycin did not result in any appreciable increase in MFI (Fig. 2.18). The data indicates the A333-N361 region of Cx45—although predicted to bind CaM—does not, and furthermore mutation to the 6E does not alter this. Altogether indicating that differential CaM binding is not a factor which contributes to the 6E phenotype.

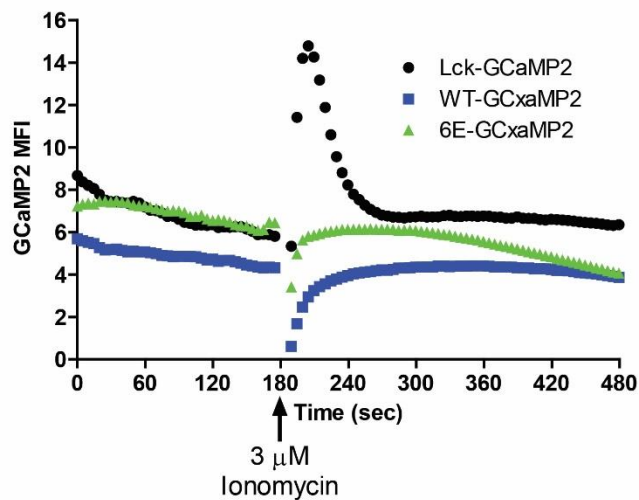
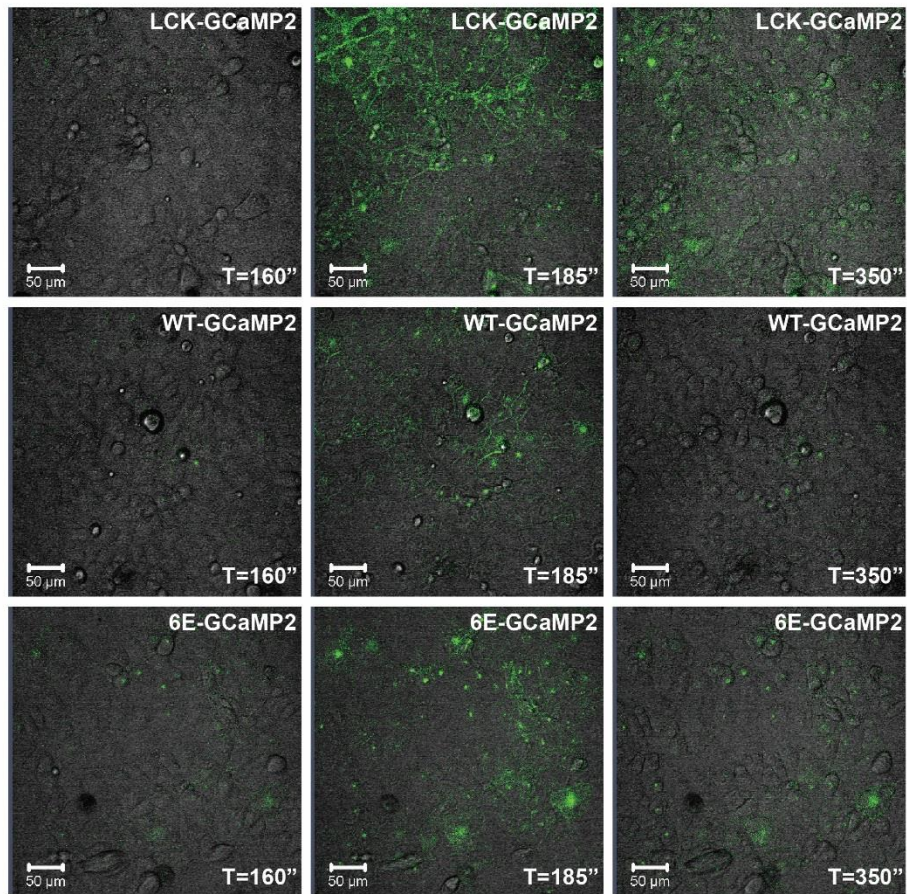


Figure 2.19. Cx45CT A333-N361 does not bind CaM.

MDCK cells were stable transfected with A) LCK-GCaMP2, B) WT-GCaMP2, or C) 6E-GCaMP2, clonally selected and live imaged. To assess CaM binding eGFP fluorescence (green) images were acquired every 5 s for 8 min. After 3 min of baseline acquisitions the dishes were treated with 3 μ M ionomycin to activate CaM. The mean fluorescent intensity of eGFP was recorded throughout.

8. Discussion

Previous work from our laboratory revealed that the Cx45 family member has a unique structural feature compared to other family members, high affinity dimerization ($K_D \sim 100$ nM) [247]. This dimerization was mediated by the region comprised of residues A333-N361, which are highly conserved (72.4%) across several species including mouse, rat, hamster, chicken, dog, and human. In fact, 5/6 of the critical hydrophobic residues are identical in all orthologs and the other highly conserved (Fig. 2.19). Based on results of a protein BLAST search with Cx45CT residues A333-N361 as the query, limited to comparisons within the human genome, no significant homology to any other protein exists, demonstrating this sequence and structure is unique to Cx45. The importance of protein binding interactions to the regulation of other CxCT domains (especially that of the Cx43CT) suggests that this interaction between Cx45CT domains, in part, influences the unique channel properties of Cx45 GJs. Furthermore, it is reasonable to posit that inhibition of this dimerization would also modulate Cx45 channel properties and function. From our studies contained herein, the inferred effects we observed through inhibiting dimerization include: increased protein at the plasma membrane due to inhibited degradation, decreased plaque formation, increased hemichannel activity, retained regulation by Ca^{+2} , increased Tyr phosphorylation, decreased interaction with β -tubulin and Nedd4, increased interaction with Drebrin, maintained interaction with ZO-1, and increased macroscopic currents.

Very few studies have characterized the functional role of the Cx45CT domain, and many were limited to a context in which Cx43 was co-expressed. In one such study, chicken Cx45 WT and CT truncation mutants (deletion of either the last 34 or 37 residues) were exogenously expressed in rat osteosarcoma cell line (ROS) which endogenously expresses Cx43 [450]. In each circumstance, the Cx45 WT or mutants were transported to the plasma membrane and the Cx45 WT and $\Delta 34$ displayed a punctate staining pattern reminiscent of what we show for Cx45 WT, however, the Cx45 $\Delta 37$ displayed a more linear distribution about the plasma membrane [451].



Figure 2.20. Sequence alignment of the Cx45CT dimerization domain (A333-N361) from different species.

Sequence alignment of the A333-N361 region using Clustal Omega to all available Cx45 RefSeq sequences revealed a high degree of conservation within this region, with 72.4% identical, 20.6% conserved, and 6.9% non-conserved residues. For clarity, the sites of point mutations in the Cx45 6E construct are indicated by the single letter code above the alignments. Degree of site conservation (excluding Cx45 6E mutations) is indicated at the bottom, * = identical, : and . = high conservation and intermediate conservation, respectively. Reprinted from Trease et al., (2017).

Notably, neither truncation deleted any of the critical hydrophobic residues previously shown to be involved in CT dimerization. One important difference between the two mutants was the ability to co-IP ZO-1, which was inversely correlated with TX-100 solubility (Cx45 Δ 37 did not co-IP ZO-1 and was more TX-100 soluble) [451]. The authors suggested the lack of association with ZO-1 may have prevented Cx45 Δ 37 from being pulled from lipid rafts, and that WT Cx45 may have a complex extended binding with ZO-1 or may harbor two smaller binding sites [451]. Previous work from our laboratory using the CT domain of mouse Cx45 did not observe an extended interaction of the Cx45CT with the PDZ2 domain of ZO-1, when compared to the binding of Cx43CT [247, 286]. However, without being able to follow the resonances of the Cx45 dimerization domain the possibility still exists that complex binding with ZO-1 occurs.

We observed a similar phenotype with the 6E, such that changes in the association with the cytoskeleton (decreased association with β -tubulin and conversely increased association of Drebrin) and proteins involved in Cx degradation (decreased binding of Nedd4) correlated with altered membrane localization, GJIC, and preferential segregation into TX-100 soluble pools. Other studies utilizing truncated forms of Cx45 highlight possible functional regulation mediated by the Cx45 CT domain, however, whether dimerization of the Cx45CT domain in these studies is a contributing factor is not clear. The aspects investigated in these studies include regulating GJ conductance, channel permeability, and the ability of Cx45 to interact with Cx43 [189, 450, 452, 453]. Koval et al. demonstrated that Cx45 Δ 37 enhanced communication of larger tracer dyes [450]. The same study also demonstrated that Cx45 channels are more selective of being the dye recipient cell than the dye donor cell compared to the truncated mutant when forming heterotypic GJs with Cx43 [450]. Similar to Koval et al., the Laing et al. study observed increased dye coupling of for the Cx45 Δ 37 as well as the Cx45 Δ 34 mutant, compared to WT Cx45 [450, 451]. We similarly observed a decrease in the co-IP of ZO-1 with Cx45 6E compared to WT (albeit non-significant) which correlated with increased TX-100 solubility, lending support to Laing's hypothesis [424, 451]. A difference we observed was the impaired communication of 6E [424]. Notably, from the results of the Kopanic et al. study, truncation of the CT at residues c-terminal to the critical Y356 would be expected to increase dimerization affinity between CTs due to decreased intrinsic disorder (as was

seen with the A333-N361 peptide) [247]. Taken together with the observation of increased dye coupling in the ROS cells with Cx45 truncations (increased dimer strength = increased communication), this further supports our hypothesis that dimerization is essential for Cx45 coupling. An interesting finding was that expression of the Cx45CT domain together with a Cx43 mutant truncated after the 4th transmembrane domain could not restore pH sensitivity to Cx43CT truncated channels, while co-expression of the Cx40CT could [229]. Another important result of the truncation studies is that if the Cx45CT was used to replace that of either Cx43 or Cx40 (i.e., Cx43-Cx45CT or Cx40-Cx45CT), they failed to form functional channels [453]. Potentially highlighting, a critical effect of Cx45CT dimerization.

Many aspects of Cx regulation involve phosphorylation of the intracellular domains [308, 326-328]. The addition of a strong negative charge arising from the phosphate group has been shown to affect the channel permeability to ions, influence the structure and positioning of the transmembrane domains thereby altering pore size, or modulate the affinities of the extensive number of protein partners which regulate Cxs. Importantly, if phosphorylation affects the rate of either channel assembly/trafficking or turnover/degradation (e.g., Nedd4; [203, 204, 447]), GJIC will be impacted. A limited number of studies have focused on determining how phosphorylation regulates Cx45. Phosphoamino acid analysis of Cx45 identified phosphorylation of Cx45 Ser, Thr, and Tyr residues [189]. Furthermore that same study determined that deletion of the final 26 residues of the Cx45 CT (containing 9 Ser) greatly reduced phosphorylation [189]. A few studies have explored differences and similarities in the regulation of Cx45 and Cx43 by Ser phosphorylation and highlight little conservation of effect. For example, PKA activation by stimulation with the cAMP analogue, 8-Br-cAMP, reduced the junctional conductance of Cx45 channels while increasing that of Cx43 [306, 454]. This was in contrast to activation of protein kinase G (PKG) by 8-Br-cGMP which was shown to have little-to-no effect on conductance of Cx45 channels, but severely impaired Cx43 junctional conductance [306, 454]. In two studies, activation of PKC by the phorbol ester PMA was shown to decrease Cx43 junctional conductance [86], however, the same studies show conflicting results for Cx45 with an increase in conductance in one [306] and decreased in the other [86]. Of note, in the Martinez et al. [86] study, decreased

junctional conductance of the Cx45 channels did not correlate with decreased transfer of the tracer NB through Cx45 channels, although it did correlate with decreased NB transfer through Cx43 channels. Finally, phosphorylation of Cx45 unlike that of Cx43 did not alter the single channel conductance of Cx45 (22 pS and 42 pS) (35). The authors suggesting phosphorylation affects the open probability of Cx45 GJ channels [306], however, taken together with the decreased junctional conductance and unaffected NB transfer it may be more likely channel permselectivity is altered.

Despite a number of differences in the regulation of Cx45 and Cx43 by Ser phosphorylation, a commonality exists in the regulation of junctional conductance by pervanadate. Through direct inhibition of Tyr phosphatases, pervanadate indirectly promotes increased Tyr phosphorylation of the CT domain of both Cx43 and Cx45 subsequently impairing GJIC [306, 455, 456]. It is, however, unclear whether the mechanism(s) (e.g., altered localization vs. open probability) that achieve this are the same. An example suggesting they may differ is Cx43 in cells treated with pervanadate localizes intracellularly [457], conversely we observed that Cx45 is still localized at the plasma membrane. A likely explanation for this is the only established Tyr kinases that phosphorylate Cx43 (Src and Tyk2; residues Y247, Y265, and Y313) disrupt Cx43 cytoskeletal anchoring by directly displacing β -tubulin and Drebrin [377, 378]. Unlike Tyk2, Src also indirectly displaces ZO-1 by competing for PDZ2 domain binding titrating ZO-1 away from Cx43 [377, 378]. Conversely to Cx43, the CT of Cx40 is capable of simultaneously interacting with Src and ZO-1 [285]. Displacement of Cx43 from the microtubules and actin cytoskeleton would explain the observed intracellular localization of Cx43. In our study, although Tyr kinases were not identified, increased basal Tyr phosphorylation of 6E correlated with a decreased (albeit not statistically significant) interaction with ZO-1 (actin) and β -tubulin (microtubules), increased association with Drebrin (actin), and a decreased interaction with Nedd4. Consistent with previous literature reports, our results further implicate ZO-1 in the regulation of GJ plaque size and accretion [458, 459], and supports the notion that β -tubulin is essential for plaque formation [167, 460, 461] while Drebrin stabilizes Cxs present at the appositional membrane [378, 379]. These studies in conjunction with our findings would explain how pervanadate had no effect on Cx45 hemichannel activity in either the presence or absence of Ca^{+2} .

Cell-cell coupling in healthy adult ventricular GJs primarily consists of Cx43, however, in end-stage heart failure or the epicardial border zone after infarct, remodeling of Cx43 (decreased expression and lateralization) sets the stage for an arrhythmic substrate. The remodeling of Cx43 although well tolerated, when coupled with aberrant upregulation of Cx45 expression (normally very low in adult ventricles) greatly enhances propensity for lethal arrhythmias [83, 431, 462]. It is likely this is in part mediated by the restrictive electrical properties of Cx45 channels (low conductance, high voltage-sensitivity), and the fact that heteromeric Cx45/Cx43 channels are more similar in electrical properties to Cx45 homomeric channels than that of Cx43 [463]. A number of studies have highlighted the tendency for Cx45/Cx43 heteromeric channels to elicit properties indicative of a dominant negative effect of Cx45 on Cx43 [31, 82, 86, 452, 464]. Furthermore, with the dimerization of Cx45CT occurring prior to channel oligomerization in the TGN, it is likely that stoichiometry within heteromeric GJ channels would favor incorporation of a minimum of two Cx45 subunits. Whether this is enough to exert the dominant negative effect remains to be explored but depending on the subunit arrangement it would not be unexpected for the dimerization of the Cx45CT to exert some steric force on the transmembrane domains potentially altering pore structure/diameter. Unfortunately, little work has been done to explore how the unique properties of Cx45 channels make its expression in the ventricles detrimental. Based on our findings in this study, Cx45CT dimerization is a structural feature essential to proper Cx45 function. Future studies should focus on determining exactly what regulatory role(s) are mediated by Cx45CT dimerization, especially if Cx45 dimerization is a key contributor to the dominant negative effect on Cx43-Cx45 heteromeric channels and whether it controls stoichiometry and subunit arrangement. Furthermore, it should be investigated how kinases and specific CT binding partners that regulate Cx43 also Cx45 function.

CHAPTER THREE

Chimeric Cx45 Proteins Confirm Cx45CT Dimerization Regulates Localization, Hemichannel Activity, and GJIC

9. Introduction

In Chapter Two, we used a mutant of Cx45 which abolished CT domain dimerization through the replacement of six hydrophobic residues with six Glu residues [424]. The absence of dimerization in that context suggested that dimerization was a key structural element required for the proper function of Cx45. Loss of dimerization correlated with increased plasma membrane localization, hemichannel activity (dye uptake and macroscopic currents), and basal Tyr phosphorylation, as well as decreased turnover, GJ plaque formation, and GJIC (measured by dye coupling). Altered cytoskeletal interactions via Drebrin, β -Tubulin, and ZO-1 were also observed. While the data offers a suggestive link between CT dimerization and channel function, a few important questions remain. Was the phenotype in part mediated by altered charge of the CT (net charge Cx45 WT = -1 vs. 6E = -7; pI Cx45 WT = 6.97 vs. 6E = 6.16)? Are there sequence or structure specific features of the dimerization domain or is the requirement simply for a dimer?

The current link between CT dimerization and GJ function is, however, only correlative at this point. This is more complex when the CT domain of the cardiac Cxs were swapped [453]. By replacing the CT domain of either Cx43 or Cx40 with that of Cx45 GJs were rendered non-functional [453]. Furthermore, replacement of the Cx45CT domain with the CT of either Cx43 or Cx40 resulted in GJs that functioned comparable to WT, albeit GJ plaque size was altered [453]. Interestingly, truncation of Cx45 at position 272 resulted in channels that failed to traffic properly, while the Cx45-Cx43CT or Cx45-Cx40CT mutants trafficked normally, which suggests that for Cx45 channels a CT domain is essential to proper trafficking [453]. Taken together this also suggests that Cx45CT dimerization may be essential for Cx45 function in the context of its own CT domain. In order to further investigate this we sought to use alternative modifications to the Cx45CT to modulate dimerization. In this Chapter, we use a combinatorial approach of biophysical, cell biology, and biochemical studies with chimeric, deletion, and scrambled Cx45 constructs to address these questions more directly. Similar to what we observed by inhibiting the dimerization with the 6E mutant, we observed increased membrane localization, TX-100 solubility, and hemichannel dye uptake in all mutants that disrupted dimerization. For mutants that maintained dimerization, we observed punctate GJ localization and GJ plaque formation (TX-100 insolubility) that were

comparable to Cx45 WT. To our surprise when we assessed GJIC by scrape loading we observed variable results suggesting a more complex mechanism regulates Cx45 coupling.

10. Materials and Methods

10.1 Expression and Purification of Recombinant GST-tagged Proteins

Constructs designed for this project are summarized in Table 4. Cx45CT WT and mutants were expressed and purified as previously described [247].

10.2 Analytical Ultracentrifugation (AUC): Sedimentation Equilibrium

AUC experiments were performed as previously described with minor modifications [247]. Briefly, purified recombinant proteins were buffer exchanged (if necessary) into 1x PBS pH 7.4 using a Nap 5 (GE Healthcare) column per manufacturer directions. Proteins were then loaded into either an AN-50Ti or AN-60Ti rotor (Beckman Coulter; Indianapolis, IN) at three concentrations (Abs_{280} nm of 0.5, 0.7, and 0.9) and speeds (15,000, 18,000, 21,000, and 24,000 RPM). Sedimentation equilibrium experiments were performed at either 7°C or 20°C with a Beckman Optima XL-I analytical ultracentrifuge. Data were collected at various rotor speeds. Absorbance scans at 280 nm were acquired after 12 hr, 14 hr, and 16 hr at each speed; attainment of equilibrium was confirmed by overlay of all four time points. Analysis of the sedimentation equilibrium data was performed using the Beckman XL-A/XL-I software package ORIGIN v6.0. Sednterp (<http://www.rasmb.bbri.org>) was used to calculate the buffer viscosities and densities as well as the partial specific volume for each protein based on the primary sequence.

10.3 Circular Dichroism (CD): Secondary Structural Analysis

CD experiments were performed as described previously [247]. Briefly, data was collected with a Jasco J-815 spectrophotometer with a Peltier temperature control system (Easton, MD). Spectra for the protein samples were acquired in 1x PBS pH 7.4. For each sample, 5 scans (wavelength range: 190–250 nm; response time: 1 s; scan rate: 50 nm/min; bandwidth 1.0 nm) were collected using a 0.01 cm quartz cell and processed using Spectral Analysis (Jasco). Spectra are presented as the averaged change in molar residual ellipticity (MRE; degree cm^2 $dmol^{-1}$) over wavelength following buffer subtraction. Protein concentrations were determined using a NanoDrop 1000 (Thermo Scientific; Wilmington, DE) at 280 nm.

Protein	Source of Chimeric Region
Cx45 WT	NA; Wild-type, K265-I396
Cx45 6E	NA; L335/L338/I342/L349/I353/Y356E
Cx45 DDSc	NA; A333-N361 randomly scrambled
Cx45 GCN4 _{LZ}	<i>S. cerevisiae</i> GCN4 R ²⁴⁹ MKQLEDKVEELLSKNYHLENEVARLKKLVGER ²⁸¹ TS (plus TS linker)
Cx45 Bsub _{VD}	<i>E. coli</i> F1/F0 ATP Synthase V ²⁵ WPPLMAAIEKRQKEIADGLASAERAH ⁵³ KD ⁵³
Cx45 Bsub _{AA}	<i>E. coli</i> F1/F0 ATP Synthase A ³¹ AIEKRQKEIADGLASAERAH ⁵⁹ KDL ⁵⁹ DLAKA ⁵⁹
Cx45 ΔDD	NA; Deletion of Cx45CT A333-N361
Cx45 40 _{MD}	<i>R. norvegicus</i> P ³⁰⁶ EEGFIHTQYGQKPEQPSGAS ³²⁶
Cx45 43 _{MD}	<i>R. norvegicus</i> Cx43 F ³³⁵ DFPDDNQNAKVAAGHELQPLAIVDQR ³⁶²

Table 4. Source of homologous and heterologous Cx45 mutants.
NA – not applicable (source is *M. musculus* Cx45)

10.4 Cell Culture and Stable Cell Line Generation

MDCK cells (gift from Dr. Paul Lampe, Fred Hutchinson Cancer Center) were cultured in Dulbecco's modified Eagle medium (Corning) at 37°C in a humidified 5% CO₂ atmosphere. Medium was supplemented with 10% FBS (Seradigm), 2 mM L-glutamine (HyClone), 1% pen-strep (Corning), and 0.2% Normocin (Invivogen). The selective agent puromycin (Tocris) was used, when appropriate, at empirically determined concentrations. 70% confluent MDCK cells were lipofected with indicated Sall linearized plasmid using MDCK Avalanche (MDCK; 2.5:3.5) in OptiMem. Transfections were carried out under antibiotic free conditions, and cells were cultured 48-72 hr prior to addition of selection media. MDCK were selected with 5 µg/mL. Cells were clonally (monoclonal) selected using Whatman paper cloning disks. Western blots and immunofluorescence were used to screen clones.

10.5 Antibodies and Immunostaining

All primary and secondary antibodies, detection reagents and concentration ranges utilized are summarized in Table 2. Cells seeded on glass coverslips were rinsed 2x with 1x PBS and then fixed and permeabilized with either ice cold methanol at -20°C for 15 min or buffered formalin (1x PBS, 3.7% formaldehyde, 0.3% TX-100) at 37°C for 30 min. Coverslips were washed 3x 5 min in 1x PBS with gentle agitation and then blocked for 60-90 min at 37°C (1x PBS containing 1% BSA and 0.3% TX-100). Coverslips were then incubated with the indicated primary antibodies diluted in blocking buffer for either 1 hr at RT or ON at 4°C. Coverslips were washed 3x with 1x PBS and then incubated with secondary antibody (if necessary) 1 hr at RT and then washed 1x for 5 min with 1x PBS containing 100 ng/mL DAPI and then 2x 5 min with 1x PBS. Coverslips were mounted with SlowFade (LifeTech) and sealed with clear nail polish and imaged. All images acquired on either a Zeiss 710 or 800 LSM microscope.

10.6 Cell Lysis for Direct Western blot

Cultured cells were rinsed 2x with 1x PBS and then incubated with protease inhibitor buffer (PIB; 1x PBS containing 1x Roche Complete + EDTA, 2 mM PMSF, 2 mM Pepstatin A) on ice for 20 min and then harvested with a cell scraper. Cell suspensions were pelleted at 1500 RPM for 5

min at 4°C. PIB was removed and cell pellet resuspended in an appropriate volume of lysis buffer (PIB + 1% TX-100, unless otherwise specified), mechanically lysed and incubated on ice for 30 min. Lysates were quantified by BCA and normalized with lysis buffer. 30 µg of total protein lysate (unless otherwise indicated) was resolved.

10.7 Western blot

Protein samples were resolved by SDS-PAGE with an appropriate gel concentration, transferred to PVDF (Millipore), blocked either 2 hr at RT or ON at 4°C with either 5% non-fat milk/PBST or 5% BSA/TBST and incubated with indicated primary antibody in blocking buffer either 1 hr at RT or ON at 4°C. Blots were washed 3x for 10 min with either PBST or TBST, and then incubated for 1 hr at RT with secondary antibody. Membranes were then washed 4x 10 min each with either PBST or TBST and detected using Signal West Femto kit (Thermo) per manufacturer protocol and exposed to autoradiography film. Quantifications were done using NIH ImageJ software using a minimum of three independent replicates.

10.8 Triton X-100 Solubility Assay

The TX-100 solubility assay was modified from a method described previously [412]. Briefly, MDCK cells grown in 10-cm dishes were washed with PBS and incubated in 1 mL PIB for 20 min at 4°C, harvested in the same buffer and gently pelleted. Supernatant was aspirated, and cell pellet was resuspended in 1 mL of fresh PIB supplemented with 50 units of Benzonase and mechanically lysed. Lysates were quantified by BCA and normalized. A total of 450 µL of cell lysate was brought to 1% SDS with 10% SDS and reserved as total lysate. Another 450 µL was brought to 1% TX-100 with 10% TX-100 in 1x PBS and incubated at 4°C for 30 min with agitation. The TX-100 lysate was then separated into non-junctional (supernatant; soluble) and junctional (pellet; insoluble) fractions by ultracentrifugation at 100,000 xg for 1 hr at 4°C. The supernatant was carefully removed and retained as the soluble fraction. The pellet was solubilized in 500 µL of solubilization buffer (1x PBS, 8 M urea, 2.5% SDS, 0.1 M DTT, 1x Roche complete + EDTA, 2 mM PMSF, and 2 µM Pepstatin A). Volume normalized samples of total lysate (T), TX-100 soluble (S) and TX-100 insoluble (I) portions were analyzed by Western blot. Soluble and insoluble fractions

were quantified as a function of total lysate. Quantification was done using NIH ImageJ software from three independent replicates.

10.9 Scrape Loading Dye Transfer Assay

Cells were scrape loaded as previously described [340]. Briefly, all buffers were pre-warmed to 37°C prior to beginning the experiment. Stable expressing MDCK clones were seeded on bovine plasma fibronectin (Sigma; 10 µg/mL) coated 35 mm live imaging dishes (CellStar). MDCK cells were transfected with Cx43 siRNA with Lipofectamine RNAiMAX (LifeTech) according to manufacturer protocol and then cultured for 48 hr prior to scrape loading. After transfection cells were washed 1x with 1x PBS and then overlaid with dye tracer mix (1x PBS containing NB). Scrapes were introduced using a fine edged micro-scalpel and incubated at RT for 1 min. Tracer dye was gently washed away with 1x PBS and media was added and the cells returned to the incubator to culture for 5 min to allow dye to transfer. Following the dye transfer period, the cells were washed with 1x PBS containing 1 mM CaCl₂ and 1 mM MgCl₂ to stop dye spread. Coverslips were then formalin fixed and stained as described above and imaged. 15 consecutive fields of view were acquired per replicate.

10.10 Hemichannel Dye Uptake Assay

To assess hemichannel activity we modified the protocol described by [442]. Briefly, all buffers were pre-warmed to 37°C prior to beginning the experiment. MDCK clones expressing either Cx45 WT or 6E were seeded on glass coverslips were cultured to approximately ~90% confluent. Some wells were pretreated with 50 µM carbenoxolone (CBX; AbCam) for 15 min prior to Ca²⁺ washout and dye uptake. The presence of CBX was maintained during dye uptake. Cells were rinsed 1x with HBSS + Ca²⁺/Mg²⁺ (LifeTech) and then 2x with HBSS – Ca²⁺/Mg²⁺ (LifeTech). Cells were then incubated at 37°C with HBSS – Ca²⁺/Mg²⁺ containing NB (0.1 mg/mL; Vector labs) for 10 min. Cells were then washed 2x with HBSS + Ca²⁺/Mg²⁺ to close hemichannels and GJs. Cells were formalin fixed and stained with streptavidin 647 conjugate (LifeTech) and imaged. Control cells were treated identically except all incubations were done in HBSS + Ca²⁺/Mg²⁺. 15 fields of view were acquired per sample.

10.11 Statistical Analysis

All data were analyzed by using GraphPad Prism 5.0 and were presented as the mean + s.e.m. Statistical analysis performed in GraphPad Prism 5.0 was either one-way ANOVA with a Bonferroni post-test comparing all samples to either Cx45 WT or 6E. P-values <0.05 were considered statistically significant.

11. Results

11.1 Design of Cx45CT Chimeric Constructs

Since our previous study made use of a single dimerization incompetent Cx45 we sought to design novel constructs that would either maintain or inhibit dimerization while assessing the requirement for any Cx45 sequence specific regulatory roles of the A333-N361 region. To accomplish this, we substituted Cx45CT A333-N361 with: a comparable helical dimer (Cx45CT GCN4_{LZ}), helical monomer (Cx45CT Bsub_{VD} and Bsub_{AA}), scrambled Cx45CT A333-N361 (Cx45CT DDSc), unstructured monomeric homologous regions of Cx40CT (Cx45CT 40_{MD}) and Cx43CT (Cx45CT 43_{MD}), and finally deletion of Cx45CT A333-N361 (Cx45CT Δ DD). A summary of the chimeric proteins (source and sequence of substitution) is contained in Table 4. To determine if the chimeric constructs would result in discernable interacting faces (i.e., hydrophobic or electrostatic) the substituted residues were modeled using a helical wheel and Cx45CT A333-N361 was included for reference (Fig. 3.1). For Cx45CT GCN4_{LZ}, as expected, helical wheel modeling revealed a substantial electrostatic face (blue colors Fig. 3.1) and validated the use of helical modeling for this purpose [465]. Cx45CT Bsub_{VD}, Bsub_{AA}, and DDSc no major electrostatic or hydrophobic faces were detected (Fig. 3.1). Cx45CT Δ DD, 40_{MD}, and 43_{MD} were not modeled as deletion of the domain removes the structure, and the structures of both regions of Cx40 and Cx43 are published [231, 277].

11.2 Biophysical Characterization of Cx45CT Mutants

Following our helical wheel modeling of the Cx45CT mutants we next wanted to test their ability to dimerize. To test this, we first expressed and purified Cx45CT WT, Cx45CT DDSc, Cx45CT GCN4_{LZ}, Cx45CT Bsub_{VD}, Cx45CT Bsub_{AA}, and Cx45CT Δ DD from *E. coli* (Cx43CT and commercial lysozyme were used as purity comparisons; Fig. 3.2). Proteins (Cx45CT WT, Cx45CT DDSc, Cx45CT GCN4_{LZ}, Cx45CT Bsub_{VD}, Cx45CT Bsub_{AA}, and Cx45CT Δ DD) were then analyzed by AUC sedimentation equilibrium at three concentrations ($Abs_{280} = 0.9, 0.7, 0.5$) across of number of rotor speeds (curves not shown). A summary of the results is contained in Table 5. For Cx45CT

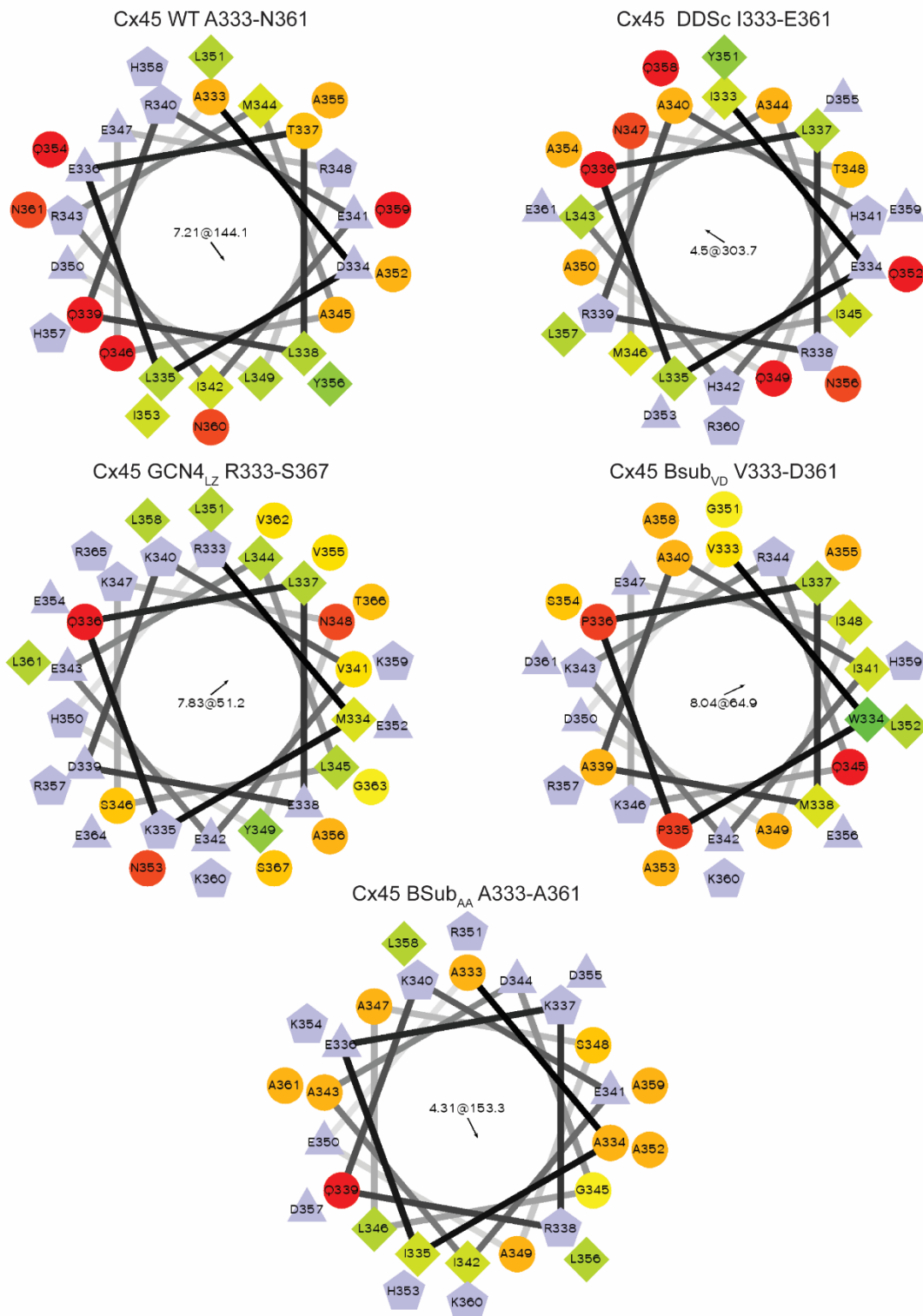


Figure 3.1. Helical wheel analysis of heterologous and scrambled Cx45 mutants. The region corresponding to A333-N361 of Cx45 WT, heterologous, and scrambled homologous mutants were modeled as α -helices and presented as a helical wheel projection. Blue colored residues are electrostatic, green colored residue are bulky hydrophobic, orange represent small side chain, and red are neutral.

WT we observed similar mass and dimerization affinity as in [247]. For Cx45CT GCN4_{LZ}, as predicted, we observed the protein in a dimer conformation as indicated by an observed mass of approximately 2-fold that of the calculated mass. Furthermore, the dimerization affinity ($K_D = 8.38$ nM) was comparable to that of other GCN4 fusion proteins and mutants from [466]. We detected Cx45CT DDSc, Bsub_{AA}, and Δ DD as monomers with observed masses similar to the calculated mass (Table 5). Although we determined a monomeric conformation for Cx45CT DDSc and Bsub_{AA} it is important to note that the observed masses are slightly below the calculated mass and therefore indicate mild degradation. Similarly, we were unable to use the data for Cx45CT Bsub_{VD} because its observed mass indicated substantial degradation (data not shown). Interestingly, for Cx45CT DDSc, although the observed mass is consistent with a monomer conformation the calculated affinity for the monomer-dimer species was 211.39 μ M (Table 5), which in the context of a connexon would be present as a dimer (CT concentration approximately 25 mM in a connexon; [231]). The affinities of Cx45CT Bsub_{AA} and Δ DD were calculated to be 1.45 M and 3.215 mM, respectively. In addition to testing the mutant Cx45CT constructs for dimerization we determined the secondary structure by circular dichroism (CD) spectroscopy (Fig. 3.3). Cx45CT WT (Fig. 3.3; black line) and 6E (Fig. 3.3; tan line) were included in the analysis as structure controls. For Cx45CT GCN4_{LZ} (Fig. 3.3; red line) were observed an increase in the helical character as compared to WT, indicated by increased positivity in the maxima at 195 nm, and more negative minima at 208 and 222 nm. This is not surprising as the length of the GCN4 substitution is 36 residues (Table 4) vs. 29 residues for Cx45CT A333-N361. Our spectra of Cx45CT Bsub_{VD} and Bsub_{AA}, both indicated a loss of helical character indicated by negative MRE values at 195 nm, and loss of the minima at 208 and 222 nm (Fig. 3.3; blue and purple lines respectively). Despite this apparent loss in secondary structure, both curves overlay with the Cx45CT 6E spectra (Fig. 3.3; tan line) and thus based on the Kopanic et al. study, the loss of secondary structure is minimal [247]. As expected for the Cx45CT Δ DD (Fig. 3.3; orange line), the spectra is consistent with deletion of the structured A333-N361 region.

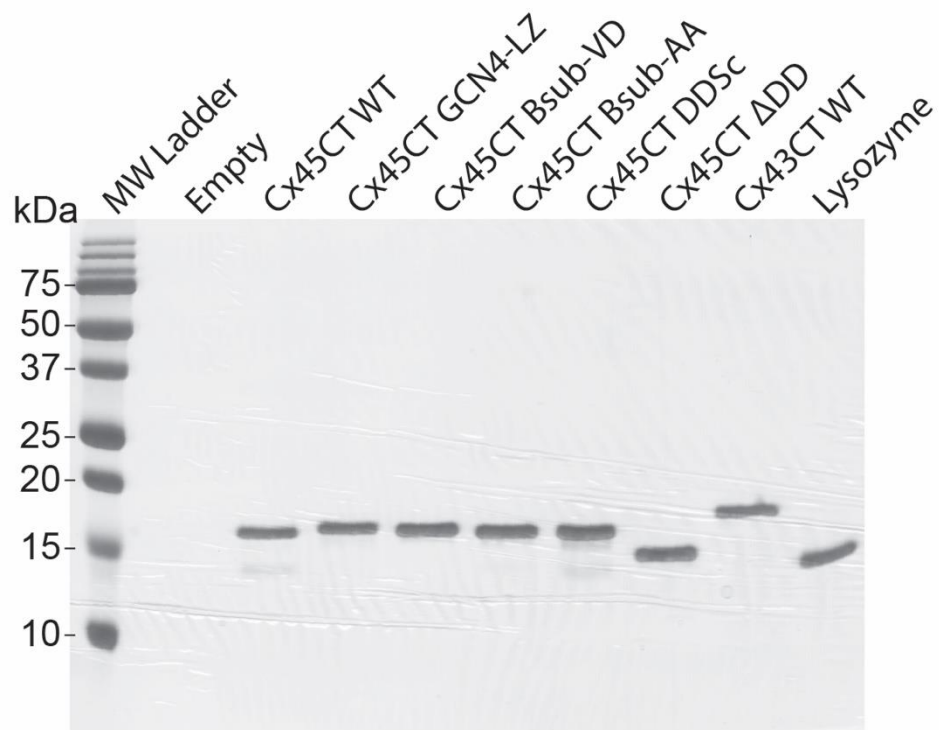


Figure 3.2. Purification of the CT domains of Cx45 WT and mutants. The CT domain of Cx45 WT, Cx45 GCN4LZ, Cx45 BsubVD, Cx45 BsubAA, Cx45 DDSc, and Cx45 ΔDD were cloned into the pGEX-KT vector, expressed in *E. coli*, and purified as in (Kopanic et al. (2014)). Resulting purity of proteins were analyzed by SDS-PAGE. Cx43CT and commercial lysozyme were added as purity controls.

Protein	M_{obs} (kDa)	M_{calc} (kDa)	Conformation	K_D
Cx45CT WT	31.098	15.006	Dimer	101.13 nM
Cx45CT GCN4 _{LZ}	32.068	15.713	Dimer	8.38 nM
Cx45CT DDSc	13.716	15.006	Monomer*	211.339 μM
Cx45CT Bsub _{AA}	12.802	14.647	Monomer	1.45 M
Cx45CT ΔDD	12.088	11.546	Monomer	3.215 mM

Table 5. Summary of observed mass and K_D for Cx45 mutants.

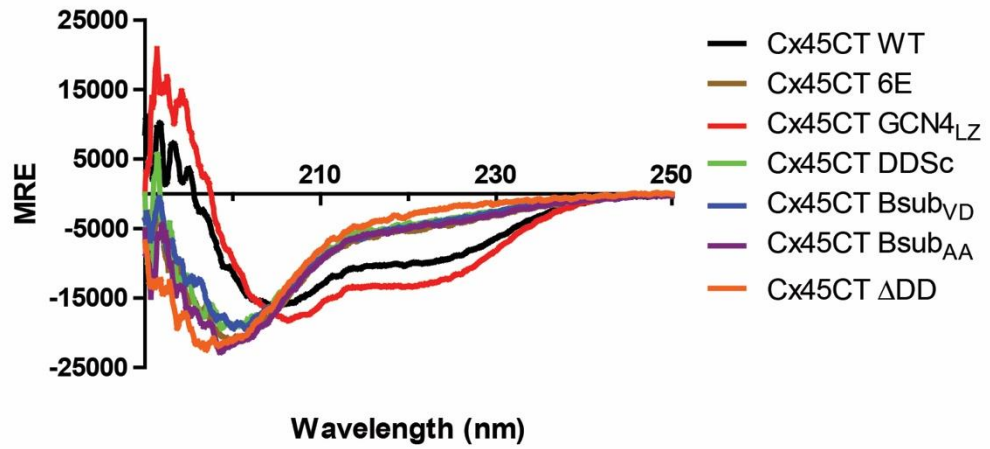


Figure 3.3. Circular dichroism spectra of Cx45CT WT and dimerization domain mutants.

The purified CT domains of the indicated Cx45 WT and mutants were analyzed for secondary structure by CD spectroscopy from 250 – 190 nm. The curves are presented as mean residual ellipticity (MRE).

11.3 Similar to Cx45 6E dimerization incompetent Cx45 mutants display increased plasma membrane localization

To further investigate the functional consequences of inhibiting (or maintaining dimerization Cx45 GCN4_{LZ} and DDSc) we made full-length stable expressing MDCK cell lines of each mutant Cx45CT construct. Similar to our characterization of Cx45 WT and 6E, we initially used immunofluorescence as a tool to determine if localization was affected by the mutations in a manner similar to the 6E cells (Fig. 3.4). Importantly, all the mutants trafficked to the plasma membrane, indicating none of them were confined to intracellular compartments or suffer from misfolding and ERAD [141, 142]. Similar to our results in the previous Chapter, for Cx45 WT we observed punctate staining along the plasma membrane and intracellularly, and linear extended immunoreactivity of the 6E. For both of the dimeric mutants (Cx45 DDSc and GCN4_{LZ}) immunolocalization of the protein was visually comparable to Cx45 WT, with punctate distribution along the plasma membrane and intracellularly (Fig. 3.4). Similar to the 6E, the immunoreactivity for Cx45 BsubAA and ΔDD was more linear and extended about the plasma membrane, with limited intracellular labeling (Fig. 3.4). Interestingly, when we immunostained the Cx45 Bsub_{VD} mutant we observed an intermediate localization phenotype, characterized by longer apparent GJ plaques than Cx45 WT but not as extended as 6E. Furthermore, there was a large contribution from small intracellular puncta (Fig. 3.4). The immunolocalization of the mutants suggests dimerization is an important regulator of Cx45 trafficking.

11.4 Loss of CT Dimerization Results in Decreased TX-100 Solubility

Following from our results in Chapter Two, we hypothesized that since we observed increased plasma membrane trafficking of the dimerization incompetent mutants, they would preferentially segregate into TX-100 soluble fractions. To test this, we lysed the MDCK cells (excluding Cx45 DDSc) mechanically and then incubated in the presence of 1% TX-100 for 1 hr to extract soluble proteins, and then fractionated the lysate by ultracentrifugation. Resulting total, TX-100 soluble, and TX-100 insoluble fractions were then analyzed by SDS-PAGE and Western blot (Fig. 3.5A). Using densitometry, five independent experiments were quantified and all mean values

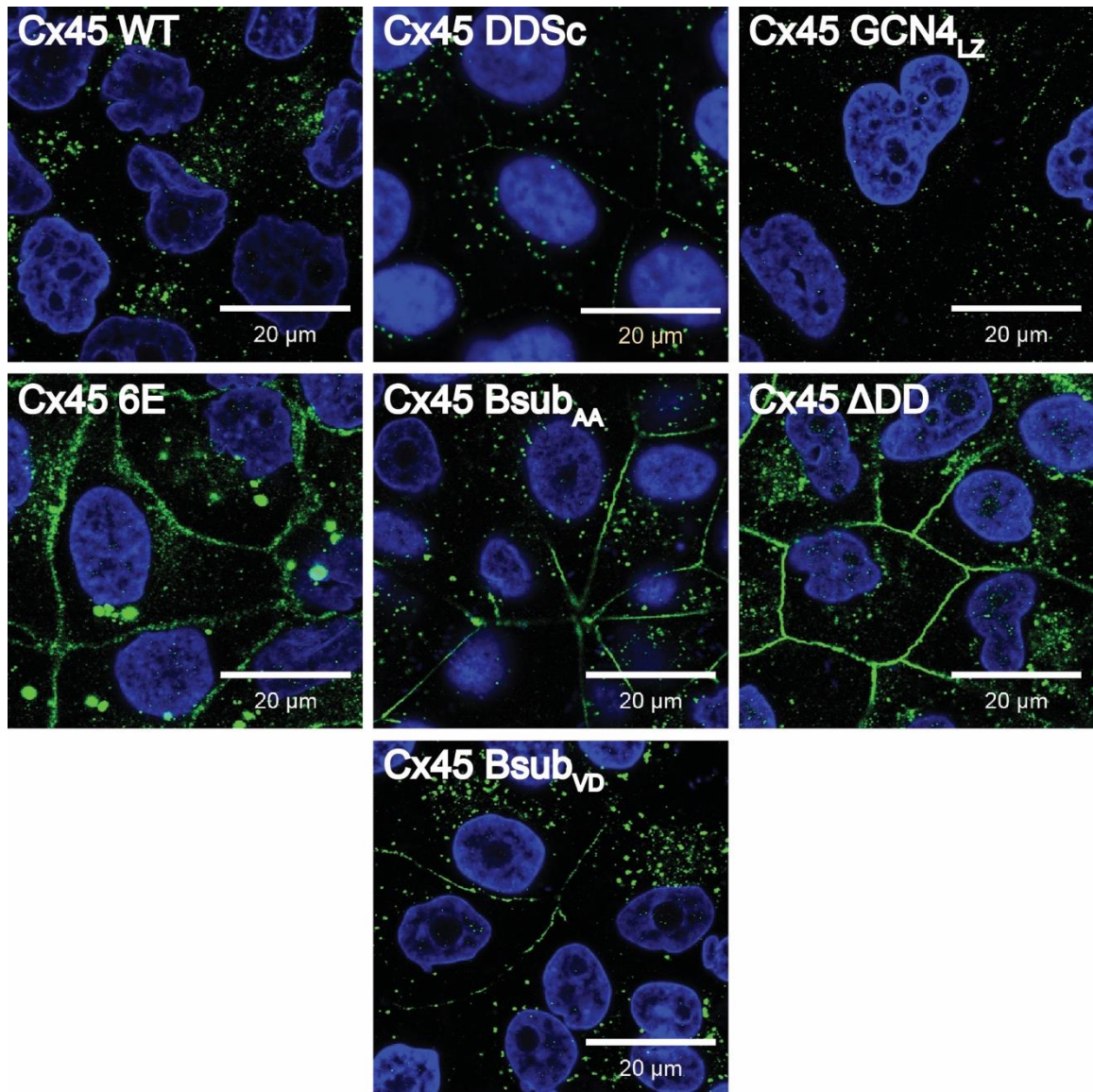


Figure 3.4. Immunofluorescence of Cx45 WT and mutants reveals altered plasma membrane localization.

MDCK cells stably expressing Cx45 WT, Cx45 DDSc, Cx45 GCN4_{LZ}, Cx45 6E, Cx45 Bsub_{AA}, Cx45 ΔDD, and Cx45 Bsub_{vD} were cultured on glass coverslips to confluence, fixed, and immunostained for Cx45 (green) and the nuclei (blue) and imaged by confocal microscopy. Scale bar = 20 μm.

cross-compared to both Cx45 WT and 6E by one-way ANOVA with a Bonferroni post-test (Fig. 3.5B; * compared to Cx45 WT, # compared to 6E). We observed a preference of Cx45 WT to segregate into the TX-100 insoluble fraction (~28.8% soluble and ~71.2% insoluble, $P < 0.001$) and 6E preferentially to the soluble fraction (~62.4% soluble and ~37.6% insoluble, $P < 0.001$). We observed Cx45 GCN4_{LZ} to segregate primarily into the insoluble fraction (~28.1% soluble and ~71.9% insoluble, $P < 0.001$), consistent with the notion that dimerization promotes GJ plaque incorporation. For Cx45 BSub_{VD}, where we observed an intermediate localization by immunostaining, our TX-100 solubility results similarly suggest an intermediate phenotype with a predominance of TX-100 insoluble segregation but to a lesser degree than either Cx45 WT or GCN4_{LZ} (~37.2% soluble and ~62.8% insoluble, $P < 0.001$). The other Bsub mutant Cx45 Bsub_{AA} also displayed an intermediate phenotype with regard to TX-100 solubility. Conversely to Cx45 Bsub_{VD}, Bsub_{AA} solubility trended towards the 6E phenotype (~55.4% soluble and ~44.6% insoluble, $P < 0.001$). Notably, despite the intermediate phenotype neither Cx45 Bsub_{VD} nor Bsub_{AA} were statistically different from Cx45 WT or 6E, respectively. Finally, as predicted by the dimer status, Cx45 Δ DD displayed a phenotype akin to 6E (~62.0% soluble and ~38.0% insoluble, $P < 0.001$). Worth noting is there is set of higher molecular weight bands of immunoreactivity detected in the Western blots of lysate from all Cx45 cell lines. These may represent nonspecific labeling of some other cellular protein, or potential phosphorylation dependent migratory isoforms, however this remains to be determined, as such these bands were not included in the quantification. Similar to the immunofluorescence images, the presence of the manipulations to the A333-N361 region require the use of an alternate antibody (α -Cx45 CT vs. α -Cx45 CL).

11.5 Dimer Incompetent Cx45 Mutants Display Increased Hemichannel Dye Uptake

Our observed TX-100 solubility in Chapter Two and increased plasma membrane localization correlated with hemichannel dye uptake when under conditions where Ca^{2+} was depleted (see Figs. 2.4, 2.9, and 2.12). We hypothesized TX-100 solubility and plasma membrane

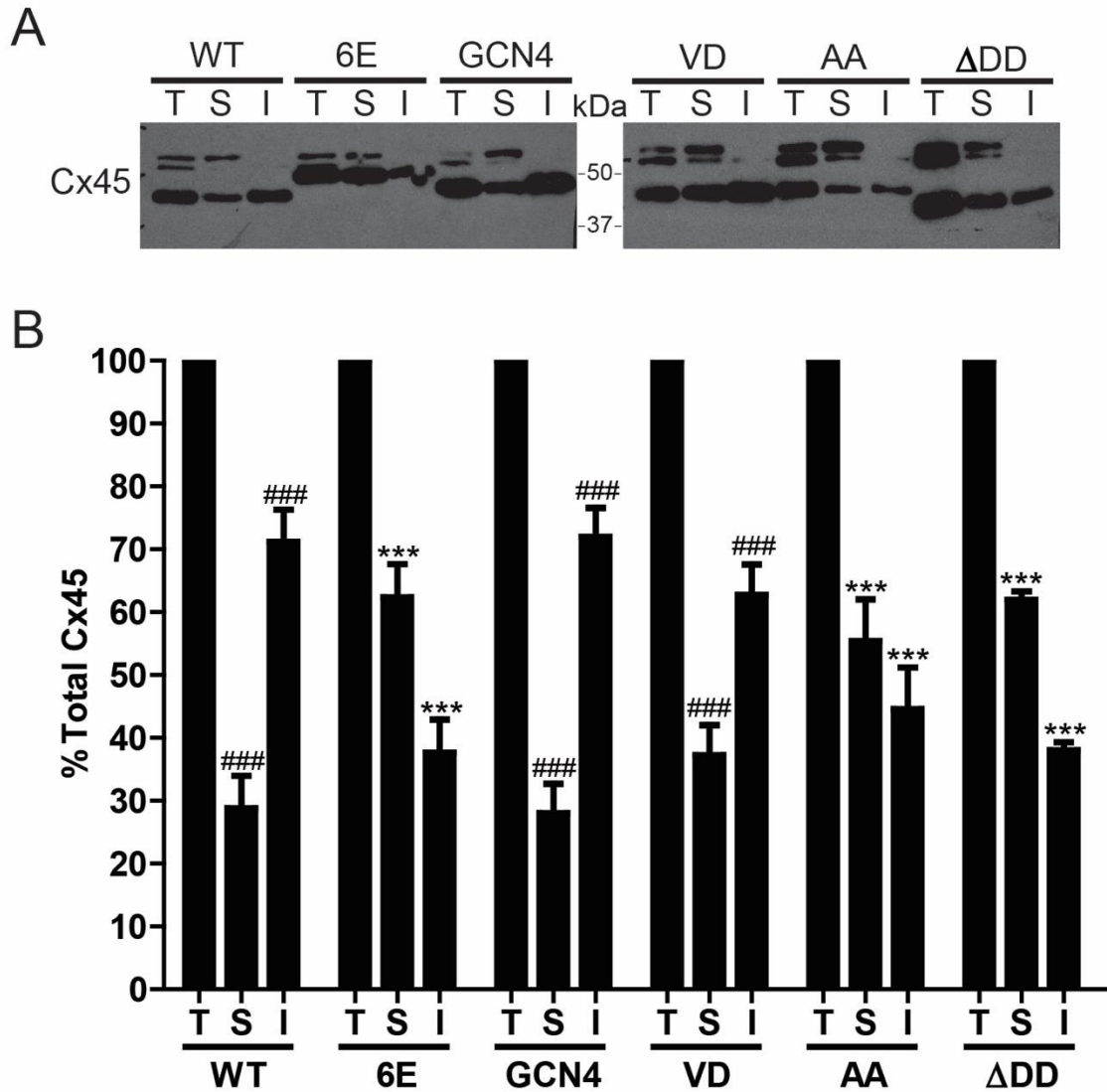


Figure 3.5. Inhibiting Cx45CT dimerization increases TX-100 solubility.

MDCK cells stably expressing Cx45 WT and mutants were cultured, lysed, extracted with TX-100, and fractionated into TX-100 soluble (non-junctional), and TX-100 insoluble (junctional) fractions. A) Representative Western blot analysis of Cx45 WT and mutant (T – total, S – soluble, I – insoluble). B) Quantification of Western blot results from 5 independent replicates. Statistical analysis is one-way ANOVA with a Bonferroni post-test to compare all samples to Cx45 WT (*) and Cx45 6E (#).

localization could be used as a predictor of hemichannel dye uptake and therefore predicted that Cx45 Bsub_{AA} and Δ DD would take up more dye than GCN4_{LZ}. To test this, we depleted cells grown on glass coverslips of Ca²⁺ in presence of NB for 10 min, fix the cells, and stained with Streptavidin-647 and imaged the coverslips. As a confirmation dye uptake was mediated by Cx hemichannels we pretreated one group of coverslips with 50 μ M CBX for 15 min prior to Ca²⁺ depletion. CBX, like La³⁺, is a potent inhibitor of Cx hemichannels at concentrations of 25-50 μ M [467]. Qualitative analysis of the images revealed all Cx45 proteins tested exhibit some degree of NB uptake when Ca²⁺ is depleted (Fig. 3.6, middle) compared to when extracellular Ca²⁺ levels were normal (Fig. 3.6, left). Similarly, all Cx45 proteins had NB uptake that returned to near control levels when the cells were pretreated with CBX (Fig. 3.6, right). Importantly, Cx45 6E, Bsub_{AA}, and Δ DD all took up more dye than WT, GCN4_{LZ}, or Bsub_{VD}. The data taken together with the TX-100 and immunofluorescent images further confirm the link between dimerization, forward trafficking, and hemichannel activity. Additionally, they suggest that membrane localization and TX-100 solubility combined can be a predictor of hemichannel activity.

11.6 Inhibiting Dimerization Correlates with Impaired GJIC

To complete our analysis of the chimeric and deletion mutants of Cx45 we measured GJIC as a function of NB dye transfer in a scrape loading experiment. Since we observed impaired GJIC for Cx45 6E in Chapter Two, we predicted increased TX-100 solubility would correlate with decreased GJIC. MDCK cells were cultured in live imaging dishes to confluence and then loaded with NB by scrape loading, cells were fixed, stained with Streptavidin-647 and imaged (Fig. 3.7). For Cx45 WT and 6E our results were comparable to those seen previously. Cx45 WT (Fig. 3.7; left-top) expressers transferred dye away from the scrape reaching 7th order transfer, while 6E (Fig. 3.7; left-middle) displayed severely impaired dye transfer yielding up to 3rd order transfer with little to no lateral transfer, suggesting networks of coupled cells are smaller in the 6E cells. We expected Cx45 GCN4_{LZ} expressing cells to be as competent as Cx45 WT cells in dye coupling, however, to our surprise transfer of NB in these cells was much more similar to that of 6E (Fig. 3.7; left-bottom).

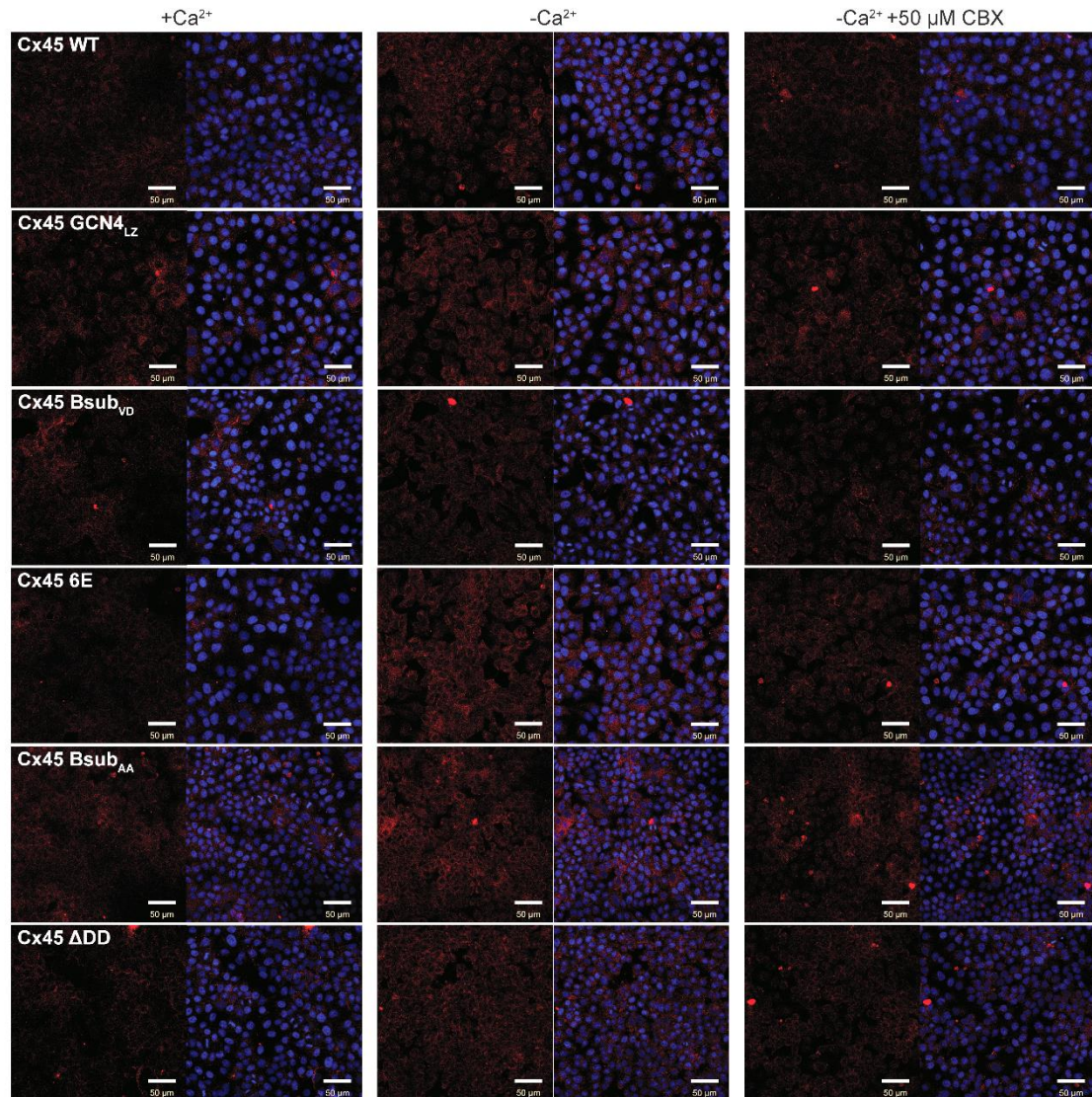


Figure 3.6. Dimerization incompetent Cx45 mutants display increased neurobiotin uptake through hemichannels.

MDCK cells stably expressing Cx45 WT or mutants were subjected to conditions that activate hemichannels activity (Ca²⁺ deprivation) and the level of NB (NB) uptake was measured. Representative fluorescent micrographs of cells loaded with NB and probed with streptavidin-647 conjugate (red). 15 random 100X FOVs were acquired per sample. Carbenoxolone (CBX) pretreatment was used to demonstrate specificity of uptake through Cx hemichannels. Nuclei are stained with DAPI (blue) to show confluence. Scale bar = 50 μm.

Comparing our results to the observations of Koval et al. and Laing et al. indicates a more complex link between Cx45CT dimerization and the regulation of GJIC [450, 451]. Since our Cx45CT GCN4_{LZ} dimer had a K_D of 8.38 nM (~17-fold that of Cx45CT WT), it suggests that increased dimerization (or alternatively some other uninvestigated aspect of this specific mutation) is impairing GJIC. Since we observed TX-100 solubility and hemichannel activity comparable to Cx45 WT in the Cx45 Bsub_{VD} mutant, we predicted it would be comparable to Cx45 WT with respect to NB dye coupling. As we predicted, Cx45 Bsub_{VD} cells were able to transfer dye to a similar extent as Cx45 WT (Fig. 3.7; right-top). Taken together with the Cx45 GCN4_{LZ} results, this mutant suggests that the A333-N361 region is not essential for Cx45 dye coupling. The results also suggest the Cx45 GCN4_{LZ} mutation itself is leading to the impairment. Scrape loading of the Cx45 Bsub_{AA} and Cx45 Δ DD (Fig. 3.7; right-middle and right-bottom, respectively) mutants revealed, like 6E, both manipulations abolishing dimerization impaired NB dye coupling.

11.7 Homologous Mutations of A333-N361 from Cx40 or Cx43 Alter Trafficking

Our Cx45 substitution mutants (except Cx45 DDSc) to this point have relied on the use of heterologous mutations and thus the potential for unintended consequences exists. Sahu et al. demonstrated Cx45 channels were still functional when the CT domain was swapped with that of either Cx40 or Cx43, despite the loss of Cx45CT dimerization [453]. We considered the possibility that in the absence of dimerization homologous mutations may preserve some features of Cx45 function. To investigate this, we engineered Cx45 mutants with A333-N361 substituted with a homologous region of either Cx40 or Cx43 and used them to generate stable MDCK cell lines (Cx45 40_{MD} and 43_{MD}; Table 5). Similar, to our previous characterizations we used immunofluorescence as an initial comparison of any phenotypic alterations. Since the structure and dimerization status of the regions of Cx40 and Cx43 have been previously described we predicted we would observe increase plasma membrane localization of both Cx45 40_{MD} and 43_{MD}. Indeed, the localization of both mutants was preferentially shifted towards a primary plasma membrane localization (Fig. 3.8). Interestingly, even though we observed increased plasma membrane localization, the pattern of immunoreactivity at the plasma membrane was more similar to Cx45 Bsub_{VD} than 6E (see Fig. 3.4) for both Cx45 40_{MD} and 43_{MD} (Fig. 3.8).

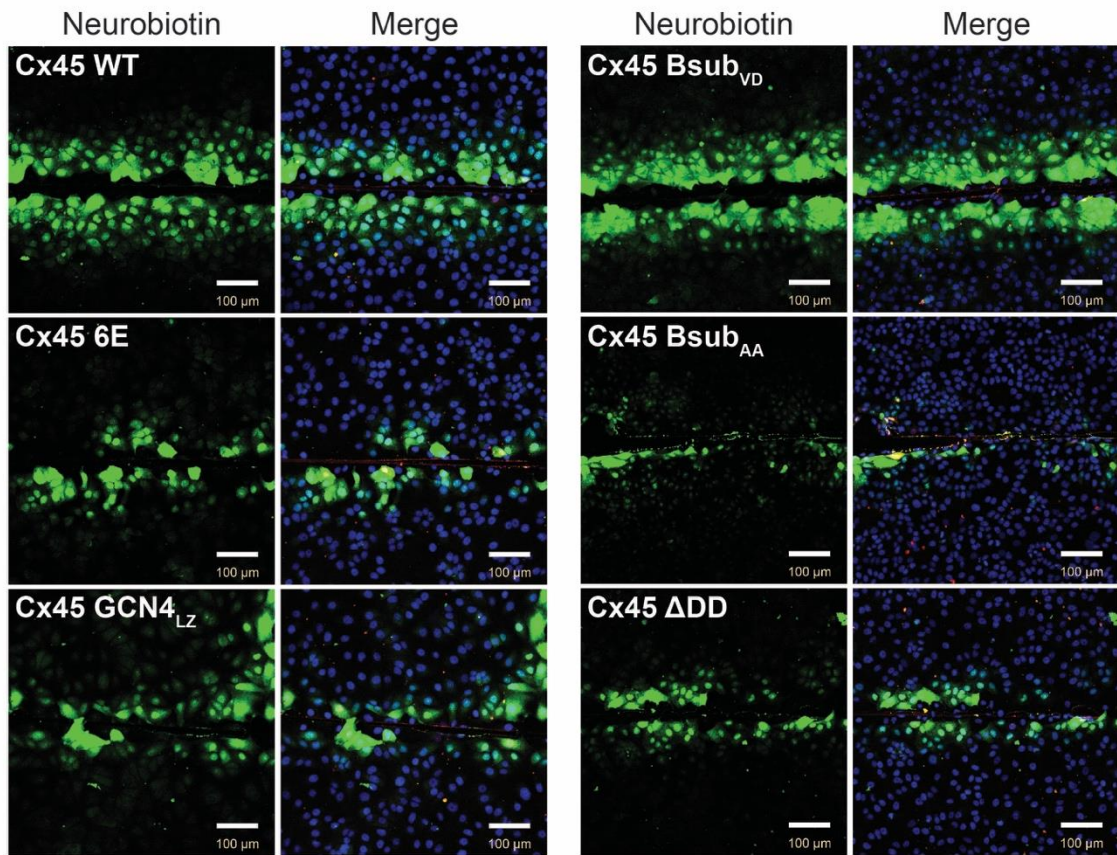


Figure 3.7. Inhibiting Cx45CT dimerization impairs cell coupling of neurobiotin. MDCK cells expressing Cx45 WT or mutants were scrape loaded with NB (green) to assess the degree of intercellular communication. Nuclei are stained with DAPI (blue). Scale bar in = 100 μm.

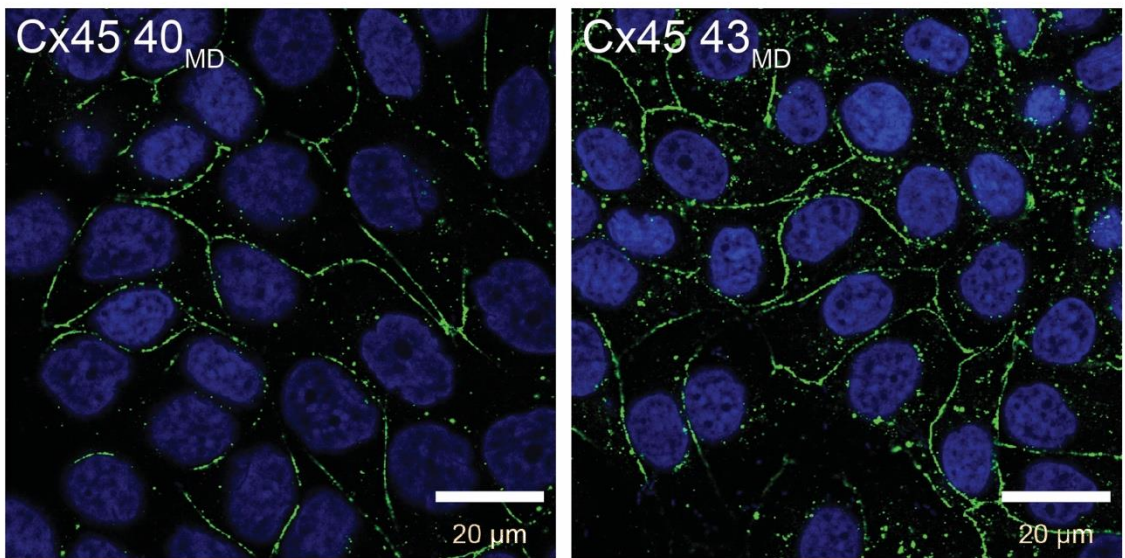


Figure 3.8. Homologous Cx45 mutants display increased plasma membrane localization. MDCK cells were stably transfected with Cx45 40_{MD} (left) or Cx45 43_{MD} (right), cultured to confluence on glass coverslips, fixed, and immunostained for Cx45 (green). Nuclei were stained with DAPI (blue). Scale bar = 20 μ m.

11.8 Cx45 40_{MD} and Cx45 43_{MD} Show Increased Hemichannel Dye Uptake

Following from observation that Cx45 40_{MD} and 43_{MD} displayed increased plasma membrane localization consistent with having dimerization inhibited we predicted they would similarly have increased NB dye uptake through hemichannels when depleted of Ca²⁺. To test this, we cultured MDCK cells expressing either Cx45 40_{MD} or 43_{MD} on glass coverslips to confluence and then depleted Ca²⁺ in the presence of NB for 10 min. Afterward incubating with NB the cells were fixed, stained with Streptavidin-647, and imaged. As we expected both Cx45 40_{MD} and 43_{MD} had increased dye uptake compared to Cx45 WT when Ca²⁺ was depleted (Fig. 3.9; bottom-middle and lower-middle). Surprisingly, Cx45 43_{MD} appeared to take up more dye than even 6E (Fig. 3.9; bottom-middle). Importantly, treatment with CBX abolished the dye uptake confirming Cx hemichannels were involved (Fig. 3.9; right panels).

11.9 Homologous A333-N361 Mutations Preserve or Enhance GJIC

We lastly wanted to determine if, similar to the Sahu et al. chimeras, the Cx45 40_{MD} and 43_{MD} proteins would yield functional GJ channels despite inhibiting Cx45CT dimerization [453]. Although, all of our heterologous mutants negatively impacted NB dye transfer (including Cx45 GCN4_{LZ}), the trend observed for the dimerization incompetent mutants was that loss of dimerization equated to impaired GJIC (Fig. 3.7). If the lack of Cx45CT dimerization (regardless of manipulation) in the context of the Cx45CT (all residues except A333-361) is essential for Cx45 GJIC, then loss of dimerization in the context of either Cx45 40_{MD} or 43_{MD} should impair GJIC. In order to test this, we cultured MDCK cells expressing either Cx45 40_{MD} or 43_{MD} in live imaging dishes to confluence, and scrape loaded the cells with NB. After the incubation with NB the dishes were fixed, stained with Streptavidin-647, and imaged. Much to our surprise unlike 6E both Cx45 40_{MD} and 43_{MD} were both able to robustly transfer NB dye (Fig. 3.10; bottom panels). Furthermore, Cx45 40_{MD} was more competent than WT in dye transfer, almost filling the entire field of view (Fig. 3.10; lower middle). Cx45 43_{MD} mediated NB transfer was comparable to that WT (Fig. 3.10; bottom). Taken together with our heterologous mutant data this supports our hypothesis that Cx45CT dimerization is an essential structural feature of Cx45 that regulates GJIC in the context of its own CT.

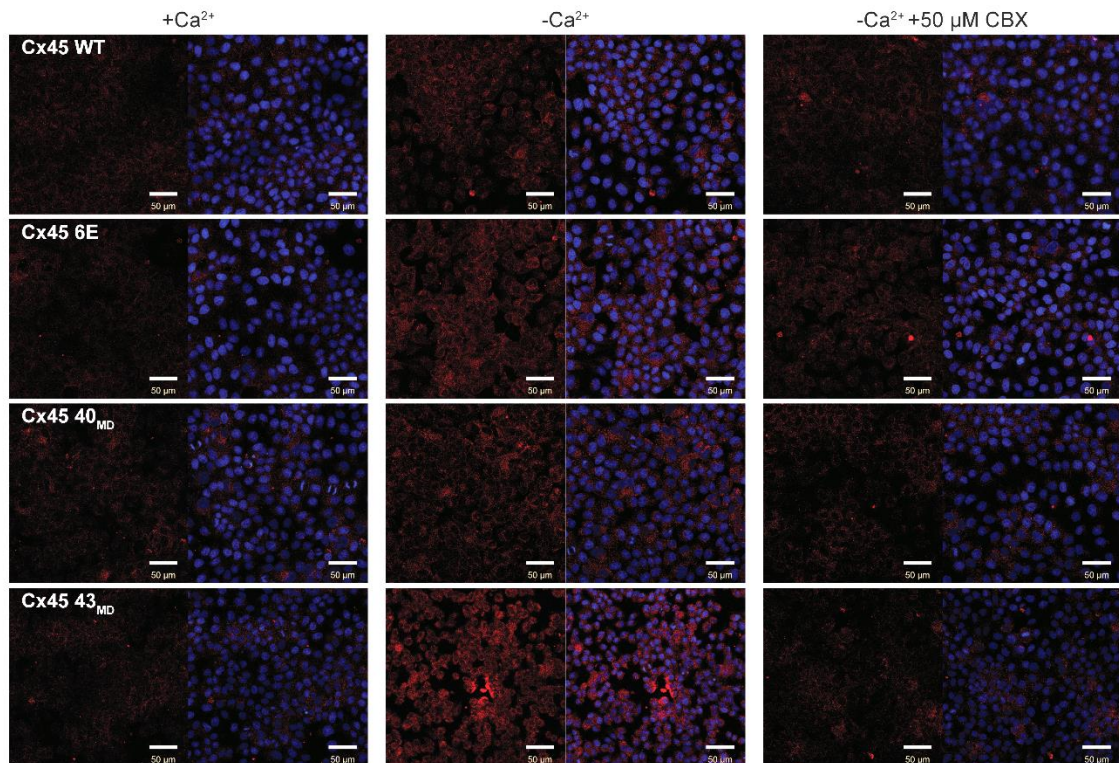


Figure 3.9. Homologous Cx45 mutants have increased hemichannel uptake of neurobiotin.

MDCK cells stably expressing Cx45 40_{MD} or Cx45 43_{MD} mutants were subjected to conditions that activate hemichannels activity (Ca²⁺ deprivation) and the level of NB uptake was measured. Representative fluorescent micrographs of cells loaded with NB and probed with streptavidin-647 conjugate (red). 15 random 100X FOVs were acquired per sample. Carbenoxolone (CBX) pretreatment was used to demonstrate specificity of uptake through Cx hemichannels. Nuclei are stained with DAPI (blue) to show confluence. Cx45 WT and 6E from Fig. 3.6 were included for ease of comparison. Scale bar = 50 μm.

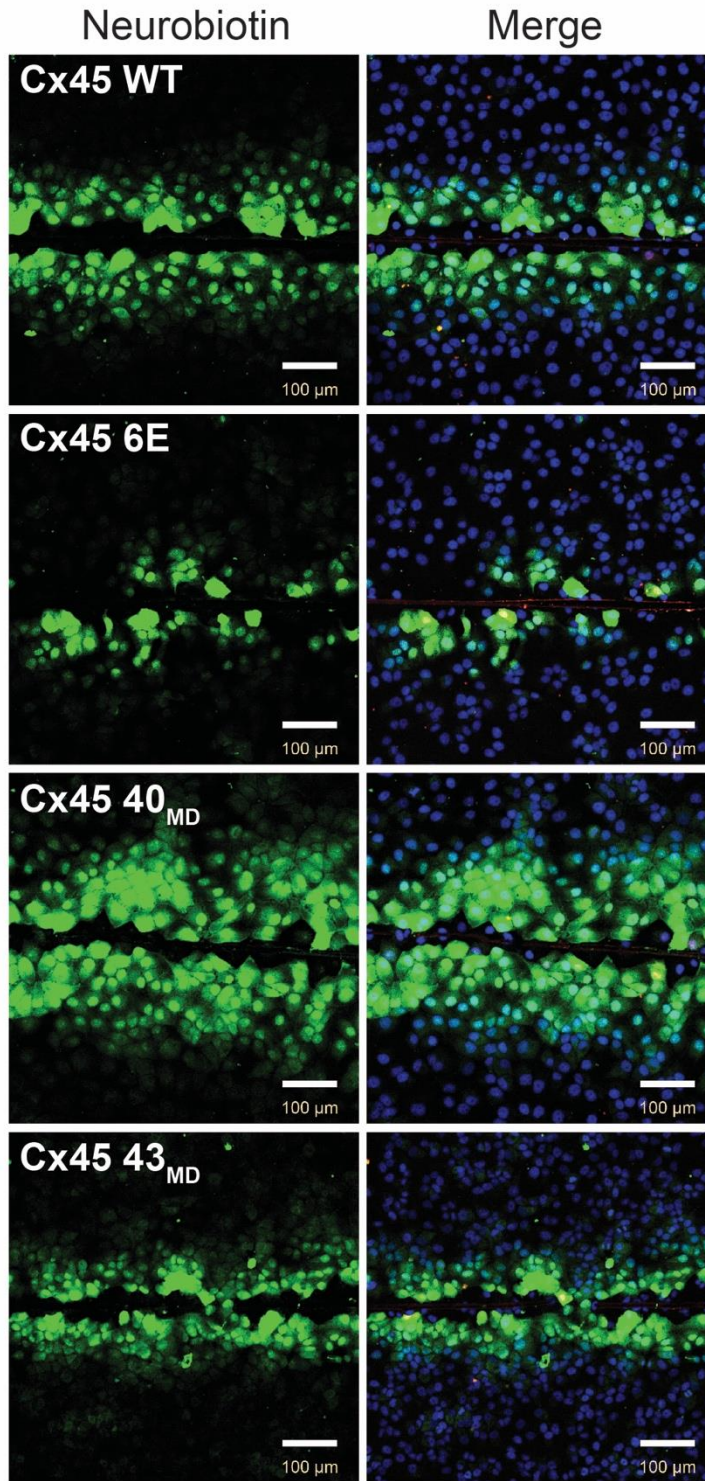


Figure 3.10. Homologous Cx45 mutant maintain or enhance neurobiotin transfer.

MDCK cells expressing Cx45 40_{MD} or Cx45 43_{MD} were cultured to confluence in live imaging dishes, scrape loaded with NB (green) and imaged. 15 fields of view per sample were acquired. Cx45 WT and 6E were included here from Fig. 3.7 for ease in comparison. Nuclei were stained with DAPI (blue). Scale bar = 100 μm.

12. Discussion

A notable similarity between the study in Chapter Two and the one contained in this Chapter is the consistent increase and more widespread plasma membrane localization of the dimerization incompetent mutants. Another similarity was the increased TX-100 solubility of these mutants. Together the pieces of data suggest the dimerization is in some manner directly linked to control mechanisms that limit the amount of the Cx45 that is present in the plasma membrane and therefore the formation of GJs. Furthermore, we observed similar increases in hemichannel dye uptake for the dimerization incompetent mutants. Although it is tempting to conclude this is directly mediated by dimerization, it seems more likely that this is a secondary effect of the increased trafficking and TX-100 solubility. Importantly, it is clear from localization of the Cx45 Δ DD (and conversely Cx45 GCN4_{LZ} and DDSc), that Cx45CT A333-N361 is not essential for the forward trafficking of Cx45 to the plasma membrane (Fig. 3.4). These data also support our conclusion that dimerization limits Cx45 membrane expression. Taken together with the turnover assay in Chapter Two, it suggests this is accomplished by positively regulating degradation and the association with Nedd4 (Fig. 2.8 and 2.16). A key difference in the studies between Chapters One and Two, was the unpredictable nature of NB dye transfer (Cx45 GCN4_{LZ} – impaired; 40_{MD} and 43_{MD} – functional). The data suggest that Cx45CT dimerization either does not regulate cell coupling or a more complex mechanism is involved. Testing the coupling ability of the Cx45 DDSc mutant will no doubt provide further insight into this possibility. Furthermore, our data highlights an important caveat in the interpretation of TX-100 solubility data, that increased solubility does not necessarily equate to decrease GJIC.

Other studies investigating functional regulation of Cx45 by the CT domain have been spurious over the last two and a half decades and narrow in focus. In one set of studies the focus was using CT truncation mutants to investigate the role of the CT in cell coupling, localization, and detergent solubility [450, 451]. In the Koval et al. study chick Cx45 truncated at position 357 (Cx45 Δ 37) expressed in ROS cells was observed to correlate with increased intercellular transfer of 7-hydroxycoumarin-carboxylic acid (HCCA), LY, and calcein [450]. Notably, this truncation is immediately following the critical Y356 in the Cx45 dimerization domain and would likely increase

the dimerization affinity. A second study from the same laboratory compared the Cx45 Δ 37 to another mutant Cx45 Δ 34 [451]. In that study, the Cx45 Δ 34 localized in a more punctate manner (similar to dimer competent Cx45 mutants) than did the Cx45 Δ 37 (which was more linear, similar to Cx45 dimer incompetent mutants) [451]. Furthermore, it was revealed that the Cx45 Δ 37 failed to co-IP ZO-1 and was also more TX-100 soluble than either Cx45 WT or Cx45 Δ 34, the authors reasoned this was due to the presence of a second or more extended binding site for ZO-1 than was previously reported for Cx43 [286, 451]. A number of pieces of data suggest that dimerization of the Cx45CT may be essential for maintaining appropriate interactions with ZO-1. The most direct piece of evidence we observed was a decrease (albeit non-significant) in the amount of ZO-1 eluted with Cx45 6E compared to WT in Chapter Two (Fig. 2.15). Although this was not directly tested in the current study, the phenotypic consistency of the dimerization incompetent mutants (increased plasma membrane localization and TX-100 solubility), all of which in some way or another result in a loss of Cx45 residues 357-361 (like Cx45 Δ 37), is consistent with the Laing et al. study Cx45 Δ 37 phenotype [451].

The nature of the loss of NB dye coupling for the heterologous (and deletion) mutants can be possibly explained by one of two theories. 1) Dimerization is a critical regulator of cell coupling either through enhancing protein-partner interactions, PTMs, or TM/EL positioning to favor docking; and 2) the heterologous (and deletion) mutations lead to unintended consequences via sequence specific mechanisms such as: gain/loss of protein partner interactions, or aberrant phosphorylation. Taken alone, the data cannot rule out the first theory, however, when considering the homologous Cx45 mutants this theory breaks down. The homologous mutants displayed comparable (Cx45 43_{MD}) and even enhanced (40_{MD}) NB dye coupling when compared to WT. This result is both interesting and consistent with the results obtained by Sahu et al. when CT truncated Cx45 was tethered with either the CT of Cx40 or Cx43 [453].

Cx45CT dimerization is a structural feature essential to controlling the amount of Cx45 present in the plasma membrane. Future studies should focus on determining how exactly ZO-1 interacts with the CT domain of Cx45 and how dimerization contributes. Furthermore, the studies of Koval et al. and Laing et al. used ROS cells to exogenously express Cx45, the ROS cells

endogenously express Cx43 (similar to the MDCK cells) [424, 450, 451]. A study focused on the regulation of heteromeric GJ channels discovered that functional Cx proteins can functionally rescue defective mutants by heterotypic pairing (docking) and are regulated normally (by the wild-type side) [452]. It is possible in the studies of Laing et al. and Koval et al. that a similar mechanism occurred, however, since the Sahu et al. study utilized Neuro-2a (N2A) cells, which lack endogenous Cx expression this would have not been a factor and lends greater support to the validity of our conclusions [450, 451, 453]. Additionally, further studies should direct their focus to understanding the role of Cx45CT dimerization in the context of heteromeric connexons.

CHAPTER FOUR

Cx45 is Regulated by Kinases Active During End-Stage Heart Failure

13. Introduction

The previous two Chapters focused on the regulation of Cx45 function by homodimerization of the CT domain, an intramolecular interaction that occurs prior to and is maintained at the GJ plaque. While protein interactions, both intra- and inter-molecular, are important for the regulation of Cxs in general, other regulatory mechanisms are critical as well. Some of the mechanisms we discussed in Chapter One include transcriptional regulation, quality control mechanisms in the ER (ERAD), gating (voltage, pH, and Ca²⁺), and diverse PTMs (ubiquitination, carboxylation, acetylation, methylation, nitrosylation, and phosphorylation). An important and widely studied modification of Cxs is phosphorylation. Despite being well characterized for Cx43, little information exists about the regulation of other Cx family members by phosphorylation. In this section, we focus on the importance of Cx phosphorylation to the function and regulation of Cx43 and Cx45.

GJs are integral membrane proteins that enable the direct exchange of ions and small cytoplasmic molecules (\leq 1kDa) between adjacent cells [468]. They mediate propagation and amplification of signaling cascades initiated by many stimuli. The 21 human Cx family members oligomerize into connexons which aggregate to form GJs [468]. Two important cardiac Cxs are Cx43 and Cx45, the latter is the focus of this Chapter. Cx43, expressed in ventricular myocytes, mediates propagation of cardiac action potentials and maintains a working cardiac rhythm [67]. Cx45 GJs, found primarily in the specialized conduction system, slow conduction velocity to allow successive atrioventricular contraction and their high voltage sensitivity (i.e., responsiveness to voltage gating) prevents current backflow [230, 464, 469]. In addition to voltage gating, Cx45 and Cx43 differ significantly in pore size, conductance, selectivity, and pH sensitivity [470, 471]. Dysregulation of GJ distribution, expression, and gating negatively impacts normal impulse propagation and can lead to arrhythmias [34, 36, 67, 71, 472]. The compartmentalization and unique channel properties of Cx45 and Cx43 strongly suggest that any alterations to expression or distribution, both associated with ischemia and heart failure, could lead to the generation of lethal arrhythmias. In end stage failing hearts, increased Cx45 at the ID, combined with Cx43 remodeling forms the basis for the arrhythmogenic substrate [432].

While Cx45 and Cx43 share high sequence homology in the transmembrane and extracellular domains, they are divergent in their cytosolic domains, especially the CTs. The CT of Cxs are involved in Ca²⁺ and pH mediated channel closure, voltage gating, trafficking, assembly and disassembly of GJs, and regular Cx turnover [149, 277, 285, 308, 473-475]. The CT domain is a hub for Cx regulation through diverse protein interactions [231, 247, 248, 285, 473, 476]. Importantly, phosphorylation alters GJ function via changes in protein partner interactions [153, 300, 306, 308, 312, 477-479]. Phosphorylation of Cx43CT is an important regulator of both increasing [153]. Phosphorylation of critical Ser residues by PKA has been attributed to enhanced forward trafficking and increasing cell coupling [160, 343]. Additionally, phosphorylation by CK1 is attributed to the P2 migratory phosphoisoform (not exclusively) and associated with increased channel openness [311]. Phosphorylation of Cx43 Ser residue 373 stimulates transfer of Cx43 from the perinexus into the GJ proper where it can participate in meaningful cell coupling [158, 159, 166, 459].

Conversely, phosphorylation is also a potent inhibitor of GJIC [153]. For example, Src phosphorylation destabilizes Cx43 GJs by loss of binding to the cytoskeletal anchoring proteins – β -tubulin, Drebrin, and ZO-1 [378, 480-483]. Src phosphorylation also induces channel closure and promotes internalization by indirectly activating PKC and MAPK (which phosphorylate S368 and S255/262/279/282, respectively), thereby decreasing GJIC [16, 376, 484]. Importantly, a number of protein partners studied in our laboratory also interact with the Cx45CT. These include Drebrin, ZO-1, Nedd4, and the GJ recycling protein TSG101 [247, 485, 486]. Notably, several of these proteins interact with the Cx45CT in regions containing several phosphorylatable residues suggesting phosphorylation may regulate the interactions [247]. Studies investigating the effects of Cx45 regulation by phosphorylation are limited, however, Ser phosphorylation of Cx45 often results in opposing effects compared to Cx43. For example, activation of PKC by PMA, triggers channel closure to subconductance states and promotes internalization and turnover of Cx43 leading to reduced GJIC, however, studies investigating the regulation of Cx45 by PKC have yielded conflicting results [86, 306, 385]. In one study, activation of PKC by the PMA resulted in increased g_j , while in another g_j was impaired (albeit to a lesser degree than Cx43) yet transfer of NB via Cx45

channels was unaffected while Cx43 did not transfer any NB [86, 306]. Interestingly, one of the earliest study to describe phosphorylation of Cx45 in any detail noted that phosphorylation of Cx45 (presumably by PKC) on far CT Ser residues promoted stability of Cx45 (another opposite of Cx43), while loss of phosphorylation correlated with decreased half-life [189]. In another study, activation of PKG by cGMP impaired communication of Cx43 channels but not those of Cx45 [487]. Taken together these findings suggest that different Cx family members are likely differentially regulated by the same kinase (if at all). Furthermore, if Cx45 is present at the ID to compensate for loss of Cx43 coupling under the same conditions it strongly suggests the same kinases will have opposing effects on Cx45 compared to Cx43.

In diseased hearts, dysregulated molecular processes lead to the activation of stress related proteins such as AngII and signal cascades via altered kinase activation [488, 489]. A number of kinases known to regulate Cx43 (and possibly Cx45) are directly activated by increased AngII levels including PKC, Pyk2 and Src [490-497]. In the heart, Pyk2 is activated downstream of AngII signaling by the AT1R due to increased $[Ca^{2+}]$ via PKC [489, 492, 498, 499]. Activation of Pyk2 links Ca^{2+} flux, integrin signaling, and G protein-coupled receptors with effectors in both the MAPK and PI3K/PDK1/Akt pathways [500-502]. Pyk2 is also activated by JAK1/2 or Src phosphorylation [499, 502-505]. Phosphorylation at Y579/580 by Src results in “enhanced” Pyk2 activation [505]. A number of *in vivo* models show Pyk2 upregulation in the adult heart in disease states, including models of hypertrophy [506, 507]. Despite these data, mechanisms defining how Pyk2 is involved in cardiac disease are limited.

The connection between Src and the pathogenesis of heart disease is well established. In the case of cardiac hypertrophy, upregulation of Src kinase expression and activity has been reported in the ventricular myocytes of spontaneously hypertensive rats [508]. The study noted decreases in the autoinhibitory phosphorylation site (Y529), and concomitant increase in phosphorylation at the active site (Y418) when compared to age-matched control Kyoto-Wistar rats [508]. Src is essential to stretch induced hypertrophy of the cardiomyocytes, a hallmark of hypertensive heart failure [509]. The study of Wang et al. demonstrated mechanical stretch of cardiomyocytes (as occurs in hypertension) activates the AT1R independently of AngII, leading to

β -arrestin2 mediated activation of Src and subsequently the ERK1/2 pathway [509]. Interestingly, the authors reported that ERK1/2 activation could be abrogated by the addition of Src inhibitors only when the initiating stimulus was mechanical stretch, not AngII mediated signaling, suggesting a bimodal role for the AT1R in the pathogenesis of hypertension induced heart failure [509]. Similar results were reported by another study in the ventricles of hypertrophic cat hearts [510]. Although both studies demonstrated a critical role of Src in the activation of the ERK1/2 cascade, the Kuppuswamy et al. study suggested a critical requirement for integrin signaling not explored in the Wang et al. report [509, 510]. Taken together these studies illustrate an important role for Src in signal transduction pathways that lead to cardiac remodeling, including the direct phosphorylation of the GJ proteins Cx43 and Cx45. Finally, in addition to Pyk2 and Src, PKC is a critical effector of AT1R signaling, and forms a feedback activation loop with Src [511].

Similar to Src and Pyk2, PKC is activated downstream of the AT1R [496, 497, 509]. The Wang et al. study discussed above demonstrated AngII independent activation of Src via mechanical stretch induced AT1R activation [509]. Notably, they also described AngII-dependent activation of PKC, mediated by the G-protein coupled receptor activity of the AT1R [509]. Several PKC isoforms have been implicated in the progression of heart disease including PKC α , PKC β , PKC γ , PKC δ , and PKC ζ (reviewed in [512]). AngII has been implicated in the activation of several of the PKC isoforms (α , $\beta(2)$, ϵ , γ , and ζ isoforms) resulting in translocation to the plasma membrane [513]. Similarly, PKC isoforms α , $\beta(2)$, and ζ were shown to be activated under hypoxic conditions mimicking ischemia [513]. In Dahl salt-sensitive rats, expression of several PKC isoforms (α , β , δ , and ϵ) increased in animals fed high-salt diet compared to low-salt diet for 11 weeks [514]. Although expression of PKC ϵ , returned to near control levels by 16 weeks high-salt, while expression of the others (α , β , and δ) remained high compared to low-salt diet controls [514]. Despite the potential involvement of several PKC isoforms in heart failure, PKC α has been implicated as particularly important. For instance, in guinea pigs subjected to aortic banding (pressure overload model) PKC α activity was shown to increase, this was however, reduced by treatment with ACE inhibitors [515]. Similarly, in rats subjected to pressure overload by aortic banding a selective upregulation of PKC α and PKC δ was reported, while PKC ϵ expression remained constant [516]. Furthermore, PKC α has

been shown to be a critical mediator of cardiac contractility [517, 518]. Importantly, genetic ablation of PKC α specifically, offered cardiac protection from heart failure induced by pressure overload and dilated cardiac myopathy, as well as partial protection from infarct induced heart failure [517, 518].

Since Cx45 is expressed in the myocytes of the ventricle in human failing hearts it is reasonable to assume that kinases activated in heart failure may regulate the function of Cx45. Based on the lack of information available on the phosphorylation of Cx45 in end-stage heart failure, the importance of AngII signaling and the kinases, Pyk2, Src, and PKC, in hypertensive models of heart failure we sought to investigate the possibility Cx45 is phosphorylated (and regulated) by these kinases using a combined approach of *in vitro*, proteomic, and molecular/cellular biology techniques.

14. Materials and Methods

14.1 Antibodies and Reagents

All antibodies and reagents for this study are contained in Table 2.

14.2 Expression and Purification of Cx45CT WT and Mutants

Constructs designed for this project are summarized in Table 6. Cloning of constructs was achieved by the purchase of a GeneBlock gene fragments (IDT) for each of the single Tyr mutants. GeneBlock gene fragments were cloned into pGEX-KT by NEBuilder (NEB) per manufacturer protocol and sequence verified by Sanger sequencing. Cx45CT WT and mutants were expressed and purified as previously described [247]. Following purification, proteins were buffer exchanged into (5 mM 3-(N-morpholino)propanesulfonic acid (MOPS), pH 7.2) using a Nap 5 (GE Healthcare) column per manufacturer protocol. Concentration of buffer exchanged proteins were determined by Abs₂₈₀ nm using a NanoDrop 1000 and Beer's Law.

14.3 Kinase Screen (Eurofins KinaseProfiler)

Cx45CT WT expressed and purified as described above. Purified protein was diluted in 1x PBS pH 7.4 to a final concentration of 200 μ M in a final volume of 1 mL, flash frozen on dry ice and shipped on dry ice to Eurofins Scientific for a custom Kinase Profiler Assay testing the Cx45CT as substrate for the indicated kinases. Substrate diluted to 20 μ M was incubated with the indicated kinase and 200 μ M ATP [γ -³³P] for 40 min at RT. Substrate was then captured by either P30 or FilterMat A filters and quantified by scintillation counter. Quantification of raw scintillation counts were achieved by averaging the value of two experimental well following subtraction of the acid buffer blank for each kinase. This value was normalized to the acid blank subtracted average of two wells of the positive control peptide for each kinase tested.

14.4 *In vitro* Phosphorylation

Buffer exchanged pure Cx45CT (K265-I396) or single Tyr mutants (Table 6) were used as substrate for *in vitro* phosphorylation by Src, Pyk2, and PKC α . Reactions were prepared, an incubated ON at 30°C and stopped by the addition of 6X SDS loading buffer, and then analyzed by SDS-PAGE and Western blot (2 nmol) or MS (15 nmol). Reactions were set up as follows:

Construct	Mutations	Remaining Tyr
Cx45CT WT	None	Y275/277/290/301/311/324/256
Cx45CT Y275	Y277/290/301/311/324/356F	Y275
Cx45CT Y277	Y275/290/301/311/324/356F	Y277
Cx45CT Y290	Y275/277/301/311/324/356F	Y290
Cx45CT Y301	Y275/277/290/311/324/356F	Y301
Cx45CT Y311	Y275/277/290/301/324/356F	Y311
Cx45CT Y324	Y275/277/290/301/311/356F	Y324
Cx45CT Y356	Y275/277/290/301/311/324F	Y356

Table 6. Cx45CT WT and single Tyr mutants.

Src: 1.5 µg of recombinant full-length active human Src, pure Cx45CT or mutants, and 500 µM ATP were combined in reaction buffer (5 mM MOPS pH 7.2, 2.5 mM β-glycerol-phosphate, 4 mM MgCl₂, 2.5 mM MnCl₂, 1.0 mM ethyleneglycol tetra acetic acid (EGTA), 0.4 mM EDTA, 0.05 mM DTT, and 40 µg/mL BSA) in a total volume of 60 µL. For negative control the kinase was substituted with reaction buffer.

Pyk2: 1.5 µg of recombinant active human Pyk2 (360-690), pure Cx45CT or mutants, and 500 µM ATP were combined in reaction buffer (5 mM MOPS pH 7.2, 2.5 mM β-glycerol-phosphate, 4 mM MgCl₂, 2.5 mM MnCl₂, 1.0 mM EGTA, 0.4 mM EDTA, 0.05 mM DTT, and 40 µg/mL BSA) in a total volume of 60 µL. For negative control the kinase was substituted with reaction buffer.

PKCα: 1.5 µg recombinant full-length active human PKCα, pure Cx45CT or mutants, 6 µL of lipid activator (0.5 mg/ml phosphatidylserine and 0.05 mg/ml diacylglycerol in 20 mM MOPS, pH 7.2, containing 1 mM CaCl₂) and 500 µM ATP were combined in reaction buffer (5 mM MOPS pH 7.2, 2.5 mM β-glycerol-phosphate, 5 mM MgCl₂, 1.0 mM EGTA, 0.4 mM EDTA, 0.05 mM DTT, 40 µg/mL BSA) in a total volume of 60 µL. For negative control the kinase was substituted with reaction buffer.

14.5 Mass Spectrometry

10 nmol of purified mouse Cx45CT (K265-I396) subjected to *in vitro* phosphorylation by the Src, Pyk2, or PKCα in Section 14.4 was resolved by SDS-PAGE, gel stained with Coomassie bright blue, and then destained with pure methanol until bands appeared. The Cx45CT bands were cut out, washed extensively with MilliQ water followed by 50% acetonitrile in MilliQ water, snap frozen on dry ice, and shipped on dry ice to the Harvard Beth Israel Deaconess Medical Center Mass Spectrometry Core Facility for post-translational mapping [519].

14.6 Validation of Mass Spectroscopy

2 nmol of purified Cx45CT WT and single Tyr mutants (Table 6) were subjected to *in vitro* phosphorylation by Src or Pyk2 as in Section 14.4. Resolved by SDS-PAGE and analyzed for phosphorylation by Western blot with a general pTyr antibody. As negative control, the kinase was omitted and replaced with reaction buffer for each protein and kinase.

14.7 Cell Culture and Stable Cell Line Generation

MDCK and LA25 cells (gifts from Dr. Paul Lampe, Fred Hutchinson Cancer Center), HeLa cells (gift from Dr. Steve Caplan, University of Nebraska Medical Center) were cultured in Dulbecco's modified Eagle medium (Corning) at 37°C in a humidified 5% CO₂ atmosphere. Medium was supplemented with 10% FBS (Seradigm), 2 mM L-glutamine (HyClone), 1% pen-strep (Corning), and 0.2% Normocin (Invivogen). The selective agent puromycin (Tocris) was used, when appropriate, at empirically determined concentrations. 70% confluent MDCK, HeLa, or LA25 cells were lipofected with Sall linearized plasmid using Lipofectamine 2000 at a 1:2 ratio in OptiMem. Transfections were carried out under antibiotic free conditions, and cells were cultured 48-72 hr prior to addition of selection media. HeLa were selected with 2 µg/mL, MDCK were selected with 5 µg/mL, and LA25 cells were selected 7 µg/mL. Cells were clonally (monoclonal) selected using Whatman paper cloning disks. Western blots and immunofluorescence were used to screen clones. For LA25 cells Src activity was modulated by culturing the cells at 35°C (permissive – Src active), 37°C (intermediate), or 40°C (non-permissive – Src inactive) for 8 hr.

14.8 Transient Transfections

HeLa cells were cultured to approximately 90% confluence and lipofected using Lipofectamine 2000 (1:2 ratio) in Optimem under antibiotic free conditions. Expression of the transgene was maintained for approximately 24 hr prior to cell lysis or subsequent experimentation.

14.9 Co-IP and Western blot

Co-IP: MDCK, LA25, or HeLa cells stably expressing Cx45 WT were seeded in either 10 or 15 cm plates and grown to confluence. Cells were rinsed 2x with 1x TBS + 1 mM EDTA and then scraped up an either 0.5 or 1.0 mL of IP lysis buffer (25 mM Tris, 150 mM NaCl, 0.25% sodium deoxycholate, 0.05% SDS, 1% TX-100 plus protease and phosphatase inhibitors). Cells were mechanically lysed and then incubated for 30 min at 4°C with rotation. Lysates were precleared with normal rabbit IgG (2 µg) bound protein G agarose for 1 hr at 4°C and then clarified by centrifugation. Clarified lysates were quantified by BCA (Pierce) and normalized. Input samples were reserved and either 2 or 5 mg of lysate was captured by IP with either 2 or 3 µg of rabbit α-

Cx45 (Alomone) or mouse α -Cx45 (Millipore) ON at 4°C. Immune-protein complexes were captured by 2 hr 4°C incubation with protein G agarose (Pierce), washed 5x with IP wash buffer (IP lysis buffer excluding sodium deoxycholate) proteins were eluted using 35-50 μ L 3x SDS sample buffer. Equal volumes of each sample were analyzed by Western blot and to avoid cross reactivity with the IP antibody a light chain specific secondary antibody (Jackson) or Veriblot (Abcam) were utilized for detection. HeLa and MDCK cells were treated with PMA (100 nM) for 1 hr prior to lysis, LA25 cells were incubated at 35°C, 37°C, and 40°C for 8 hr prior to lysis. **Western blot:** Protein samples were resolved by SDS-PAGE with an appropriate gel concentration, transferred to PVDF (Millipore), blocked either 2 hr at RT or ON at 4°C with either 5% non-fat milk/PBST or 5% BSA/TBST and incubated with indicated primary antibody in blocking buffer either 1 hr at RT or ON at 4°C. Blots were washed 3x for 10 min with either PBST or TBST, and then incubated for 1 hr at RT with secondary antibody. Membranes were then washed 4x 10 min each with either PBST or TBST and detected using Signal West Femto kit (Thermo) per manufacturer protocol and exposed to autoradiography film. Quantifications were done using NIH ImageJ software using a minimum of three independent replicates.

14.10 Antibodies and Immunostaining

All primary and secondary antibodies, detection reagents and concentration ranges utilized are summarized in Table 2. Cells seeded on glass coverslips were rinsed 2x with 1x PBS and then fixed and permeabilized with either ice cold methanol at -20°C for 15 min or buffered formalin (1x PBS, 3.7% formaldehyde, 0.3% TX-100) at 37°C for 30 min. For LA25 cells, the cells were incubated at 35°C, 37°C, and 40°C for 8 hr prior to fixation. Coverslips were washed 3x 5 min in 1x PBS with gentle agitation and then blocked for 60-90 min at 37°C (1x PBS containing 1% BSA and 0.3% TX-100). Coverslips were then incubated with the indicated primary antibodies diluted in blocking buffer for either 1 hr at RT or ON at 4°C. Coverslips were washed 3x with 1x PBS and then incubated with secondary antibody (if necessary) 1 hr at RT and then washed 1x for 5 min with 1x PBS containing 100 ng/mL DAPI and then 2x 5 min with 1x PBS. Coverslips were mounted with SlowFade (LifeTech) and sealed with clear nail polish and imaged. All images acquired on either Zeiss 710 or 800 LSM microscope.

14.11 Scrape Loading Dye Transfer Assay

Cells were scrape loaded as previously described [340]. Briefly, all buffers were pre-warmed to 37°C prior to beginning the experiment. Stable expressing HeLa or LA25 clones were seeded on bovine plasma fibronectin (Sigma; 10 µg/mL) coated 35 mm live imaging dishes (CellStar). After appropriate treatments cells were washed 1x with 1x PBS and then overlaid with dye tracer mix (1x PBS containing NB and Texas Red Dextran). LA25 cells were incubated for 8 hr at either 35°C or 40°C prior to scrape loading. HeLa cells were either transiently transfected with v-Src for 24 hr, treated with PMA (100 nM) for 1 hr, or serum starved for 24 hr and then treated with either epidermal growth factor (EGF) (100 ng/mL) or human insulin (100 nM) for 1 hr and then scrape loaded. Scrapes were introduced using a fine edged micro-scalpel and incubated at RT for 4 min. Tracer dye was gently washed away with 1x PBS and media was added and the cells returned to the incubator to culture for 6 min to allow dye to transfer. Following the dye transfer period, the cells were washed with 1x PBS containing 1 mM CaCl₂ and 1 mM MgCl₂ to stop dye spread. Dishes were then formalin fixed and stained as described above and imaged. 15 consecutive fields of view were acquired per replicate. Dye spread was quantified using an ROI tool in NIH ImageJ measuring the dye spread as a function of total area of field of view. Data is presented as mean ± SD.

14.12 TX-100 Solubility Assay

The TX-100 solubility assay was modified from a method described previously [412]. Briefly, MDCK, LA25, or HeLa cells stably expressing Cx45 grown in 10-cm dishes were washed with PBS, scraped into in 1 mL of fresh PIB and mechanically lysed by sonication (10 s at power 3). Lysates were quantified by BCA and normalized to 1.5 mg/mL. A total of 450 µL of cell lysate was brought to 1% SDS with 10% SDS and reserved as total lysate. Another 450 µL was brought to 1% TX-100 with 10% TX-100 in 1x PBS and incubated at 4°C for 30 min with agitation. The TX-100 lysate was then separated into non-junctional (supernatant; soluble) and junctional (pellet; insoluble) fractions by ultracentrifugation at 100,000 xg for 1 hr at 4°C. The supernatant was carefully removed and retained as the soluble fraction. The pellet was solubilized in 500 µL of solubilization buffer (1x PBS, 8 M urea, 2.5% SDS, 0.1 M DTT, 1x Roche complete + EDTA, 2 mM

PMSF, and 2 μM Pepstatin A). Volume normalized samples of total lysate (T), TX-100 soluble (S) and TX-100 insoluble (I) portions were analyzed by Western blot. MDCK cells were treated prior to analysis for the indicated time with PMA (100 nM) or 15 min with 100 μM pervanadate (freshly prepared). HeLa cells were transiently transfected for 24 hr with v-Src prior to analysis. LA25 cells were incubated at 35°C and 40°C for 8 hr prior to analysis. Soluble and insoluble fractions were quantified as a function of total lysate. Quantification was done using NIH ImageJ software from three independent replicates. Data is presented as the mean \pm s.e.m.

14.13 Circular Dichroism (CD): Secondary Structural Analysis

Peptides for Cx45 A333-N361 (A333-N361 npY356, and A333-N361 pY356) were purchased from LifeTein. CD experiments were performed as described previously [247]. Briefly, data was collected with a Jasco J-815 spectrophotometer with a Peltier temperature control system (Easton, MD). Spectra for the protein samples were acquired in 1x PBS pH 7.4 at 7°C. For each sample, 5 scans (wavelength range: 190–250 nm; response time: 1 s; scan rate: 50 nm/min; bandwidth 1.0 nm) were collected using a 0.01 cm quartz cell and processed using Spectral Analysis (Jasco). Spectra are presented as the averaged change in molar residual ellipticity (MRE; degree $\text{cm}^2 \text{dmol}^{-1}$) over wavelength following buffer subtraction. Peptide concentrations were determined using a NanoDrop 2000 (Thermo Scientific; Wilmington, DE) at 205 nm.

14.14 Analytical Ultracentrifugation (AUC): Sedimentation Equilibrium

AUC experiments were performed as previously described with minor modifications [247]. Peptides for Cx45 A333-N361 (npY356 and pY356) were purchased from LifeTein. Briefly, peptides were extensively dialyzed against 1x PBS pH 7.4 prior to sample preparation. Proteins were then loaded into either an AN-50Ti or AN-60Ti rotor (Beckman Coulter; Indianapolis, IN) at three concentrations ($\text{Abs}_{280} \text{ nm}$ of 0.5, 0.7, and 0.9) and speeds (24,000, 30,000, and 36,000 RPM). Sedimentation equilibrium experiments were performed at 7°C with a Beckman Optima XL-I analytical ultracentrifuge. Data were collected at various rotor speeds. Absorbance scans at 280 nm were acquired after 12 hr, 14 hr, and 16 hr at each speed; attainment of equilibrium was confirmed by overlay of all four time points. Analysis of the sedimentation equilibrium data was performed using the Beckman XL-A/XL-I software package ORIGIN v6.0. Sednterp

(<http://www.rasmb.bbri.org>) was used to calculate the buffer viscosities and densities as well as the partial specific volume for each protein based on the primary sequence.

14.15 Statistical Analysis

All data were analyzed by using GraphPad Prism 5.0 and were presented as the mean \pm s.e.m (TX-100) or mean \pm SD (scrape loading). Statistical analysis performed in GraphPad Prism 5.0 was either one-way ANOVA with a Newman-Keuls post-hoc analysis comparing all groups, or two-tailed Student's T-Test where appropriate. P-values <0.05 were considered statistically significant.

15. Results

15.1 Screen Identifies Kinases that Phosphorylate the Cx45CT

Little is known about the regulation of Cx45 by kinases and phosphorylation. Several studies have identified Cx45 as a phosphoprotein and correlative links from various phosphorylating conditions and some effect on Cx45 function [86, 189, 385, 487, 520]. Despite these advances the relationship between Cx45, specific kinase(s), the sites phosphorylated, and the physiological outcome remain unclear. Consequently, we set out to investigate how phosphorylation regulates Cx45 function, identify several kinases and the residues of Cx45 they phosphorylate.

Using a discovery-based approach, we expressed and purified recombinant mouse Cx45CT (K265-I396; see Fig. 3.2 for representative purity) as in [247]. After purification, the protein was buffer exchanged into 1x PBS pH 7.4 and submitted to Eurofins Scientific for custom KinaseProfiler Assay. We screened a total of 40 kinases for the Cx45CT. Phosphorylated Cx45CT or control peptide were captured by either FMA (Fig. 4.1A) or P30 filtermat (Fig. 4.1B) and signal determined by scintillation. The results of the screen are summarized in Fig. 4.1A and Fig. 4.1B, data presented is the mean percent of control peptide for each kinase after subtracting the signal of acid blanks. Any kinase producing greater than 50% of control signal on either filtermat was considered a positive result. A number of kinases relevant to cardiac function and disease (Fig. 4.1A and Fig. 4.1B; red bars) were able to phosphorylate the Cx45CT with at least 50% of control peptide signal, including: Src, JAK2, PKC isoforms (α , β , and δ), Pyk2, and TAK1. Based on our results and the importance that Src, PKC α , and Pyk2 have in the heart and interconnected signaling pathways (see introduction for this Chapter) we chose to focus our efforts on validating and characterizing the effects of these kinases.

15.2 Src, Pyk2, and PKC α Interact with Cx45 in HeLa Cells.

HeLa cells express Src, Pyk2, and PKC α , and thus were chosen to determine if the kinases are capable of interacting with Cx45. To test this, we generated a HeLa cell line stable expressing

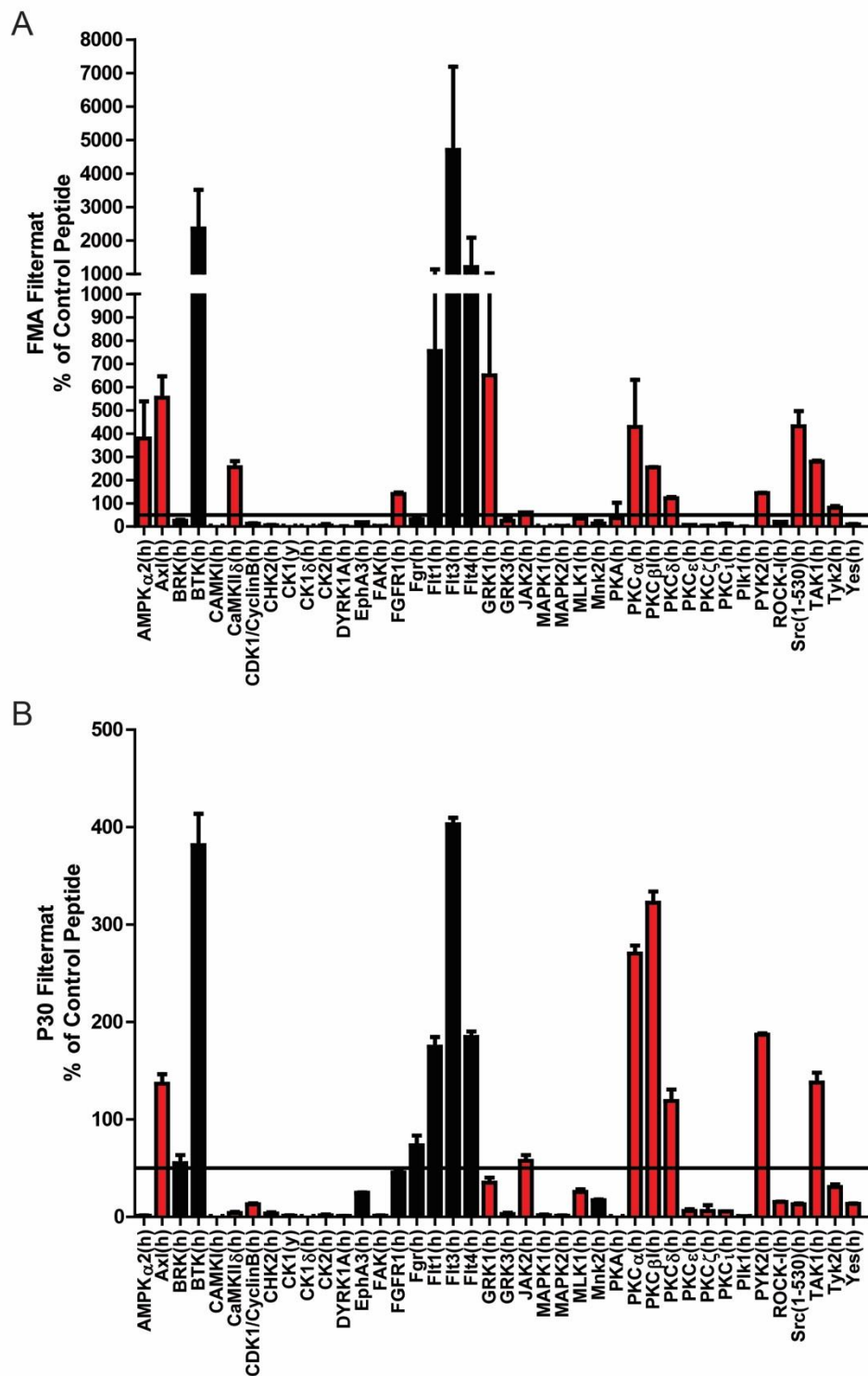


Figure 4.1. Kinase screen reveals several kinases phosphorylate Cx45CT *in vitro*.

Cx45CT (K265-I396) was expressed in *E. coli* and purified as described in Kopanic et al. (2014). Pure Cx45CT was submitted to Eurofins Scientific as test-substrate for phosphorylation in their KinaseProfiler assay. Cx45CT data is presented as the percent signal of positive control substrate for each kinase captured on A) FMA filtermat and B) P30 filtermat. Red bars represent kinases relevant to cardiac disease. Horizontal black bars correspond 50% of positive control peptide signal.

Cx45 and used a co-IP experiment to determine if the kinases interact with Cx45 under basal conditions. Lysates from the stable Cx45 expressing HeLa cells were subjected to IP ON with either an antibody against the CL domain of Cx45 or normal rabbit IgG, and then captured with resin conjugated with Protein G. Eluates were resolved by SDS-PAGE and Western blotted for Cx45, Src, Pyk2, PKC α , and p21 activated kinase 2 (PAK2). PAK2 was used as a negative control. Representative results from our co-IP experiment are shown in Fig. 4.2. We observed that Cx45 was able to co-IP Src, Pyk2, and PKC α as indicated by the presence of immunoreactivity for each kinase. Furthermore, the amount that was detected by co-IP of Cx45 was greater in all three cases compared to the background signal pulled down by normal rabbit IgG. Importantly, PAK2 immunoreactivity was not detected in either the lane corresponding to the IgG control nor the α -Cx45 lane validating our positive results and indicating our washing conditions were appropriate. Although, our results for Src are not as pronounced as either Pyk2 or PKC α , they are further supported by the NMR data in the Kopanic et al. study and consistent with the moderate K_D suggesting a more transient interaction potential [247].

15.3 Src Regulates Cx45 Phosphorylation in LA25 Cells

Having detected an interaction between Src and Cx45 using co-IP, we sought to determine if Src regulates the phosphorylation state of Cx45. To accomplish this, we generated LA25 cells that stably express Cx45. LA25 cells are useful in the study of regulation by Src because they express a temperature sensitive mutant of v-Src where the activity is modulated by incubating at alternative temperatures (35°C – Src permissive, 37°C – intermediate, 40°C – Src non-permissive) [325]. We incubated LA25 cells that stably express Cx45 for 8 hr at 35°C, 37°C, and 40°C, then lysed the cells and enriched for Cx45 by IP using antibodies raised against both the CL and the CT domain (Fig. 4.3). Eluates were resolved by SDS-PAGE and Western blotted using antibodies against general pTyr, Src, and PAK2. When Cx45 was captured using an antibody against the CL

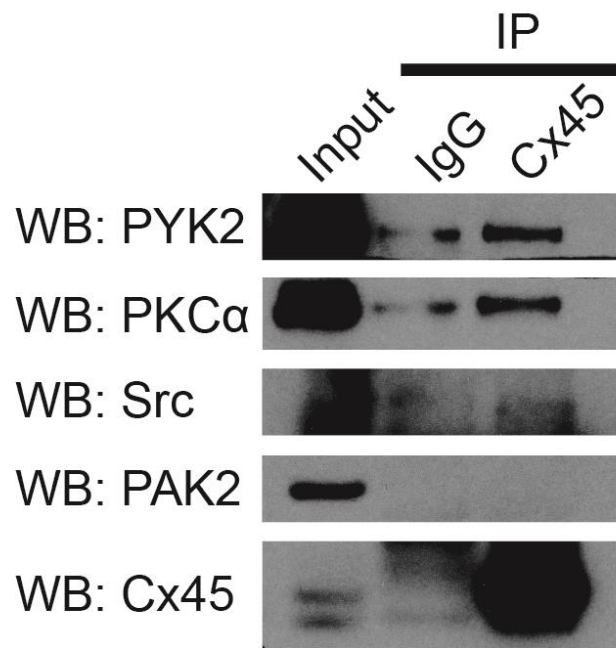


Figure 4.2. Co-IP of Src, Pyk2, and PKCα by Cx45.

HeLa cells stably expressing Cx45 were cultured and lysed. Cx45 was enriched by IP from the lysate using antibody raised against the CL domain. Eluates were resolved by SDS-PAGE, and Western blotted for the indicated kinases. Normal rabbit IgG and PAK2 were used as negative controls.

domain we observed a temperature (and Src activity) dependent increase in the amount of Src associated with Cx45, while no PAK2 was observed to co-IP, in support of the data obtained in HeLa cells (Fig. 4.3; middle). Additionally, general pTyr immunoreactivity was also detected, and increased in intensity as Src activity increased, however, based on molecular weight, the observed pTyr signal was actually derived from Cx43 also pulled-down by Cx45 (LA25 endogenously express Cx43). Any general pTyr signal for Cx45 was being obscured by the large IgG heavy chain immunoreactivity. To circumvent this, we also used an antibody against the CT domain to IP Cx45, and analyzed those eluates simultaneously (Fig. 4.3; top). When using this antibody, we observed a loss of detectable immunoreactivity to Src, suggesting the antibody against the CT domain was blocking (or disrupting) the interaction. However, we now observed two sets of bands of general pTyr immunoreactivity that increased in intensity with increasing Src activity, one consistent with the molecular weight of Cx43 and the other consistent with the molecular weight of Cx45 (Fig. 4.3; top). Interestingly, when analyzing the inputs, we observed a temperature dependent increase in the total expression of Cx45, where increasing Src activity correlated with increased Cx45 expression (Fig. 4.3; bottom).

15.4 v-Src Activity Does Not Alter Cx45 Localization in LA25 Cells

Since we observed a temperature dependent increase in the Tyr phosphorylation of Cx45 in LA25 cells we hypothesized this would correlate with a difference in protein localization following incubation at the Src permissive, intermediate, and non-permissive temperatures. We tested this by culturing the Cx45 expressing LA25 on glass coverslips to confluence and then incubating for 8 hr at the various temperatures followed by chemical fixation and immunofluorescent staining. Confocal imaging of the stained coverslips revealed little-to-no difference in the gross morphology (localization or plaque size) of Cx45 GJs (Fig. 4.4; Cx45 in red). We also immunostained Cx43 (Fig. 4.4; Cx43 in green) to determine if the both Cx45 and Cx43 co-localized under each condition. We visually observed similar colocalization between Cx45 and Cx43 under each temperature (Fig. 4.4; overlap in yellow).

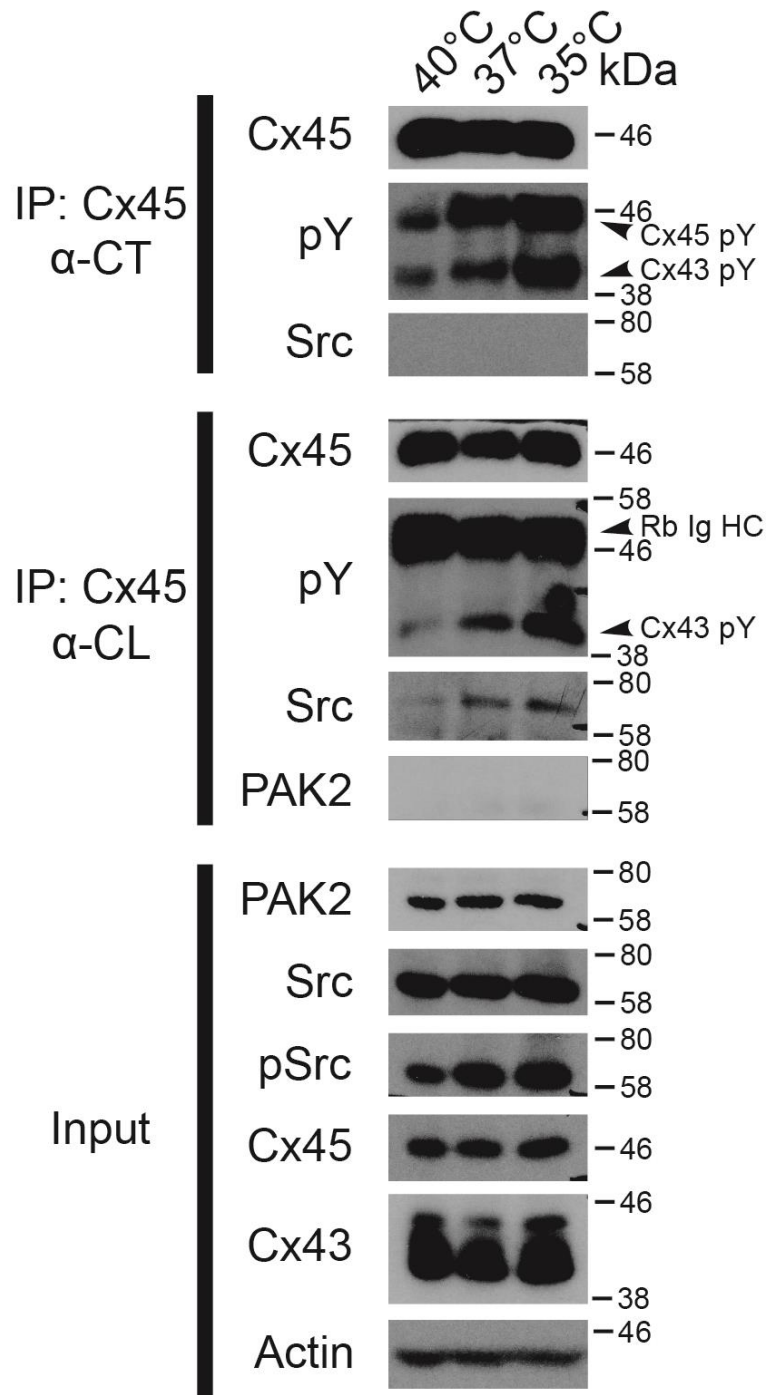


Figure 4.3. Cx45 Tyr phosphorylation increases with Src activity in LA25 cells.

LA25 cells engineered to stably express Cx45 were cultured at Src non-permissive (40°C), intermediate (37°C), and Src permissive (35°C) temperatures. Cx45 was captured by IP using antibodies raised against either the CT or CL domain. Eluates were analyzed by SDS-PAGE and Western blotted for general pTyr and Src. PAK2 was used as negative control.

15.5 v-Src Disrupts Cx45 GJ Plaque Formation in LA25 and HeLa Cells

In our immunofluorescence of Cx45 in LA25 cells at the Src permissive temperature we observed little-to-no change in the localization of Cx45 compared to the Src non-permissive temperature. We therefore hypothesized that Src activity would not affect GJ plaque formation. To test this, we cultured LA25 cells stably expressing Cx45 to confluence and then incubated the cells for 8 hr at either 35°C or 40°C. The cells were then lysed, extracted with TX-100, and fractionated into soluble (non-junctional) and insoluble (junctional) Cx45 by ultracentrifugation. The resulting fractions were resolved by SDS-PAGE and Western blotted for Cx45. Representative immunoblots are presented in Fig. 4.5A. At the Src non-permissive temperature we observed approximately 50% of the Cx45 immunoreactivity in each the soluble and insoluble fractions (Fig. 4.5A; left lanes, S – 50.5% vs. I – 49.5%, ns, N=3). Conversely, when incubated at the Src permissive temperature for 8 hr we observed a shift of Cx45 immunoreactivity from the junctional to the non-junctional pool. Quantification of the results of three independent experiments indicated this was a statistically significant change (Fig. 4.5, right lanes; S – 57.9% vs. I – 42.1%; one-way ANOVA, $P < 0.0001$, N=3;). When comparing non-permissive to permissive Src temperatures we observed a significant difference in both the soluble and insoluble Cx45 pools (Fig. 4.5; S – 40°C 50.5% vs. 35°C 57.9%, one-way ANOVA, $P < 0.01$; I – 40°C 49.5% vs. 35°C 42.1%, one-way ANOVA, $P < 0.01$). To determine if this effect was isolated to LA25 cells, we tested the response of Cx45 to transient transfection of v-Src in Cx45 expressing HeLa cells. HeLa cells stably expressing Cx45 were grown to 90% confluent and transiently transfected with v-Src or empty plasmid for approximately 24 hr prior to analysis. The obtained fractions were analyzed by SDS-PAGE and Western blot (Fig. 4.5B). Similar to observations in LA25, under control conditions Cx45 was evenly partitioned between the junctional and non-junctional pools (Fig. 4.5B; left lanes). Additionally, and again similar to the results we obtained from LA25 cells, v-Src resulted in a statistically significant shift of Cx45 from the insoluble to the soluble fraction (Fig. 4.5B; right lanes; one-way ANOVA; $P < 0.001$ comparing control to v-Src, N= 3). Quantification of three independent experiments indicated when v-Src was expressed Cx45 in the soluble pool was 65.0% of the total, while the insoluble Cx45 represented 35.0% of total (Fig. 4.5B; graph). This was compared to control transfection conditions where Cx45

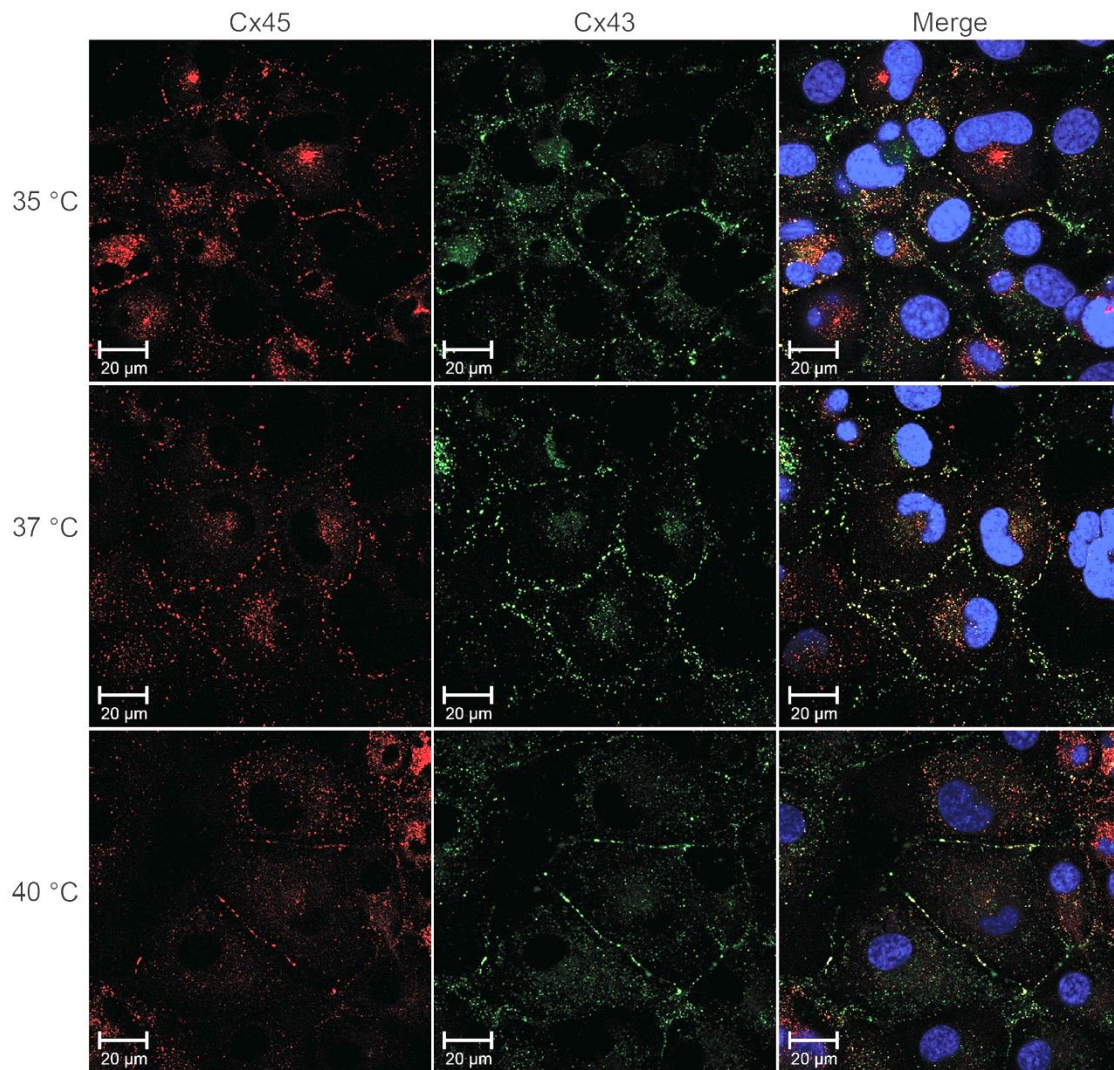


Figure 4.4. Src activity does not appreciably alter the localization of Cx45 in LA25 cells.

LA25 cells stably expressing Cx45 were grown on glass coverslips, fixed, and immunostained for Cx45 (red), Cx43 (green), and nuclei (DAPI, blue). Prior to fixation cells were incubated for 8 hr at the Src permissive, intermediate, and non-permissive temperatures.

in the soluble pool was 51.9% of total, while the insoluble pool was 48.1% of total. Interestingly, although we did not quantitate the difference in the amount of total Cx45 between either control condition (empty plasmid transfection or 40°C) and the Src active condition (v-Src transfection or 35°C), we did observe an apparent increase in total Cx45 expression when Src was active, similar to in Fig. 4.3. This may explain how little-to-no difference in the localization or GJ plaque distribution was observed in LA25 cells by immunofluorescence (Fig. 4.4). Finally, in the HeLa cells we observed a larger shift from junctional to non-functional pools of Cx45 as compared to LA25, this is likely due to the difference in time before analysis (~24 hr for v-Src transfection in HeLa vs. ~8 hr for v-Src permissive temperature in LA25).

15.6 v-Src Negatively Regulates Cx45 GJIC in HeLa Cells

Our observation of decreased junctional segregation of Cx45 in both HeLa cells and LA25 led us to hypothesize that Src active conditions would decrease Cx45 GJIC as measured by scrape loading transfer of NB. Since we observed a larger change in the segregation of Cx45 in HeLa cells we reasoned this cell line would more reliably show a phenotypic change in communication if one existed. Furthermore, since HeLa cells are deficient of endogenous Cx expression, they allow us to study the effects of Src on Cx45 function in isolation. We tested this by culturing stable Cx45 expressing HeLa cells in live imaging dishes, scrape loaded them with NB, fixed, stained with Streptavidin-488, and imaged. Representative immunofluorescent micrographs of our results are presented in Fig. 4.6. Under control conditions NB dye was transferred away from the line of the scrape an average 4-5 cell layers (Fig. 4.6; top). However, when cells were transfected with v-Src for ~24 hr, NB dye transfer was impaired, with only 1-2 layers of cells on average showing staining for NB (Fig. 4.6; bottom).

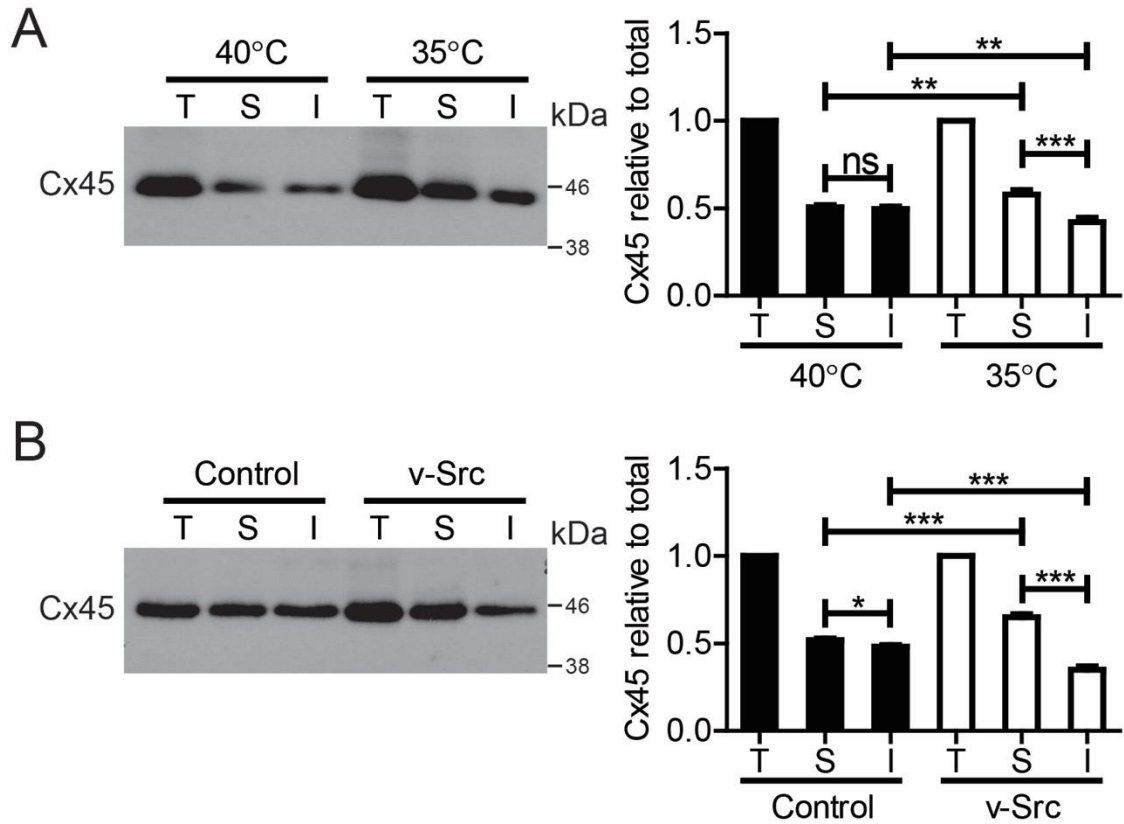


Figure 4.5. Src activity disrupts Cx45 GJ plaque formation in LA25 and HeLa cells.

TX-100 solubility assays were used to determine the effect of Src on Cx45 GJ plaque formation in A) LA25 cells incubated for 8 hr at either the Src non-permissive or permissive temperatures or B) HeLa cells transiently transfected with v-Src for 24 hr. Quantification was done from three independent experiments using NIH ImageJ for densitometry. Statistics are one-way ANOVA with a Newman-Keuls post-hoc comparison. *P <0.05, **P <0.01. ***P <0.001

15.7 Physiological Activation of Src by EGF Enhances Cx45 GJIC

Transfection of v-Src results in substantial Src activation [295]. It is possible that this nonphysiological level of activation influences GJIC in ways that do not directly involve GJ proteins, such as remodeling of actin cytoskeletal networks [521]. A more physiological stimulus for activating c-Src is stimulation of the EGFR with EGF [522]. In order to test whether acute (and more physiological) stimuli altered Cx45 GJIC, we starved HeLa cells stably expressing Cx45 of serum for 24 hr and then treated with EGF for 1 hr before scrape loading the cells with NB and Texas Red Dextran. After scrape loading the cells were fixed, stained with Streptavidin-488 and imaged. We acquired a minimum of 15 non-overlapping fields of view per replicate. To quantify dye spread we used the drawing tool of NIH ImageJ to draw regions of interest around the dye spread and measured the area as function of percent of the field of view. Representative fluorescent micrographs are presented in Fig. 4.7. GJIC of NB under serum starvation conditions was not appreciably different from under standard growth media conditions (compare Fig. 4.7 top to Fig. 4.6 top). We measured the spread of the serum starved cells to be $18.75 \pm 2.51\%$ ($n = 114$). When cells were treated for 1 hr with EGF prior to scrape loading we observed a statistically significant increase in dye spread (18.75% (control) to $25.09 \pm 2.40\%$ (EGF), $n = 82$; one-way ANOVA; $P < 0.0001$). In order to confirm that the upregulation of GJIC was specific to the signaling of the EGFR (and Src downstream) and not a function of a general stress response, we similarly serum starved the cells for 24 hr and then treated the cells with human insulin for 1 hr before scrape loading. When treated with insulin we observed little-to-no change in the NB dye spread compared to serum starved control (18.75% vs. $18.98 \pm 2.09\%$, $n = 45$; ns). Taken together the results suggest that acute phosphorylation effects activated by EGF enhance Cx45 mediated cell coupling.

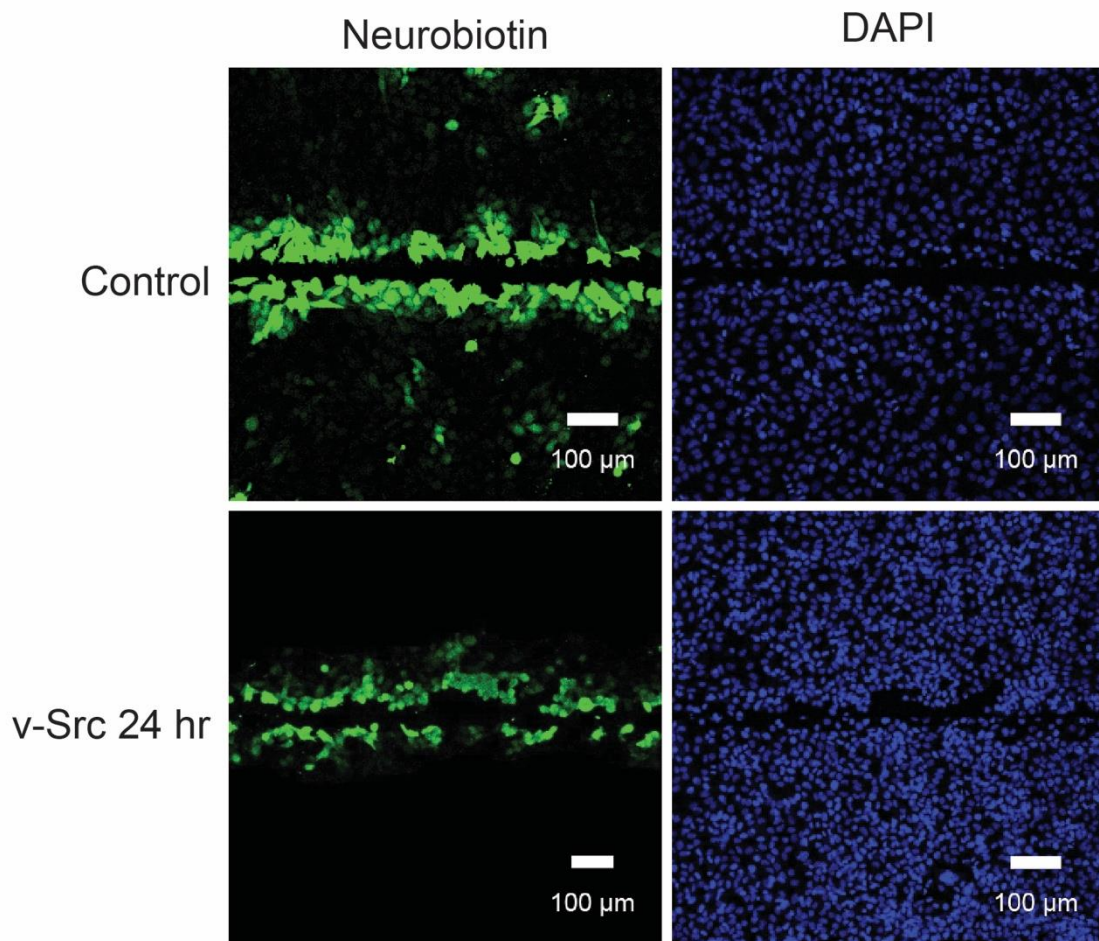


Figure 4.6. Transfection with v-Src impairs Cx45 GJIC.

HeLa cells stably expressing Cx45 were cultured in glass bottom dishes, scrape loaded with NB, fixed, stained with Streptavidin-488, and imaged. NB dye transfer (green) was assessed visually. Nuclei are stained with DAPI (blue) to illustrate cell confluence.

15.8 Acute Exposure to Pervanadate Increases GJ Plaque Formation

To further investigate the effects of acute phosphorylation on Cx45 we used pervanadate to transiently increase Tyr phosphorylation of Cx45 (see Fig. 2.12B). We tested the segregation of Cx45 into junctional and non-junctional pools after pervanadate exposure. MDCK cells were grown to confluence, treated with fresh pervanadate for 15 min, lysed, extracted, and fractionated the protein by ultracentrifugation. Notably, 15 min of pervanadate treatment in our experience has been the longest we can treat cells without observing significant loss of viability. Representative Western blot analysis of the total, soluble, and insoluble fractions of Cx45 are shown in Fig. 4.8A. Quantification of three independent experiments by densitometry indicated a statistically significant increase in the junctional (insoluble) fraction of Cx45 after pervanadate treatment. The insoluble portions of Cx45 under control conditions was $37.6 \pm 0.92\%$ and increased to $45.6 \pm 4.2\%$ when treated with pervanadate (Fig. 4.8.B and C; T-test, $P < 0.05$). The data taken together with scrape loading data suggest acute and chronic effects on GJIC can be diverse.

15.9 PMA Enhances Anchoring of Cx45 to Cytoskeleton in MDCK and HeLa Cells

In addition to Src and Pyk2, we also detected phosphorylation of the Cx45CT by PKC α in our kinase screen. Although several studies have examined the potential role for PKC regulation of Cx45 by phosphorylation, the results have not been consistent [86, 189, 306, 385, 520]. Consequently, we wanted to assess the potential effects of activation of PKC α on Cx45 in our own hands. Since the Hertlein et al. study suggested phosphorylation by PKC α promoted Cx45 stability through the use of various mutants where loss of phosphorylatable Cx45 Ser residues correlated with decreased protein stability, we sought to examine mechanistically how this may occur [189]. In order to address this, MDCK or HeLa cells stably expressing Cx45 were cultured, treated for 1 hr with PMA (or vehicle), and then analyzed by IP and Western blot for several proteins as well as general Tyr and Ser phosphorylation. Representative Western blot for MDCK (Fig. 4.9) and HeLa (Fig. 4.10) cells are presented here. In MDCK cells following treatment with PMA, we observed an increase in the active pool of Pyk2 (activated downstream of PKC α via Src [489, 492, 498, 499]) as assessed by increase Pyk2 (pY402). This indicated our treatment with PMA was successful in activating PKC. Furthermore, when we blotted for general pSer and pTyr, we observed a PMA

dependent increase in both Cx45 Ser and Tyr phosphorylation (Fig. 4.9; black arrows). Importantly, we observed this increase in total phosphorylation to correlate with increased association with the cytoskeletal anchoring proteins ZO-1, Drebrin (Fig. 4.9; black arrow), and β -tubulin. The increases in association of the cytoskeletal anchoring proteins is consistent the conclusions made by the Hertlein et al. study on the stability of Cx45 [189]. Since the MDCK cells endogenously express Cx43, we wanted to confirm our results in a cell line devoid of Cx43. We used our Cx45 stable expressing HeLa cells to test this. Following the same approach as in the MDCK cells, we cultured HeLa cells, treated for one hr with PMA, and analyzed the cells by IP and blotting for general phosphorylation and the cytoskeletal protein partners. Similar to MDCK, PMA treatment for one hr induced activation of Pyk2 (Fig. 4.10). We also detected increased activation of Src by Western blotting for Src (pY416) and total Src. Interestingly, total levels of Src were observed to increase, but not proportionally to the increase in detected active Src. Finally, we directly determined that PMA activated PKC α blotting with an antibody against PKC α (pT638), observing an increase in the active form of PKC α (Fig. 4.10; comparing total levels of PKC α and pT638). Notably, treatment with PMA reduced the total expression of PKC α in both MDCK and HeLa cells. An early study of Cx45 phosphorylation by Laing et al. demonstrated that activation of PKC by PMA in a smooth muscle-like cell derived from embryonic rat heart (BWEM cells) resulted in decreased expression of Cx45 [385]. It is likely the differences in observed total Cx45 expression levels may be cell line specific, herein we demonstrate this effect occurs in two diverse cell lines confirming our results were not impacted by co-expression of Cx43. In addition to increased total expression of Cx45, we observed PMA dependent increases in both Ser and Tyr phosphorylation in HeLa cells, consistent with our results in MDCK cells. Interestingly, the Laing et al. study, suggested that in BWEM, cells activation of PKC with PMA did not alter Cx45 phosphorylation levels by radiography of [³²P] metabolically labeled cells [385]. This difference either highlights a cell-type specific pathway, differences in treatment times and concentrations (30 min and 50 nM in Laing et al.; 1 hr and 100 nM herein), or limitations in the ability of the Cx45 antibody used in the Laing et al. study to IP all phosphoisoforms of Cx45 [385]. While all are reasonable possibilities the latter has been observed for Cx43 (for example see [523]). In combination with our results from two diverse cell lines and the observation

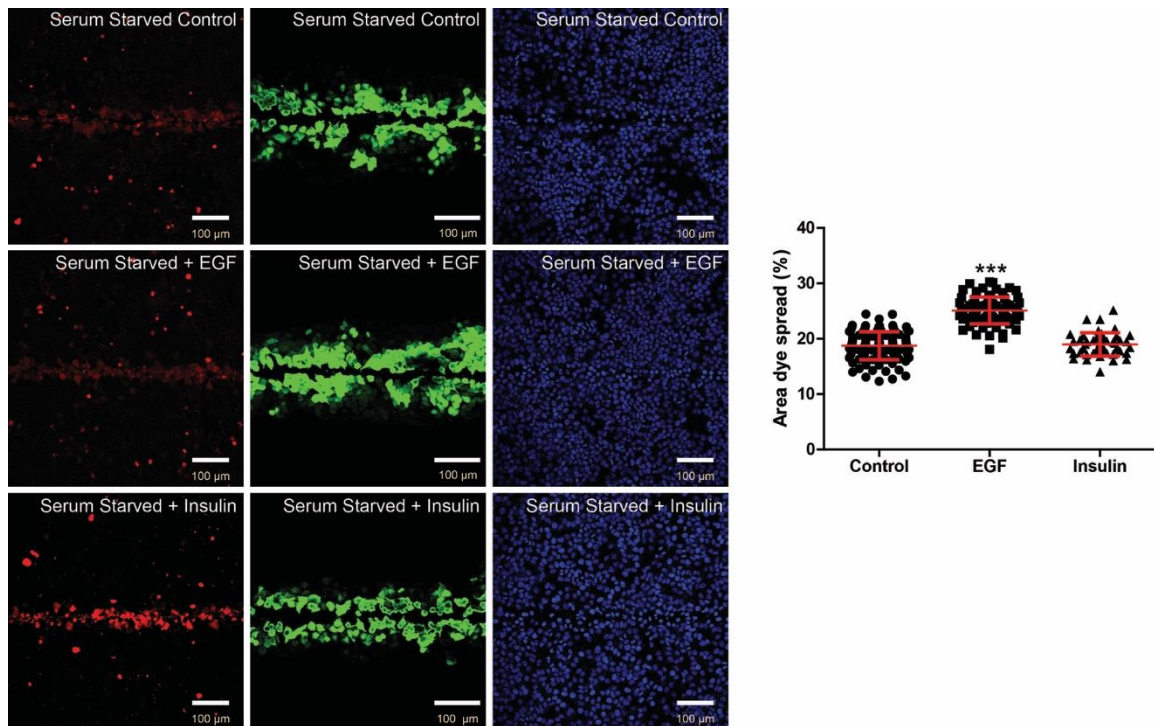


Figure 4.7. More physiologically relevant activation of Src by stimulation of the EGFR by EGF enhances Cx45 GJIC.

HeLa cells stably expressing Cx45 were culture to confluence in glass bottom dishes, serum starved for 24 hr, and then treated with either EGF (100 ng/mL) or insulin (100 nM) for 1 hr. Cells were then scrape loaded with NB and Texas Red Dextran, fixed, stained with Streptavidin-488, and imaged. NB dye spread was measured as a function of total area of field of view from a minimum of 10 non-overlapping fields of view in each of three independent replicates. Statistics are one-way ANOVA with a Newman-Keuls post-hoc comparison. ***P <0.0001

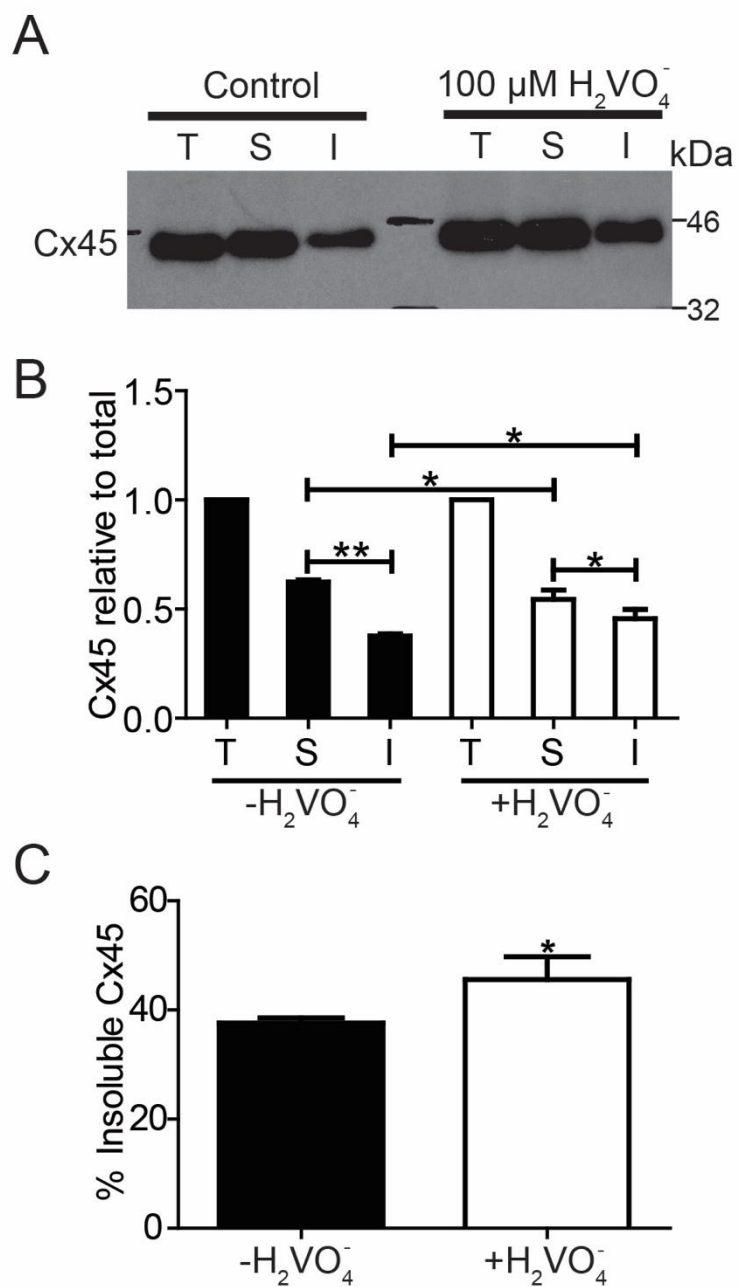


Figure 4.8. Acute pervanadate treatment enhances Cx45 GJ plaque incorporation.

MDCK cells stably expressing Cx45 were cultured to confluence and then treated with 100 μM pervanadate for 15 min to increase total Tyr phosphorylation. Cells were then lysed, extracted with TX-100 and fractionated into total (T), non-junctional (soluble – S), or junctional (insoluble – I) pools of Cx45. A) Representative Western blot of the fractionation of Cx45. B) Quantification of three independent experiments by densitometry. C) Comparison of the total amount of insoluble Cx45. Statistics for B) are one-way ANOVA with a Newman-Keuls post-hoc comparison and (*P <0.05, **P <0.01) C) Two-tailed Student's T-Test (*P <0.05).

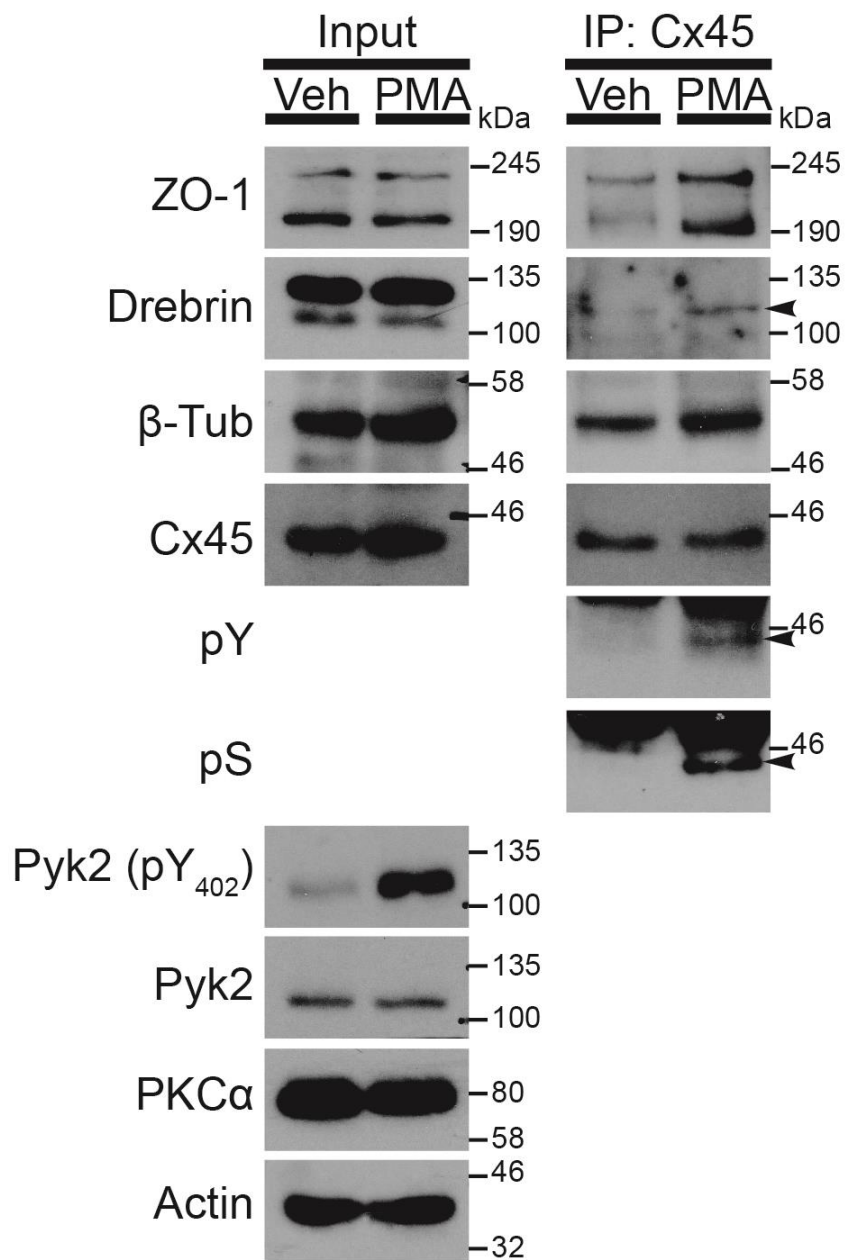


Figure 4.9. PMA increases Cx45 Tyr and Ser phosphorylation and enhances cytoskeletal anchoring in MDCK cells.

MDCK cells stably expressing Cx45 were cultured and treated for 1 hr with 100 nM PMA and lysed. Lysates were subjected to IP with an antibody against the Cx45 CL and Western blotted with antibodies against general pSer, pTyr, Drebrin, β-tubulin, and ZO-1. Phosphorylation of Pyk2 (pY₄₀₂) was used as a marker for PKC activation.

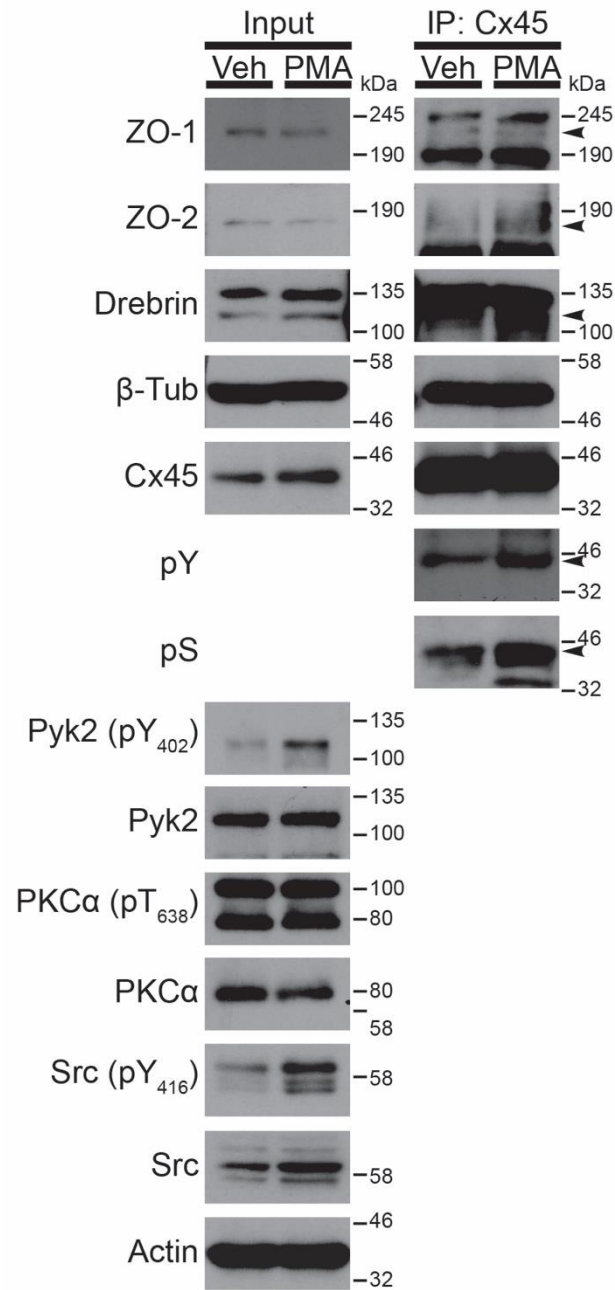


Figure 4.10. PMA increases Cx45 Ser and Tyr phosphorylation and enhances interactions with cytoskeletal anchors in HeLa cells.

HeLa cells stably expressing Cx45 were cultured and treated for 1 hr with 100 nM PMA and lysed. Lysates were subjected to IP with an antibody against the Cx45 CL and Western blotted with antibodies against general pSer, pTyr, Drebrin, β-tubulin, ZO-1, and ZO-2. Phosphorylation of PKCα (pT638), Pyk2 (pY402), and Src (pY416) were used as marker of PKC activation.

that some Cx43 antibodies are conformation specific, it is highly likely this is the case and presents an important caveat in the analysis of IP of phosphorylated proteins when changes in the amount of precipitated protein are detected. When blotting for cytoskeletal partners, we observed an appreciable increase in the association of Drebrin, ZO-1 and ZO-2 pulled-down by Cx45 after PMA (a second tight-junction actin cytoskeletal anchoring protein). We were unable to test the association of ZO-2 with Cx45 in MDCK cells as the available antibodies were not reactive to canine ZO-1, however, our observations of increased ZO-1 and Drebrin are consistent with the results we obtained in MDCK cells (Fig. 4.9). For β -tubulin little-to-no change in the amount that came down with Cx45 was observed between vehicle and PMA treated cells (Fig. 4.10). It is possible that regulation of the microtubule network in HeLa cells (a cancer line) and MDCK cells (a kidney epithelial line) by signal transduction is different. Another possibility is that species specific differences in the primary sequence of β -tubulin or binding site for β -tubulin on Cx45 may result in different outcomes.

15.10 Treatment with PMA Does Not Affect Cx45 GJ Plaque Formation

Following our observation of increased association of the cytoskeleton anchors β -tubulin, Drebrin, ZO-1, and ZO-2 we hypothesized this would correlate with an increase in the amount of Cx45 present in the junctional pools. We therefore tested this by TX-100 solubility assay and analyzed the results by SDS-PAGE and Western blot. To test this in absence of any influence from Cx43, we treated and analyzed Cx45 from our stable HeLa line. We initially treated cells for 1 hr with PMA as we did in our IP experiments previously. Comparing levels of junctional and non-junctional Cx45 after 1 hr of PMA we observed little-to-no change in the immunoreactivity of Cx45 (Fig. 4.11A and B; S – 47.2% vs. 49.0%, I – 52.8% vs. 51.0%, ns). In order to determine if time-dependent changes may occur beyond the 1 hr treatment period, we additionally treated cells for 2 and 4 hr and evaluated them in the same manner (Fig. 4.11A and B). Similar to 1 hr of PMA treatment, we observed little-to-no change in either the soluble or insoluble pools of Cx45 (Fig. 4.11B; 2 hr S – 51.8% vs. 53.0%, I – 48.2% vs. 47.0%, ns; 4 hr S – 49.3% vs. 49.5%, I – 50.7% vs. 50.5%, ns). Finally, to determine if minute changes were present we compared the vehicle-to-PMA

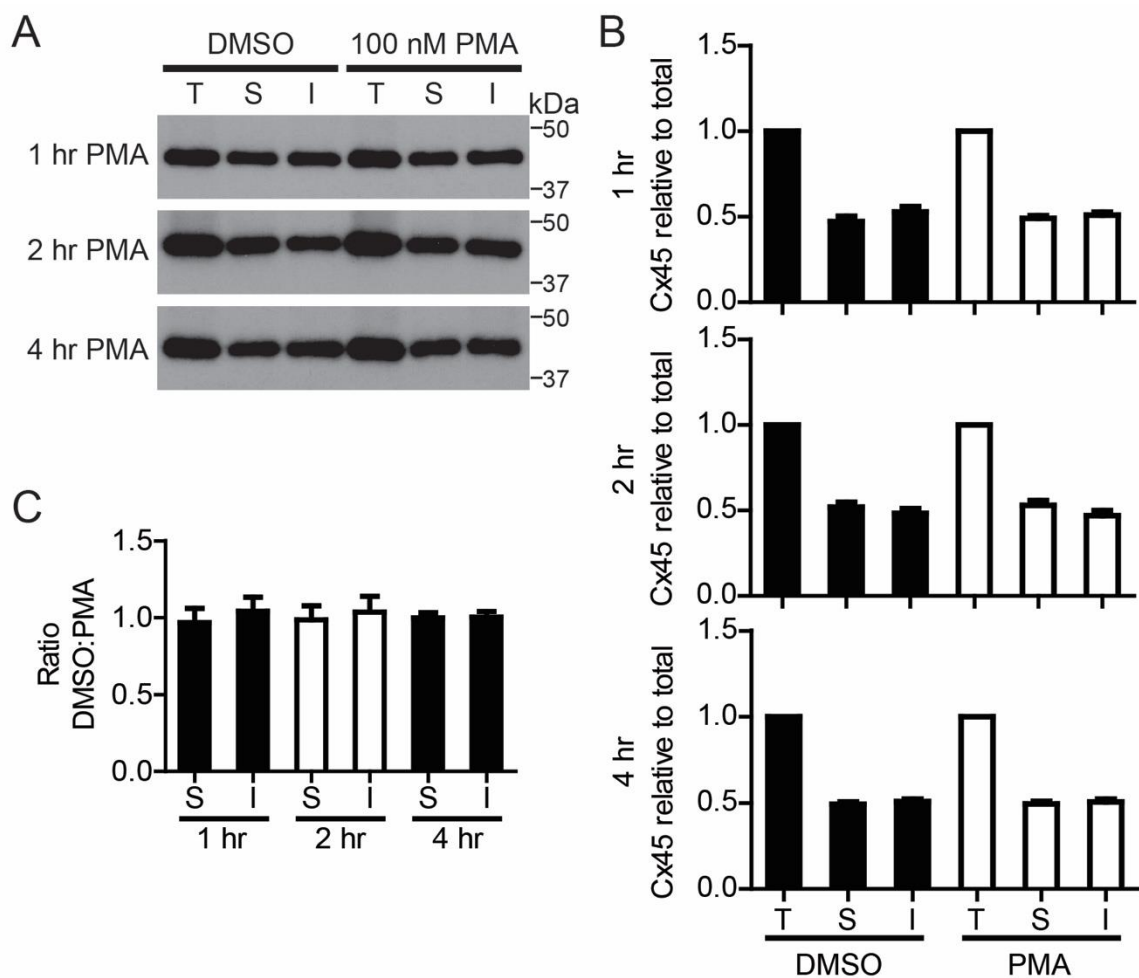


Figure 4.11. PMA does not affect Cx45 GJ plaque stability.

HeLa cells stably expressing Cx45 were cultured and treated with 100 nM PMA for 1, 2, and 4 hr periods and then lysed, extracted with TX-100, and fractionated into total (T), non-junctional (soluble – S), and junctional (insoluble – I) Cx45 pools by ultracentrifugation. Resulting fractions were analyzed by SDS-PAGE and Western blot. A) Representative Western blots of Cx45 fractions. B) Quantification of three independent replicates using densitometry by ImageJ. C) Ratio of vehicle:PMA treated samples of the S and I fractions at each time point. Statistical analysis used was one-way ANOVA with a Newman-Keuls post-hoc comparison.

ratios at each time-point for both soluble and insoluble pools of Cx45 (Fig. 4.11C; 1 hr S – 0.969, I – 1.04; 2 hr S – 0.986, I – 1.03; 4 hr S – 0.998, I – 1.00). Consistent with our direct quantification by densitometry no difference was detected between vehicle and PMA treatments at any time point.

15.11 Activation of PKC by Treatment with PMA Impairs Cx45 GJIC

Stemming from our observation that PMA did not alter the GJ plaque incorporation of Cx45 and the previous conflicting reports on the effects of PMA on Cx45 GJIC we sought to evaluate this in our own hands as well. In the van Veen et al. study ROS cells were used which endogenously co-express Cx43 [306]. Conversely, the Martinez et al. study used HeLa cells to study Cx45 in the absence of influence from other Cx family members [86]. In order to assess the effect of PMA on Cx45 in isolation in our study we similarly used HeLa cells. After culturing HeLa cells expressing Cx45 to confluence, the cells were treated for 1 hr with PMA and scrape loaded with NB, fixed, stained, and imaged. Representative fluorescent micrographs are presented in Fig. 4.12. Importantly, NB dye spread was observed in vehicle treated cells comparably to the untreated cells in Fig. 4.6. When quantified as a function of area of field of view vehicle treated cells were observed to have a total dye spread of $23.6 \pm 2.46\%$ of the field area. When cells were treated with PMA communication was still observed, however, the total area of dye spread was significantly reduced (Fig. 4.12; vehicle 23.6% vs. PMA $19.74 \pm 3.26\%$; T-Test; $P < 0.0001$). This observation is in conflict with the dye transfer results presented by the Martinez et al. study [86].

15.12 MS Identifies Cx45 Residues Phosphorylated by Src, Pyk2, and PKC α

Functionally, we have provided several pieces of data that suggest activation of Src, Pyk2 (indirectly), and PKC α regulate Cx45. Unfortunately, without explicit knowledge of the residues phosphorylated by each of the kinases, attribution of a given effect to a specific kinase remains correlative at best. For Cx43 phosphoisoform specific antibodies are essentially responsible for our

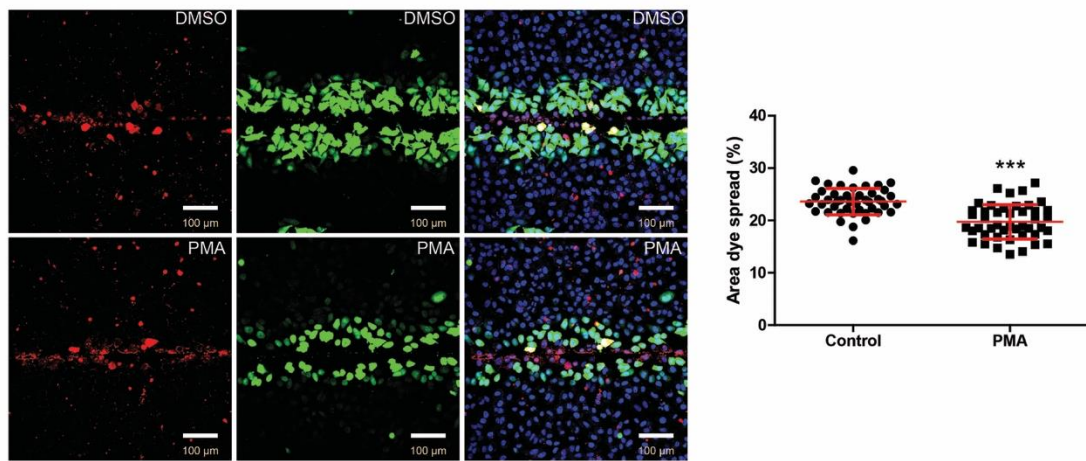


Figure 4.12. Treatment with PMA impairs Cx45 GJIC in HeLa cells.

HeLa cells stably expressing Cx45 were culture to confluence in glass bottom dishes then treated with either vehicle or PMA (100 nM) for 1 hr. Cells were then scrape loaded with NB and Texas Red Dextran, fixed, stained with Streptavidin-488, and imaged. NB dye spread was measured as a function of total area of field of view from a minimum of 15 non-overlapping fields of view in each of three independent replicates. Statistics are two-tailed Student's T-Test. ***P < 0.0001

current degree of understanding of the regulation of Cx43 by phosphorylation (reviewed in [524]). Regrettably, while several high-quality commercial Cx43 phosphoisoform specific antibodies exist, there are currently none for Cx45. In order to lay the groundwork for the development of phosphoisoform specific Cx45 antibodies and simultaneously identify Cx45 residues phosphorylated by Src, Pyk2, and PKC α we purified Cx45CT (K265-I396; for example of purification, see Fig. 3.2) and phosphorylated it *in vitro* with Src (recombinant human full-length, Sigma), Pyk2 (recombinant human residues 360-690, SignalChem), or PKC α (recombinant human full-length, SignalChem). The resulting phospho- and non-phosphoproteins were resolved by SDS-PAGE and the bands corresponding to Cx45CT were cut from the gel and submitted to the Beth Israel Deaconess Mass Spectrometry Core Facility at Harvard for PTM mapping. A summary of the residues identified as phosphorylated by each kinase is presented in Fig 4.13. For Src (Fig. 4.13A) Tyr residues 324 and 356—the latter is present in the Cx45CT dimerization domain—were identified by peptides that mapped to this region containing mass shifts of 80 Da, consistent with a phosphoryl moiety (data not shown). Similar to Src, for Pyk2 phosphorylated Cx45CT we also identified Tyr residues 324 and 356 (Fig. 4.13B, peptides detected not shown). Interestingly, for Cx43CT our laboratory has also detected identical phosphorylation by MS from Src and Pyk2 [295]. When we phosphorylated Cx45CT with PKC α and analyzed by MS we observed phosphorylation of several Ser residues and one Thr residue (Fig. 4.13C). Specifically, we observed Ser phosphorylation on residues 326, 376, 378, 381, 381, 384, and 385; and detected Thr phosphorylation on residue 392 (Fig. 4.13C; peptides detected not shown). Of note, T392 is immediately followed by a Ser residue, so the possibility exists that this is erroneous placement of the phosphate during analysis, however, this remains to be tested.

15.13 Cx45CT Mutants Confirm MS and Identify Additional Phosphorylated Tyrosines

Although MS identified only two Tyr residues phosphorylated by either Src or Pyk2, at least one other Tyr (Y301) has been identified as phosphorylated in other studies utilizing high through-put MS that did not directly investigate Cx phosphorylation [525, 526]. Furthermore, despite

A
GSKRRELD DPGAYNYPFTWNTPSAPPGYNI AVKPDQIQYTEL
SNAKIAYKQNKANIAQEQQY³²⁴GSHEEHL PADLET LQREIRMA
QERLDLAIQAY³⁵⁶HHQNNPHGPREKKAKVGSKSGSNKSSISS
KSGDGKTSVWI

B
GSKRRELD DPGAYNYPFTWNTPSAPPGYNI AVKPDQIQYTEL
SNAKIAYKQNKANIAQEQQY³²⁴GSHEEHL PADLET LQREIRMA
QERLDLAIQAY³⁵⁶HHQNNPHGPREKKAKVGSKSGSNKSSISS
KSGDGKTSVWI

C
GSKRRELD DPGAYNYPFTWNTPSAPPGYNI AVKPDQIQYTEL
SNAKIAYKQNKANIAQEQQYGS³²⁶HEEHL PADLET LQREIRMA
QERLDLAIQAYHHQNNPHGPREKKAKVGSKS³⁷⁶GS³⁷⁸NKS³⁸¹
S³⁸²IS³⁸⁴S³⁸⁵KSGDGKT³⁹²SVWI

Figure 4.13. MS reveals residues of Cx45CT phosphorylated *in vitro* by Src, Pyk2, and PKC α . Cx45CT (K265-I396) was expressed in *E. coli*, purified as in Kopanic et al. (2014), and *in vitro* phosphorylated by Src, Pyk2, or PKC α . Reactions were resolved by SDS-PAGE, the bands for Cx45CT were cut out and submitted to the Beth Israel Deaconess Mass Spectrometry Core Facility at Harvard for PTM mapping. Summary of residues phosphorylated (red) by A) Src, B) Pyk2, and C) PKC α .

the high sensitivity of MS as a tool for identifying PTMs, there are limitations to its use, such as the inherent failure of some peptides to fly in MALDI-TOF [320, 527]. Additionally, the high-throughput discovery-type nature of MS requires subsequent validation of through the use of low-throughput methods due to the high kinase concentration used in the reaction which can result in aberrant hyperphosphorylation. In order to validate the results of our MS analysis on Src and Pyk2 phosphorylated Cx45CT we generated single Tyr mutants of Cx45CT (Table 6) where all CT Tyr residues (7 total) except 1 were mutated to Phe to focus analysis to phosphorylation on a specific residue. We in vitro phosphorylated Cx45CT WT and each of the 7 single Tyr mutants with either Src (Fig. 4.14A) or Pyk2 (Fig. 4.14B), resolved the resulting proteins by SDS-PAGE, and then Western blotted for pTyr using a general pTyr antibody. In addition to validating the MS data, this method allows for determining the “primary” target of the specific kinase as it will be the mutant with the highest degree of pTyr signal detected. As negative control a second reaction was prepared replacing the kinase volume with excess reaction buffer. For Src we observed robust phosphorylation of Cx45CT WT as expected. When analyzing the single Tyr mutants, Cx45CT Y324 displayed the highest degree of pTyr signal, followed by Y301, then Y275, and finally Y356. The data validates Tyr residues 324 and 356 as phosphorylated by Src (as detected in the MS data), and identified novel Tyr residues 275, and 301. Importantly, the data identifies Cx45 Tyr residue 324 as the primary target for Src. For Pyk2 we followed an identical approach to validate the residues identified by MS. Similar to Src, we observed phosphorylation on the MS identified sites as well as additional residues. In order of decreasing signal strength, we observed Tyr phosphorylation of Cx45CT WT > Y324 > Y301 ≈ Y277 > Y275 ≈ Y356. Our results therefore validate the MS identified Tyr residues (324 and 356) as well as identified novel Tyr residues (275, 277, and 301), of which Tyr 324 is also the primary target for Pyk2.

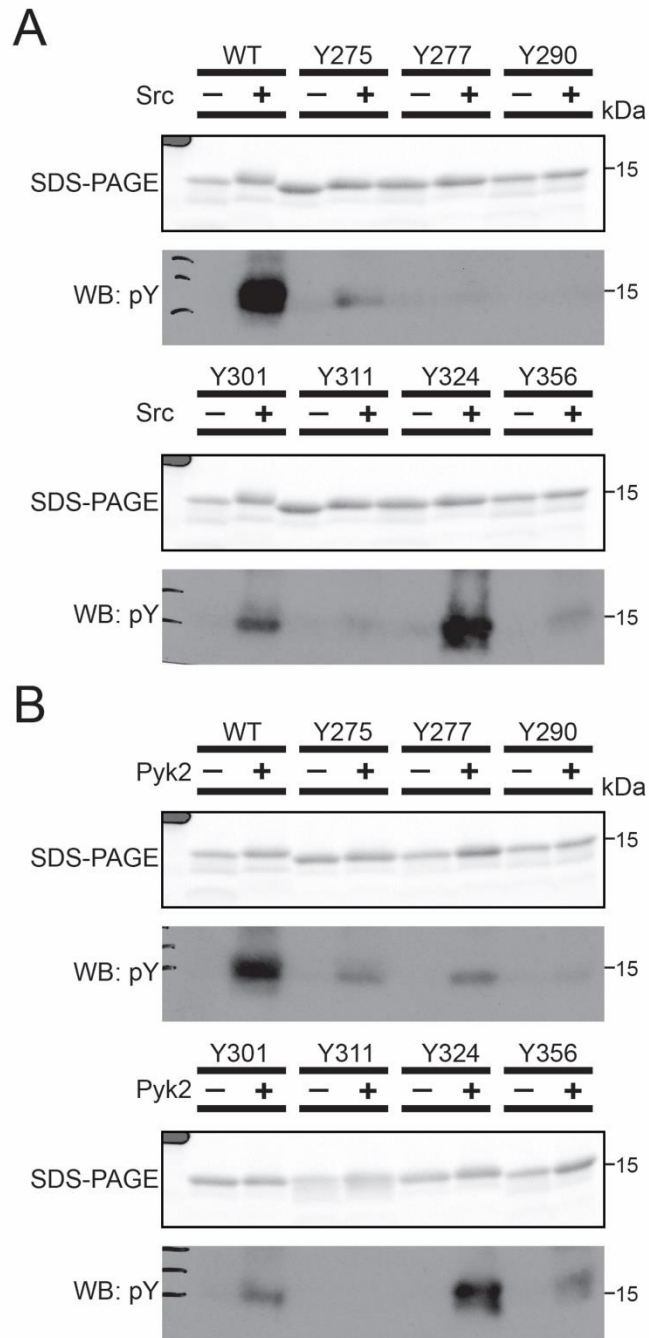


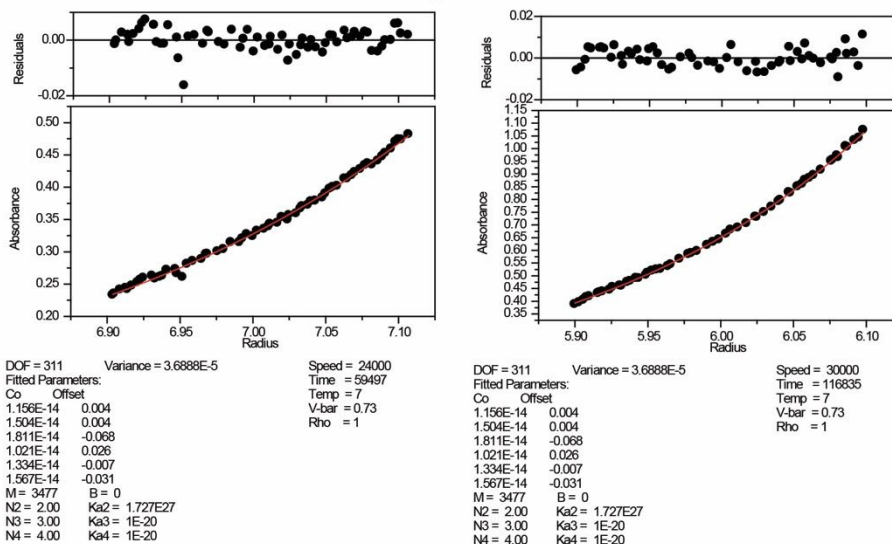
Figure 4.14. Cx45CT single Tyr mutants reveal novel phosphorylated residues and validate *in vitro* MS results.

Cx45CT WT (K265-I396) and mutants where all but the indicated Tyr residue have been mutated to Phe, were *in vitro* phosphorylated by A) Src or B) Pyk2. Reactions were resolved by SDS-PAGE and Western blotted with a general pTyr antibody to detect phosphorylation.

15.14 Phosphorylation of Y356 Reduces Cx45CT A333-N361 Dimerization Affinity

Although Y324 was identified as the primary target for both Src and Pyk2, we have significant interest in Y356 as it is identified as a critical residue mediating the dimerization of the Cx45CT domain [247]. As such we sought to determine if phosphorylation of Y356 would affect Cx45CT dimerization. To test this, we purchased peptides (LifeTein) corresponding to Cx45CT A333-N361 that was either not phosphorylated on Y356 (npY356) or was phosphorylated on Y356 (pY356) and subjected them to AUC sedimentation equilibrium (example curves shown in Fig. 4.15). Importantly, analysis of observed mass revealed both peptides sedimented primarily as dimers (npY356 – 7.332 ± 0.17 kDa; pY356 – 6.541 ± 0.12 kDa). However, based on calculated molecular weight the npY356 peptide (3.458 kDa), the observed mass suggests a small contribution from the presence of higher order oligomers. Previous characterization of recombinant Cx45CT A333-N361 observed a similar phenomenon, where the recombinant peptide (including a linker not present in the synthesized peptide) sedimented with a mass consistent with a primarily tetrameric arrangement [247]. In the same study the K_D for the monomer-dimer species was calculated to be 141 nM [247]. We did not calculate the K_D for the npY356 peptide, however for the pY365 peptide we calculated the K_D and determined it to be 531 ± 284 μ M. Taken together the data indicates phosphorylation of Cx45 Y356 severely impacts the affinity of dimerization.

Cx45CT A333-N361
1x PBS pH 7.4 7°C



Cx45CT A333-N361 pY356
1x PBS pH 7.4 7°C

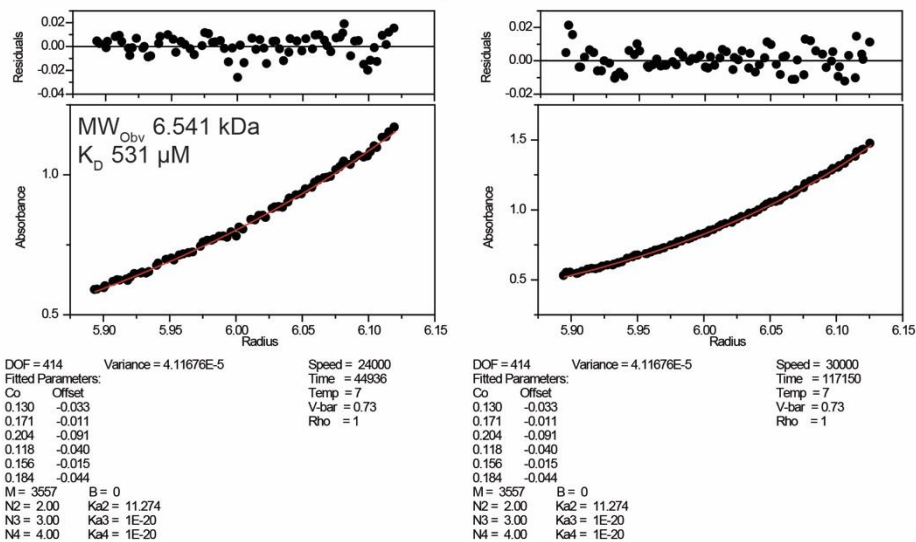


Figure 4.15. Phosphorylation of Y356 reduces the dimerization affinity of Cx45 A333-N361 by an order of seven magnitudes.

Peptides corresponding to A333-N361 with or without phosphorylation of Y356 were synthesized by LifeTein. Peptides were dialyzed into 1x PBS pH 7.4 and their oligomeric status was assessed by AUC sedimentation equilibrium. Observed mass and dimerization affinity for the A333-N361 (pY356) peptide are inlaid on the left plots. Plots shown are for speeds: 24,000 (left) and 30,000 (right) RPM.

15.15 Cx45 Y356 Phosphorylation Does Not Alter Structure of A333-N361

Although there are many mechanisms by which phosphorylation may be reducing the dimerization affinity of Cx45 A333-A361, one possibility is that phosphorylation may alter the secondary structure of residues A333-N361. Any change in structure that results in loss of the hydrophobic face of the A333-N361 (either by loss of helix entirely or by “over-tightening” it as acetonitrile does) would reasonably alter the K_D of the homodimerization. To test whether phosphorylation of Y356 affects A333-N361 secondary structure both npY356 and pY356 peptides were subjected to CD spectroscopy to analyze overall secondary structure (Fig. 4.16). Similar to what was observed in our previous study, the secondary structure of the npY356 (Fig. 4.16; black line) peptide is consistent with that of an α -helix, indicated by the presence of a local maxima at 195 nm, and two local minima at 208 and 222 nm respectively. When phosphorylated on Y356 (Fig. 4.16; red line), we observed a decrease in the magnitude of the local maxima at 195 nm, as well as a slight positive change in magnitude (i.e., less negative) for the local minima at 208 and 222 nm. This suggests there may be a mild decrease in the total amount of helical character, however, the overall trace is consistent with an α -helical structure and we therefore conclude that phosphorylation has not significantly altered the structure of the peptide. On a technical note, the difference observed in the traces could also be explained by differences in calculated MRE as this is a function that is concentration dependent. Phosphorylation of Tyr residues reduces the extinction from $1,490 \text{ M}^{-1}\text{cm}^{-1}$ (ExPasy ProtParam value for Tyr) to $\sim 650 \text{ M}^{-1}\text{cm}^{-1}$, thereby reducing the reliability of A_{280} in determining concentration [528]. To circumvent this, A_{205} (measures the peptide bond absorbance [529]) was utilized, however, the effect of phosphorylation of side chains on the A_{205} of peptide to our knowledge has not been explored, and thus the possibility exists that even using A_{205} may introduce a margin of error that modestly affects analysis.

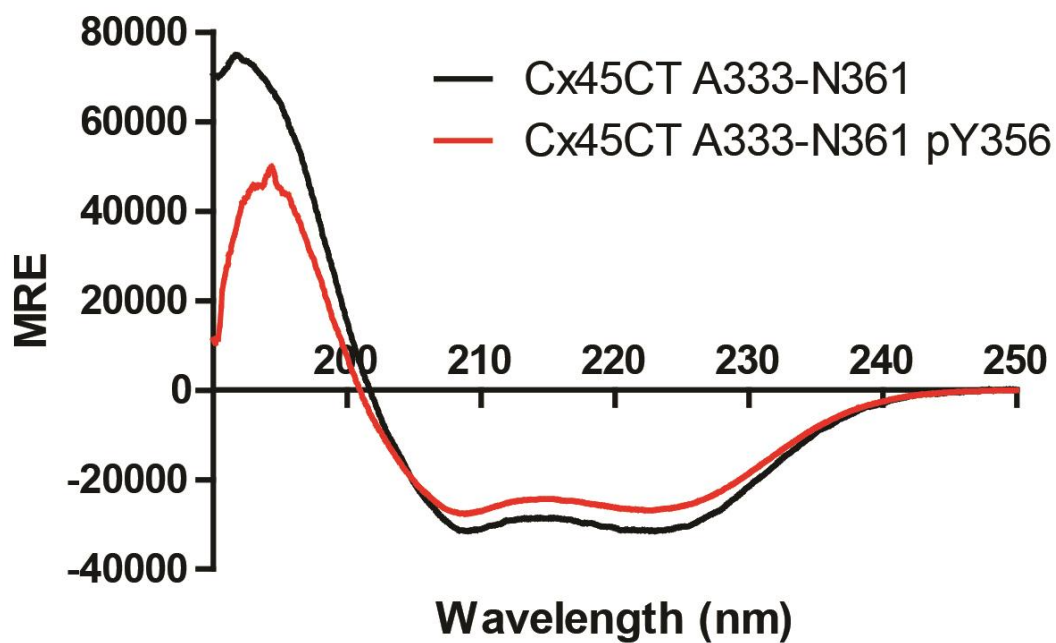


Figure 4.16. Phosphorylation of Y356 does not alter A333-N361 secondary structure.

Peptides corresponding to A333-N361 with or without phosphorylation of Y356 were synthesized by LifeTein. Peptides were dialyzed against 1x PBS pH 7.4 and then the secondary structure was assessed by CD spectroscopy from 190 – 250 nm. The curves are presented as mean residual ellipticity (MRE).

15.16 Phosphomimetic Cx45 Y356E Localizes Similar to Cx45 WT

As one final experiment, we hypothesized phosphorylation of Cx45 Y356 may regulate Cx45 in cells since it reduced the affinity of the dimer. To test this, we created a phosphomimetic mutant Cx45 Y356E and used that to generate a stable expressing MDCK cell line. As we have on numerous accounts, we used immunofluorescence of the localization of Cx45 as an indicator of major phenotypic changes in trafficking, plaque incorporation, or degradation. Representative immunofluorescent micrographs of Cx45 WT and Y356E expressed in MDCK cells are presented as Fig. 4.17. Cx45 (green) is seen in both Cx45 WT and Y356E as primarily punctate GJ plaques studding the cell surface with a significant contribution of intracellular puncta as well. This was not surprising, as phosphorylation of the Tyr reduced dimerization affinity, but since the concentration of CT domain present in the connexon would be in excess of 500 μM ([CT] in connexon \sim 25 mM; [231]), even the CT of phosphorylated Cx45 would still be present primarily as a dimer. Furthermore, the use of Glu as a substitution for pTyr, although well accepted in the GJ field is not a perfect mimetic, as it lacks the ring stacking interactions and the negative charge is not equivalent.

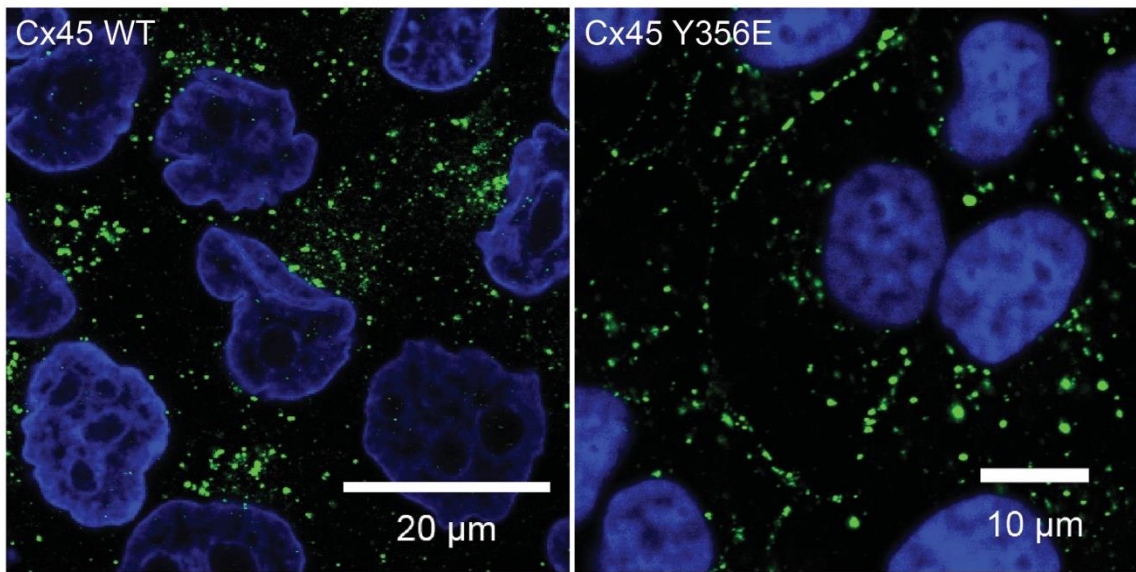


Figure 4.17. Phosphomimetic Cx45 Y356E similarly to Cx45 WT.

MDCK stably expressing Cx45 Y356E were cultured on glass coverslips, fixed, and immunostained for Cx45 (green) and imaged on a Zeiss LSM 800 confocal microscope. Nuclei were stained with DAPI (blue). Cx45 WT from Fig. 3.4 has been included for ease of comparison. Scale bar for Cx45 WT = 20 μm , and for Y356E = 10 μm .

16. Discussion

In this Chapter, we have presented numerous observations confirming and expanding upon previous reports that Cx45 is a phosphoprotein [189, 385]. Although, these previous studies detected Cx45 phosphorylation [189, 385], and in some cases attributed functional effects of activation of a specific kinase [86, 306, 385], no direct connections to a specific kinase or phosphorylated residue were presented. We used an *in vitro* screen to identify several kinases that phosphorylate the Cx45CT. Specifically, a number of the kinases that were able to phosphorylate the Cx45CT are known to be involved in AngII signaling [491, 492, 498, 499, 504, 509]. Upregulation of AngII in the bloodstream is a hallmark of both hypertensive patients and those suffering from end-stage heart failure [530]. Similarly, Cx45 expression in the myocytes of ventricles has been shown to increase in a number of models of heart disease and in human patient samples [67, 75, 79, 82]. The understanding how phosphorylation of Cx45 affects its function in context of heart disease is critical for the development of novel therapeutic targets. Importantly, while Cx45 expression increases in the ventricles, Cx43 expression is reduced [67, 71, 75, 84, 531]. Residual Cx43 has therefore been demonstrated to form heteromeric channels with Cx45 and suggested to form the basis for arrhythmias via altered electrical properties of the resultant heteromeric channels [31, 86, 87]. Despite this notion, work in native cardiac murine GJs has suggested that the presence of Cx45 in the ventricles did not alter the organ level electrical properties of the heart (i.e., ECG, QRS duration, etc.) [83]. Additionally, the study identified a number of Cx45 residues phosphorylated *in vitro* by CaMKII and CK1, several of which we also identified as phosphorylated by PKC [83]. One caveat to the study of Bao et al. is their focus on the outcome of Cx45/Cx43 heteromeric channels in healthy hearts [83]. While this is important, it does little to examine how the presence of Cx45 alters electrical properties of the heart in the diseased state, which is notably characterized by a vastly altered kinase landscape, including increased expression and activation of PKC, Pyk2, and Src [491, 492, 498, 499, 504, 509].

Our results demonstrate the Cx45CT domain is efficiently phosphorylated *in vitro* and *in cyto* by Src, leading to impaired and enhanced GJIC under chronic and acute Src activation, respectively. When v-Src was overexpressed, we observed a decrease in the total amount of

junctional (TX-100 insoluble) Cx45, that correlated with impaired transfer of NB dye and increased Tyr phosphorylation. The loss in junctional Cx45 was consistent between both LA25 cells at the Src permissive temperature and HeLa cells transiently transfected with v-Src. Surprisingly, we did not observe a gross change in the localization or punctate GJ staining of Cx45 in LA25 when Src was active, which has been demonstrated for Cx43 [325]. The mechanism behind this remains to be determined, however, one possibility is the anecdotal increase in total Cx45 expression when Src was overexpressed (HeLa) or active (LA25). Contrastingly, we observed an increase in NB dye transfer when we treated HeLa cells with EGF to achieve more physiological levels of Src activation. Our results with EGF treatment highlight a difference in the regulation of Cx45 and Cx43 by the EGFR signaling. A study by Warn-Cramer et al. studying the regulation of Cx43 used EGF to treat cells and measured the Cx43 mediated g_j and observed a rapid decrease in coupling within 4 minutes of treatment [532]. The authors attributed this effect specifically to the Cx43 MAPK sites, as mutation of S255,279,282 prevented the downregulation of GJIC by EGF treatments [532]. For Cx45 in our system, whether this is directly linked to Src or alternate pathways activated by EGF remains to be determined. Regardless, the result indicates a dichotomy may exist between acute and chronic stimulation of signaling pathways or alternatively low vs. high levels of phosphorylation. This is supported by variable results of several studies using EGF to affect GJIC [533-539]. In the bulk of these studies EGF treatment disrupted GJIC on a short time frame (30 min to 1 hr), however in the study by Vikhamar et al. an increase in Cx43 mediated GJIC was observed 2-3 hr after treatment with EGF [533-539]. The authors speculated this may be a function of the low native coupling observed in the K7 cells they used in the study [539]. Another acute effect we observed was the increase in junctional Cx45 in MDCK cells treated with pervanadate, a stimulus we previously demonstrated increases the amount of total Tyr phosphorylation on Cx45 [424]. Due to the very short test period it is unclear what the fate of the Cx45 protein would have been 30-45 min later. Finally, for Src we detected phosphorylation on Y275, Y301, Y324, and Y356, of which Y324 was the apparent primary target.

In addition to regulation by Src, our results suggest that Cx45 GJIC is also modulated by PKC as well. Although we did not detect alterations in the GJ plaque dynamics of Cx45 in response

to PKC activation, we did observe a number of phenomena worth discussing. First, we observed increased ability of Cx45 to co-IP several cytoskeletal proteins when cells were treated with the PKC activator PMA. In both HeLa cells and MDCK we observed an increase in the amount of Drebrin and ZO-1 that precipitated with Cx45. In HeLa cells, we additionally detected an increase in the amount of ZO-2 pulled down, which we were unable to assess in MDCK cells due to antibody recognition issues. The only non-consistent change in protein partner binding we observed was for β -Tubulin, in MDCK we observed an increase while in HeLa no change. Notably, when cells were treated with PMA we observed an increase in the total levels of Cx45 Ser and Tyr phosphorylation indicating that PMA is activating a Tyr kinase downstream of PKC that can phosphorylate Cx45, perhaps Src [511]. Although we have not explored the signaling pathway in detail to determine which kinases are contributing to the phosphorylation of Cx45 subsequent to PMA treatment, the enhanced associations linking Cx45 to the structural network of the cell is of particular interest. This is in contrast to Cx43, whose association with the cytoskeleton is generally disrupted by increased Tyr phosphorylation [286, 295, 325, 378]. A notable difference between Cx43 and Cx45 is the binding sites for the cytoskeletal proteins (predicted: β -Tubulin (R267-P273; MAPred [540]); empirically determined: Drebrin (T283-K312; Sorgen Laboratory, unpublished data) and ZO-1 (K371-I396; Kopanic et al. [247])) is the lack of Tyr residues phosphorylated by Src, except Drebrin which has one Tyr phosphorylated by Src while Cx43 has three in the Drebrin binding domain [295]. Consistent with the conclusions of Hertlein et al., the increased affinity of cytoskeletal proteins and correlated stability (at least to 4 hr) suggest that phosphorylation of Cx45 by PKC contributes to Cx45 GJ stability [189]. Importantly, residues identified by Hertlein et al. to contribute to Cx45 stability in their study were identified as phosphorylated by PKC in our MS analysis [189]. In contrast to the studies of van Veen and Martinez et al., we observed a PMA dependent decrease in NB transfer [86, 306]. Few differences exist between our study and that of van Veen et al. that may explain the difference in our results, HeLa cells expressing mouse Cx45 were utilized in each study, the major differences are the method of detection (macroscopic conductance vs. dye coupling) and the timeframe addressed (0-5 min vs. 1 hr after addition of PMA). It is possible that on our time scale we are observing effects mediated by downstream effectors of PKC, however to this will need

to be addressed directly by future studies. Similar to the van Veen et al. study, Martinez et al. used HeLa cells expressing mouse Cx45, they however measured both macroscopic conductance and dye coupling [86]. Key differences in these two studies are the concentration of PMA used to treat cells (100 nM vs. 200 nM) and the timeframe of analyses, which for the Martinez et al. study was more in line with our own [86, 306]. Although, Martinez et al. concluded no statistical difference in the NB dye transfer of Cx45 channels after 30 min of PMA, they did observe a non-statistical decrease [86]. It is possible this decrease would have become more pronounced at 1 hr if that assay had been continued. Indeed, when they measured macroscopic conductance after 1 hr of PMA treatment they did note a reduction in g_j [86].

The study of contributions to the regulation of Cx45 by Pyk2 at this point are merely correlative. We observed an increase in Pyk2 activity as measured by autophosphorylation of Y402 when cells were treated with PMA. In fact, lack of high-quality selective inhibitors for Pyk2 make investigating its role in phosphorylating Cx45 difficult to separate from either Src or PKC. Despite this, our results have shown a number of Cx45 residues that are phosphorylated by Pyk2, all but one of which (Y277) are also targeted by Src. We have observed a similar trend for the phosphorylation of Cx43 by Pyk2 and Src as well (Sorgen Laboratory, unpublished data). Current models link Src and Pyk2 activity the scaffolding protein Paxillin, where Src is required for enhanced activation of Pyk2 via phosphorylation of residues Y579/580 on Pyk2 [505, 541]. Due to the physical link (Paxillin) between these two kinases and the reliance of Pyk2 on Src for its full activity, it is unlikely Pyk2 is ever the “lone gunman” kinase, but rather fine-tunes the effects of Src. The development of inhibitors selective for Pyk2 will no doubt be essential for delineating its specific role in regulating Cx45 (and Cx43).

Although knowledge of the regulation of Cx43 by phosphorylation is broad, that of Cx45 is quite limited. Very few studies investigate the outcome of activation of specific kinase programs on Cx45 function and those that have do not make a direct link to phosphorylation of any specific residue of Cx45. In this Chapter, we have used a diverse set of approaches (biophysical, cellular and molecular biology, and proteomics) to investigate phosphorylation of Cx45. Our results confirm previous studies that have demonstrated Cx45 is a phosphoprotein and expand on the notion that

Cx45 is regulated by kinases active downstream of the AT1R [189, 385]. Additionally, our results suggest that important differences may exist in the regulation of Cx45 by kinases when compared to Cx43, a feature that may contribute to maintained Cx45 expression in the ventricles of diseased hearts as well as the arrhythmogenic substrate.

CHAPTER FIVE

Cross-regulation of the Cardiac Connexins: Cx45 Protects Cx43 From Kinase Initiated Turnover

17. Introduction

In Chapter Four we characterized the phosphorylation of Cx45 by kinases (Src, Pyk2, PKC α) active downstream of the AT1R [491, 492, 498, 499, 504, 509]. Additionally, all three of the kinases similarly phosphorylate Cx43 (Pyk2 – Sorgen Laboratory, unpublished data) [296, 300]. The effects of Src and PKC on Cx43 mediated GJIC are well characterized and lead to the down-regulation of coupling through either channel closure, loss of cytoskeletal anchoring and internalization, or the combination of these [19, 286, 295, 296, 300, 325, 337, 339, 351, 372-376, 480, 482-484, 542]. Our results in Chapter Four suggest that aspects of the regulation of Cx45 by these kinases, at least in the acute stage are different than that of Cx43 (EGF increased Cx45 GJIC and PMA enhanced cytoskeletal anchoring supporting plaque stability). Since Cx45 and Cx43 can form heteromeric channels the question arises how these kinases would affect the regulation of heteromeric channels. It stands to reason that in cells that express two or more Cx family members compatible to form heteromeric channels, that regulation of all aspects of the heteromeric channels are likely more complex than either individual counterpart. Indeed, a number of observations support this. For example, dye coupling properties of Cx43-Cx45 heteromeric channels in HeLa cells fail to couple LY (anionic) while NB dye coupling is maintained, suggesting Cx45 exerts a dominant negative effect on Cx43 [86]. Similarly, in NRK cells stably transfected with the lens Cx56 (NRK-Cx56), the current-voltage relationship was altered compared to that of untransfected NRK cells (endogenously express Cx43) [543]. Specifically, the untransfected NRK cells displayed a decay of current following a voltage pulse of >50 mV and the rate of decay was proportional to the magnitude of the voltage pulse [543]. Conversely, the NRK-Cx56 cells maintained current conductance following the voltage pulse without appreciable decay, suggesting that the presence of Cx43-Cx56 heteromeric [543]. Finally, two studies examining the formation of heteromeric channels between Cx43 and Cx40 in vascular smooth muscle cells observed significant differences in dye permeability and channel electrical properties [544, 545]. Although all of these studies highlight differences in channel properties formed from intermixing of Cx family members, only the Martinez et al. study investigated the regulation of the heteromeric channels by phosphorylation [86]. In their study, they noted that NB coupling of Cx45 homomeric channels were unaffected by

addition of PMA (contrary to our results in Chapter Four), however, when Cx43 was co-expressed they observed significant reductions in NB dye coupling, suggesting the presence of Cx43 exerted some regulatory role on Cx45 in response to phosphorylation [86].

Studies have hinted at the potential for heteromeric channel formation in the failing heart. In the ventricles of human patients with heart failure, Yamada et al. noted an increase in the protein expression of Cx45 by approximately 2-fold, that correlated with an increase in immunostaining by 3.5-fold compared to non-failing hearts [82]. Notably, Cx45 mRNA levels in the failing hearts was unaltered suggesting that Cx45 protein stability was increased by some mechanism in the failing hearts [82]. Additionally, the presence of Cx45 in the failing heart increases the susceptibility to tachyarrhythmias [432]. While the mechanisms of how Cx45 expression was upregulated and maintained in these systems was not explored, altered regulation by kinases maybe a contributing factor. Notably, in Chapter Four, when we immunostained Cx45 and Cx43 in the stable Cx45 expressing LA25 cells we observed Cx43 still present at the GJ plaque where it colocalized with Cx45 at the Src permissive temperature contrary to what was observed in our previous study by Li et al. [340]. We therefore sought to investigate the potential cross-regulation of Cx45 on Cx43 in heteromeric channels in LA25 cells.

18. Materials and Methods

18.1 Antibodies and Reagents

All antibodies and reagents for this study are contained in Table 2.

18.2 Cell Culture and Stable Cell Line Generation

LA25 cells (gifts from Dr. Paul Lampe, Fred Hutchinson Cancer Center) were cultured in Dulbecco's modified Eagle medium (Corning) at 37°C in a humidified 5% CO₂ atmosphere. Medium was supplemented with 10% FBS (Seradigm), 2 mM L-glutamine (HyClone), 1% pen-strep (Corning), and 0.2% Normocin (Invivogen). The selective agent puromycin (Tocris) was used, when appropriate, at empirically determined concentrations. 70% confluent LA25 cells were lipofected with Sall linearized plasmid using Lipofectamine 2000 at a 1:2 ratio in OptiMem. Transfections were carried out under antibiotic free conditions, and cells were cultured 48-72 hr prior to addition of selection media. LA25 cells were selected 7 µg/mL. Cells were clonally (monoclonal) selected using Whatman paper cloning disks. Western blots and immunofluorescence were used to screen clones. Src activity, in LA25 cells, was modulated by culturing the cells at 35°C (permissive – Src active), 37°C (intermediate), or 40°C (non-permissive – Src inactive) for 8 hr.

18.3 siRNA Knock-down of Exogenous Cx45

Parental (Cx45⁻) LA25 cells or those stably expressing Cx45 (Cx45⁺) at approximately 60% confluent were lipofected with stealth siRNA designed against the exogenous mouse Cx45 using Lipofectamine RNAiMAX according to manufacturer protocol under antibiotic free conditions, cells were cultured 48 hr prior to any analysis. Complexes were generated in OptiMem. siRNA was designed using the Invitrogen design tool against the coding region (CDS) of accession number NM_001159382.1. siRNA duplex sequence: 5'-UUUGCUUGUAGGCAAUCUUAGCAUU-3' and 5'-AAUGCUAAGAUUGCCUACAAGCAAA-3'

18.4 Antibodies and Immunostaining

All primary and secondary antibodies, detection reagents and concentration ranges utilized are summarized in Table 2. Cells seeded on glass coverslips were rinsed 2x with 1x PBS and then fixed and permeabilized with either ice cold methanol at -20°C for 15 min or buffered formalin (1x

PBS, 3.7% formaldehyde, 0.3% TX-100) at 37°C for 30 min. LA25 cells were incubated at 35°C, 37°C, and 40°C for 8 hr prior to fixation. For siRNA mediated knock-down of exogenous Cx45, at 60% confluence cells were transiently transfected with siRNA as described in 18.3. Coverslips were washed 3x 5 min in 1x PBS with gentle agitation and then blocked for 60-90 min at 37°C (1x PBS containing 1% BSA and 0.3% TX-100). Coverslips were then incubated with the indicated primary antibodies diluted in blocking buffer for either 1 hr at RT or ON at 4°C. Coverslips were washed 3x with 1x PBS and then incubated with secondary antibody (if necessary) 1 hr at RT and then washed 1x for 5 min with 1x PBS containing 100 ng/mL DAPI and then 2x 5 min with 1x PBS. Coverslips were mounted with SlowFade (LifeTech) and sealed with clear nail polish and imaged. All images acquired on either Zeiss 710 or 800 LSM microscope.

18.5 Scrape Loading Dye Transfer Assay

Cells were scrape loaded as previously described [340]. Briefly, all buffers were pre-warmed to 37°C prior to beginning the experiment. Cx45⁻ or Cx45⁺ LA25 cells were seeded on bovine plasma fibronectin (Sigma; 10 µg/mL) coated 35 mm live imaging dishes (CellStar). After appropriate treatments cells were washed 1x with 1x PBS and then overlaid with dye tracer mix (1x PBS containing NB). LA25 cells were incubated for 8 hr at either 35°C or 40°C prior to scrape loading. Scrapes were introduced using a fine edged micro-scalpel and incubated at RT for 4 min. Tracer dye was gently washed away with 1x PBS and media was added and the cells returned to the incubator to culture for 6 min to allow dye to transfer. Following the dye transfer period, the cells were washed with 1x PBS containing 1 mM CaCl₂ and 1 mM MgCl₂ to stop dye spread. Dishes were then formalin fixed and stained as described above and imaged. 15 consecutive fields of view were acquired per replicate. Dye spread was quantified using an ROI tool in NIH ImageJ measuring the dye spread as a function of total area of field of view.

18.6 TX-100 Solubility Assay

The TX-100 solubility assay was modified from a method described previously [412]. Briefly, Cx45⁻ or Cx45⁺ LA25 cells were grown in 10-cm dishes were washed with PBS, scraped into in 1 mL of fresh PIB and mechanically lysed by sonication (10 s at power 3). Lysates were quantified by BCA and normalized to 1.5 mg/mL. A total of 450 µL of cell lysate was brought to 1%

SDS with 10% SDS and then reserved as total lysate. Another 450 μ L was brought to 1% TX-100 with 10% TX-100 in 1x PBS and incubated at 4°C for 30 min with agitation. The TX-100 lysate was then separated into non-junctional (supernatant; soluble) and junctional (pellet; insoluble) fractions by ultracentrifugation at 100,000 xg for 1 hr at 4°C. The supernatant was carefully removed and retained as the soluble fraction. The pellet was solubilized in 500 μ L of solubilization buffer (1x PBS, 8 M urea, 2.5% SDS, 0.1 M DTT, 1x Roche complete + EDTA, 2 mM PMSF, and 2 μ M Pepstatin A). Volume normalized samples of total lysate (T), TX-100 soluble (S) and TX-100 insoluble (I) portions were analyzed by Western blot. LA25 cells were incubated at either 35°C or 40°C for 8 hr prior to analysis. Soluble and insoluble fractions were quantified as a function of total lysate. Specifically, for Cx43 quantification was done using samples resolved on a 15% SDS-PAGE to ensure collapse of the multiple phosphorylation depended migratory forms into a single band. Quantification was done using NIH ImageJ software from three independent replicates.

18.7 Statistical Analysis

All data were analyzed by using GraphPad Prism 5.0 and were presented as the mean + s.e.m. Statistical analysis performed in GraphPad Prism 5.0 was either one-way ANOVA with a Newman-Keuls post-hoc analysis comparing all groups, or two-tailed Student's T-Test where appropriate. P-values <0.05 were considered statistically significant.

19. Results

19.1 Cx45 Prevents Src Mediated Turnover of Cx43 Containing GJs

Since we observed a maintenance of Cx43 immunoreactivity consistent with GJ plaques in LA25 cells expressing Cx45 at the Src permissive temperature in Fig. 4.4 we hypothesized this would correlate with reduced TX-100 solubility. To test this, we cultured Cx45⁻ or Cx45⁺ LA25 cells to confluence, then incubated them for 8 hr at either the Src non- or permissive temperatures. Expression of Cx45 was assessed in both Cx45⁻ or Cx45⁺ LA25 cells by Western (Fig. 5.1A) Cells were lysed, extracted and resolved by SDS-PAGE and analyzed by Western blot for Cx43 (we used a high percentage gel to collapse Cx43 phosphoisoforms into a single band for ease of quantification) (Fig. 5.1B). At the Src non-permissive temperatures, we observed no difference in the junctional pool of Cx43 regardless of Cx45 expression (Fig. 5.1C, dashed lines; Cx45⁻ 56.5% vs. Cx45⁺ 55.9%, ns, N=3). When comparing the Src permissive to the Src non-permissive temperature within each group (i.e., Cx45⁻ to Cx45⁻), we observed a significant decrease in the amount of junctional Cx43 at the Src permissive temperature compared to the non-permissive (Fig. 5.1B, solid lines; Cx45⁻ 40°C – 56.5% vs. 35°C – 30.7%, $P < 0.0001$; Cx45⁺ 40°C – 55.9% vs. 35°C – 39.6%, $P < 0.0001$, N=3). Finally, when comparing the amount of non-junctional and junctional Cx43 between the Cx45⁻ and Cx45⁺ LA25 cells at the Src permissive temperature, we observed a difference in the degree of change in Cx43 (Fig. 5.1C, dashed lines; Cx45⁻ 30.7% vs. Cx45⁺ 39.6%, $P < 0.05$, N=3). In Cx45⁻ LA25 cells we observed only 35% of Cx43 remaining in the junctional pool, while for Cx45⁺ LA25 this was ~45%. Suggesting that Cx45 was stabilizing some of the Cx43 at the GJ plaque. In parallel, we resolved Cx43 on our standard 10% SDS-PAGE gel to display the multiple migratory forms (Fig. 5.1D).

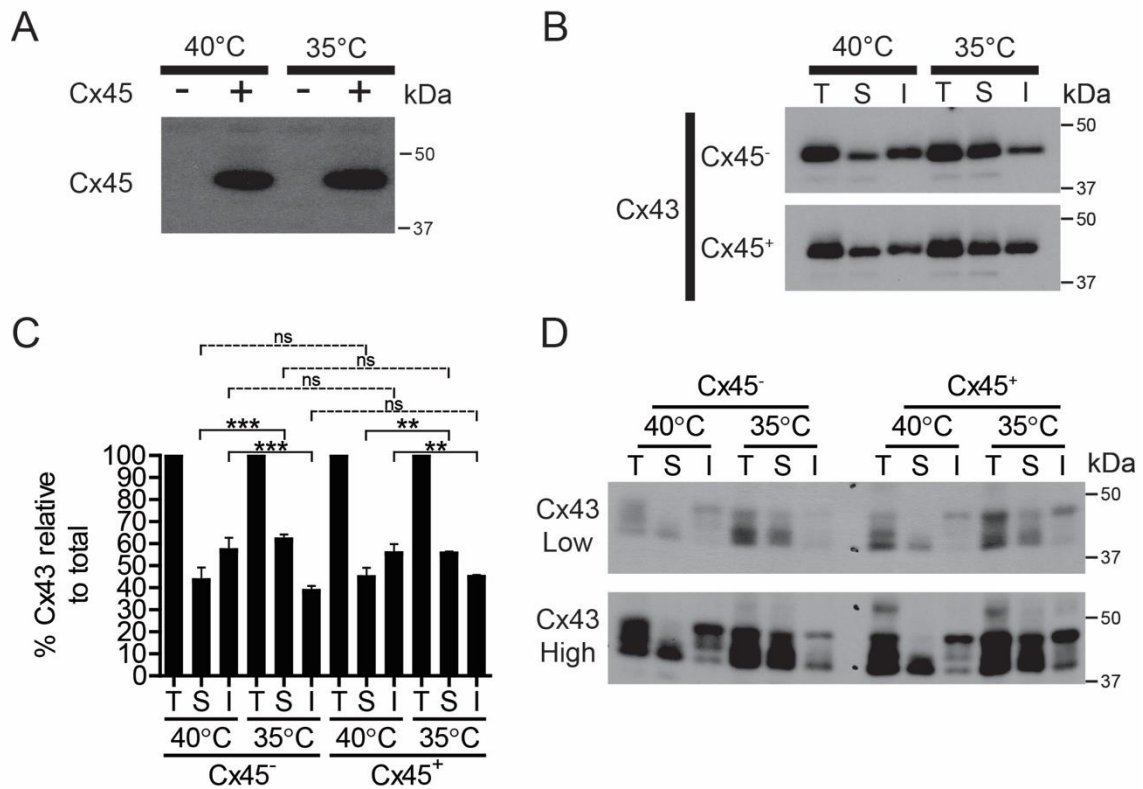


Figure 5.1. Cx45 mutates the effect of Src on Cx43, reducing the transition of junctional to non-junctional Cx43.

Cx45⁻ and Cx45⁺ LA25 cells were cultured to confluence and incubated at 40°C or 35°C for 8 hr. Cx43 was extracted with TX-100 and fractionated into total (T), non-junctional (TX-100 soluble, S) and junctional (TX-100 insoluble, I) fractions by ultracentrifugation. A) Representative Western blot showing the expression of Cx45 in the Cx45⁻ and Cx45⁺ LA25 cell lines B) Representative Western blot of resulting fractions analyzed by 15% SDS-PAGE and probed for Cx43. C) Quantification of 15% blots from three independent experiments. D). Representative Western blot of Cx43 fractions resolved on 10% SDS-PAGE demonstrating multiple electrophoretic forms of Cx43. Statistics are one-way ANOVA with a Newman-Keuls post-hoc analysis, *P < 0.05, ***P < 0.0001.

19.2 Knock-down of Exogenous Cx45 Results in Src Mediated Cx43 Turnover

To follow up with our TX-100 data from the previous experiment, we hypothesized that the increase in Cx43 GJ stability in the Cx45⁺ LA25 cells would be lost if expression of Cx45 was abrogated. We cultured Cx45⁺ LA25 cells on glass coverslips to 60% confluent and then treated with siRNA designed against the exogenous Cx45 for 48 hr. Following siRNA treatment, the cells were maintained for 8 hr at the Src non-, intermediate, or permissive temperatures, fixed and immunostained the cells. Representative immunofluorescent micrographs are presented in Fig. 5.2. As expected when LA25⁺ were treated with siRNA, we observed a stark decrease in the expression of Cx45 indicating the knock-down was successful (Fig. 5.2; red; right panels). This was surprisingly more efficient at the Src permissive temperature than either intermediate or non-permissive. Immunoreactivity of Cx43 in the mock transfected LA25⁺ was similar in pattern and degree at all three temperatures (Fig. 5.2; green; left panels), however, when Cx45 was knocked down we observed a Src activity dependent loss of Cx43 immunoreactivity (Fig. 5.2; green; right panels). In fact, after 8 hr at the Src permissive temperature the majority of Cx43 staining was completely lost. Furthermore, few if any GJ plaques were observed. Taken together with the TX-100 data, this further supports the hypothesis that Cx45 protects Cx43 from the effects of Src.

19.3 Presence of Cx45 Does Not Protect Against Src Mediated Channel Closure

Our immunostaining and TX-100 data suggest that expression of Cx45 is a factor that contributes to maintained GJIC in cells expressing Cx43 when Src is active. We wanted to test this using scrape loading transfer of NB in Cx45⁻ and Cx45⁺ LA25 cells. Experimentally, we cultured either Cx45⁻ or Cx45⁺ LA25 in glass bottom dishes to confluence, incubated them at 35°C or 40°C for 8 hr, and then scrape loaded them with NB. Following loading the cells were fixed, stained with Streptavidin-488, and imaged. Representative fluorescent images are presented in Fig. 5.3. Dye spread was quantified as a function of the percent of total area in the field of view. At the Src non-permissive temperature, we observed no difference in the amount of NB transfer between Cx45⁻ or Cx45⁺ LA25 cells (Fig. 5.3, top panels, green; Cx45⁻ 53.9 ± 7.67% vs. Cx45⁺ 53.2 ± 5.95%). To

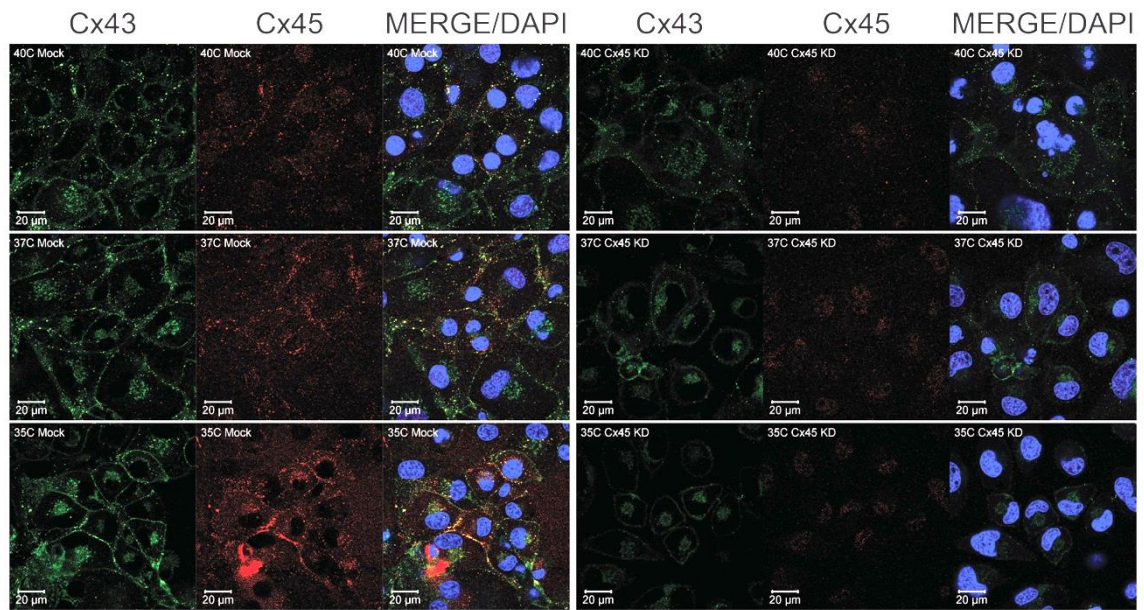


Figure 5.2. Knock-down of exogenous Cx45 restores Cx43 lability when Src is active.

Cx45⁻ and Cx45⁺ LA25 cells were cultured to ~60% confluent on glass coverslips and either mock transfected (left panels) or transfected with siRNA designed against the exogenous Cx45 (right panels). After 48 hr of siRNA or mock transfection the cells were incubated at the Src non-permissive, intermediate, or permissive temperature for 8 hr, followed by fixation and immunostaining for Cx43 (green) and Cx45 (red). Nuclei were stained with DAPI (blue). Scale bars = 20 μ m.

our surprise, we observed a Src dependent decrease in the amount of NB dye transfer at the Src permissive temperature for both cell lines (Fig. 5.3, bottom panels, green; Cx45⁻ 28.1 ± 5.53% vs. Cx45⁺ 27.6 ± 5.80%). Quantification indicated the degree of change in GJIC in response to Src activation was comparable between Cx45⁻ and Cx45⁺ LA25 cells (Fig. 5.3; right). Taking into consideration our observation of Src mediated loss of coupling in HeLa cells when transiently transfected with v-Src, the possibility exists that our model is resulting in aberrantly high levels of phosphorylation not physiologically relevant. It would be interesting to determine how these cells respond to EGF treatment.

19.4 Cx43 Maintained in GJs by Cx45 Shows Altered Phosphorylation Patterns

Since we observed a comparable Src dependent decrease in GJIC in both Cx45⁻ and Cx45⁺ LA25 cells, yet a decrease in the amount of Cx43 GJ disassembly, we wanted to determine whether the phosphorylation pattern of the residual junctional Cx43 was consistent with that of open or closed channel conformations. To test this, we probed only the insoluble fraction of Cx43 from our experiment in Section 19.1 with several phosphospecific antibodies for Cx43 and normalized to the amount of total insoluble Cx43 (Fig. 5.4). For Src phosphorylation sites, we probed Cx43 with antibodies against pY247, pY265, and pY313. For pY247 we observed a non-significant increase (2.03-fold for Cx45⁺ at 35°C compared to 40°C; 1.66-fold for Cx45⁻ at 35°C compared to 40°C, N=3) in the amount of pY247 relative to total insoluble Cx43 (Fig. 5.4; top right panel). For the primary Cx43 Src phosphorylation site, Y265 (first site phosphorylated by Src to generate SH2 binding site), we observed a statistically significant increase (1.42-fold Cx45⁺ at 35°C compared to 40°C; 1.01-fold change in Cx45⁻ at 35°C compared to 40°C, P <0.05, N=3) in the amount of pY265 in the Cx45⁺ LA25 cells at 35°C compared to Cx45⁻ (Fig. 5.4; upper-central right panel). For Cx43 Y313, we observed comparable levels of phosphorylation in the insoluble fraction of both Cx45⁻ and Cx45⁺ LA25 cells at the Src permissive temperature (Fig. 5.4; center right panel; 1.76-fold for Cx45⁺ at 35°C compared to 40°C; 1.82-fold for Cx45⁻ at 35°C compared to 40°C, ns, N=3). In addition to the Src phosphorylation sites, we also probed the Cx43 MAPK sites (S279/282)

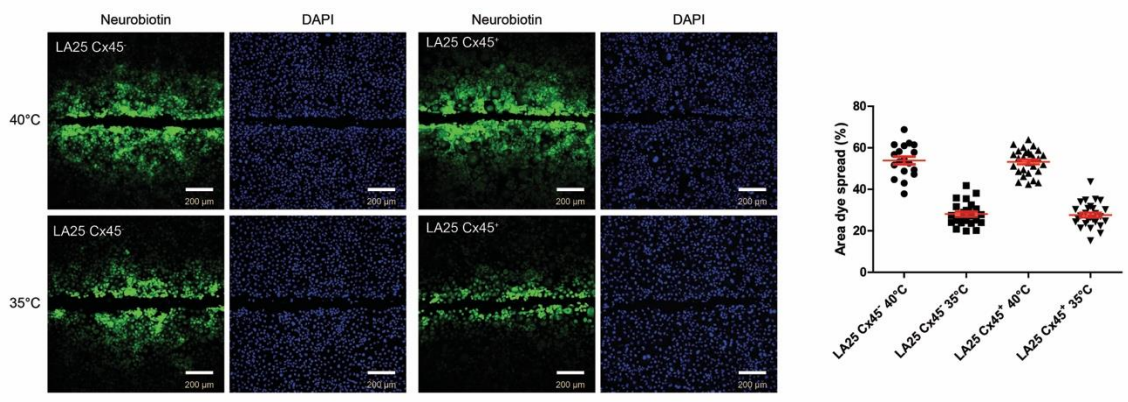


Figure 5.3. Cx45 does not prevent Src mediated downregulation of GJIC in LA25 cells. Cx45⁻ and Cx45⁺ LA25 cells were cultured to confluence in glass bottom dishes and subsequently incubated for 8 hr at either 40°C (top panels) or 35°C (lower panels) and then scrape loaded with NB dye. Following scrape loading the cells were fixed and stained with Streptavidin-488 (green) and DAPI (blue) to show cell confluence, and then imaged. The degree of NB dye transfer was quantitated in ImageJ by measuring the total area of dye spread as a function of total area of field of view. Images were acquired from a minimum of 10 non-overlapping fields of view from each of three independent replicates.

for phosphorylation and our results indicate the presence of Cx45 significantly reduced the degree of phosphorylation at S279/282 (Fig. 5.4 lower-center right panel; 1.71-fold for Cx45⁺ at 35°C compared to 40°C; 4.14-fold for Cx45⁻ at 35°C compared to 40°C, P <0.05, N=3). Finally, we probed the insoluble Cx43 for phosphorylation of S368 (PKC site). Similar to the MAPK sites, we observed a significant decrease in the amount of S368 phosphorylation in the Cx45⁺ LA25 cells (1.07-fold change at 35°C compared to 40°C for Cx45⁺; 2.27-fold increase for Cx45⁻ at 35°C compared to 40°C; P <0.0001, N=3). Taken together, the data suggest that the co-expression of Cx45 is altering the phosphorylation landscape of Cx43 in response to increased Src activity. Although we did not directly compare the levels of Cx43 phosphorylation at 40°C, it is worth noting that we did observe increased Cx43 phosphorylation on Y247 and Y265 by co-expression of Cx45 alone, the significance of this observation is unclear at this time.

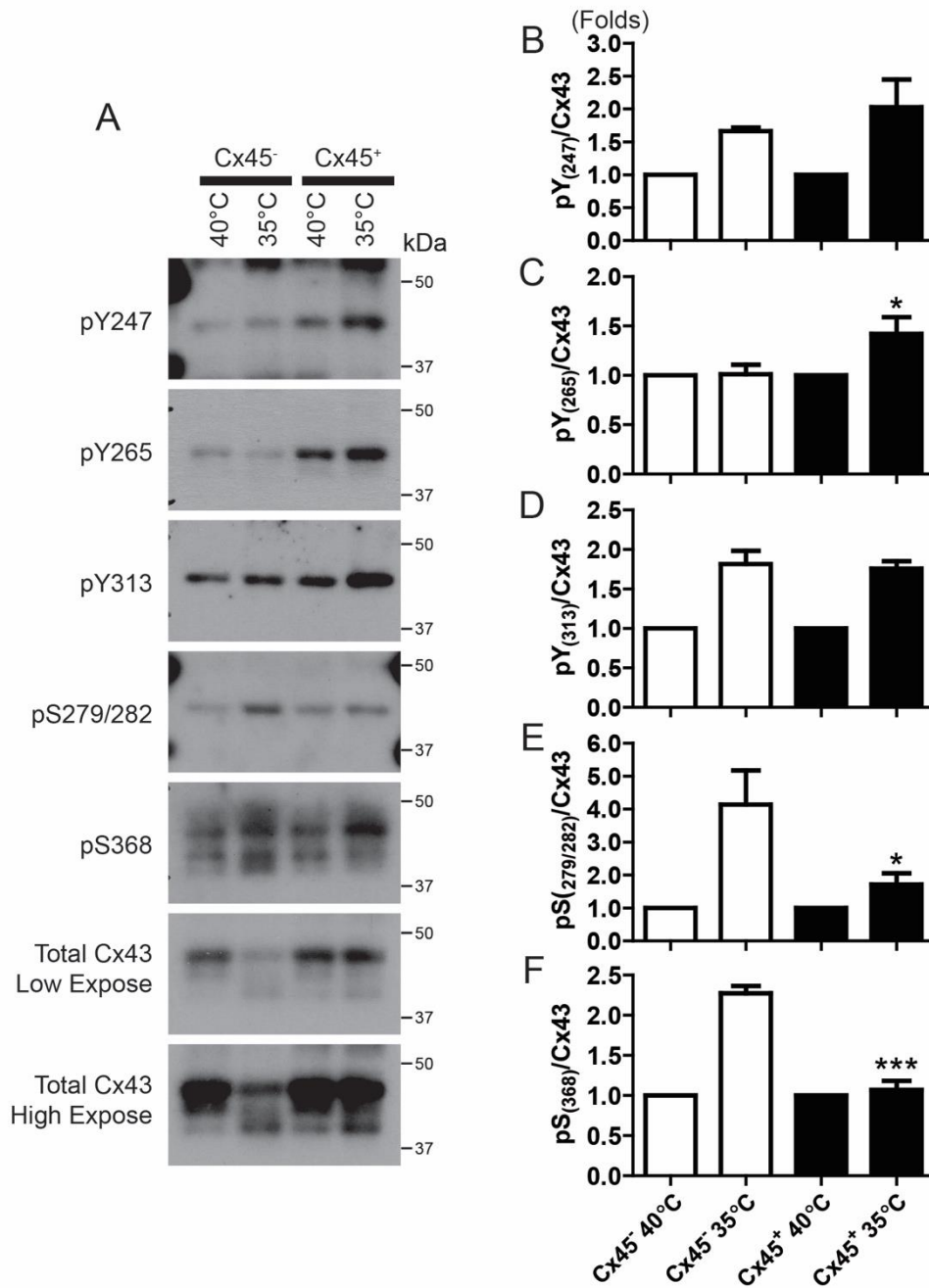


Figure 5.4. Cx43 is maintained the GJ plaque with altered phosphorylation landscape when Cx45 is co-expressed in LA25 cells.

Cx45⁻ and Cx45⁺ LA25 cells were cultured to confluence and incubated at 40°C or 35°C for 8 hr. Cx43 was extracted with TX-100 and fractionated into total (T), non-junctional (TX-100 soluble, S) and junctional (TX-100 insoluble, I) fractions by ultracentrifugation. Resulting insoluble fractions were resolved by SDS-PAGE and Western blotted for total Cx43, and Cx43 phosphorylation at residues Y247, Y265, Y313, S272/282, and S368. A) Representative Western blots of total and phospho Cx43 from the insoluble fractions. B-F) Quantitation of Cx43 phosphorylation in the insoluble pool relative to total insoluble Cx43. Statistics are one-way ANOVA with a Bonferroni multiple comparison test comparing Cx45⁻ to Cx45⁺ in each temperature group. *P < 0.05, ***P < 0.0001

20. Discussion

Although the existence of heteromeric oligomerization of Cxs has been accepted for over a decade, studies investigating them are not plentiful. Of the studies that do explore the consequences of heteromeric channel formation, a vast majority have focused on aspects of channel trafficking, GJIC, and gating (reviewed in [546, 547]). For example, Berthoud et al. demonstrated altered the voltage dependence in heteromeric channels composed of Cx43 and Cx56, compared to homomeric Cx43 channels [543]. Similarly, in N2a cells Brink et al. demonstrated channels composed of intermixed Cx37 and Cx43 displayed conductance/voltage relationships different from either family member alone [548]. Consistent with the Brink et al. and Berthoud et al. studies, a study by He et al. attributed altered GJ channel properties in Ar75 (rat vascular smooth muscle cells) to the co-expression of Cx40 and Cx43 [543, 544, 548]. Specifically, they reported changes in voltage sensitivity and residual conductance at high voltage in the Ar75 compared to cell lines only expressing either Cx40 or Cx43 [544]. A 2008 study by the Dupont group examined the effects of co-expressing Cx45 and Cx43 in HeLa and rat lung epithelial (RLE) cells and concluded that expression of Cx45 significantly reduced GJ plaque size [88]. Notably, several studies have examined the ability of wild-type Cxs to rescue trafficking (and functional) defects of mutant Cxs (both homomeric and heteromeric) [452, 549-551]. Finally, Martinez et al. also investigated heteromeric channels composed of Cx43 and Cx45 in HeLa cells, reporting that co-expression reduced the dye permeability of the cells to LY, and resulted in the appearance of single channel conductance recording that could not be attributed to Cx43 or Cx45 alone [86]. In the same study, the authors examined the effects of PKC activation by PMA to determine if heteromeric Cx43/Cx45 channels would respond to PKC more complexly than either homomeric counterpart [86]. Compared to Cx43 homomeric GJs PKC similarly affected Cx43/Cx45, rapidly reducing conductance and dye coupling, while compared to Cx45 PKC had much less pronounced effect on conductance and did not affect dye coupling [86]. To our knowledge, the Martinez et al. study is unique in investigating the link between response to kinase activation and connexon composition [86]. Despite this, the data presented in the study only suggests a casual role for the

kinase and did little to explore the mechanism leading to altered function in of the Cx43/Cx45 heteromers.

In this Chapter we took a cellular biology approach to begin to understand the outcome of having two heterocompatible Cxs co-expressed in the context of Src kinase activation. Although the work is preliminary it suggests that a heteromeric channels respond more complexly to regulatory stimuli such as phosphorylation. One example we presented is the ability of Cx45 to protect Cx43 from Src mediated turnover assessed by detergent solubility. Although the amount of retained insoluble Cx43 in the Cx45⁺ cells was only ~10% greater than in Cx45⁻ cells this actually represents a substantial rescue of ~40%. Supporting our detergent solubility results, a second example is when exogenous Cx45 was knocked down by siRNA, we observed Src activity dependent loss of Cx43 GJs and expression that was not observed when Cx45 was expressed. The significance of these results is two-fold, on one hand this could maintain coupling potential and promote communication, however, due to the dominant negative effect of Cx45 on Cx43, in the heart, this could explain why aberrant expression of Cx45 leads to arrhythmia while lateralization and reduction in expression of Cx43 alone does not [72, 73, 76, 82, 84, 432, 438]. Although we observed an increase in Cx43 retention at the GJ plaque, we did not observe a functional rescue in terms of dye coupling. This raises the question: Why does heteromeric mixing of Cx43 and Cx45 result in plaque maintenance if the channels are still closed? It is possible that this is a protective mechanism that would retain a working quantity of Cx43 at the GJ plaque poised to reopen upon more favorable conditions thus promoting GJIC. This supposition is consistent with studies describing: 1) A similar mechanism may occur involving CaM and its interaction with Cx32, in which reduced Tyr phosphorylation of Cx32 by EGFR stimulation has was reported in the presence of CaM [298]. 2) An interaction of CaM with the CT domain of Cx43 that would in part prevent the internalization of Cx43 by blocking the Nedd4 and AP2 binding sites, potentially preventing ubiquitination and subsequent clathrin mediated endocytosis (Sorgen Laboratory, unpublished data). Furthermore, our probing of the insoluble fraction of Cx43 with phosphospecific antibodies supports this as we observed a significant decrease in the percentage of Cx43 that was phosphorylated by MAPK, which would reduce the affinity of Cx43 for Nedd4 and consequently

reduce binding of AP2 [203, 382]. Consistent with MAPK phosphorylation of Cx43 occurring simultaneously as phosphorylation by PKC, the decrease in phosphorylation of S279/282 correlated with a decrease in phosphorylation of S368 [325]. While this data is consistent with the decrease in both turnover and phosphorylation of S279/282, the functional significance is unclear at this time. In order to obtain a clearer picture, the ability to interrogate phosphorylation of Cx43 at the CK1 and PKA sites (S325,328,330 and S365, respectively) would be essential. Nevertheless, the data supports the concept that regulatory complexity increases as Cx proteins intermingle.

The work in this Chapter raises important novel questions about heteromeric channels: 1) What determines which Cx family member is dominant, is it a function of stoichiometry? 2) Does protomer arrangement within the connexon contribute to the regulation? 3) Do heteromeric channels respond bimodally in response to acute/chronic signaling pathway activation (e.g., 1 hr EGF vs. v-*Src* transfection for 24 hr)? 4) Physiologically speaking, what is the advantage of maintaining GJs in the plasma membrane in situations that would normally lead to turnover? 4) Furthermore, what does this reflect in terms of potential therapeutic value? Future studies should focus efforts on addressing these questions as well as expanding them to other heterocompatible Cx co-expression systems especially under endogenous or *in vivo* conditions.

CHAPTER SIX

Regulation of Cx32 by Ephrin Receptors and TC-PTP

The bulk of data presented in this Chapter is published Trease et al.

(2018), Journal of Biochemistry [552]

21. Introduction

GJ are comprised of tight knit arrays of membrane channels that connect the cytoplasm of adjacent cell and function to allow the passive transport of ions, small metabolites, and signaling molecules between coupled cells. Their function is important for several cellular and tissue processes including cell growth, maintenance, differentiation, and tissue synchronization. Of the 21 human family members, Cx32 is the primary GJ protein in both liver and brain, as well as the reproductive tissues [553]. Mice harboring Cx32 KO suffer from increased incidence of spontaneous tumors in the liver and are more susceptible to chemically induced liver tumors as well [554, 555]. Additionally, other pathological conditions arise in Cx32 KO mice including impaired innervated bile secretion, increases release of the enzyme amylase from the pancreas, and loss of myelination in the peripheral nervous system [556-559]. Mutations in Cx32 are an etiological source of the X-linked CMTX syndrome. Over 400 unique mutations have been identified in Cx32, encompassing every domain of Cx32 [560]. Many of the mutations affect Cx32 GJ function by impairing trafficking, gating properties, selectivity, interactions with protein partners, or the phosphorylation status [561].

Phosphorylation is a critical regulator of every point in the Cx life cycle, such as accretion, turnover, the regulation of channel opening/closure, and modulating the affinities for binding of protein partners [328]. The intracellular domains of Cx32 contain 12 Ser residues (NT, 2; CL, 1; CT, 9) and has been phosphorylated *in vitro* by CaMKII, PKA, and PKC [365, 478, 562]. Although demonstration of changes in Cx32 phosphorylation status were not assessed, activation of the MAP kinase p38, correlated with differentiation of rat mammary epithelial cells [563]. In addition to Ser residues the intracellular domains of Cx32 also contains two Tyr residues (NT, Y7; CT, Y243). A third Tyr (Y211) is present in a membrane juxtaposed region of the Cx32CT, however, may not be accessible to cytoplasmic enzymes. If Y211 is accessible it is unlikely to interact with any proteins (including enzymes) due to steric hindrance from the plasma membrane itself. Cx32 was shown to be Tyr phosphorylated in purified liver membranes by stimulation of the RTK EGFR, and this phosphorylation was prevented when excess CaM was present [248, 365]. Although Cx32 Tyr phosphorylation was detected, neither the specific residue(s) phosphorylation nor the effect on

Cx32 GJ function were determined [365]. Phosphorylation of Y7 was detected in a MS study utilizing exogenous Cx32 expression in HeLa cells, however, potential kinases targeting this site were not revealed [274]. The lack of information on the kinases involved, sites phosphorylated, and downstream effects of Cx32 Tyr phosphorylation, we screened the Cx32NT and Cx32CT *in vitro* for candidate kinases and identified the Ephrin type-B receptor 1 (EphB1) and Ephrin type-A receptor 1 (EphA1) as novel Tyr kinases which phosphorylate Cx32.

Both Eph receptors and ligands (the ephrins) are integral membrane proteins and mediate both forward (Eph receptor) and reverse (ephrin) signaling in response to cell-cell contact. Signaling downstream of the Eph receptor has been shown to influence cell migration and sorting during development, modulate adhesion, neuronal injury repair, and importantly GJ [366, 564-566]. Cx43 was demonstrated to co-IP EphB4, and when EphB4 was activated in primary rodent cardiomyocytes Cx43 GJIC was inhibited [567]. Along the same lines it was shown by another group that GJIC was reduced in ectopic ephrin boundaries and Cx43 localization was influenced via interaction with ephrin-B1 [366]. Taken together these studies highlight a potential mechanism by which cell coupling via GJs is regulated by cell-cell contact through Eph receptors and ephrins that is both dependent and independent of phosphorylation of the GJ proteins. Whether the phosphorylation of Cxs by Eph receptors is direct and whether this mechanism is general to multiple Cx family members remains to be investigated.

In this study, we reveal that Eph receptors (EphB1 and EphA1) phosphorylate the Cx32CT on residue Y243, and consequently (and conversely to what would be expected for Cx43) increase GJIC. We also identify T-Cell Protein Tyr Phosphatase (TC-PTP) as a phosphatase that can dephosphorylate Cx32CT residue pY243. This study provides further support that the outcome of Cx phosphorylation by a given kinase is determined not by the kinase but by the cx family member, and thus characterization of the same kinase for each Cx family member is essential for a complete understanding of the regulation of Cxs by phosphorylation.

22. Materials and Methods

22.1 Cell Culture and Treatments

Cx32 WT, Y243F, and Y243E cloned into the pD2529 vector as described previously, were stably expressed in HeLa cells (ATCC) [424]. HeLa and Caco2 cells were grown in Dulbecco's modified Eagle's medium (Hyclone, Thermo Fisher Scientific Inc.) supplemented with 10% FBS (Hyclone, Thermo Fisher Scientific Inc.) and antibiotics. FHC cells were cultured in DMEM:F12 supplemented with 25 mM HEPES, 10 ng/mL cholera toxin, 0.005 mg/mL insulin and transferrin, 100 ng/mL hydrocortisone, 20 ng/mL human recombinant EGF, 10% FBS, and antibiotics. All cells were cultured in an atmosphere of humidified 5% CO₂ at 37°C. Where appropriate, cells were transiently transfected with either EphA1, EphB1, or a combination of either in conjunction with TC-PTP₁₋₃₁₄ using Lipofectamine 2000 (Invitrogen) according to manufacturer protocol. For single and combination transfections, the amount of plasmid for the Eph receptor and TC-PTP₁₋₃₁₄ was equivalent. Cells were treated for 1 hr at 37°C with 1 µg/mL of either EphA1-Fc or EphB2-Fc (SinoBiological) approximately 24 hr after transfection.

22.2 Antibodies and Immunostaining

The following antibodies were used in this study: Cx32 monoclonal antibody (Sigma-Aldrich); Cx32 polyclonal antibody (LifeTech); EphB1 and EphA1 antibodies (Cell Signaling); EphA1 antibody (Cell Signaling); TC-PTP antibodies against the N-terminus and C-terminus (Sigma-Aldrich); general pTyr antibody (Cell Signaling).

Cells were immunostained as described previously [424]. Briefly, cells grown on cover slips to ~60% confluence were fixed with 2% para-formaldehyde for 15 min. Cells were blocked for 30 min at room temperature (RT) by MPS buffer (1x PBS, 1% Goat Serum) containing 0.2% TX-100 for permeabilization. Then, cells were immunostained with appropriate primary antibodies at RT for 1 hr, followed by several PBS-0.5% Tween washes. Secondary antibodies (Alexa 594-conjugated goat arabbit antibody and/or Alexa 488-conjugated goat amouse antibody) were applied for 1 hr at RT. Images of immunostained cells were acquired with a Zeiss 510 Meta Confocal Laser Scanning Microscope using a 63×1.4 numerical aperture objective with appropriate filters.

22.3 Co-IP and Western blot

Cx32 expressing HeLa cells were lysed in complete lysis buffer (50 mM Tris-HCl [pH 7.4], 150 mM NaCl, 0.5% Na-deoxycholate, 1% TX-100, 5 mM NaF, and one-half tablet of Complete protease inhibitor (Roche) in 20 ml buffer), maintained on ice for 30 min, precleared with protein G beads for 30 min at 4°C, and then spun at 12,000 rpm for 15 min. Total protein was assessed using the BCA protein assay kit (Pierce). 2 mg of protein lysate was incubated with 2 µg of αCx32 or mouse IgG (4 hr at 4°C) and then incubated with 100 µl of protein G sepharose (GE Healthcare) (overnight (ON) at 4°C). The sepharose was washed 4x with cold lysis buffer and the co-IP was analyzed by SDS-PAGE and Western blot. AEphB1 monoclonal antibody was used to detect EphB1 co-IP with Cx32.

Protein levels were detected by SDS-PAGE and Western blot. One exception for detecting Tyr phosphorylation was that 5 mM Na₃VO₄ was added in the blocking buffer and primer antibody buffer in order to minimize the loss of phosphorylation. Western blot data were scanned and quantified using Image J as described in [424].

22.4 GST Pull Downs

The GST pull down assay was modified from [203]. Briefly, purified GST, GST-Cx32NT, or GST-Cx32CT were bound to glutathione-Sepharose beads in buffer containing 25 mM Tris-HCl (pH=7.4), 150 mM NaCl, 0.1% TX-100, 1 mM DTT, 0.1 mM EDTA and one-half tablet of Complete protease inhibitor in 20 ml buffer. 5 mg of either purified TC-PTP₁₋₃₁₄ was incubated with the GST control or either fusion GST-fusion protein ON at 4°C on a rotating wheel. Beads were washed 5 times with buffer and bound proteins were eluted with SDS-PAGE sample buffer and analyzed by Western blot.

To pull down Cx32 binding partners, 4 mg of MDA-MB-231 cell lysate protein (in cell lysis buffer containing 25 mM Tris-HCl (pH 7.4), 150 mM NaCl, 0.5% TX-100, 0.5% sodium deoxycholate, 2 mM EDTA, PhosSTOP (Roche), and Complete protease inhibitor) were incubated with GST-fusion Cx32CT or the GST control for 6 hr at 4°C on a rotating wheel. Beads were washed 5 times with cell lysis buffer and bound proteins were eluted with SDS-PAGE sample buffer and analyzed by Western blot.

22.5 NMR-HSQC Experiment

NMR data were acquired using a 600 MHz Varian INOVA NMR Spectrometer outfitted with a Bruker cryo-probe at the NMR Facility of the University of Nebraska Medical Center. Cx32CT₂₁₇₋₂₈₃ and TC-PTP₁₋₃₁₄ were expressed and purified as described previously [248, 340]. Gradient-enhanced two-dimensional ¹⁵N-HSQC experiments were acquired to detect backbone amide bond resonances from the ¹⁵N-Cx32CT (30 μM) in the absence and presence of different concentration of unlabeled TC-PTP₁₋₃₁₄.

For testing the interaction with CaM, peptides corresponding to Cx32CT₂₁₇₋₂₆₆ (not phosphorylated, nopY243) or Cx32CT₂₁₇₋₂₆₆ pY243 were purchased (LifeTein) and ¹⁵N-CaM was expressed recombinantly and purified by affinity chromatography using a Phenyl HP column (Amersham). Pure CaM was eluted with Tris-EGTA, dialyzed extensively against water, and lyophilized. Gradient-enhanced two-dimensional ¹⁵N-HSQC experiments were acquired to detect backbone amide bond resonances from the ¹⁵N-CaM (300 μM) in the absence and presence of different concentration of either unlabeled Cx32CT₂₁₇₋₂₆₆ nopY243 or Cx32CT₂₁₇₋₂₆₆ pY243. A similar approach was used to test the impact of pY243 on the interaction with hDlg. ¹⁵N-HSQC experiments were acquired to detect backbone amide bond resonances from ¹⁵N-Cx32CT WT or Y243E (50 μM) in the absence and presence of unlabeled synapse associated protein 97-guanylate kinase (SAP97-GUK₇₀₁₋₉₂₄) domain. SAP97-GUK₇₀₁₋₉₂₄ was purified as in [248]. NMR spectra were processed using NMRPipe [568] and analyzed with NMRView [569]. Binding affinity from the ¹⁵N-HSQC titration experiments were calculated by GraphPad Prism 5 (GraphPad Software, Inc.).

22.6 In vitro Phosphatase Assay

Cx32 phospho-peptide pY243 (HRLSPEpYKQNEIN) was used in the malachite green assay (Millipore) to detect if they are substrates of TC-PTP *in vitro*. Positive and negative controls were DADEpYL (described in [570]) and ARKRlpYPP (described in [571]), respectively. Peptides and enzyme were dissolved and diluted in reaction buffer (60 mM HEPES [pH 7.2], 150 mM NaCl, 1 mM EDTA, 0.17 mM DTT, 0.83% glycerol, 0.017% BSA, and 0.002% Brij-35) and temperature-equilibrated for 15 min at RT. 500 μM of each peptide was added into a 96-well plate, and then TC-PTP₁₋₃₁₄ was added to each peptide at different time points. The final concentration of TC-PTP₁₋₃₁₄

was 0.6 nM. All reactions were terminated by adding 100 μ l malachite green solution and incubated for 15 min at RT to allow color development. Absorbance at 650 nm was read using a SpectraMax 190 spectrometer (Molecular devices).

The Malachite green assay was also used to measure the kinetic parameters of de-phosphorylation [570]. The reaction was performed in 96-well plates with a final volume of 25 μ l. A standard curve of KH_2PO_4 , used for calculating the release of inorganic phosphate, was determined on the same plate as the reaction samples. Different concentrations of peptides [substrate] were combined with 1.2 nmol TC-PTP₁₋₃₁₄. Time points of the reaction were sampled from 0-15 min to calculate the initial velocity (v) versus [substrate]. Lineweaver-Burk double-reciprocal plot (rearranged from the Michaelis-Menten equation) was created based on $1/v$ and $1/[\text{substrate}]$. The kinetic parameters were determined by the linear equation from the Lineweaver-Burk double-reciprocal plot. All the reactions were conducted at pH 7.5, 25°C. The reported results were calculated from three independent experiments.

22.7 Scrape Loading Assay

Cells were scrape-loaded as described in [248]. Briefly, either HeLa cells expressing Cx32 WT or the Y243E mutant and Caco2 cells were seeded on cover slips 24 hr before performing the assay. Cell culture medium from 100% confluent cells was removed and replaced with 1 ml of PBS containing 0.25% Lucifer Yellow and Texas Red-conjugated fluorescent dextran (10 kDa, 1.5 mg/ml; fixable). Cells were scrape-loaded with a sterile scalpel by two longitudinal scratches and then incubate at RT for 1 min for HeLa cells and 4 min for Caco2. Cells were washed quickly 3x with warm PBS (containing MgCl_2 and CaCl_2) or cell culture medium followed by incubating at 37°C for 5 min. After incubation, cells were washed 2 times with warm PBS, and fixed with 3.7% buffered paraformaldehyde for 15 min. 0.1 M glycine was used to quench autofluorescence for 15 min. Cover slips were mounted on glass slides in a droplet of SlowFade (Invitrogen). The result was confirmed by repeating the experiment 3 times and for each trial, capturing 4 side-by-side images. The method to quantify dye transfer was described previously [248]. Briefly, cells with Lucifer yellow were counted while the cells with dextran, which indicated the initially loaded cells, were excluded.

22.8 Statistical Analysis

All data were analyzed by GraphPad Prism 5.0 and presented as the mean \pm standard deviation (\pm S.D.). Either Student's T-Test or one-way ANOVA with Newman-Keuls post hoc analysis was used to compare differences between all groups, where appropriate. $P < 0.05$ was considered to be statistically significant.

23. Results

23.1 EphB1 directly interacts and phosphorylates the Cx32CT domain

We initially used the web-based software tools GPS 2.0, NetPhos 2.0 Server, and KinasePhos 2.0 to predict kinases that could phosphorylate Tyr residues on the NT and CT domains of Cx32 (data not shown). Based on our *in silico* analysis, we chose five candidate Tyr kinases to screen against the Cx32 NT and CT domains. We submitted purified Cx32NT (M1-G21; Y7) and Cx32CT (C217-C283; Y243) as substrates to Eurofins Scientific for the *in vitro* screen (KinaseProfiler; Fig. 6.1A). Of the five kinases EphB1 and Ron both phosphorylated the Cx32 CT domain with greater than 50% and 40% of control peptide signal, respectively. EphB1 also phosphorylated the Cx32NT to a level similar to that of the Cx32CT. Based on the importance of Cx43CT Tyr phosphorylation in regulating Cx43 channel function, we sought to validate the Cx32CT screen, and thus tested the ability of the EphB1, Ron, and EGFR (negative control) to phosphorylate the purified Cx32CT in our laboratory. Our results, consistent with the Eurofins screen, demonstrated clear phosphorylation of the Cx32CT domain by EphB1 and Ron kinase (Fig. 6.1B). Although we were unable to detect Tyr phosphorylation of the Cx32CT by EGFR, work from Diez *et al.* used autoradiography to demonstrate that EGFR can phosphorylate IP enriched Cx32 *in vitro* [365]. This may suggest in our system the degree of phosphorylation was below the detection limit of the general pTyr antibody, or alternatively that stimulation of EGFR leads to a cascade that ultimately results in phosphorylation of Cx32 by some other downstream kinase. We next sought to confirm an interaction of Cx32 with EphB1 and Ron using a GST pull down assay. To accomplish this we purified GST alone, GST-Cx32NT, GST-Cx32CT and used these constructs as bait for EphB1 and Ron from HeLa (expressing EphB1 and Ron, but not Cx32) cell lysate (Fig. 6.1C). We were able to successfully pull down EphB1 with the GST-Cx32CT, but not either GST or GST-Cx32NT. The amount of EphB1 pulled down by the GST-Cx32CT was increased by the addition of the chemical crosslinker DTSSP (3,3'-dithiobis[sulfosuccinimidylpropionate]; indicating the interaction was stabilized [572]).

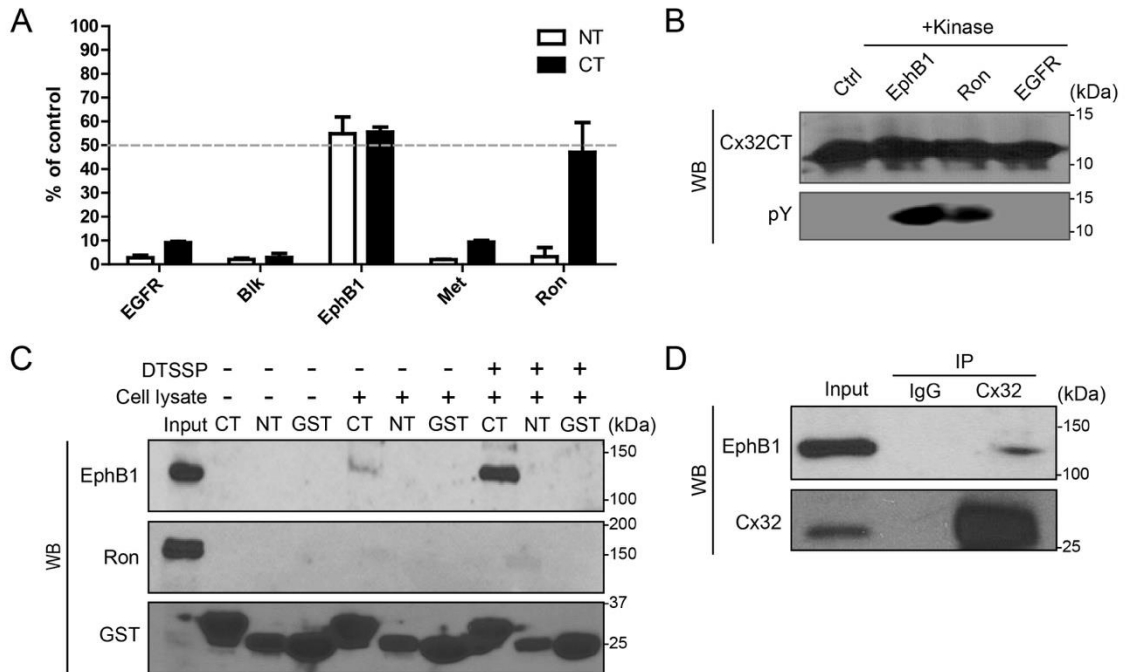


Figure 6.1. EphB1 phosphorylates the Cx32CT domain *in vitro*.

A) The Cx32NT and CT domains were used as a substrate for the human EGFR, Blk, EphB1, Met, and Ron kinases (performed by Eurofins Scientific). The amount of Cx32NT and CT phosphorylation was compared with a positive control peptide for each kinase (% of control signal). The dashed line highlights 50% of the control signal. B) An *in vitro* kinase assay for the Cx32CT was performed in our laboratory to repeat the kinase screen performed by Eurofins Scientific (EphB1, Ron, and EGFR). A general anti-phospho-tyrosine antibody was used to detect the phosphorylation level by Western blot. Control group used buffer to substitute the kinases in the reactions. C) Purified GST alone, GST-Cx32CT (CT), or GST-Cx32NT (NT) bound on glutathione-agarose beads were incubated without (-) or with (+) HeLa cell lysate and the pulled down proteins were analyzed by Western blot using anti-EphB1 or anti-Ron antibodies. The chemical cross-linker DTSSP was used to capture the weak and/or transient interactions. D) Co-IP was performed in HeLa cells stably expressing Cx32. Lysates were captured by IP with anti-Cx32 or IgG and then blotted for Cx32 and EphB1. Reprinted from Trease et al., (2018).

Further confirming the interaction, co-IP revealed that EphB1 could complex with full-length Cx32 from transfected HeLa cells (Fig. 6.1D). Although we detected robust phosphorylation of the Cx32CT by Ron kinase *in vitro*, detection of Ron kinase in the GST pull down was very low, and was not improved by the addition of DTSSP, nor was Ron detected to complex with Cx32 from transfected HeLa cells in co-IP (data not shown). Thus, Ron was not included in any following assays, highlighting a caveat in this type of *in vitro* screen where the phosphorylation *in vitro* does not always correlate with a detectable interaction in cells.

23.2 TC-PTP interacts with and dephosphorylates Cx32CT residue pY243

Previous work from our laboratory demonstrated that TC-PTP dephosphorylates Cx43 residues Y247 and Y265, which promotes increased GJIC [340]. It is currently unknown whether TC-PTP is able to target and dephosphorylate other Cx family members (e.g., Cx32 pY243). We hypothesized TC-PTP may mediate a general mechanism by which Cx family members are dephosphorylated and such sought to determine if it directly interacts with the Cx32CT domain. To address this, we performed NMR titration experiments comparing purified Cx32CT alone to that of Cx32CT mixed with the purified catalytic domain of TC-PTP (TC-PTP₁₋₃₁₄). We acquired ¹⁵N-HSQC spectra at a number of molar ratios of ¹⁵N-labeled Cx32CT₂₁₇₋₂₈₃ and unlabeled TC-PTP₁₋₃₁₄ (Fig. 6.2A). We observed changes in the ¹⁵N-Cx32CT spectra in response to increasing amount of TC-PTP, such that at a 1:1 molar ratio, residues C217-S266 of Cx32CT (including Y243) had broadened beyond detection (highlighted on the Cx32CT sequence in Fig. 6.2B; red peaks on spectra).

The loss of ¹⁵N-Cx32CT signal from increasing TC-PTP₁₋₃₁₄ concentrations was plotted and fit according to the nonlinear least square method allowing for the determination of the K_D (Fig. 6.2C), which was determined to be $19.9 \pm 4.5 \mu\text{M}$. To validate the NMR results we did a GST pull down experiment with purified GST alone, GST-Cx32CT, or GST-Cx32NT as bait. The purified proteins were incubated on glutathione-Sepharose with purified TC-PTP₁₋₃₁₄, washed, and analyzed by SDS-PAGE and Western blot. Analysis revealed a band consistent with the molecular

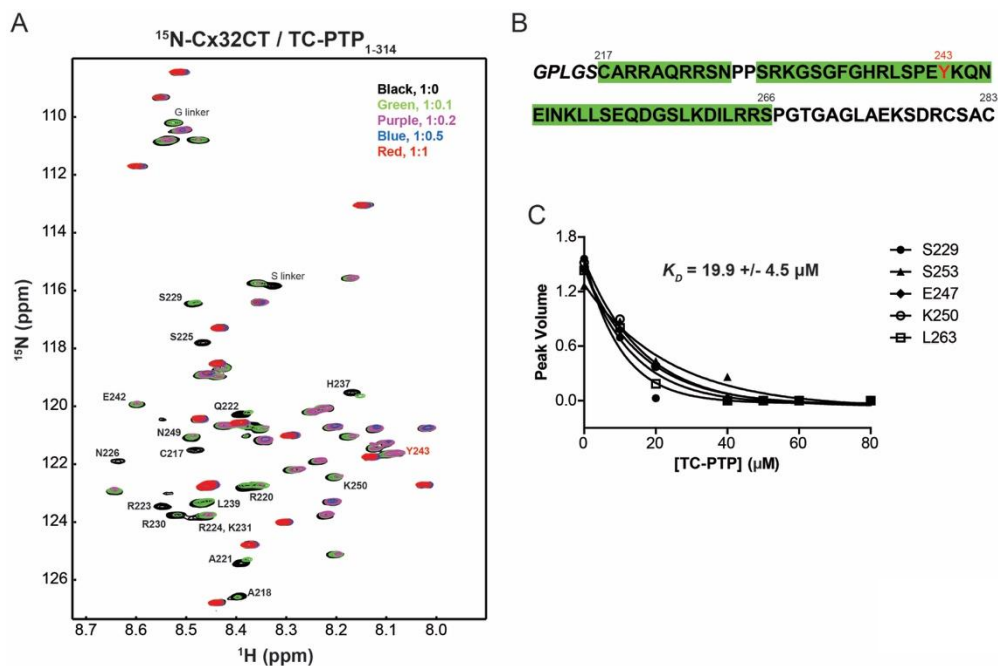


Figure 6.2. Cx32CT residues affected by the direct interaction with TC-PTP.

A) Overlaid ^{15}N -HSQC spectra of the ^{15}N -Cx32CT alone (residues 217-283; 30 μM) and in the presence of different concentrations of unlabeled TC-PTP₁₋₃₁₄. The cross-peak color changes according to the concentration ratio. The strongly affected peaks are labeled. B) Amino acid sequence of Cx32CT. Residues affected by the addition of TC-PTP₁₋₃₁₄ are highlighted in green. In red is Cx32 residues Y243. C) K_D for the TC-PTP₁₋₃₁₄ interaction with Cx32CT was estimated by fitting the decrease in signal intensity as a function of TC-PTP₁₋₃₁₄ concentration. Represented are a subset of the residues used to calculate the K_D . Reprinted from Trease et al., (2018).

weight of TC-PTP₁₋₃₁₄, whose identity was confirmed as TC-PTP using an α TC-PTP NT antibody that was pulled down by GST-Cx32CT, but not GST alone nor GST-Cx32NT (Fig. 6.3A, B). Taken together with the NMR this demonstrates that TC-PTP directly interacts with the Cx32CT. We also tested if GST-Cx32CT could pull down full length TC-PTP from HeLa cell lysate confirming by Western blot (Fig. 6.3C).

Having confirmed a direct interaction between the Cx32CT and TC-PTP, we next sought to determine if TC-PTP dephosphorylates Cx32 Y243. To test this, we ordered a peptide corresponding to Cx32 residues H237-N249 phosphorylated on Y243 and incubated it with TC-PTP₁₋₃₁₄ *in vitro*. Using the Malachite green assay kit (Millipore) we observed an increase in the absorbance of the reactions containing TC-PTP₁₋₃₁₄ over time, indicating an accumulation of inorganic phosphate (Fig. 6.3D). This confirmed that TC-PTP can dephosphorylate Cx32 Y243. Importantly, when compared to the positive control peptide for TC-PTP we observed comparable affinity of TC-PTP for both substrates as determined from the kinetic data in Table 7 ($k_{cat}/K_m \cdot 10^{-6}$; 2.24 ± 0.18 vs. 2.42 ± 0.47).

23.3 EphB1 phosphorylates and TC-PTP dephosphorylates Cx32 in HeLa cells

Having demonstrated that EphB1 and TC-PTP modulate phosphorylation of Cx32 Y243 *in vitro* we next wanted to determine if this effect could be reproduced in cells. We therefore transiently transfected HeLa cells which stably expressed exogenous Cx32 WT with either EphB1 alone or in conjunction with the TC-PTP₁₋₃₁₄. We measured the level of Tyr phosphorylation by IP of Cx32 and Western blotting with a general phospho-Tyr antibody (Fig. 6.4A, left lane). In the control condition (no EphB1 or TC-PTP) we were unable to detect any Tyr phosphorylation on Cx32; however, increased Tyr phosphorylation was detected when cells were transfected with EphB1 and activated with the soluble ligand (Fig. 6.4A, middle lane). This effect was partially reversed by the co-transfection of TC-PTP₁₋₃₁₄ with EphB1 (Fig. 6.4A, right lane).

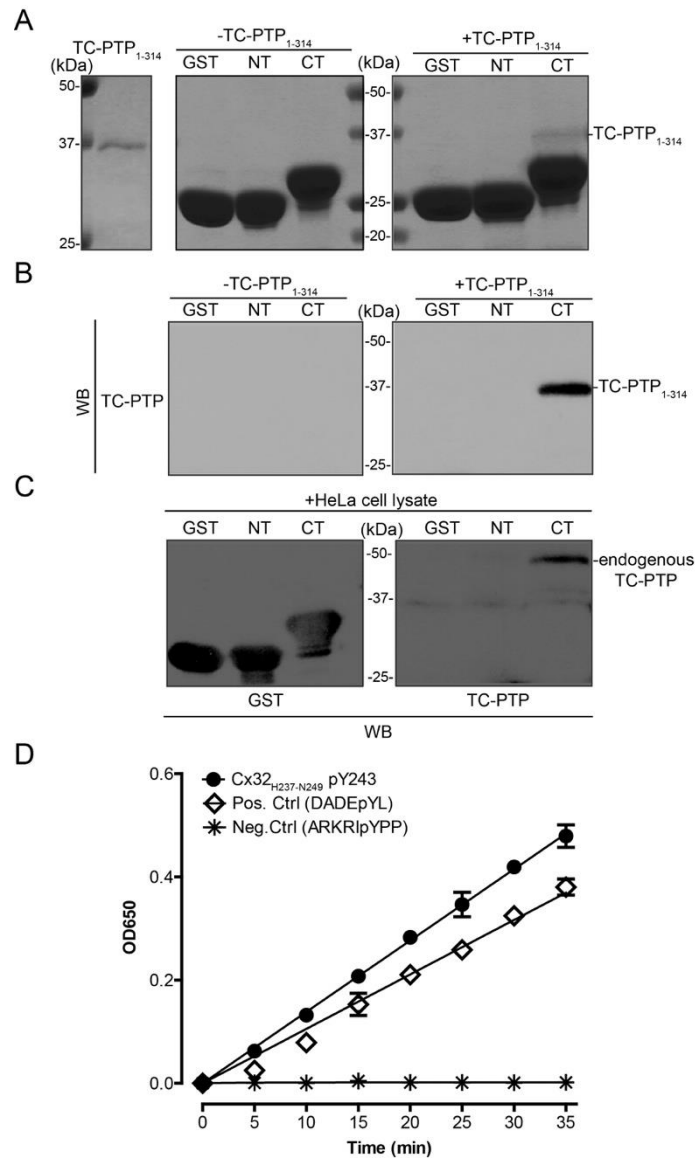


Figure 6.3. TC-PTP interacts with the Cx32CT domain and dephosphorylates pY243.

A) Purified GST, GST-Cx32NT, or GST-Cx32CT on glutathione sepharose beads were incubated without (-) or with (+) purified TC-PTP catalytic domain (residues 1-314). After washes, samples were run on SDS-PAGE gel and stained with Coomassie Blue. B) GST pull down samples were blotted with the anti-TC-PTP NT antibody. The TC-PTP catalytic domain is 36 kDa. C) Purified GST, GST-Cx32NT, or GST-Cx32CT bound on glutathione beads were incubated with HeLa cell lysate containing endogenous TC-PTP. Pulled down proteins were analyzed by Western blot using anti-TC-PTP NT or anti-GST antibodies. D) Plot of the Malachite green assay shows the time course of Cx32 phospho-peptides containing pY243 dephosphorylated by the TC-PTP catalytic domain (1.2 nmol). Data were recorded based on readings at OD650. Each experiment was repeated three times. Reprinted from Trease et al., (2018).

Peptide	K_m (mM)	k_{cat} (s^{-1})	$k_{cat}/K_m \times 10^{-6}$ ($M^{-1}s^{-1}$)
Positive control*#	0.022±0.001	52.8±10.6	2.42±0.47
pY243*	0.028±0.007	63.3±13.8	2.24±0.18

*All data were collected at pH 7.5, 25°C.

Table 7. Kinetic constants for dephosphorylation of Cx32 pY243 by TC-PTP₁₋₃₁₄.
 Reprinted from Trease et al., (2018).

Despite no detected interaction of the Cx32NT with EphB1 in our GST pull down (Fig. 6.2), phosphorylation of the Cx32NT Y7 by EphB1 was detected *in vitro*, so we wanted to test if this residue was phosphorylated in HeLa cells [274]. To accomplish this, we generated a Cx32 Y243F mutant and created a stable expressing HeLa cell line. We used IP to enrich either Cx32 WT or Cx32 Y243F from these cells and interrogated the level of Tyr phosphorylation by Western blot (Fig. 6.4B). When the stable cells were transiently transfected with EphB1 we observed increased Cx32 WT phosphorylation. Exogenous activation of the EphB1 receptor with a soluble version of the high-affinity ligand ephrin-B2-Fc further increased the degree of Cx32 WT phosphorylation. Confirming the specificity of EphB1 for phosphorylating Cx32 Y243 (not Y7 or Y211), no appreciable Cx32 phosphorylation was detectable from cells expressing the Cx32 Y243F mutant.

23.4 Cx32 Y243E increases GJIC

In order to determine the specific effects of Y243 phosphorylation on Cx32 function, we generated a Y243E mutant in addition to the Y243F mutant. Use of this mutant allows us to interpret the effects of specific site phosphorylation as the mutation ensures there is enough “phosphorylated” protein produced to observe a biological response. Use of the Glu substitutions for phosphorylated Tyr residues is common accepted in the GJ field as a reasonable mimetic for phosphorylation, often times reproducing the effects of *bona fide* phosphorylation (e.g., [344, 573]). Here, HeLa cells either transiently or stably expressing Cx32 WT, Cx32 Y243F, or Y243E were used to determine the impact of Y243 phosphorylation on Cx32 GJIC. We first wanted to determine if phosphorylation altered subcellular localization of Cx32 and therefore immunostained HeLa cells transiently transfected with Cx32 WT, Cx32 Y243F, or Cx32 Y243E (Fig. 6.5A). Our results suggest that mimicking phosphorylation of Y243 did not disrupt trafficking to the plasma membrane or the ability of the cells to make GJ plaques, as the Cx32 Y243E made GJ plaques of apparently similar size and number (Fig. 6.5A; white arrows) although this was not directly quantified.

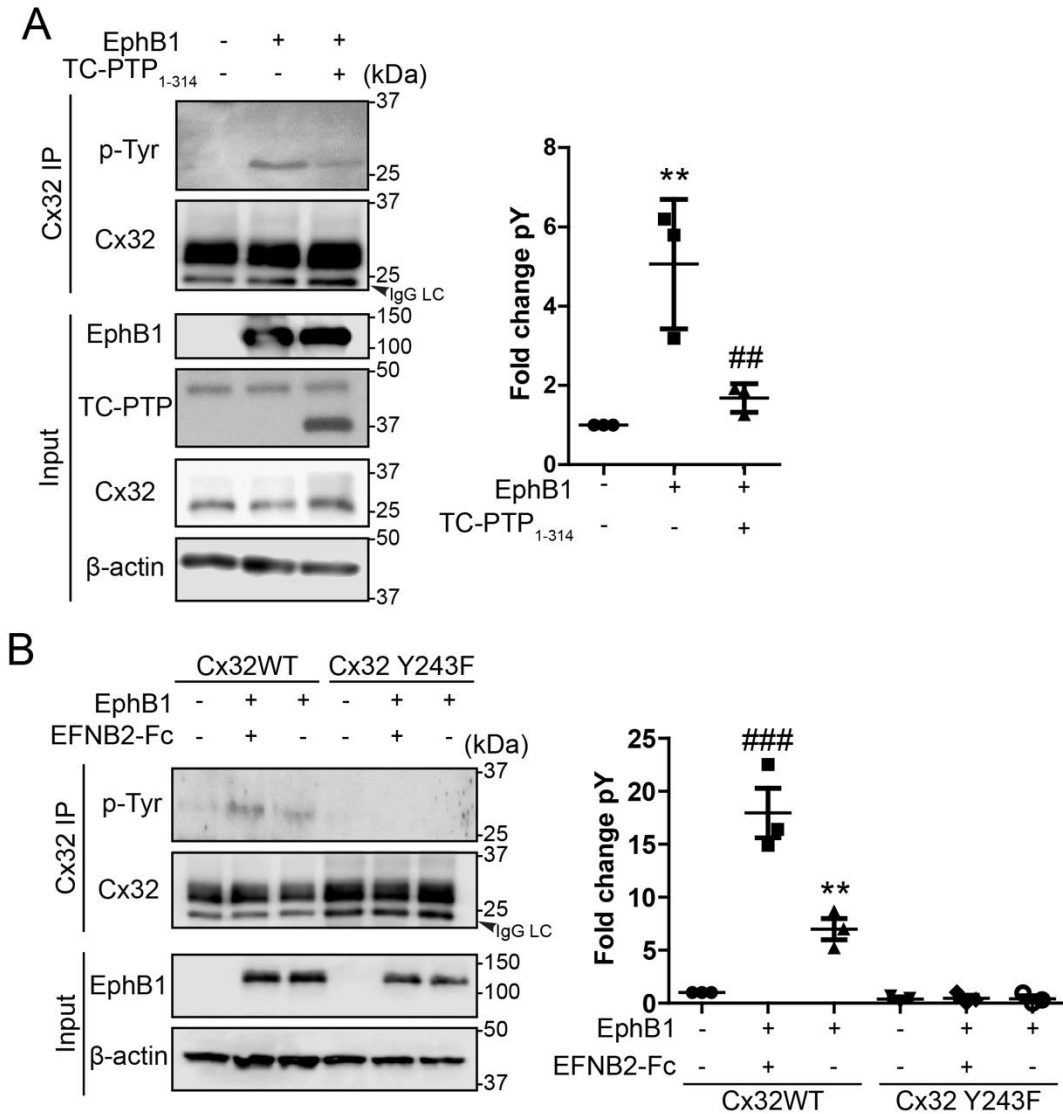


Figure 6.4. EphB1 increases and TC-PTP decreases the Tyr phosphorylation level on Cx32.

A) HeLa cells stably expressing Cx32 were transfected with EphB1 and/or the TC-PTP catalytic domain (residues 1-314). Cx32 was enriched by IP and tyrosine phosphorylation was detected with a general phospho-tyrosine antibody. The level of tyrosine phosphorylation was quantified by densitometry from three independent experiments. ** $P < 0.01$ (compared to control); ## $P < 0.01$ (compared to EphrinB1) (One-way ANOVA). B) HeLa cells stably expressing Cx32 wild-type (WT) or the Y243F mutant were transfected with EphB1. EphrinB2-Fc was used to activate the EphB1 receptor. Cx32 was similarly enriched by IP and the level of tyrosine phosphorylation detected by Western blot. ** $P < 0.01$ (compared to control); *** $P < 0.001$ (compared to EphrinB1) (One-way ANOVA). Black arrows indicate IgG light chain. Reprinted from Trease et al., (2018).

Interestingly, the Cx32 Y243F mutant (mimicking non-phosphorylated Cx32 Y243) failed to make any observable GJ plaques. To confirm this, we made stable expressing HeLa cell lines, as expected, the localization and propensity to form GJ plaques mirrored that of the transient transfections (Fig. 6.5A). To assess if the mutations affected protein expression levels we analyzed stable cell lysates by Western blot (Fig. 6.5B). We determined that the expression of Cx32 WT was 2-fold that of Cx32 Y243E (54% of WT), and approximately 6.5-fold that of Cx32 Y243F (14% of WT), as a result we excluded Cx32 Y243F from any functional assay. Finally, to test the effect of Y243 phosphorylation on cell coupling we measured the junctional transfer of the fluorescent tracer LY by scrape loading assay (Fig. 6.5C). Although we observed an approximate 50% reduction in the amount of Cx32 Y243E compared to Cx32 WT, we were surprised to observe a significant increase in the number of cells positive for LY but negative for the labeled dextran. This data suggests that phosphorylation of Cx32 Y243 positively regulates GJIC.

23.5 EphA1 also phosphorylates Cx32 on the CT domain

Following from our experiments establishing EphB1 as a kinase that phosphorylates and thereby regulates Cx32, we were curious if other Eph receptor family members also phosphorylated Cx32. To test this, we purified Cx32CT (C217-C283; Y243) and submitted it to Eurofins Scientific for *in vitro* kinase screening with all other available Eph receptor family members (KinaseProfiler). To validate the screen, EphB1 and Yes were screened as positive and negative controls, respectively. Of the Eph receptors screened, only EphA1 was able to phosphorylate the Cx32CT *in vitro* (Fig. 6.6A). Compared to control peptide it phosphorylated the Cx32CT at ~67% (Fig. 6.6A). The phosphorylation by EphB1 was comparable to the previous screen, and Yes kinase did not detectably phosphorylate the Cx32CT. Following our workflow for EphB1 we next transiently transfected human EphA1 into the Cx32 stable expressing HeLa cell line and activated the receptor with the soluble ligand, ephrin-A1-Fc. To determine the level of Tyr phosphorylation we captured Cx32 by IP and Western blotted with a general pTyr antibody (Fig. 6.6B). Like when transfected with EphB1 we observed a significant increase in Cx32 Tyr phosphorylation when EphA1 was expressed, that was further increased upon activation with the ligand (Fig. 6.6B).

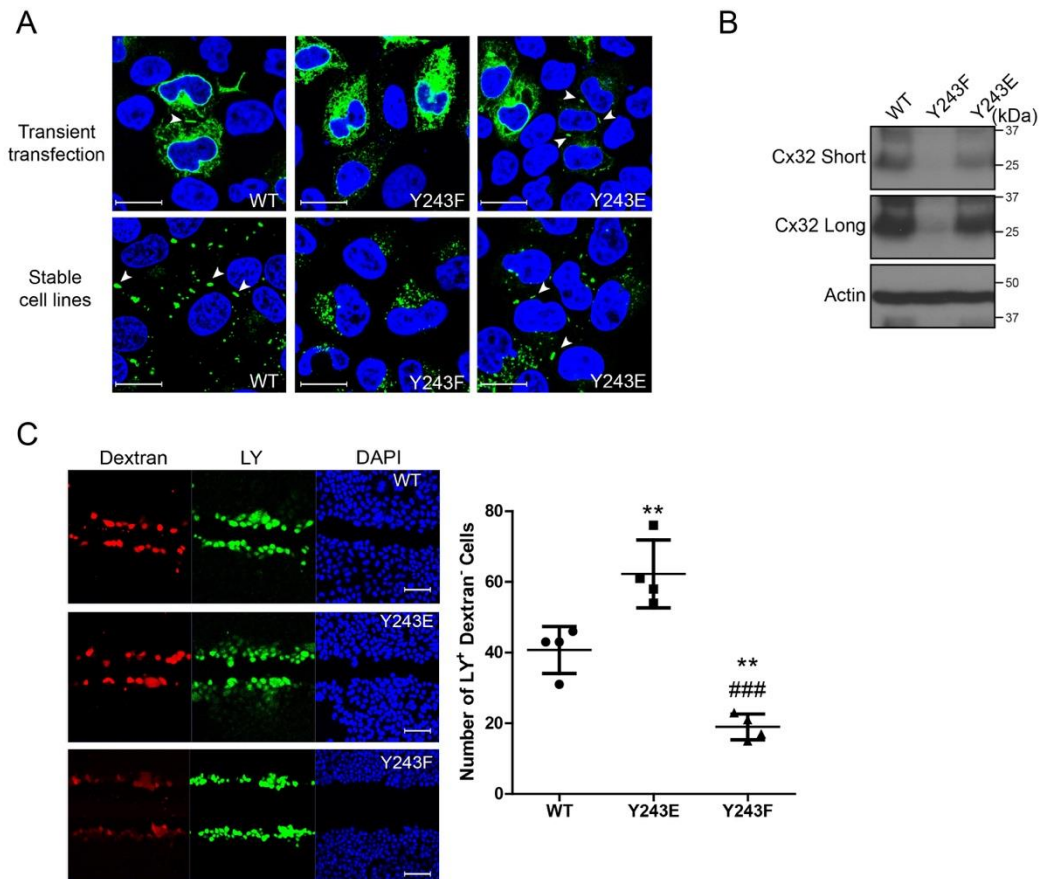


Figure 6.5. Cx32 Y243E increases GJIC.

A) Immunostaining of Cx32 WT, Y243F, and Y243E transiently (top) and stable (bottom) expressed in HeLa cells. Green: Cx32; Blue: DAPI. White arrow shows gap junction plaques. Scale bar is 20 μm . (B) Western blot of Cx32 expression in stable Cx32 WT, Y243F, and Y243E HeLa cells. (C) GJIC of Cx32 WT, Y243F, Y243E were investigated using the scraping loading dye transfer assay. Cells grown on glass coverslips were scrape loaded with Lucifer Yellow (LY, green) and Texas Red-conjugated dextran (red). Nuclei were stained by DAPI to show the confluence of cells. Scale bar is 100 μm . ** $P < 0.01$ (T-Test). Modified from Trease et al., (2018).

Since our work to this stage was completed using exogenous expression systems we sought to determine if phosphorylation would occur under endogenous expression conditions. We screened a number of cell lines (colon cancer, cholangiocyte, and cholangiocarcinoma lines) at our disposal for expression of Cx32 and EphA1 (Fig. 6.6C). We determined that Caco2 cells (human colon cancer line) expressed reasonable levels of Cx32 and EphA1 and thus tested whether EphA1 could phosphorylate Cx32 (Fig. 6.6D). We observed a significant increase in Cx32 Tyr phosphorylation when the Caco2 cells were treated with the soluble ephrin-A1-Fc, confirming the results we obtained from the overexpression system (Fig. 6.6D).

Having observed a significant increase in GJIC in our Cx32 Y243E expressing HeLa cells (Fig. 6.5), suggesting that phosphorylation of Y243 enhanced the dye transfer we predicted that activation of EphA1 in Caco2 cells would have a similar result. We therefore treated Caco2 cells with ephrin-A1-Fc and used scrape loading to determine if GJIC was increased subsequent to receptor activation. Our results indicate that similar to the phosphomimetic Cx32 Y243E mutant, activation of EphA1 enhanced GJIC in Caco2 cells (29 vs. 12 cells receiving dye; Fig. 6.6E). Finally, we were curious if the expression of EphA1, EphB1, and Cx32 was specific to the cancer state of the Caco2 cells, so we compared the levels of expression in Caco2 cells to their normal counterpart fetal human colon (FHC) cells by Western blot (Fig. 6.6F). To our surprise compared to Caco2 cell FHC cells expressed EphA1 and Cx32, but not EphB1, while the FHC only expressed EphB1. This may suggest a developmental role for EphB1 in colon, or oncogenic conditioning in the cancer cells, however, further investigation is needed. The data taken together suggest a role for Eph receptors in regulating Cx32 mediated cell coupling, and further reinforce the validity of using phosphomimetic mutants to ascertain the function of specific phosphorylation sites.

23.6 Phosphorylation at Y243 has little-to-no effect on the Cx32CT interaction with calmodulin or synapse-associated protein 97

A number of mechanisms by which phosphorylation affects the function of Cxs have been described in the literature, including: altering trafficking and assembly, accretion, open probability, channel gating, or modulation of protein partner binding (e.g., [204, 378]). Having demonstrated

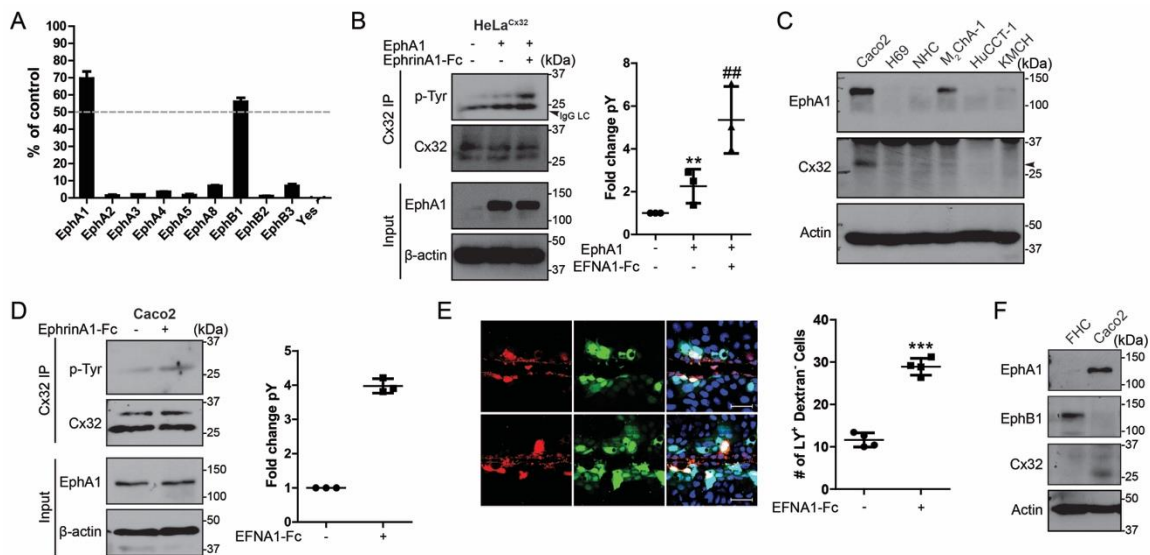


Figure 6.6. EphA1 phosphorylation of Cx32 increases gap junction intercellular communication *in vitro* and *in cyto*.

A) Cx32CT was used as a substrate for a number of different Eph receptor isoforms. EphB1 and Yes were used as positive and negative control, respectively. The amount of Cx32CT phosphorylation was compared with a positive control peptide for each kinase (% of control signal). The dashed line highlights the 50% of the control signal. B) HeLa cells stably expressing Cx32 were transfected with EphA1. EphrinA1-Fc was used to activate EphA1 receptor. Cx32 was captured by IP and the tyrosine phosphorylation level detected by Western blot. ** $P < 0.01$ (one-way ANOVA). Black arrows indicate IgG light chain. C) Western blot analysis of several cell lines screening for endogenous expression of Cx32 and EphA1. D) Cx32 was enriched by IP from Caco2 cells stimulated with EphrinA1-Fc and probed for tyrosine phosphorylation by Western blot. E) Caco2 cells cultured on glass coverslips were stimulated with EphrinA1-Fc and scrape loaded with Lucifer Yellow (LY, green) and Texas Red-conjugated dextran (red). Nuclei were stained by DAPI to show the confluence of cells. Scale bar is 100 μm . *** $P < 0.0001$ (T-Test). F) Western blot analysis comparing endogenous expression levels of EphA1, EphB1, and Cx32 in fetal human colon (FHC) and Caco2 cells. Modified from Trease et al., (2018).

that phosphorylation of Cx32 Y243 enhances GJIC we were curious what the mechanism behind this may be. Previously our laboratory reported direct interactions between either CaM or SAP97, and the Cx32CT in a region which includes Y243 (CaM: C217-S266; SAP97: C217-Q245) [248]. We hypothesized that phosphorylation of Y243 may modulate the association of these proteins with the Cx32CT. To test this, we used NMR ¹⁵N-HSQC titrations with either unlabeled Cx32 (C217-S266, pY243; ¹⁵N-CaM; Fig. 6.7) or ¹⁵N-Cx32CT Y243E (unlabeled SAP97₇₀₁₋₉₂₄; Fig. 6.8). Little-to-no difference was observed in the NMR spectra in the experiments between the non- and phosphorylated (or phosphomimetic) Cx32, indicating phosphorylation of Y243 alone does not significantly affect the interaction of Cx32CT with CaM or SAP97.

Although our results show that phosphorylation of Y243 alone do not modulate the binding of either CaM nor SAP97 to the Cx32CT, it is possible that a requirement for multiple phosphorylations exists. There are three Ser residues in close proximity to Y243 that have been detected as phosphorylated (e.g., all *in vitro*: S229, PKC; S233, PKA and PKC; and Ser240, PKC) [274, 478]. It may be that cooperativity between phosphorylation at Y243 and one (or more) of the Ser residues may alter the binding of CaM and SAP97. An additional possibility is that phosphorylation of Y243 may not alter protein partner binding at all, but rather alter channel properties such as gating, open probability, or permselectivity. Interestingly, the presence of CaM was shown to reduce the degree of Cx32 phosphorylation by EGFR and may represent a mechanism by which CaM mediates or maintains the closure of Cx32 channels by negating the effect of Y243 phosphorylation or preventing it altogether [239, 240, 298].

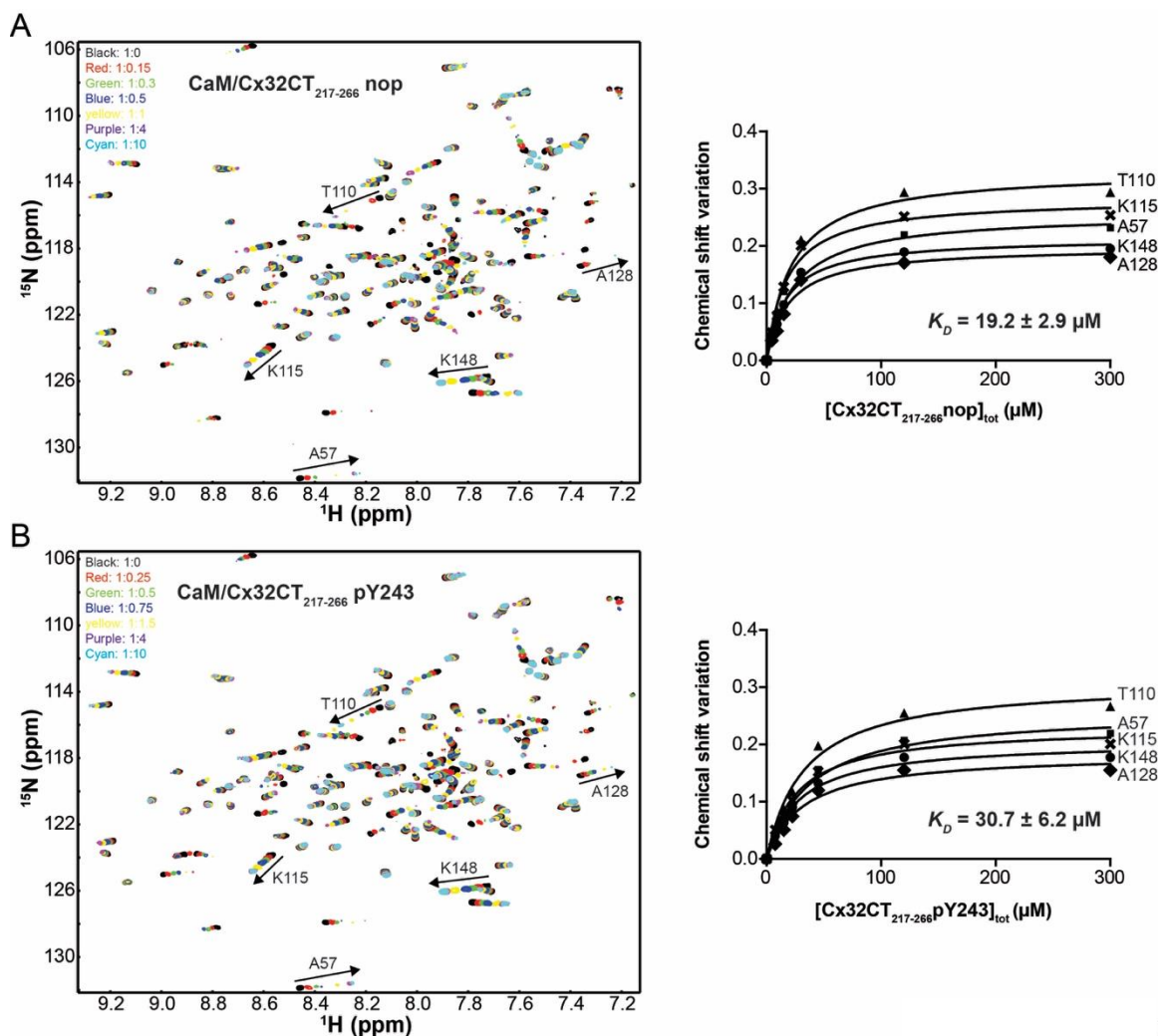


Figure 6.7. Phosphorylation of Cx32 Y243 has little-to-no effect on the interaction with CaM. ^{15}N -HSQC spectra of purified ^{15}N -CaM (30 μM) titrated with either (A) Cx32CT₂₁₇₋₂₆₆ nop (no phosphorylation) or (B) Cx32CT₂₁₇₋₂₆₆ pY243 peptides at various molar ratios. The K_D for each interaction was estimated by fitting the change in chemical shift. Represented are a subset of the CaM residues used to calculate the K_D . Reprinted from Trease et al., (2018).

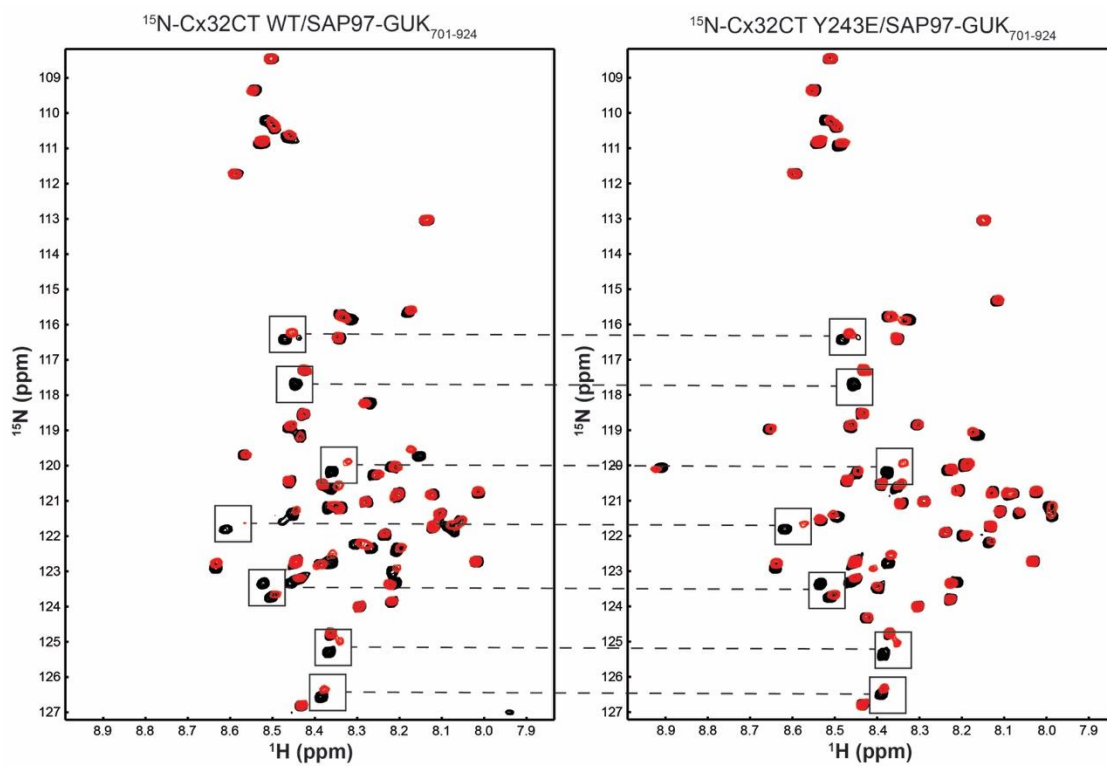


Figure 6.8. Phosphorylation of Cx32 Y243 has no effect on the interaction with SAP97.

^{15}N -HSQC spectra of purified ^{15}N -Cx32CT WT (left) or Y243E (right) ($50\ \mu\text{M}$) in the presence (red) or absence (black) of the SAP97 GUK domain (residues 701-924). For easier comparison, the main peaks affected by the SAP97-GUK $_{701-924}$ domain for both constructs have been boxed and linked. Reprinted from Trease et al., (2018).

24. Discussion

Although our report of the regulation of Cx32 GJIC by Eph receptors is novel, others have reported links between Cxs (Cx43 and Cx36) and Eph receptors. Notably, when GJIC was measured, the studies all reported an impairment of communication. In one such study examining the relationship of Cx43 and the EphB4 receptor, Cx43 was shown to co-IP the EphB4 receptor. Additionally, when the receptor was activated in primary cardiomyocytes GJ coupling was impaired [567]. A second study demonstrated co-IP of ephrin-B1 (high affinity ligand of EphB2) and Cx43 [366]. The same study also showed that when ephrin-B1 was bound by EphB2 in NIH3T3 cells Cx43 was internalized and consequently GJIC was disrupted [366]. Another study examining the formation and function of GJs in zebra fish cap cells demonstrated that both unidirectional (activation of either Eph receptor or ephrin) and bidirectional Ephrin signaling (activation of both Eph receptor and ephrin) completely blocked transfer of LY dye at the boundary of two cell populations [566]. Although the authors did not directly measure GJIC, a fourth study, demonstrated Cx36 expression was required for EphA receptor mediated insulin secretion in pancreatic β cells [574]. In the study, siRNA mediated knock-down of Cx36 reduced insulin secretion to that of control levels (inactive EphA5), however, supplementing the cells with cDNA to Cx36 cDNA rescued insulin secretion [574].

In the current study, we have shown that Cx32 Y243 is phosphorylated by EphB1 and EphA1. Use of phosphomimetic Cx32 (Y243E) suggested phosphorylation of this site increased GJIC in HeLa cells and did so through mechanisms that did not apparently affect number or size of the GJ plaques. A result that was reproducible by activation of the EphA1 receptor in an endogenous expression system (Caco2 cells). Interestingly, in hepatocytes, phosphorylation of Cx32 S233 was also shown to correlate with increased GJIC [478]. We have additionally demonstrated that the phosphatase TC-PTP dephosphorylates Cx32CT residue pY243 both *in vitro* and in the context of cells, and based on our scrape loading assays would reduce Cx32 GJIC. This contrasts with reports for Cx43, where Tyr phosphorylation (specifically Y247, Y265, and Y313) decreases GJIC by disrupting cytoskeletal anchoring and thereby GJ stability [323, 325, 328, 575-577]. These and our studies contained herein, therefore suggest that Cx phosphorylation by the

same kinase can have largely diverse effects of the regulation of different Cx family members. The number of reports of differences in response to activation of the same kinase is increasing. A good example of this is differential regulation of Cx43 and Cx45, where activation of PKA was shown to reduce Cx45 g_j while that of Cx43 was increased [306, 454]. Another example is PKG activation seemingly has no effect on Cx45 channels while it reduced Cx43 g_j [306, 454]. Response to PKC activation similarly has been shown to be divergent between Cx43 and both Cx45 and Cx37, where Cx43 channel function (g_j and dye coupling) is inhibited by PKC while one study showed Cx45 g_j increased, and a second showed although Cx45 g_j had a mild decrease, its ability to couple NB was unaffected [86]. For Cx37, PKC activation was shown to increase GJIC, again highlighting an opposite effect than what has been observed for Cx43 GJ channels [446].

Although our study has demonstrated phosphorylation of Cx32 by Eph receptors positively regulates GJIC, the relevance to human physiology remains to be determined. Using data curated within the Human Protein Atlas, expression of Cx32 is primarily found in the foregut and lower portion of the digestive tract (appendix, liver, gallbladder, gastrointestinal tract), renal (kidney), and reproductive systems (both male and female) ([578]; www.proteinatlas.org). Importantly, the EphA1 receptor is also expressed in all of these systems, suggesting that this mechanism of Cx32 regulation is likely common in these systems. EphB1 expression, however, is more restricted and relatively low. In the testes, however, EphB1 expression is relatively high and is therefore likely to contribute to the regulation of Cx32 GJIC there. Although alternate mechanisms of Eph receptor activation have been described (e.g., soluble ephrin-A1 secretion in HeLa cells [579, 580]), canonical activation of EphA1 and EphB1 by their respective ephrin ligands [581] is dependent on cell-cell contact. A similarity to this is the requirement of cell-cell contact for GJs to assemble. It is therefore likely in cells and tissues that express either EphA1 or EphB1 and Cx32, that this contact would result in the increased Cx32 phosphorylation and subsequent increases in GJIC. Furthermore, any pathological dysregulation in the expression of either the receptors, ligands, or Cx32, or aberrant cell interactions (e.g., implantation of metastatic cancer cell at site of metastasis) could lead to aberrant Cx32/Eph signaling [565, 582, 583]. While our work demonstrates

phosphorylation of Cx32 Y243 (independent of the kinase) enhances GJIC, future studies should determine what physio- and pathological conditions Cx32/Eph signaling is relevant to.

Current research on Cx phosphorylation utilizing diverse techniques and systems have demonstrated that Cx regulation by phosphorylation can be traced to similarly diverse mechanisms including changes in Cx structure, localization, trafficking/assembly, protein partner binding, turnover, and channel gating (reviewed in [328, 338]). The identification of stimuli and signal transductions which lead to phosphorylation of Cxs have greatly improved our understanding of the regulation of Cxs by kinase programs (reviewed in [328]) and are of potential clinical significance. However, comprehensive understanding of the regulation of Cxs phosphorylation will require identification of all kinases that phosphorylate Cxs and characterization of the effect(s) of the sites phosphorylated. This study is important because it demonstrates phosphorylation of a specific Cx32 residue (Y243) modulates GJIC, and further supports the notion that the effect of Cx phosphorylation by a given kinase is dictated by the Cx family member rather than the kinase, and therefore investigation of the effects on other Cx family members is essential.

CHAPTER SEVEN

Conclusions and Future Directions

25. Summary and Conclusions

GJs are critical mediators of juxtacrine signaling through the direct transfer of cytosolic constituents from one cell to the next, thereby regulating processes essential to tissue and organ homeostasis and function, including electrical and metabolic continuity, among others. Regulation of GJ proteins is diverse and complex, relying on the coordination of many hierarchical mechanisms ranging from gene expression to PTM. The importance of GJ function to many essential physiological processes (organ development, contraction in the heart, insulin release in the pancreas, neuronal plasticity, vision, hearing, etc.) makes them attractive therapeutic targets. However, to develop therapeutic approaches for the modulation of GJ function a clear understanding of mechanisms which: 1) differentiate one family member from another, 2) regulate channel function, 3) block or restore coupling, and 4) are associated with disease, is essential. In the previous Chapters, we have described the current state of GJ knowledge with a primary focus on 2 out of the 21 human family members (Cx43 and Cx45), as well as presented studies contributing to the advancement of that knowledge specifically on Cx45. Our studies focused on highlighting the regulation of Cx45 by both structural and post-translational (phosphorylation) features and described a regulatory landscape that is both similar and dissimilar to Cx43, reinforcing the need to fully characterize each Cx protein individually in order to design novel therapeutics. Our additional study on the regulation of Cx32 by phosphorylation further supports this notion.

The intimate relationship that exists between the structure and function of proteins is not a new concept and holds true for the regulation of Cxs as well. Our laboratory has historically made its primary focus delineating this relationship by investigating the CT domain of several Cxs [231, 247, 248, 284, 287, 312]. While the CT domain is primarily unstructured for most Cxs, they easily adopt structure from the influence other proteins or phosphorylation (for examples see [248, 312, 377]). The CT domain of one unique Cx, Cx45, was reported previously by our laboratory to contain a static α -helical domain that led to high-affinity ($K_D \sim 141$ nM) dimerization of the recombinant CT domain when in solution [247]. In the work presented in Chapters Two and Three, we followed up on this to investigate the functional implications of Cx45CT dimerization with the hypothesis that at

least in part, CT dimerization contributes to the uniquely (at least among cardiac Cxs) restrictive channel properties elicited by Cx45 channels [424]. While the CT domains of other Cxs adopt helical structure when tethered to their 4th TM domain, in the presence of protein partners, or when phosphorylated, Cx45 is, to our knowledge, the only described to date with a static α -helix in the absence of protein partners, phosphorylation or tethering to the 4th TM domain [247, 248, 284, 312, 377]. Notably, the region of the Cx45CT domain when compared to all proteins in the human proteome by BLAST is unique [424]. Since Cx45 expression in the ventricles has been linked to arrhythmias, the existence of this unique domain (and structure) would make an attractive target for therapeutics if modulation of the dimerization interaction alters channel function in any way. By inhibiting dimerization of the Cx45CT domain of full-length Cx45 through homologous mutants (6E, DDSc, 40_{MD}, 43_{MD}, and Δ DD), and heterologous mutants (GCN4_{LZ}, Bsub_{VD}, and Bsub_{AA}) we were able to link the presence of dimerization to tightly regulated forward trafficking and proper plaque formation, while the absence of dimerization uniformly increased the plasma membrane expression, hemichannel activity, and detergent solubility. Importantly, the dimerization of Cx45 appears to influence Cx45 channel function in a manner that is directly opposite that of Cx43. Dimerization of Cx43CT domains in a pH dependent manner serves to close the channel in ischemic conditions, perhaps a mechanism that prevents the spread of necrotic factors from the cells in the infarct to the healthy cells outside the epicardial border zone [72, 84, 222, 224, 473]. It is also probable, that since dimerization of Cx45CT domains influence the function of Cx45 homomeric channels, that it is also a contributing factor to the dominant negative phenotype Cx45 exerts on Cx43 in heteromeric channels [86, 87]. Since we observed Cx45CT dimerization preceding oligomerization of connexons in the TGN, this is almost certainly a factor that controls both stoichiometry and subunit arrangement in heteromeric channels. Two factors that are likely to influence channel function in unique ways. Supporting this are studies done on the glutamate based NMDA receptor, which are composed of two subunits each of GluN1/GluN2a that adopt an alternating arrangement such that the two GluN1 subunits and the two GluN2a subunits are diagonal to each other in the tetrad forming the receptor and pore [584]. How subunit arrangement affects Cx function remains to be determined. Future efforts to investigate the structural regulation

of Cx45 should delineate the atomic structure of the dimer interface. By accomplishing this it may be possible under certain circumstances (such as conditions that would phosphorylate Y356, thereby reducing dimer affinity) to design small molecules capable of disrupting a weakened dimer, consequently modulating Cx45 GJIC. Additionally, the role of dimerization should be addressed in the context of heteromeric channels. Determining how heteromeric Cx43/Cx45 channels form in terms of stoichiometry and subunit arrangement may offer unique insights into how dimerization alters pore structure or channel permeability. It would be reasonable to predict that two Cx45 protomers side-by-side would likely have a smaller influence than two positions across from each other. Although no results have been published, a study using atomic force microscopy is currently underway investigating the allowed subunit arrangement and stoichiometries of two β -Cx (Cx26 and Cx32; Jorge Contreras, personal communication). Finally, studies should focus on identifying unique protein partners that preferentially bind on Cx45CT over the dimerization domain, as this may offer alternate therapeutic targets that may be specific to Cx45 without needing to overcome the high energetic costs required to disrupt the dimerization.

In addition to the regulation by a static structural feature another notable difference in the regulation of different Cx family members is the response to phosphorylation. Cx43, the canonical Cx family member, has been thoroughly (albeit not exhaustively) characterized with respect to regulation by kinases and phosphorylation [524]. Since every aspect of the Cx43 life cycle is regulated by phosphorylation it is highly likely, phosphorylation is a general mechanism of Cx regulation. Indeed, this is supported by studies identifying phosphorylation of multiple family members and reporting functional effects of kinase activating conditions *in vitro* and *in vivo* [86, 158, 159, 189, 283, 294, 301, 306, 307, 311, 324, 325, 344, 351, 356, 363, 385, 446, 464, 478, 543]. We characterized the regulation of Cx45 by kinases downstream of the AT1R that would be active in hypertension and in failing hearts [491, 492, 498, 499, 504, 509]. Our results are the first to show definitive evidence of direct phosphorylation of Cx45 by Src, Pyk2, and PKC α .

Previous studies have implicated PKC (non-specifically) in the regulation of Cx45 but direct evidence of phosphorylation was lacking [86, 189]. Conversely, CaMKII has been shown to phosphorylate Cx45 *in vitro*, notably four of the seven Ser residues phosphorylated by CaMKII

(S381,381,384,385) are also phosphorylated in our samples by PKC α , suggesting the two kinases may serve overlapping or compensatory roles in the regulation of Cx45 in different cell types or under different physiological or pathophysiological states [83]. Additionally, a subset of the Ser phosphorylated by CaMKII were also phosphorylated *in vitro* by CK1, two of those (plus one additional not phosphorylated by CaMKII) were also phosphorylated in our study by PKC α (five of seven for CaMKII; S326,382,384 for PKC α) [83]. Whether all of these residues are actually phosphorylated *in cyto* or *in vivo* remains to be determined. Regardless of the kinase, based on the work of Hertlein et al. phosphorylation of Ser residues in the last 26 amino acids of Cx45 would likely contribute to GJ stability, similar to what we observed in MDCK cells stimulated with PMA [189]. A noteworthy difference between Cx43 and Cx45, is the redistribution of Cx43 from the plasma membrane following addition of PMA [585]. Speculatively, the enhancement of association with cytoskeletal partners following PMA could explain increased stability of Cx45 vs. Cx43. To address this more directly, validation of the residues phosphorylated by PKC α is essential, as well as determining biophysically how phosphorylation affects the association with specific protein partners. It is unclear if in the heart (if the same phenomenon occurs) whether this would be protective or pathological. Since PKC α attenuation offers a cardioprotective effect, it is likely that the its phosphorylation and subsequent stabilization of Cx45 would be conversely pathological [518].

Currently, the effect of PKC (via activation with PMA) on Cx45 is controversial, two separate studies highlighted opposing effects, in one the g_j was increased while in the other it decreased while NB transfer was unaffected [86, 306]. Our results do little to settle the controversy, as we report a decrease in NB transfer upon treatment with PMA. It is unclear if this is a result of parallel pathway activation from PMA treatment such as we observed in MDCK and HeLa cells, differences in timescale or concentration used, or a combination thereof. The use of selective inhibitors of PKC, MAPK, and Src would prove effective in teasing this out. It is interesting that we observed an increase in both total Cx45 and Cx45 Tyr phosphorylation when PKC is activated. Although we did not determine the exact residues phosphorylated, the activation of Pyk2 and Src downstream of PKC may suggest they have phosphorylated Cx45 under these conditions, leading

to a more complex effect than that of phosphorylation by PKC alone. Certainly, PMA is resulting in either direct or transactivation of both of these pathways as we detected increased ratios of active to total Pyk2 (MDCK and HeLa) and Src (HeLa). Future studies should focus on teasing out the exact contributions of each of these kinases downstream of PKC, as well as validate the phosphorylated residues with cellular and *in vivo* models. Subsequently, it would be important to use phosphomimetic mutants to begin to tease out the functional importance of each individual phosphorylation site as well as in combination.

The role of Src in regulating Cx43 has been well described by several studies [296, 325, 375, 376, 484]. Activation of Src leads to increased phosphorylation of several Tyr and Ser residues of Cx43 and relies on the convergence of a number of signaling pathways mediated by Src activity [325, 484]. Most notably Src activation leads to the recruitment and activation of MAPK which phosphorylates Cx43 on S255,279,282 [325]. A unified theme of Src activation for Cx43 regardless of the initial stimulus (EGF, PMA, v-Src transfection, etc.) leads to channel closure and internalization accomplished by the direct and indirect displacement of cytoskeletal anchoring proteins and recruitment of turnover/internalization machinery [286, 295, 328, 378]. When we treated MDCK and HeLa cells with PMA we observed activation of Src (in HeLa) and Pyk2 (HeLa and MDCK) that correlated with increased Tyr phosphorylation and increased association with Drebrin, ZO-1, ZO-2, and β -Tubulin. This suggests that the molecular mechanisms that mediate the association of Cx45 with these proteins differ from that of Cx43. Despite this difference we observed Src mediated loss of GJIC, under conditions in which Src was chronically active (transient transfection of constitutively active v-Src, or Src permissive temperatures in LA-25). This was starkly contrasted by acute activation of Src through stimulation of the EGFR, which resulted in upregulation of GJIC. Therefore, with respect to Src kinase, it seems Cx45 (and thus perhaps other Cxs) has a bimodal response. Interestingly, several kinases have been reported to lead to different (and many times opposite) effects when acutely vs. chronically active (reviewed in [586-590]). For example, acute activation of p38 MAPK has prohypertrophic effects, while chronic activation seems to abrogate cardiac hypertrophy [590]. Another example is Protein Kinase D 1 (PKD1) in the heart, which acutely functions to mediate cardiomyocyte metabolism by the stimulation of glucose uptake,

however, when chronically activated (in conjunction with PKD3) PKD1 mediated gene transcription that promotes the development of hypertrophy [591]. Src kinase itself is a good example of the dichotomous effects of acute vs. chronic kinase activation, acutely Src functions to regulate angiogenic factors and vascular permeability, however, chronic activation leads to cellular transformation [592-594].

Subsequent studies should focus on clarifying the differences observed between acute vs. chronic activation of Src as well as examine the effects of inhibiting Src *in cyto* and *in vivo* with the goal of determining how pathways parallel to Src may contribute. Furthermore, it would be advantageous to explore the potential that other Src family kinases also regulate Cx45. Biophysically, studies could investigate how activation by PMA leads to increased Tyr phosphorylation and why this does not affect the binding of cytoskeletal protein partners. Finally, an intimate relationship exists between Src and Pyk2, it should be investigated exactly what contribution each of these kinases make to the regulation of Cx45.

Although the initial goal of Chapter Four was to investigate the regulation of Cx45 by three kinases downstream of the AT1R, investigating the role of Pyk2 was not directly achievable beyond our *in vitro* work and co-IP. We were able to demonstrate that Pyk2 phosphorylates Cx45 on residues similar (albeit not identical) to Src. Work currently ongoing in our laboratory studying the phosphorylation of Cx43 by Pyk2 has revealed a similar effect, with Pyk2 phosphorylating Cx43 residues that are also phosphorylated by Src (Sorgen Laboratory, unpublished data). A challenge in investigating the direct phosphorylation of Pyk2 is the requirement of Src for “enhanced” activation of Pyk2, as well as the lack of selective inhibitors that do not also target focal adhesion kinase [505]. Additionally, Src and Pyk2 (when active) are physically linked via the scaffolding protein Paxillin [541]. In addition to demonstrating Pyk2 phosphorylates the Cx45CT domain, we were able to show that Pyk2 can complex with Cx45 using co-IP from Cx45 expressing HeLa cells, to this end the interaction and resultant regulation of Cx45 warrants further investigation. Notably, our study did not explore the involvement of upstream effectors including the AT1R, however, collaboratively our laboratory has tested the effects of prolonged exposure to AngII in a mouse model and consistent with the study of Yamada et al. demonstrated that Cx45 expression in the

ventricles is increased as a function of hypertrophic remodeling (Sorgen and Beuve Collaboration, unpublished data; [82]). Our *in vitro* and *in cyto* data, in combination with the collaborative animal model, numerous studies illustrating the importance of the AT1R in activation of the Src-Pyk2-PKC α axis in heart failure, and differences observed between Cx43 and Cx45, strongly suggests that expression and function of Cx45 is regulated in end-stage heart failure differently than Cx43 by the same kinase programming [72, 286, 295, 323, 378, 424, 488, 491-499, 504, 515, 530, 595, 596]. Future studies should primarily focus on the establishing the AT1R-Src-Pyk2-PKC α axis and how it relates to Cx45 function specifically in cardiac derived primary cells or cell lines. With the plethora of identified phosphorylation sites on Cx45 from this dissertation it would be beneficial to develop the first phosphorylation site specific antibodies against Cx45, this would be invaluable in terms of better understanding molecular mechanisms and temporal regulation of phosphorylation. Furthermore, as mentioned above for PKC α , it would be useful to employ phosphomimetic mutants to better understand the importance of individual sites of phosphorylation, and how those may alter the binding of protein partners or modulate channel properties directly.

Another aspect of Cx regulation that we explored herein, is the potential for cross-regulation between family members. Several studies describe altered channel properties or plaque formation when more than one heterocompatible Cx family member is expressed in the same cell type (for examples see [86-88, 476]). In our study we demonstrated co-expression of Cx45 with Cx43 in LA-25 cells was able to protect Cx43 from Src mediated turnover, while it did not prevent Src mediated channel closure as measured by NB transfer. Interestingly, though GJIC was reduced Cx43 maintained at the GJ plaque was not marked by phosphorylation for channel closure nor primed for ubiquitination and internalization. The implications of these observations are complex. In terms of turnover and channel closure the co-expression of Cx45 has greatly altered how Cx43 would normally respond [325]. However, the lack of GJIC when Cx43 is not marked for channel closure suggest that Cx45 is either marked for closure (exerting dominant negative effect on Cx43), or permselectivity of the heteromeric channels has been altered by phosphorylation. Without explicit knowledge of the specific Cx45 residues phosphorylated and their functional importance, the first possibility is difficult to explore. The possibility that permselectivity is altered, is supported

by a recent study of Cx43 describing altered permselectivity in CK1 site nonphospho- and phosphomimetic mutants [597]. Whether this is a potential mechanism leading to the loss of GJIC in our system remains to be determined. The significance of this set of experiments is the idea that if this occurs in the heart it may be a causal factor leading to arrhythmia. Loss of Cx43 alone in the heart is generally well tolerated, even to expression levels as low as 50% of normal, however, even modest expression of Cx45 in these conditions promotes the development of lethal arrhythmias [432, 437, 598]. In the case of reduced Cx43 expression, channel conductance properties are maintained, however, the inclusion of Cx45 in the ensuing heteromeric channels greatly alters the conductive properties and consequently impulse propagation [86, 87]. It therefore stands that any mechanism which promotes the formation of Cx43/Cx45 heteromeric channels may therefore be pathological. Additionally, this suggests that regulation of Cxs when intermixed is not always predictable from regulation of the individual family members. Based on our findings future studies should focus on characterizing the regulation of Cx43/Cx45 heteromeric channels *in vivo*, putting an emphasis on the response to kinase activation. Similarly, as previously suggested, it would be important to determine what degree of connexon incorporation (i.e. stoichiometry) is required for Cx45 to exert its dominant negative effect. Finally, if the regulation of heteromeric channels is unique in comparison to either homomeric channel, it is possible that this may similarly present as a unique therapeutic target, thus the therapeutic potential of modulating the function of heteromeric channel should be explored.

Finally, we explored the regulation of Cx32 a β -subtype Cx, by Eph receptors EphA1 and EphB1, and the phosphatase TC-PTP. Our results indicate that EphA1 and EphB1 both phosphorylate Cx32, on residue Y243 in the CT domain. In cells this is reversed by TC-PTP. A unifying theme of this dissertation has been highlighting differences in the regulation of the Cx family members studied, as compared to Cx43. The goal of which, has been to substantiate the importance of thoroughly characterizing each family member with respect to protein interactions and phosphorylation, two critical mediators of GJ function. Notably, comparing Cx43 and Cx32, phosphorylation by Eph family receptors has opposite effects. For Cx43 activation of EphB4 in cardiomyocytes disrupted GJIC [366]. Similarly, activation EphB2 by the ligand ephrin-B1 in

NIH3T3 cells also resulted in loss of Cx43 mediated coupling [567]. Additional examples of differences between Cx43 and exist between Cx45 and Cx43 as presented in the Chapters contained herein, as well as in response to activation of PKA, PKC, and PKG [86, 306, 454]. Another example is differential responses of Cx37 and Cx43 to PKC [364]. These reports and our studies in Chapters Two through Six clearly define a heterogeneous response of different Cx family members to the same stimulus and therefore warrant direct investigation of each Cx family member with respect to the same stimulus.

References

- [1] E.C. Beyer, V.M. Berthoud, Gap junction structure: unraveled, but not fully revealed, *F1000Res* 6 (2017) 568.
- [2] M. Yeager, Structure of cardiac gap junction intercellular channels, *J Struct Biol* 121(2) (1998) 231-45.
- [3] M. Yeager, N.B. Gilula, Membrane topology and quaternary structure of cardiac gap junction ion channels, *J Mol Biol* 223(4) (1992) 929-48.
- [4] M. Yeager, A.L. Harris, Gap junction channel structure in the early 21st century: facts and fantasies, *Curr Opin Cell Biol* 19(5) (2007) 521-8.
- [5] M. Yeager, B.J. Nicholson, Structure of gap junction intercellular channels, *Curr Opin Struct Biol* 6(2) (1996) 183-92.
- [6] D.J. Muller, G.M. Hand, A. Engel, G.E. Sosinsky, Conformational changes in surface structures of isolated connexin 26 gap junctions, *EMBO J* 21(14) (2002) 3598-607.
- [7] R.R. Shivers, L.K. McVicar, Gap junctions revealed by freeze-fracture electron microscopy, *Microsc Res Tech* 31(5) (1995) 437-45.
- [8] P. Phelan, Innexins: members of an evolutionarily conserved family of gap-junction proteins, *Biochimica et biophysica acta* 1711(2) (2005) 225-45.
- [9] P. Phelan, J.P. Bacon, J.A. Davies, L.A. Stebbings, M.G. Todman, L. Avery, R.A. Baines, T.M. Barnes, C. Ford, S. Hekimi, R. Lee, J.E. Shaw, T.A. Starich, K.D. Curtin, Y.A. Sun, R.J. Wyman, Innexins: a family of invertebrate gap-junction proteins, *Trends Genet* 14(9) (1998) 348-9.
- [10] G. Sohl, P.A. Nielsen, J. Eiberger, K. Willecke, Expression profiles of the novel human connexin genes hCx30.2, hCx40.1, and hCx62 differ from their putative mouse orthologues, *Cell communication & adhesion* 10(1) (2003) 27-36.
- [11] K. Willecke, J. Eiberger, J. Degen, D. Eckardt, A. Romualdi, M. Guldenagel, U. Deutsch, G. Sohl, Structural and functional diversity of connexin genes in the mouse and human genome, *Biol Chem* 383(5) (2002) 725-37.
- [12] J. Eiberger, J. Degen, A. Romualdi, U. Deutsch, K. Willecke, G. Sohl, Connexin genes in the mouse and human genome, *Cell communication & adhesion* 8(4-6) (2001) 163-5.
- [13] G. Sohl, K. Willecke, An update on connexin genes and their nomenclature in mouse and man, *Cell communication & adhesion* 10(4-6) (2003) 173-80.
- [14] M.S. Nielsen, L.N. Axelsen, P.L. Sorgen, V. Verma, M. Delmar, N.H. Holstein-Rathlou, Gap junctions, *Compr Physiol* 2(3) (2012) 1981-2035.
- [15] N.S. Heyman, D.T. Kurjiaka, J.F. Ek Vitorin, J.M. Burt, Regulation of gap junctional charge selectivity in cells coexpressing connexin 40 and connexin 43, *American journal of physiology. Heart and circulatory physiology* 297(1) (2009) H450-9.
- [16] M. Pahuja, M. Anikin, G.S. Goldberg, Phosphorylation of connexin43 induced by Src: regulation of gap junctional communication between transformed cells, *Experimental cell research* 313(20) (2007) 4083-90.
- [17] S.K. Li, S.W. Shan, H.L. Li, A.K. Cheng, F. Pan, S.P. Yip, M.M. Civan, C.H. To, C.W. Do, Characterization and Regulation of Gap Junctions in Porcine Ciliary Epithelium, *Invest Ophthalmol Vis Sci* 59(8) (2018) 3461-3468.
- [18] A.R. Hood, X. Ai, S.M. Pogwizd, Regulation of cardiac gap junctions by protein phosphatases, *J Mol Cell Cardiol* 107 (2017) 52-57.
- [19] J.S. Alstrom, L.W. Stroemlund, M.S. Nielsen, N. MacAulay, Protein kinase C-dependent regulation of connexin43 gap junctions and hemichannels, *Biochem Soc Trans* 43(3) (2015) 519-23.
- [20] A.B. Belousov, The regulation and role of neuronal gap junctions during neuronal injury, *Channels (Austin)* 6(5) (2012) 390-2.
- [21] A.B. Belousov, The regulation and role of neuronal gap junctions during development, *Commun Integr Biol* 4(5) (2011) 579-81.
- [22] B.A. Boswell, J.K. VanSlyke, L.S. Musil, Regulation of lens gap junctions by Transforming Growth Factor beta, *Mol Biol Cell* 21(10) (2010) 1686-97.

- [23] D. Lin, D.L. Boyle, D.J. Takemoto, IGF-I-induced phosphorylation of connexin 43 by PKC γ : regulation of gap junctions in rabbit lens epithelial cells, *Invest Ophthalmol Vis Sci* 44(3) (2003) 1160-8.
- [24] H.P. Bode, L. Wang, D. Cassio, M.F. Leite, M.V. St-Pierre, K. Hirata, K. Okazaki, M.L. Sears, P. Meda, M.H. Nathanson, J.F. Dufour, Expression and regulation of gap junctions in rat cholangiocytes, *Hepatology* 36(3) (2002) 631-40.
- [25] A.D. Martinez, J.C. Saez, Regulation of astrocyte gap junctions by hypoxia-reoxygenation, *Brain Res Brain Res Rev* 32(1) (2000) 250-8.
- [26] J.C. Saez, A.D. Martinez, M.C. Branes, H.E. Gonzalez, Regulation of gap junctions by protein phosphorylation, *Braz J Med Biol Res* 31(5) (1998) 593-600.
- [27] J. Hu, I.A. Cotgreave, Differential regulation of gap junctions by proinflammatory mediators in vitro, *J Clin Invest* 99(10) (1997) 2312-6.
- [28] D.C. Spray, S. Bai, R.D. Burk, J.C. Saez, Regulation and function of liver gap junctions and their genes, *Prog Liver Dis* 12 (1994) 1-18.
- [29] R.D. Veenstra, Developmental changes in regulation of embryonic chick heart gap junctions, *The Journal of membrane biology* 119(3) (1991) 253-65.
- [30] A. Matsumoto, A.P. Arnold, G.A. Zampighi, P.E. Micevych, Androgenic regulation of gap junctions between motoneurons in the rat spinal cord, *J Neurosci* 8(11) (1988) 4177-83.
- [31] E.C. Beyer, J. Gemel, A. Martinez, V.M. Berthoud, V. Valiunas, A.P. Moreno, P.R. Brink, Heteromeric mixing of connexins: compatibility of partners and functional consequences, *Cell communication & adhesion* 8(4-6) (2001) 199-204.
- [32] M. Rackauskas, V. Neverauskas, V.A. Skeberdis, Diversity and properties of connexin gap junction channels, *Medicina (Kaunas)* 46(1) (2010) 1-12.
- [33] M. Kumai, K. Nishii, K. Nakamura, N. Takeda, M. Suzuki, Y. Shibata, Loss of connexin45 causes a cushion defect in early cardiogenesis, *Development* 127(16) (2000) 3501-12.
- [34] D.E. Gutstein, G.E. Morley, H. Tamaddon, D. Vaidya, M.D. Schneider, J. Chen, K.R. Chien, H. Stuhlmann, G.I. Fishman, Conduction slowing and sudden arrhythmic death in mice with cardiac-restricted inactivation of connexin43, *Circ Res* 88(3) (2001) 333-9.
- [35] S.C. Juneja, K.J. Barr, G.C. Enders, G.M. Kidder, Defects in the germ line and gonads of mice lacking connexin43, *Biol Reprod* 60(5) (1999) 1263-70.
- [36] A.G. Reaume, P.A. de Sousa, S. Kulkarni, B.L. Langille, D. Zhu, T.C. Davies, S.C. Juneja, G.M. Kidder, J. Rossant, Cardiac malformation in neonatal mice lacking connexin43, *Science* 267(5205) (1995) 1831-4.
- [37] Y. Gao, D.C. Spray, Structural changes in lenses of mice lacking the gap junction protein connexin43, *Invest Ophthalmol Vis Sci* 39(7) (1998) 1198-209.
- [38] J.J. Kelly, J.L. Esseltine, Q. Shao, E.W. Jabs, J. Sampson, M. Auranen, D. Bai, D.W. Laird, Specific functional pathologies of Cx43 mutations associated with oculodentodigital dysplasia, *Mol Biol Cell* 27(14) (2016) 2172-85.
- [39] D.W. Laird, Syndromic and non-syndromic disease-linked Cx43 mutations, *FEBS Lett* 588(8) (2014) 1339-48.
- [40] T. Huang, Q. Shao, A. MacDonald, L. Xin, R. Lorentz, D. Bai, D.W. Laird, Autosomal recessive GJA1 (Cx43) gene mutations cause oculodentodigital dysplasia by distinct mechanisms, *J Cell Sci* 126(Pt 13) (2013) 2857-66.
- [41] Q. Shao, Q. Liu, R. Lorentz, X.Q. Gong, D. Bai, G.S. Shaw, D.W. Laird, Structure and functional studies of N-terminal Cx43 mutants linked to oculodentodigital dysplasia, *Mol Biol Cell* 23(17) (2012) 3312-21.
- [42] R. Lorentz, Q. Shao, T. Huang, G.I. Fishman, D.W. Laird, Characterization of gap junction proteins in the bladder of Cx43 mutant mouse models of oculodentodigital dysplasia, *The Journal of membrane biology* 245(5-6) (2012) 345-55.
- [43] E. McLachlan, I. Plante, Q. Shao, D. Tong, G.M. Kidder, S.M. Bernier, D.W. Laird, ODDD-linked Cx43 mutants reduce endogenous Cx43 expression and function in osteoblasts and inhibit late stage differentiation, *J Bone Miner Res* 23(6) (2008) 928-38.
- [44] R. Dobrowolski, A. Sommershof, K. Willecke, Some oculodentodigital dysplasia-associated Cx43 mutations cause increased hemichannel activity in addition to deficient gap junction channels, *The Journal of membrane biology* 219(1-3) (2007) 9-17.

- [45] E. McLachlan, J.L. Manias, X.Q. Gong, C.S. Lounsbury, Q. Shao, S.M. Bernier, D. Bai, D.W. Laird, Functional characterization of oculodentodigital dysplasia-associated Cx43 mutants, *Cell communication & adhesion* 12(5-6) (2005) 279-92.
- [46] X.Z. Liu, Y. Yuan, D. Yan, E.H. Ding, X.M. Ouyang, Y. Fei, W. Tang, H. Yuan, Q. Chang, L.L. Du, X. Zhang, G. Wang, S. Ahmad, D.Y. Kang, X. Lin, P. Dai, Digenic inheritance of non-syndromic deafness caused by mutations at the gap junction proteins Cx26 and Cx31, *Hum Genet* 125(1) (2009) 53-62.
- [47] S. Melchionda, M. Bicego, E. Marciano, A. Franze, M. Morgutti, G. Bortone, L. Zelante, M. Carella, P. D'Andrea, Functional characterization of a novel Cx26 (T55N) mutation associated to non-syndromic hearing loss, *Biochem Biophys Res Commun* 337(3) (2005) 799-805.
- [48] G. Mese, E. Londin, R. Mui, P.R. Brink, T.W. White, Altered gating properties of functional Cx26 mutants associated with recessive non-syndromic hearing loss, *Hum Genet* 115(3) (2004) 191-9.
- [49] A. Forge, N.K. Marziano, S.O. Casalotti, D.L. Becker, D. Jagger, The inner ear contains heteromeric channels composed of cx26 and cx30 and deafness-related mutations in cx26 have a dominant negative effect on cx30, *Cell communication & adhesion* 10(4-6) (2003) 341-6.
- [50] Y.C. Wang, C.Y. Kung, M.C. Su, C.C. Su, H.M. Hsu, C.C. Tsai, C.C. Lin, S.Y. Li, Mutations of Cx26 gene (GJB2) for prelingual deafness in Taiwan, *Eur J Hum Genet* 10(8) (2002) 495-8.
- [51] A. Murgia, E. Orzan, R. Polli, M. Martella, C. Vinanzi, E. Leonardi, E. Arslan, F. Zacchello, Cx26 deafness: mutation analysis and clinical variability, *J Med Genet* 36(11) (1999) 829-32.
- [52] G. Richard, T.W. White, L.E. Smith, R.A. Bailey, J.G. Compton, D.L. Paul, S.J. Bale, Functional defects of Cx26 resulting from a heterozygous missense mutation in a family with dominant deaf-mutism and palmoplantar keratoderma, *Hum Genet* 103(4) (1998) 393-9.
- [53] Y. Kim, K.G. Choi, K.D. Park, K.S. Lee, K.W. Chung, B.O. Choi, X-linked dominant Charcot-Marie-Tooth disease with connexin 32 (Cx32) mutations in Koreans, *Clin Genet* 81(2) (2012) 142-9.
- [54] M. Bicego, S. Morassutto, V.H. Hernandez, M. Morgutti, F. Mammano, P. D'Andrea, R. Bruzzone, Selective defects in channel permeability associated with Cx32 mutations causing X-linked Charcot-Marie-Tooth disease, *Neurobiol Dis* 21(3) (2006) 607-17.
- [55] E. Nelis, S. Simokovic, V. Timmerman, A. Lofgren, H. Backhovens, P. De Jonghe, J.J. Martin, C. Van Broeckhoven, Mutation analysis of the connexin 32 (Cx32) gene in Charcot-Marie-Tooth neuropathy type 1: identification of five new mutations, *Hum Mutat* 9(1) (1997) 47-52.
- [56] E.C. Beyer, L. Ebihara, V.M. Berthoud, Connexin mutants and cataracts, *Frontiers in pharmacology* 4 (2013) 43.
- [57] C.W. Lo, Role of gap junctions in cardiac conduction and development: insights from the connexin knockout mice, *Circ Res* 87(5) (2000) 346-8.
- [58] S.A. Bernstein, G.E. Morley, Gap junctions and propagation of the cardiac action potential, *Adv Cardiol* 42 (2006) 71-85.
- [59] C.W. Lo, A. Wessels, Cx43 gap junctions in cardiac development, *Trends Cardiovasc Med* 8(6) (1998) 264-9.
- [60] M. Delmar, Gap junctions as active signaling molecules for synchronous cardiac function, *Journal of cardiovascular electrophysiology* 11(1) (2000) 118-20.
- [61] A.G. Kleber, Gap junctions and conduction of cardiac excitation, *Heart Rhythm* 8(12) (2011) 1981-4.
- [62] S. Rohr, Role of gap junctions in the propagation of the cardiac action potential, *Cardiovasc Res* 62(2) (2004) 309-22.
- [63] Y. Rudy, R.M. Shaw, Cardiac excitation: an interactive process of ion channels and gap junctions, *Adv Exp Med Biol* 430 (1997) 269-79.
- [64] J.E. Saffitz, R.H. Hoyt, R.A. Luke, H. Lee Kanter, E.C. Beyer, Cardiac myocyte interconnections at gap junctions Role in normal and abnormal electrical conduction, *Trends Cardiovasc Med* 2(2) (1992) 56-60.
- [65] S. Alcolea, M. Theveniau-Ruissy, T. Jarry-Guichard, I. Marics, E. Tzouanacou, J.P. Chauvin, J.P. Briand, A.F. Moorman, W.H. Lamers, D.B. Gros, Downregulation of connexin 45 gene products during mouse heart development, *Circ Res* 84(12) (1999) 1365-79.

- [66] T. Desplantez, D. Halliday, E. Dupont, R. Weingart, Cardiac connexins Cx43 and Cx45: formation of diverse gap junction channels with diverse electrical properties, *Pflugers Arch* 448(4) (2004) 363-75.
- [67] N.J. Severs, A.F. Bruce, E. Dupont, S. Rothery, Remodelling of gap junctions and connexin expression in diseased myocardium, *Cardiovasc Res* 80(1) (2008) 9-19.
- [68] M.M. Kreuzberg, K. Willecke, F.F. Bukauskas, Connexin-mediated cardiac impulse propagation: connexin 30.2 slows atrioventricular conduction in mouse heart, *Trends Cardiovasc Med* 16(8) (2006) 266-72.
- [69] M.M. Kreuzberg, J.W. Schrickel, A. Ghanem, J.S. Kim, J. Degen, U. Janssen-Bienhold, T. Lewalter, K. Tiemann, K. Willecke, Connexin30.2 containing gap junction channels decelerate impulse propagation through the atrioventricular node, *Proc Natl Acad Sci U S A* 103(15) (2006) 5959-64.
- [70] M.M. Kreuzberg, M. Liebermann, S. Segschneider, R. Dobrowolski, H. Dobrzynski, R. Kaba, G. Rowlinson, E. Dupont, N.J. Severs, K. Willecke, Human connexin31.9, unlike its orthologous protein connexin30.2 in the mouse, is not detectable in the human cardiac conduction system, *J Mol Cell Cardiol* 46(4) (2009) 553-9.
- [71] N.J. Severs, E. Dupont, S.R. Coppen, D. Halliday, E. Inett, D. Baylis, S. Rothery, Remodelling of gap junctions and connexin expression in heart disease, *Biochimica et biophysica acta* 1662(1-2) (2004) 138-48.
- [72] F. Kieken, N. Mutsaers, E. Dolmatova, K. Virgil, A.L. Wit, A. Kellezi, B.J. Hirst-Jensen, H.S. Duffy, P.L. Sorgen, Structural and molecular mechanisms of gap junction remodeling in epicardial border zone myocytes following myocardial infarction, *Circ Res* 104(9) (2009) 1103-12.
- [73] J.E. Saffitz, K.Y. Hames, S. Kanno, Remodeling of gap junctions in ischemic and nonischemic forms of heart disease, *The Journal of membrane biology* 218(1-3) (2007) 65-71.
- [74] J.E. Saffitz, A.G. Kleber, Effects of mechanical forces and mediators of hypertrophy on remodeling of gap junctions in the heart, *Circ Res* 94(5) (2004) 585-91.
- [75] N.J. Severs, E. Dupont, N. Thomas, R. Kaba, S. Rothery, R. Jain, K. Sharpey, C.H. Fry, Alterations in cardiac connexin expression in cardiomyopathies, *Adv Cardiol* 42 (2006) 228-42.
- [76] A.L. Wit, Remodeling of cardiac gap junctions: the relationship to the genesis of ventricular tachycardia, *J Electrocardiol* 34 Suppl (2001) 77-83.
- [77] Z.B. Yu, J.J. Sheng, [Remodeling of cardiac gap junctions and arrhythmias], *Sheng Li Xue Bao* 63(6) (2011) 586-92.
- [78] Y. Zhang, E.M. Kanter, K.A. Yamada, Remodeling of cardiac fibroblasts following myocardial infarction results in increased gap junction intercellular communication, *Cardiovasc Pathol* 19(6) (2010) e233-40.
- [79] E. Dupont, T. Matsushita, R.A. Kaba, C. Vozzi, S.R. Coppen, N. Khan, R. Kaprielian, M.H. Yacoub, N.J. Severs, Altered connexin expression in human congestive heart failure, *J Mol Cell Cardiol* 33(2) (2001) 359-71.
- [80] B. Bastide, L. Neyses, D. Ganten, M. Paul, K. Willecke, O. Traub, Gap junction protein connexin40 is preferentially expressed in vascular endothelium and conductive bundles of rat myocardium and is increased under hypertensive conditions, *Circ Res* 73(6) (1993) 1138-49.
- [81] E. Dupont, Y. Ko, S. Rothery, S.R. Coppen, M. Baghai, M. Haw, N.J. Severs, The gap-junctional protein connexin40 is elevated in patients susceptible to postoperative atrial fibrillation, *Circulation* 103(6) (2001) 842-9.
- [82] K.A. Yamada, J.G. Rogers, R. Sundset, T.H. Steinberg, J. Saffitz, Up-regulation of connexin45 in heart failure, *Journal of cardiovascular electrophysiology* 14(11) (2003) 1205-12.
- [83] M. Bao, E.M. Kanter, R.Y. Huang, S. Maxeiner, M. Frank, Y. Zhang, R.B. Schuessler, T.W. Smith, R.R. Townsend, H.W. Rohrs, V.M. Berthoud, K. Willecke, J.G. Laing, K.A. Yamada, Residual Cx45 and its relationship to Cx43 in murine ventricular myocardium, *Channels (Austin)* 5(6) (2011) 489-99.
- [84] E. Macia, E. Dolmatova, C. Cabo, A.Z. Sosinsky, W. Dun, J. Coromilas, E.J. Ciaccio, P.A. Boyden, A.L. Wit, H.S. Duffy, Characterization of gap junction remodeling in epicardial border zone of healing canine infarcts and electrophysiological effects of partial reversal by rotigaptide, *Circ Arrhythm Electrophysiol* 4(3) (2011) 344-51.
- [85] S. Elenes, A.D. Martinez, M. Delmar, E.C. Beyer, A.P. Moreno, Heterotypic docking of Cx43 and Cx45 connexons blocks fast voltage gating of Cx43, *Biophys J* 81(3) (2001) 1406-18.

- [86] A.D. Martinez, V. Hayrapetyan, A.P. Moreno, E.C. Beyer, Connexin43 and connexin45 form heteromeric gap junction channels in which individual components determine permeability and regulation, *Circ Res* 90(10) (2002) 1100-7.
- [87] G. Zhong, N. Akoum, D.A. Appadurai, V. Hayrapetyan, O. Ahmed, A.D. Martinez, E.C. Beyer, A.P. Moreno, Mono-Heteromeric Configurations of Gap Junction Channels Formed by Connexin43 and Connexin45 Reduce Unitary Conductance and Determine both Voltage Gating and Metabolic Flux Asymmetry, *Frontiers in Physiology* 8(346) (2017).
- [88] K. Grikscheit, N. Thomas, A.F. Bruce, S. Rothery, J. Chan, N.J. Severs, E. Dupont, Coexpression of connexin 45 with connexin 43 decreases gap junction size, *Cell communication & adhesion* 15(1) (2008) 185-93.
- [89] T. Miller, G. Dahl, R. Werner, Structure of a gap junction gene: rat connexin-32, *Biosci Rep* 8(5) (1988) 455-64.
- [90] C.L. Anderson, M.A. Zundel, R. Werner, Variable promoter usage and alternative splicing in five mouse connexin genes, *Genomics* 85(2) (2005) 238-44.
- [91] M. Oyamada, K. Takebe, Y. Oyamada, Regulation of connexin expression by transcription factors and epigenetic mechanisms, *Biochimica et biophysica acta* 1828(1) (2013) 118-33.
- [92] M. Oyamada, Y. Oyamada, T. Takamatsu, Regulation of connexin expression, *Biochimica et biophysica acta* 1719(1-2) (2005) 6-23.
- [93] I. Pfeifer, C. Anderson, R. Werner, E. Oltra, Redefining the structure of the mouse connexin43 gene: selective promoter usage and alternative splicing mechanisms yield transcripts with different translational efficiencies, *Nucleic Acids Res* 32(15) (2004) 4550-62.
- [94] R. Sullivan, C. Ruangvoravat, D. Joo, J. Morgan, B.L. Wang, X.K. Wang, C.W. Lo, Structure, sequence and expression of the mouse Cx43 gene encoding connexin 43, *Gene* 130(2) (1993) 191-9.
- [95] A. Jacob, E.C. Beyer, Mouse connexin 45: genomic cloning and exon usage, *DNA Cell Biol* 20(1) (2001) 11-9.
- [96] B.E. Teunissen, M.F. Bierhuizen, Transcriptional control of myocardial connexins, *Cardiovasc Res* 62(2) (2004) 246-55.
- [97] M. Hernandez, Q. Shao, X.J. Yang, S.P. Luh, M. Kandouz, G. Batist, D.W. Laird, M.A. Alaoui-Jamali, A histone deacetylation-dependent mechanism for transcriptional repression of the gap junction gene cx43 in prostate cancer cells, *Prostate* 66(11) (2006) 1151-61.
- [98] H. Kim, W.D. Pennie, Y. Sun, N.H. Colburn, Differential functional significance of AP-1 binding sites in the promoter of the gene encoding mouse tissue inhibitor of metalloproteinases-3, *Biochem J* 324 (Pt 2) (1997) 547-53.
- [99] B.E. Teunissen, A.T. Jansen, S.C. van Amersfoort, T.X. O'Brien, H.J. Jongsma, M.F. Bierhuizen, Analysis of the rat connexin 43 proximal promoter in neonatal cardiomyocytes, *Gene* 322 (2003) 123-36.
- [100] C. Tacheau, J. Fontaine, J. Loy, A. Mauviel, F. Verrecchia, TGF-beta induces connexin43 gene expression in normal murine mammary gland epithelial cells via activation of p38 and PI3K/AKT signaling pathways, *J Cell Physiol* 217(3) (2008) 759-68.
- [101] H. Negoro, A. Kanematsu, M. Imamura, Y. Kimura, R. Matsuoka, M. Tanaka, Y. Tabata, O. Ogawa, Regulation of connexin 43 by basic fibroblast growth factor in the bladder: transcriptional and behavioral implications, *J Urol* 185(6) (2011) 2398-404.
- [102] M. Zi, T.E. Kimura, W. Liu, J. Jin, J. Higham, S. Khariche, G. Hao, Y. Shi, W. Shen, S. Prehar, A. Mironov, L. Neyses, M.F. Bierhuizen, M.R. Boyett, H. Zhang, M. Lei, E.J. Cartwright, X. Wang, Mitogen-activated protein kinase kinase 4 deficiency in cardiomyocytes causes connexin 43 reduction and couples hypertrophic signals to ventricular arrhythmogenesis, *The Journal of biological chemistry* 286(20) (2011) 17821-30.
- [103] X. Chen, J.M. Wu, K. Hornischer, A. Kel, E. Wingender, TiProD: the Tissue-specific Promoter Database, *Nucleic Acids Res* 34(Database issue) (2006) D104-7.
- [104] S. Zaffran, M. Frasch, Early signals in cardiac development, *Circ Res* 91(6) (2002) 457-69.
- [105] B.G. Bruneau, Transcriptional regulation of vertebrate cardiac morphogenesis, *Circ Res* 90(5) (2002) 509-19.
- [106] L. Dupays, T. Jarry-Guichard, D. Mazurais, T. Calmels, S. Izumo, D. Gros, M. Theveniau-Ruissy, Dysregulation of connexins and inactivation of NFATc1 in the cardiovascular system of Nkx2-5 null mutants, *J Mol Cell Cardiol* 38(5) (2005) 787-98.

- [107] V.L. Linhares, N.A. Almeida, D.C. Menezes, D.A. Elliott, D. Lai, E.C. Beyer, A.C. Campos de Carvalho, M.W. Costa, Transcriptional regulation of the murine Connexin40 promoter by cardiac factors Nkx2-5, GATA4 and Tbx5, *Cardiovasc Res* 64(3) (2004) 402-11.
- [108] H. Kasahara, H. Wakimoto, M. Liu, C.T. Maguire, K.L. Converso, T. Shioi, W.Y. Huang, W.J. Manning, D. Paul, J. Lawitts, C.I. Berul, S. Izumo, Progressive atrioventricular conduction defects and heart failure in mice expressing a mutant Csx/Nkx2.5 homeoprotein, *J Clin Invest* 108(2) (2001) 189-201.
- [109] H. Kasahara, T. Ueyama, H. Wakimoto, M.K. Liu, C.T. Maguire, K.L. Converso, P.M. Kang, W.J. Manning, J. Lawitts, D.L. Paul, C.I. Berul, S. Izumo, Nkx2.5 homeoprotein regulates expression of gap junction protein connexin 43 and sarcomere organization in postnatal cardiomyocytes, *J Mol Cell Cardiol* 35(3) (2003) 243-56.
- [110] M. Pashmforoush, J.T. Lu, H. Chen, T.S. Amand, R. Kondo, S. Pradervand, S.M. Evans, B. Clark, J.R. Feramisco, W. Giles, S.Y. Ho, D.W. Benson, M. Silberbach, W. Shou, K.R. Chien, Nkx2-5 pathways and congenital heart disease; loss of ventricular myocyte lineage specification leads to progressive cardiomyopathy and complete heart block, *Cell* 117(3) (2004) 373-86.
- [111] R.J. Blaschke, N.D. Hahurij, S. Kuijper, S. Just, L.J. Wisse, K. Deissler, T. Maxelon, K. Anastassiadis, J. Spitzer, S.E. Hardt, H. Scholer, H. Feitsma, W. Rottbauer, M. Blum, F. Meijlink, G. Rappold, A.C. Gittenberger-de Groot, Targeted mutation reveals essential functions of the homeodomain transcription factor Shox2 in sinoatrial and pacemaking development, *Circulation* 115(14) (2007) 1830-8.
- [112] R.A. Espinoza-Lewis, L. Yu, F. He, H. Liu, R. Tang, J. Shi, X. Sun, J.F. Martin, D. Wang, J. Yang, Y. Chen, Shox2 is essential for the differentiation of cardiac pacemaker cells by repressing Nkx2-5, *Dev Biol* 327(2) (2009) 376-85.
- [113] V. Ionta, W. Liang, E.H. Kim, R. Rafie, A. Giacomello, E. Marban, H.C. Cho, SHOX2 overexpression favors differentiation of embryonic stem cells into cardiac pacemaker cells, improving biological pacing ability, *Stem Cell Reports* 4(1) (2015) 129-42.
- [114] F.A. Ismat, M. Zhang, H. Kook, B. Huang, R. Zhou, V.A. Ferrari, J.A. Epstein, V.V. Patel, Homeobox protein Hop functions in the adult cardiac conduction system, *Circ Res* 96(8) (2005) 898-903.
- [115] F. Liu, M.D. Levin, N.B. Petrenko, M.M. Lu, T. Wang, L.J. Yuan, A.L. Stout, J.A. Epstein, V.V. Patel, Histone-deacetylase inhibition reverses atrial arrhythmia inducibility and fibrosis in cardiac hypertrophy independent of angiotensin, *J Mol Cell Cardiol* 45(6) (2008) 715-23.
- [116] S.S. Zhang, K.H. Kim, A. Rosen, J.W. Smyth, R. Sakuma, P. Delgado-Olguin, M. Davis, N.C. Chi, V. Puvindran, N. Gaborit, T. Sukonnik, J.N. Wylie, K. Brand-Arzamendi, G.P. Farman, J. Kim, R.A. Rose, P.A. Marsden, Y. Zhu, Y.Q. Zhou, L. Miquerol, R.M. Henkelman, D.Y. Stainier, R.M. Shaw, C.C. Hui, B.G. Bruneau, P.H. Backx, Iroquois homeobox gene 3 establishes fast conduction in the cardiac His-Purkinje network, *Proc Natl Acad Sci U S A* 108(33) (2011) 13576-81.
- [117] K.J. Boogerd, L.Y. Wong, V.M. Christoffels, M. Klarenbeek, J.M. Ruijter, A.F. Moorman, P. Barnett, Msx1 and Msx2 are functional interacting partners of T-box factors in the regulation of Connexin43, *Cardiovasc Res* 78(3) (2008) 485-93.
- [118] V.M. Christoffels, W.M. Hoogaars, A. Tessari, D.E. Clout, A.F. Moorman, M. Campione, T-box transcription factor Tbx2 represses differentiation and formation of the cardiac chambers, *Dev Dyn* 229(4) (2004) 763-70.
- [119] N. Kapoor, G. Galang, E. Marban, H.C. Cho, Transcriptional suppression of connexin43 by TBX18 undermines cell-cell electrical coupling in postnatal cardiomyocytes, *The Journal of biological chemistry* 286(16) (2011) 14073-9.
- [120] A.C. Fijnvandraat, R.H. Lekanne Deprez, V.M. Christoffels, J.M. Ruijter, A.F. Moorman, TBX5 overexpression stimulates differentiation of chamber myocardium in P19C16 embryonic carcinoma cells, *J Muscle Res Cell Motil* 24(2-3) (2003) 211-8.
- [121] N.V. Munshi, J. McAnally, S. Bezprozvannaya, J.M. Berry, J.A. Richardson, J.A. Hill, E.N. Olson, Cx30.2 enhancer analysis identifies Gata4 as a novel regulator of atrioventricular delay, *Development* 136(15) (2009) 2665-74.
- [122] M. Vinken, E. De Rop, E. Decrock, E. De Vuyst, L. Leybaert, T. Vanhaecke, V. Rogiers, Epigenetic regulation of gap junctional intercellular communication: more than a way to keep cells quiet?, *Biochimica et biophysica acta* 1795(1) (2009) 53-61.

- [123] F. Rinaldi, E.M. Hartfield, L.A. Crompton, J.L. Badger, C.P. Glover, C.M. Kelly, A.E. Rosser, J.B. Uney, M.A. Caldwell, Cross-regulation of Connexin43 and beta-catenin influences differentiation of human neural progenitor cells, *Cell Death Dis* 5 (2014) e1017.
- [124] Z. Ai, A. Fischer, D.C. Spray, A.M. Brown, G.I. Fishman, Wnt-1 regulation of connexin43 in cardiac myocytes, *J Clin Invest* 105(2) (2000) 161-71.
- [125] Y. Komiya, R. Habas, Wnt signal transduction pathways, *Organogenesis* 4(2) (2008) 68-75.
- [126] A. Schiavi, A. Hudder, R. Werner, Connexin43 mRNA contains a functional internal ribosome entry site, *FEBS Lett* 464(3) (1999) 118-22.
- [127] R. Werner, IRES elements in connexin genes: a hypothesis explaining the need for connexins to be regulated at the translational level, *IUBMB Life* 50(3) (2000) 173-6.
- [128] A. Hudder, R. Werner, Analysis of a Charcot-Marie-Tooth disease mutation reveals an essential internal ribosome entry site element in the connexin-32 gene, *The Journal of biological chemistry* 275(44) (2000) 34586-91.
- [129] M.M. Falk, N.B. Gilula, Connexin membrane protein biosynthesis is influenced by polypeptide positioning within the translocon and signal peptidase access, *The Journal of biological chemistry* 273(14) (1998) 7856-64.
- [130] A.C. Borel, S.M. Simon, Biogenesis of polytopic membrane proteins: membrane segments of P-glycoprotein sequentially translocate to span the ER membrane, *Biochemistry* 35(33) (1996) 10587-94.
- [131] A.C. Borel, S.M. Simon, Biogenesis of polytopic membrane proteins: membrane segments assemble within translocation channels prior to membrane integration, *Cell* 85(3) (1996) 379-89.
- [132] K.S. Crowley, S. Liao, V.E. Worrell, G.D. Reinhart, A.E. Johnson, Secretory proteins move through the endoplasmic reticulum membrane via an aqueous, gated pore, *Cell* 78(3) (1994) 461-71.
- [133] K.S. Crowley, G.D. Reinhart, A.E. Johnson, The signal sequence moves through a ribosomal tunnel into a noncytoplasmic aqueous environment at the ER membrane early in translocation, *Cell* 73(6) (1993) 1101-15.
- [134] W. Mothes, S.U. Heinrich, R. Graf, I. Nilsson, G. von Heijne, J. Brunner, T.A. Rapoport, Molecular mechanism of membrane protein integration into the endoplasmic reticulum, *Cell* 89(4) (1997) 523-33.
- [135] M.M. Falk, Biosynthesis and structural composition of gap junction intercellular membrane channels, *Eur J Cell Biol* 79(8) (2000) 564-74.
- [136] V. Su, A.F. Lau, Connexins: mechanisms regulating protein levels and intercellular communication, *FEBS Lett* 588(8) (2014) 1212-20.
- [137] S. Das, T.D. Smith, J.D. Sarma, J.D. Ritzenthaler, J. Maza, B.E. Kaplan, L.A. Cunningham, L. Suaud, M.J. Hubbard, R.C. Rubenstein, M. Koval, ERp29 restricts Connexin43 oligomerization in the endoplasmic reticulum, *Mol Biol Cell* 20(10) (2009) 2593-604.
- [138] F. Kieken, G. Spagnol, V. Su, A.F. Lau, P.L. Sorgen, NMR structure note: UBA domain of CIP75, *J Biomol NMR* 46(3) (2010) 245-50.
- [139] J.L. Kopanic, B. Schlingmann, M. Koval, A.F. Lau, P.L. Sorgen, V.F. Su, Degradation of gap junction connexins is regulated by the interaction with Cx43-interacting protein of 75 kDa (CIP75), *Biochem J* 466(3) (2015) 571-85.
- [140] X. Li, V. Su, W.E. Kurata, C. Jin, A.F. Lau, A novel connexin43-interacting protein, CIP75, which belongs to the Ubl-UBA protein family, regulates the turnover of connexin43, *The Journal of biological chemistry* 283(9) (2008) 5748-59.
- [141] V. Su, C. Hoang, D. Geerts, A.F. Lau, CIP75 (connexin43-interacting protein of 75 kDa) mediates the endoplasmic reticulum dislocation of connexin43, *Biochem J* 458(1) (2014) 57-67.
- [142] V. Su, R. Nakagawa, M. Koval, A.F. Lau, Ubiquitin-independent proteasomal degradation of endoplasmic reticulum-localized connexin43 mediated by CIP75, *The Journal of biological chemistry* 285(52) (2010) 40979-90.
- [143] M. Koval, J.E. Harley, E. Hick, T.H. Steinberg, Connexin46 is retained as monomers in a trans-Golgi compartment of osteoblastic cells, *J Cell Biol* 137(4) (1997) 847-57.
- [144] L.S. Musil, D.A. Goodenough, Multisubunit assembly of an integral plasma membrane channel protein, gap junction connexin43, occurs after exit from the ER, *Cell* 74(6) (1993) 1065-77.

- [145] M.M. Falk, L.K. Buehler, N.M. Kumar, N.B. Gilula, Cell-free synthesis and assembly of connexins into functional gap junction membrane channels, *EMBO J* 16(10) (1997) 2703-16.
- [146] M.M. Falk, N.M. Kumar, N.B. Gilula, Membrane insertion of gap junction connexins: polytopic channel forming membrane proteins, *J Cell Biol* 127(2) (1994) 343-55.
- [147] J. Das Sarma, F. Wang, M. Koval, Targeted gap junction protein constructs reveal connexin-specific differences in oligomerization, *The Journal of biological chemistry* 277(23) (2002) 20911-8.
- [148] D.W. Laird, M. Castillo, L. Kasprzak, Gap junction turnover, intracellular trafficking, and phosphorylation of connexin43 in brefeldin A-treated rat mammary tumor cells, *J Cell Biol* 131(5) (1995) 1193-203.
- [149] A.F. Thevenin, T.J. Kowal, J.T. Fong, R.M. Kells, C.G. Fisher, M.M. Falk, Proteins and mechanisms regulating gap-junction assembly, internalization, and degradation, *Physiology (Bethesda)* 28(2) (2013) 93-116.
- [150] A. Akhmanova, M.O. Steinmetz, Microtubule +TIPs at a glance, *J Cell Sci* 123(Pt 20) (2010) 3415-9.
- [151] M.A. Welte, Bidirectional transport along microtubules, *Curr Biol* 14(13) (2004) R525-37.
- [152] S.S. Zhang, R.M. Shaw, Trafficking highways to the intercalated disc: new insights unlocking the specificity of connexin 43 localization, *Cell communication & adhesion* 21(1) (2014) 43-54.
- [153] P.L. Sorgen, A.J. Trease, G. Spagnol, M. Delmar, M.S. Nielsen, Protein(-)Protein Interactions with Connexin 43: Regulation and Function, *Int J Mol Sci* 19(5) (2018).
- [154] U. Lauf, B.N. Giepmans, P. Lopez, S. Braconnot, S.C. Chen, M.M. Falk, Dynamic trafficking and delivery of connexons to the plasma membrane and accretion to gap junctions in living cells, *Proc Natl Acad Sci U S A* 99(16) (2002) 10446-51.
- [155] A.R. Dukic, P. Gerbaud, J. Guibourdenche, B. Thiede, K. Tasken, G. Pidoux, Ezrin-anchored PKA phosphorylates serine 369 and 373 on connexin 43 to enhance gap junction assembly, communication, and cell fusion, *Biochem J* (2017).
- [156] A.R. Dukic, L.H. Haugen, G. Pidoux, E. Leithe, O. Bakke, K. Tasken, A protein kinase A-ezrin complex regulates connexin 43 gap junction communication in liver epithelial cells, *Cell Signal* 32 (2017) 1-11.
- [157] D.C. Spray, A.P. Moreno, J.A. Kessler, R. Dermietzel, Characterization of gap junctions between cultured leptomeningeal cells, *Brain Res* 568(1-2) (1991) 1-14.
- [158] C.A. Dunn, P.D. Lampe, Injury-triggered Akt phosphorylation of Cx43: a ZO-1-driven molecular switch that regulates gap junction size, *J Cell Sci* 127(Pt 2) (2014) 455-64.
- [159] C.A. Dunn, V. Su, A.F. Lau, P.D. Lampe, Activation of Akt, not connexin 43 protein ubiquitination, regulates gap junction stability, *The Journal of biological chemistry* 287(4) (2012) 2600-7.
- [160] G. Pidoux, P. Gerbaud, J. Dompierre, B. Lygren, T. Solstad, D. Evain-Brion, K. Tasken, A PKA-ezrin-Cx43 signaling complex controls gap junction communication and thereby trophoblast cell fusion, *J Cell Sci* 127(Pt 19) (2014) 4172-85.
- [161] N. Batra, M.A. Riquelme, S. Burra, J.X. Jiang, 14-3-3 θ facilitates plasma membrane delivery and function of mechanosensitive connexin 43 hemichannels, *J Cell Sci* 127(Pt 1) (2014) 137-46.
- [162] N. Batra, M.A. Riquelme, S. Burra, R. Kar, S. Gu, J.X. Jiang, Direct regulation of osteocytic connexin 43 hemichannels through AKT kinase activated by mechanical stimulation, *The Journal of biological chemistry* 289(15) (2014) 10582-91.
- [163] D.J. Park, T.A. Freitas, C.J. Wallick, C.V. Guyette, B.J. Warn-Cramer, Molecular dynamics and in vitro analysis of Connexin43: A new 14-3-3 mode-1 interacting protein, *Protein Sci* 15(10) (2006) 2344-55.
- [164] D.J. Park, C.J. Wallick, K.D. Martyn, A.F. Lau, C. Jin, B.J. Warn-Cramer, Akt phosphorylates Connexin43 on Ser373, a "mode-1" binding site for 14-3-3, *Cell communication & adhesion* 14(5) (2007) 211-26.
- [165] M.M. Falk, Connexin-specific distribution within gap junctions revealed in living cells, *J Cell Sci* 113 (Pt 22) (2000) 4109-20.
- [166] A.W. Hunter, R.J. Barker, C. Zhu, R.G. Gourdie, Zonula occludens-1 alters connexin43 gap junction size and organization by influencing channel accretion, *Mol Biol Cell* 16(12) (2005) 5686-98.

- [167] R.M. Shaw, A.J. Fay, M.A. Puthenveedu, M. von Zastrow, Y.N. Jan, L.Y. Jan, Microtubule plus-end-tracking proteins target gap junctions directly from the cell interior to adherens junctions, *Cell* 128(3) (2007) 547-60.
- [168] G. Richard, F. Rouan, C.E. Willoughby, N. Brown, P. Chung, M. Ryyanen, E.W. Jabs, S.J. Bale, J.J. DiGiovanna, J. Uitto, L. Russell, Missense mutations in GJB2 encoding connexin-26 cause the ectodermal dysplasia keratitis-ichthyosis-deafness syndrome, *Am J Hum Genet* 70(5) (2002) 1341-8.
- [169] D.B. Zimmer, C.R. Green, W.H. Evans, N.B. Gilula, Topological analysis of the major protein in isolated intact rat liver gap junctions and gap junction-derived single membrane structures, *The Journal of biological chemistry* 262(16) (1987) 7751-63.
- [170] C.J. Wei, R. Francis, X. Xu, C.W. Lo, Connexin43 associated with an N-cadherin-containing multiprotein complex is required for gap junction formation in NIH3T3 cells, *The Journal of biological chemistry* 280(20) (2005) 19925-36.
- [171] Y. Wang, B. Rose, An inhibition of gap-junctional communication by cadherins, *J Cell Sci* 110 (Pt 3) (1997) 301-9.
- [172] R. Govindarajan, S. Chakraborty, K.E. Johnson, M.M. Falk, M.J. Wheelock, K.R. Johnson, P.P. Mehta, Assembly of connexin43 into gap junctions is regulated differentially by E-cadherin and N-cadherin in rat liver epithelial cells, *Mol Biol Cell* 21(23) (2010) 4089-107.
- [173] K. Fujimoto, A. Nagafuchi, S. Tsukita, A. Kuraoka, A. Ohokuma, Y. Shibata, Dynamics of connexins, E-cadherin and alpha-catenin on cell membranes during gap junction formation, *J Cell Sci* 110 (Pt 3) (1997) 311-22.
- [174] J.C. Wu, R.Y. Tsai, T.H. Chung, Role of catenins in the development of gap junctions in rat cardiomyocytes, *J Cell Biochem* 88(4) (2003) 823-35.
- [175] G. Spagnol, A.J. Trease, L. Zheng, M. Gutierrez, I. Basu, C. Sarmiento, G. Moore, M. Cervantes, P.L. Sorgen, Connexin43 Carboxyl-Terminal Domain Directly Interacts with beta-Catenin, *Int J Mol Sci* 19(6) (2018).
- [176] A. Salameh, Life cycle of connexins: regulation of connexin synthesis and degradation, *Adv Cardiol* 42 (2006) 57-70.
- [177] D.W. Laird, Life cycle of connexins in health and disease, *Biochem J* 394(Pt 3) (2006) 527-43.
- [178] M.G. Hopperstad, M. Srinivas, D.C. Spray, Properties of gap junction channels formed by Cx46 alone and in combination with Cx50, *Biophys J* 79(4) (2000) 1954-66.
- [179] J. Sun, S. Ahmad, S. Chen, W. Tang, Y. Zhang, P. Chen, X. Lin, Cochlear gap junctions coassembled from Cx26 and 30 show faster intercellular Ca²⁺ signaling than homomeric counterparts, *Am J Physiol Cell Physiol* 288(3) (2005) C613-23.
- [180] R.F. Fallon, D.A. Goodenough, Five-hour half-life of mouse liver gap-junction protein, *J Cell Biol* 90(2) (1981) 521-6.
- [181] O. Traub, J. Look, D. Paul, K. Willecke, Cyclic adenosine monophosphate stimulates biosynthesis and phosphorylation of the 26 kDa gap junction protein in cultured mouse hepatocytes, *Eur J Cell Biol* 43(1) (1987) 48-54.
- [182] O. Traub, J. Look, R. Dermietzel, F. Brummer, D. Hulser, K. Willecke, Comparative characterization of the 21-kD and 26-kD gap junction proteins in murine liver and cultured hepatocytes, *J Cell Biol* 108(3) (1989) 1039-51.
- [183] L.S. Musil, B.A. Cunningham, G.M. Edelman, D.A. Goodenough, Differential phosphorylation of the gap junction protein connexin43 in junctional communication-competent and -deficient cell lines, *J Cell Biol* 111(5 Pt 1) (1990) 2077-88.
- [184] D.W. Laird, K.L. Puranam, J.P. Revel, Turnover and phosphorylation dynamics of connexin43 gap junction protein in cultured cardiac myocytes, *Biochem J* 273(Pt 1) (1991) 67-72.
- [185] P.D. Lampe, Analyzing phorbol ester effects on gap junctional communication: a dramatic inhibition of assembly, *J Cell Biol* 127(6 Pt 2) (1994) 1895-905.
- [186] B.J. Darrow, J.G. Laing, P.D. Lampe, J.E. Saffitz, E.C. Beyer, Expression of multiple connexins in cultured neonatal rat ventricular myocytes, *Circ Res* 76(3) (1995) 381-7.
- [187] D.M. Larson, M.J. Wroblewski, G.D. Sagar, E.M. Westphale, E.C. Beyer, Differential regulation of connexin43 and connexin37 in endothelial cells by cell density, growth, and TGF-beta1, *Am J Physiol* 272(2 Pt 1) (1997) C405-15.

- [188] M.A. Beardslee, J.G. Laing, E.C. Beyer, J.E. Saffitz, Rapid turnover of connexin43 in the adult rat heart, *Circ Res* 83(6) (1998) 629-35.
- [189] B. Hertlein, A. Butterweck, S. Haubrich, K. Willecke, O. Traub, Phosphorylated carboxy terminal serine residues stabilize the mouse gap junction protein connexin45 against degradation, *The Journal of membrane biology* 162(3) (1998) 247-57.
- [190] J.G. Laing, P.N. Tadros, K. Green, J.E. Saffitz, E.C. Beyer, Proteolysis of connexin43-containing gap junctions in normal and heat-stressed cardiac myocytes, *Cardiovasc Res* 38(3) (1998) 711-8.
- [191] V.M. Berthoud, S. Bassnett, E.C. Beyer, Cultured chicken embryo lens cells resemble differentiating fiber cells in vivo and contain two kinetic pools of connexin56, *Exp Eye Res* 68(4) (1999) 475-84.
- [192] E.L. Hertzberg, J.C. Saez, R.A. Corpina, C. Roy, J.A. Kessler, Use of antibodies in the analysis of connexin 43 turnover and phosphorylation, *Methods* 20(2) (2000) 129-39.
- [193] D.M. Larson, K.H. Seul, V.M. Berthoud, A.F. Lau, G.D. Sagar, E.C. Beyer, Functional expression and biochemical characterization of an epitope-tagged connexin37, *Mol Cell Biol Res Commun* 3(2) (2000) 115-21.
- [194] J.K. VanSlyke, S.M. Deschenes, L.S. Musil, Intracellular transport, assembly, and degradation of wild-type and disease-linked mutant gap junction proteins, *Mol Biol Cell* 11(6) (2000) 1933-46.
- [195] R. Windoffer, B. Beile, A. Leibold, S. Thomas, U. Wilhelm, R.E. Leube, Visualization of gap junction mobility in living cells, *Cell Tissue Res* 299(3) (2000) 347-62.
- [196] M.A. Thomas, N. Zosso, I. Scerri, N. Demaurex, M. Chanson, O. Staub, A tyrosine-based sorting signal is involved in connexin43 stability and gap junction turnover, *J Cell Sci* 116(Pt 11) (2003) 2213-22.
- [197] D.T. Yamaguchi, D. Ma, Mechanism of pH regulation of connexin 43 expression in MC3T3-E1 cells, *Biochem Biophys Res Commun* 304(4) (2003) 736-9.
- [198] K. Jordan, R. Chodock, A.R. Hand, D.W. Laird, The origin of annular junctions: a mechanism of gap junction internalization, *J Cell Sci* 114(Pt 4) (2001) 763-73.
- [199] W.L. Di, E.L. Rugg, I.M. Leigh, D.P. Kelsell, Multiple epidermal connexins are expressed in different keratinocyte subpopulations including connexin 31, *J Invest Dermatol* 117(4) (2001) 958-64.
- [200] G. Richard, Connexins: a connection with the skin, *Exp Dermatol* 9(2) (2000) 77-96.
- [201] G. Gaietta, T.J. Deerinck, S.R. Adams, J. Bouwer, O. Tour, D.W. Laird, G.E. Sosinsky, R.Y. Tsien, M.H. Ellisman, Multicolor and electron microscopic imaging of connexin trafficking, *Science* 296(5567) (2002) 503-7.
- [202] L.S. Musil, A.C. Le, J.K. VanSlyke, L.M. Roberts, Regulation of connexin degradation as a mechanism to increase gap junction assembly and function, *The Journal of biological chemistry* 275(33) (2000) 25207-15.
- [203] K. Leykauf, M. Salek, J. Bomke, M. Frech, W.D. Lehmann, M. Durst, A. Alonso, Ubiquitin protein ligase Nedd4 binds to connexin43 by a phosphorylation-modulated process, *J Cell Sci* 119(Pt 17) (2006) 3634-42.
- [204] G. Spagnol, F. Kieken, J.L. Kopanic, H. Li, S. Zach, K.L. Stauch, R. Grosely, P.L. Sorgen, Structural Studies of the Nedd4 WW Domains and their Selectivity for the Cx43 Carboxyl-terminus, *The Journal of biological chemistry* (2016).
- [205] M.M. Falk, R.M. Kells, V.M. Berthoud, Degradation of connexins and gap junctions, *FEBS Lett* 588(8) (2014) 1221-9.
- [206] R.M. Kells-Andrews, R.A. Margraf, C.G. Fisher, M.M. Falk, Connexin-43 K63-polyubiquitylation on lysines 264 and 303 regulates gap junction internalization, *J Cell Sci* 131(15) (2018).
- [207] D. Gonzalez, J.M. Gomez-Hernandez, L.C. Barrio, Molecular basis of voltage dependence of connexin channels: an integrative appraisal, *Prog Biophys Mol Biol* 94(1-2) (2007) 66-106.
- [208] V.K. Verselis, C.S. Ginter, T.A. Bargiello, Opposite voltage gating polarities of two closely related connexins, *Nature* 368(6469) (1994) 348-51.
- [209] S. Oh, J.B. Rubin, M.V. Bennett, V.K. Verselis, T.A. Bargiello, Molecular determinants of electrical rectification of single channel conductance in gap junctions formed by connexins 26 and 32, *The Journal of general physiology* 114(3) (1999) 339-64.

- [210] P.E. Purnick, S. Oh, C.K. Abrams, V.K. Verselis, T.A. Bargiello, Reversal of the gating polarity of gap junctions by negative charge substitutions in the N-terminus of connexin 32, *Biophys J* 79(5) (2000) 2403-15.
- [211] P. Brink, Gap junction voltage dependence. A clear picture emerges, *The Journal of general physiology* 116(1) (2000) 11-2.
- [212] F.F. Bukauskas, V.K. Verselis, Gap junction channel gating, *Biochimica et biophysica acta* 1662(1-2) (2004) 42-60.
- [213] A. Revilla, C. Castro, L.C. Barrio, Molecular dissection of transjunctional voltage dependence in the connexin-32 and connexin-43 junctions, *Biophys J* 77(3) (1999) 1374-83.
- [214] L.C. Barrio, J. Capel, J.A. Jarillo, C. Castro, A. Revilla, Species-specific voltage-gating properties of connexin-45 junctions expressed in *Xenopus* oocytes, *Biophys J* 73(2) (1997) 757-69.
- [215] D. Manthey, F. Bukauskas, C.G. Lee, C.A. Kozak, K. Willecke, Molecular cloning and functional expression of the mouse gap junction gene connexin-57 in human HeLa cells, *The Journal of biological chemistry* 274(21) (1999) 14716-23.
- [216] A. Revilla, M.V. Bennett, L.C. Barrio, Molecular determinants of membrane potential dependence in vertebrate gap junction channels, *Proc Natl Acad Sci U S A* 97(26) (2000) 14760-5.
- [217] F.F. Bukauskas, A. Bukauskiene, M.V. Bennett, V.K. Verselis, Gating properties of gap junction channels assembled from connexin43 and connexin43 fused with green fluorescent protein, *Biophys J* 81(1) (2001) 137-52.
- [218] C.G. Bevans, A.L. Harris, Regulation of connexin channels by pH. Direct action of the protonated form of taurine and other aminosulfonates, *The Journal of biological chemistry* 274(6) (1999) 3711-9.
- [219] R. Eckert, pH gating of lens fibre connexins, *Pflugers Arch* 443(5-6) (2002) 843-51.
- [220] B. Liu, L.C. Wang, D.D. Belke, Effects of temperature and pH on cardiac myofilament Ca²⁺ sensitivity in rat and ground squirrel, *Am J Physiol* 264(1 Pt 2) (1993) R104-8.
- [221] R. Werner, E. Levine, C. Rabadan-Diehl, G. Dahl, Gating properties of connexin32 cell-cell channels and their mutants expressed in *Xenopus* oocytes, *Proc Biol Sci* 243(1306) (1991) 5-11.
- [222] D.C. Spray, R. Hanstein, S.V. Lopez-Quintero, R.F. Stout, Jr., S.O. Suadicani, M.M. Thi, Gap junctions and Bystander Effects: Good Samaritans and executioners, *Wiley Interdiscip Rev Membr Transp Signal* 2(1) (2013) 1-15.
- [223] G.E. Morley, S.M. Taffet, M. Delmar, Intramolecular interactions mediate pH regulation of connexin43 channels, *Biophys J* 70(3) (1996) 1294-302.
- [224] M. Delmar, W. Coombs, P. Sorgen, H.S. Duffy, S.M. Taffet, Structural bases for the chemical regulation of Connexin43 channels, *Cardiovasc Res* 62(2) (2004) 268-75.
- [225] J.F. Ek-Vitorin, G. Calero, G.E. Morley, W. Coombs, S.M. Taffet, M. Delmar, PH regulation of connexin43: molecular analysis of the gating particle, *Biophys J* 71(3) (1996) 1273-84.
- [226] J.F. Ek, M. Delmar, R. Perzova, S.M. Taffet, Role of histidine 95 on pH gating of the cardiac gap junction protein connexin43, *Circ Res* 74(6) (1994) 1058-64.
- [227] C. Peracchia, X.C. Wang, Connexin domains relevant to the chemical gating of gap junction channels, *Braz J Med Biol Res* 30(5) (1997) 577-90.
- [228] X.G. Wang, C. Peracchia, Connexin 32/38 chimeras suggest a role for the second half of inner loop in gap junction gating by low pH, *Am J Physiol* 271(5 Pt 1) (1996) C1743-9.
- [229] K. Stergiopoulos, J.L. Alvarado, M. Mastroianni, J.F. Ek-Vitorin, S.M. Taffet, M. Delmar, Hetero-domain interactions as a mechanism for the regulation of connexin channels, *Circ Res* 84(10) (1999) 1144-55.
- [230] N. Palacios-Prado, S.W. Briggs, V.A. Skeberdis, M. Pranevicius, M.V. Bennett, F.F. Bukauskas, pH-dependent modulation of voltage gating in connexin45 homotypic and connexin45/connexin43 heterotypic gap junctions, *Proc Natl Acad Sci U S A* 107(21) (2010) 9897-902.
- [231] D. Bouvier, G. Spagnol, S. Chenavas, F. Kieken, H. Vitrac, S. Brownell, A. Kellezi, V. Forge, P.L. Sorgen, Characterization of the structure and intermolecular interactions between the connexin40 and connexin43 carboxyl-terminal and cytoplasmic loop domains, *The Journal of biological chemistry* 284(49) (2009) 34257-71.

- [232] H. Ripps, H. Qian, J. Zakevicius, Pharmacological enhancement of hemi-gap-junctional currents in *Xenopus* oocytes, *J Neurosci Methods* 121(1) (2002) 81-92.
- [233] V. Valiunas, Biophysical properties of connexin-45 gap junction hemichannels studied in vertebrate cells, *The Journal of general physiology* 119(2) (2002) 147-64.
- [234] E.B. Trexler, F.F. Bukauskas, M.V. Bennett, T.A. Bargiello, V.K. Verselis, Rapid and direct effects of pH on connexins revealed by the connexin46 hemichannel preparation, *The Journal of general physiology* 113(5) (1999) 721-42.
- [235] S. Liu, S. Taffet, L. Stoner, M. Delmar, M.L. Vallano, J. Jalife, A structural basis for the unequal sensitivity of the major cardiac and liver gap junctions to intracellular acidification: the carboxyl tail length, *Biophys J* 64(5) (1993) 1422-33.
- [236] C.J. Fearnley, H.L. Roderick, M.D. Bootman, Calcium signaling in cardiac myocytes, *Cold Spring Harb Perspect Biol* 3(11) (2011) a004242.
- [237] W. Lopez, J. Ramachandran, A. Alsamarah, Y. Luo, A.L. Harris, J.E. Contreras, Mechanism of gating by calcium in connexin hemichannels, *Proc Natl Acad Sci U S A* 113(49) (2016) E7986-E7995.
- [238] Q. Xu, R.F. Kopp, Y. Chen, J.J. Yang, M.W. Roe, R.D. Veenstra, Gating of connexin 43 gap junctions by a cytoplasmic loop calmodulin binding domain, *Am J Physiol Cell Physiol* 302(10) (2012) C1548-56.
- [239] C. Peracchia, A. Sotkis, X.G. Wang, L.L. Peracchia, A. Persechini, Calmodulin directly gates gap junction channels, *The Journal of biological chemistry* 275(34) (2000) 26220-4.
- [240] C. Peracchia, X.G. Wang, L.L. Peracchia, Slow gating of gap junction channels and calmodulin, *The Journal of membrane biology* 178(1) (2000) 55-70.
- [241] G.S. Burr, C.K. Mitchell, Y.J. Keflemariam, R. Heidelberger, J. O'Brien, Calcium-dependent binding of calmodulin to neuronal gap junction proteins, *Biochem Biophys Res Commun* 335(4) (2005) 1191-8.
- [242] M.M. Lurtz, C.F. Louis, Intracellular calcium regulation of connexin43, *Am J Physiol Cell Physiol* 293(6) (2007) C1806-13.
- [243] Y. Zhou, W. Yang, M.M. Lurtz, Y. Chen, J. Jiang, Y. Huang, C.F. Louis, J.J. Yang, Calmodulin mediates the Ca²⁺-dependent regulation of Cx44 gap junctions, *Biophys J* 96(7) (2009) 2832-48.
- [244] C. Peracchia, K.C. Young, X.G. Wang, L.L. Peracchia, Is the voltage gate of connexins CO₂-sensitive? Cx45 channels and inhibition of calmodulin expression, *The Journal of membrane biology* 195(1) (2003) 53-62.
- [245] Y. Chen, Y. Zhou, X. Lin, H.C. Wong, Q. Xu, J. Jiang, S. Wang, M.M. Lurtz, C.F. Louis, R.D. Veenstra, J.J. Yang, Molecular interaction and functional regulation of connexin50 gap junctions by calmodulin, *Biochem J* 435(3) (2011) 711-22.
- [246] Y. Zhou, W. Yang, M.M. Lurtz, Y. Ye, Y. Huang, H.W. Lee, Y. Chen, C.F. Louis, J.J. Yang, Identification of the calmodulin binding domain of connexin 43, *The Journal of biological chemistry* 282(48) (2007) 35005-17.
- [247] J.L. Kopanic, M.H. Al-mugotir, F. Kieken, S. Zach, A.J. Trease, P.L. Sorgen, Characterization of the connexin45 carboxyl-terminal domain structure and interactions with molecular partners, *Biophys J* 106(10) (2014) 2184-95.
- [248] K. Stauch, F. Kieken, P. Sorgen, Characterization of the structure and intermolecular interactions between the connexin 32 carboxyl-terminal domain and the protein partners synapse-associated protein 97 and calmodulin, *The Journal of biological chemistry* 287(33) (2012) 27771-88.
- [249] R. Dodd, C. Peracchia, D. Stolady, K. Torok, Calmodulin association with connexin32-derived peptides suggests trans-domain interaction in chemical gating of gap junction channels, *The Journal of biological chemistry* 283(40) (2008) 26911-20.
- [250] K. Torok, K. Stauffer, W.H. Evans, Connexin 32 of gap junctions contains two cytoplasmic calmodulin-binding domains, *Biochem J* 326 (Pt 2) (1997) 479-83.
- [251] J. Zou, M. Salarian, Y. Chen, Y. Zhuo, N.E. Brown, J.R. Hepler, J.J. Yang, Direct visualization of interaction between calmodulin and connexin45, *Biochem J* 474(24) (2017) 4035-4051.
- [252] J.S. Wolenski, Regulation of calmodulin-binding myosins, *Trends Cell Biol* 5(8) (1995) 310-6.

- [253] S.S. Taylor, M.M. Keshwani, J.M. Steichen, A.P. Kornev, Evolution of the eukaryotic protein kinases as dynamic molecular switches, *Philos Trans R Soc Lond B Biol Sci* 367(1602) (2012) 2517-28.
- [254] S.S. Taylor, A.P. Kornev, Protein kinases: evolution of dynamic regulatory proteins, *Trends Biochem Sci* 36(2) (2011) 65-77.
- [255] P.E. Wright, H.J. Dyson, Intrinsically disordered proteins in cellular signalling and regulation, *Nat Rev Mol Cell Biol* 16(1) (2015) 18-29.
- [256] J. Burgi, B. Xue, V.N. Uversky, F.G. van der Goot, Intrinsic Disorder in Transmembrane Proteins: Roles in Signaling and Topology Prediction, *PLoS One* 11(7) (2016) e0158594.
- [257] G. Mese, G. Richard, T.W. White, Gap junctions: basic structure and function, *J Invest Dermatol* 127(11) (2007) 2516-24.
- [258] E.C. Beyer, G.M. Lipkind, J.W. Kyle, V.M. Berthoud, Structural organization of intercellular channels II. Amino terminal domain of the connexins: sequence, functional roles, and structure, *Biochimica et biophysica acta* 1818(8) (2012) 1823-30.
- [259] J.W. Kyle, P.J. Minogue, B.C. Thomas, D.A. Domowicz, V.M. Berthoud, D.A. Hanck, E.C. Beyer, An intact connexin N-terminus is required for function but not gap junction formation, *J Cell Sci* 121(Pt 16) (2008) 2744-50.
- [260] B.D. Kalmatsky, S. Bhagan, Q. Tang, T.A. Bargiello, T.L. Dowd, Structural studies of the N-terminus of Connexin 32 using ¹H NMR spectroscopy, *Arch Biochem Biophys* 490(1) (2009) 9-16.
- [261] M.P. Piechocki, R.M. Toti, M.J. Fernstrom, R.D. Burk, R.J. Ruch, Liver cell-specific transcriptional regulation of connexin32, *Biochimica et biophysica acta* 1491(1-3) (2000) 107-22.
- [262] S. Maeda, S. Nakagawa, M. Suga, E. Yamashita, A. Oshima, Y. Fujiyoshi, T. Tsukihara, Structure of the connexin 26 gap junction channel at 3.5 Å resolution, *Nature* 458(7238) (2009) 597-602.
- [263] B.C. Thomas, P.J. Minogue, V. Valiunas, G. Kanaporis, P.R. Brink, V.M. Berthoud, E.C. Beyer, Cataracts are caused by alterations of a critical N-terminal positive charge in connexin50, *Invest Ophthalmol Vis Sci* 49(6) (2008) 2549-56.
- [264] J.E. Common, D. Becker, W.L. Di, I.M. Leigh, E.A. O'Toole, D.P. Kelsell, Functional studies of human skin disease- and deafness-associated connexin 30 mutations, *Biochem Biophys Res Commun* 298(5) (2002) 651-6.
- [265] G. Richard, L.E. Smith, R.A. Bailey, P. Itin, D. Hohl, E.H. Epstein, Jr., J.J. DiGiovanna, J.G. Compton, S.J. Bale, Mutations in the human connexin gene GJB3 cause erythrokeratoderma variabilis, *Nat Genet* 20(4) (1998) 366-9.
- [266] S.M. Deschenes, J.L. Walcott, T.L. Wexler, S.S. Scherer, K.H. Fischbeck, Altered trafficking of mutant connexin32, *J Neurosci* 17(23) (1997) 9077-84.
- [267] J. Shibayama, W. Paznekas, A. Seki, S. Taffet, E.W. Jabs, M. Delmar, H. Musa, Functional characterization of connexin43 mutations found in patients with oculodentodigital dysplasia, *Circ Res* 96(10) (2005) e83-91.
- [268] C.K. Abrams, M.M. Freidin, V.K. Verselis, M.V. Bennett, T.A. Bargiello, Functional alterations in gap junction channels formed by mutant forms of connexin 32: evidence for loss of function as a pathogenic mechanism in the X-linked form of Charcot-Marie-Tooth disease, *Brain Res* 900(1) (2001) 9-25.
- [269] W. Roscoe, G.I. Veitch, X.Q. Gong, E. Pellegrino, D. Bai, E. McLachlan, Q. Shao, G.M. Kidder, D.W. Laird, Oculodentodigital dysplasia-causing connexin43 mutants are non-functional and exhibit dominant effects on wild-type connexin43, *The Journal of biological chemistry* 280(12) (2005) 11458-66.
- [270] X.Q. Gong, Q. Shao, S. Langlois, D. Bai, D.W. Laird, Differential potency of dominant negative connexin43 mutants in oculodentodigital dysplasia, *The Journal of biological chemistry* 282(26) (2007) 19190-202.
- [271] T. Lazic, K.A. Horii, G. Richard, D.I. Wasserman, R.J. Antaya, A report of GJB2 (N14K) Connexin 26 mutation in two patients--a new subtype of KID syndrome?, *Pediatr Dermatol* 25(5) (2008) 535-40.
- [272] A. Terrinoni, A. Codispoti, V. Serra, E. Bruno, B. Didona, M. Paradisi, S. Nistico, E. Campione, B. Napolitano, L. Diluvio, G. Melino, Connexin 26 (GJB2) mutations as a cause of the KID syndrome with hearing loss, *Biochem Biophys Res Commun* 395(1) (2010) 25-30.

- [273] A. Terrinoni, A. Codispoti, V. Serra, B. Didona, E. Bruno, R. Nistico, M. Giustizieri, M. Alessandrini, E. Campione, G. Melino, Connexin 26 (GJB2) mutations, causing KID Syndrome, are associated with cell death due to calcium gating deregulation, *Biochem Biophys Res Commun* 394(4) (2010) 909-14.
- [274] D. Locke, I.V. Koreen, A.L. Harris, Isoelectric points and post-translational modifications of connexin26 and connexin32, *FASEB journal : official publication of the Federation of American Societies for Experimental Biology* 20(8) (2006) 1221-3.
- [275] Z. Wang, K.L. Schey, Phosphorylation and truncation sites of bovine lens connexin 46 and connexin 50, *Exp Eye Res* 89(6) (2009) 898-904.
- [276] V.M. Unger, N.M. Kumar, N.B. Gilula, M. Yeager, Three-dimensional structure of a recombinant gap junction membrane channel, *Science* 283(5405) (1999) 1176-80.
- [277] H.S. Duffy, P.L. Sorgen, M.E. Girvin, P. O'Donnell, W. Coombs, S.M. Taffet, M. Delmar, D.C. Spray, pH-dependent intramolecular binding and structure involving Cx43 cytoplasmic domains, *The Journal of biological chemistry* 277(39) (2002) 36706-14.
- [278] A.G. Fort, D.C. Spray, Trifluoroethanol reveals helical propensity at analogous positions in cytoplasmic domains of three connexins, *Biopolymers* 92(3) (2009) 173-82.
- [279] M. Oyamada, Y. Oyamada, T. Kaneko, T. Takamatsu, Regulation of gap junction protein (connexin) genes and function in differentiating ES cells, *Methods Mol Biol* 185 (2002) 63-9.
- [280] A. Seki, W. Coombs, S.M. Taffet, M. Delmar, Loss of electrical communication, but not plaque formation, after mutations in the cytoplasmic loop of connexin43, *Heart Rhythm* 1(2) (2004) 227-33.
- [281] P.E. Martin, E.T. Mambetisaeva, D.A. Archer, C.H. George, W.H. Evans, Analysis of gap junction assembly using mutated connexins detected in Charcot-Marie-Tooth X-linked disease, *J Neurochem* 74(2) (2000) 711-20.
- [282] J. Zou, M. Salarian, Y. Chen, R. Veenstra, C.F. Louis, J.J. Yang, Gap junction regulation by calmodulin, *FEBS Lett* 588(8) (2014) 1430-8.
- [283] V.M. Berthoud, E.C. Beyer, W.E. Kurata, A.F. Lau, P.D. Lampe, The gap-junction protein connexin 56 is phosphorylated in the intracellular loop and the carboxy-terminal region, *Eur J Biochem* 244(1) (1997) 89-97.
- [284] G. Spagnol, M. Al-Mugotir, J.L. Kopanic, S. Zach, H. Li, A.J. Trease, K.L. Stauch, R. Grosely, M. Cervantes, P.L. Sorgen, Secondary structural analysis of the carboxyl-terminal domain from different connexin isoforms, *Biopolymers* 105(3) (2016) 143-62.
- [285] D. Bouvier, F. Kieken, A. Kellezi, P.L. Sorgen, Structural changes in the carboxyl terminus of the gap junction protein connexin 40 caused by the interaction with c-Src and zonula occludens-1, *Cell communication & adhesion* 15(1) (2008) 107-18.
- [286] P.L. Sorgen, H.S. Duffy, P. Sahoo, W. Coombs, M. Delmar, D.C. Spray, Structural changes in the carboxyl terminus of the gap junction protein connexin43 indicates signaling between binding domains for c-Src and zonula occludens-1, *The Journal of biological chemistry* 279(52) (2004) 54695-701.
- [287] R. Grosely, F. Kieken, P.L. Sorgen, (1)H, (1)(3)C, and (1)(5)N backbone resonance assignments of the connexin43 carboxyl terminal domain attached to the 4th transmembrane domain in detergent micelles, *Biomol NMR Assign* 7(2) (2013) 299-303.
- [288] K. Pogoda, P. Kameritsch, M.A. Retamal, J.L. Vega, Regulation of gap junction channels and hemichannels by phosphorylation and redox changes: a revision, *BMC Cell Biol* 17 Suppl 1 (2016) 11.
- [289] D. Locke, S. Bian, H. Li, A.L. Harris, Post-translational modifications of connexin26 revealed by mass spectrometry, *Biochem J* 424(3) (2009) 385-98.
- [290] S. Urschel, T. Hoher, T. Schubert, C. Alev, G. Sohl, P. Worsdorfer, T. Asahara, R. Dermietzel, R. Weiler, K. Willecke, Protein kinase A-mediated phosphorylation of connexin36 in mouse retina results in decreased gap junctional communication between All amacrine cells, *The Journal of biological chemistry* 281(44) (2006) 33163-71.
- [291] P.D. Lampe, A.F. Lau, Regulation of gap junctions by phosphorylation of connexins, *Arch Biochem Biophys* 384(2) (2000) 205-15.
- [292] J.L. Solan, P.D. Lampe, Key connexin 43 phosphorylation events regulate the gap junction life cycle, *The Journal of membrane biology* 217(1-3) (2007) 35-41.

- [293] W.R. Lowenstein, Regulation of cell-to-cell communication by phosphorylation, *Biochem Soc Symp* 50 (1985) 43-58.
- [294] J.C. Saez, D.C. Spray, A.C. Nairn, E. Hertzberg, P. Greengard, M.V. Bennett, cAMP increases junctional conductance and stimulates phosphorylation of the 27-kDa principal gap junction polypeptide, *Proc Natl Acad Sci U S A* 83(8) (1986) 2473-7.
- [295] L. Zheng, H. Li, A. Cannon, A.J. Trease, G. Spagnol, H. Zheng, S. Radio, K. Patel, S. Batra, P.L. Sorgen, Phosphorylation of Cx43 residue Y313 by Src contributes to blocking the interaction with Drebrin and disassembling gap junctions, *J Mol Cell Cardiol* 126 (2018) 36-49.
- [296] L.W. Loo, J.M. Berestecky, M.Y. Kanemitsu, A.F. Lau, pp60src-mediated phosphorylation of connexin 43, a gap junction protein, *The Journal of biological chemistry* 270(21) (1995) 12751-61.
- [297] W.E. Kurata, A.F. Lau, p130gag-fps disrupts gap junctional communication and induces phosphorylation of connexin43 in a manner similar to that of pp60v-src, *Oncogene* 9(1) (1994) 329-35.
- [298] J.A. Diez, M. Elvira, A. Villalobo, The epidermal growth factor receptor tyrosine kinase phosphorylates connexin32, *Molecular and cellular biochemistry* 187(1-2) (1998) 201-10.
- [299] B.J. Warn-Cramer, W.E. Kurata, A.F. Lau, Biochemical analysis of connexin phosphorylation, *Methods Mol Biol* 154 (2001) 431-46.
- [300] P.D. Lampe, E.M. TenBroek, J.M. Burt, W.E. Kurata, R.G. Johnson, A.F. Lau, Phosphorylation of connexin43 on serine368 by protein kinase C regulates gap junctional communication, *J Cell Biol* 149(7) (2000) 1503-12.
- [301] B.J. Warn-Cramer, P.D. Lampe, W.E. Kurata, M.Y. Kanemitsu, L.W. Loo, W. Eckhart, A.F. Lau, Characterization of the mitogen-activated protein kinase phosphorylation sites on the connexin-43 gap junction protein, *The Journal of biological chemistry* 271(7) (1996) 3779-86.
- [302] J.X. Yan, N.H. Packer, A.A. Gooley, K.L. Williams, Protein phosphorylation: technologies for the identification of phosphoamino acids, *J Chromatogr A* 808(1-2) (1998) 23-41.
- [303] Y. Chen, H.Z. Hu, J.W. Wu, Q.Y. Peng, G. Yang, Z.G. Liao, [Changes of connexin 43 in rabbit with early myocardial ischemia], *Sichuan Da Xue Xue Bao Yi Xue Ban* 35(2) (2004) 191-3.
- [304] H.H. Chen, C.J. Baty, T. Maeda, S. Brooks, L.C. Baker, T. Ueyama, E. Gursoy, S. Saba, G. Salama, B. London, A.F. Stewart, Transcription enhancer factor-1-related factor-transgenic mice develop cardiac conduction defects associated with altered connexin phosphorylation, *Circulation* 110(19) (2004) 2980-7.
- [305] R.M. Pelletier, C.D. Akpovi, L. Chen, N.M. Kumar, M.L. Vitale, Complementary expression and phosphorylation of Cx46 and Cx50 during development and following gene deletion in mouse and in normal and orchitic mink testes, *Am J Physiol Regul Integr Comp Physiol* 309(3) (2015) R255-76.
- [306] T.A. van Veen, H.V. van Rijen, H.J. Jongsma, Electrical conductance of mouse connexin45 gap junction channels is modulated by phosphorylation, *Cardiovasc Res* 46(3) (2000) 496-510.
- [307] J. Liu, J.F. Ek Vitorin, S.T. Weintraub, S. Gu, Q. Shi, J.M. Burt, J.X. Jiang, Phosphorylation of connexin 50 by protein kinase A enhances gap junction and hemichannel function, *The Journal of biological chemistry* 286(19) (2011) 16914-28.
- [308] P.D. Lampe, A.F. Lau, The effects of connexin phosphorylation on gap junctional communication, *Int J Biochem Cell Biol* 36(7) (2004) 1171-86.
- [309] J.L. Solan, P.D. Lampe, Connexin43 phosphorylation: structural changes and biological effects, *Biochem J* 419(2) (2009) 261-72.
- [310] L.S. Musil, D.A. Goodenough, Biochemical analysis of connexin43 intracellular transport, phosphorylation, and assembly into gap junctional plaques, *J Cell Biol* 115(5) (1991) 1357-74.
- [311] C.D. Cooper, P.D. Lampe, Casein kinase 1 regulates connexin-43 gap junction assembly, *The Journal of biological chemistry* 277(47) (2002) 44962-8.
- [312] R. Grosely, J.L. Kopanic, S. Nabors, F. Kieken, G. Spagnol, M. Al-Mugotir, S. Zach, P.L. Sorgen, Effects of phosphorylation on the structure and backbone dynamics of the intrinsically disordered connexin43 C-terminal domain, *The Journal of biological chemistry* 288(34) (2013) 24857-70.
- [313] E. Kinoshita, E. Kinoshita-Kikuta, T. Koike, Separation and detection of large phosphoproteins using Phos-tag SDS-PAGE, *Nat Protoc* 4(10) (2009) 1513-21.

- [314] C.L. Smith, C. Debouck, M. Rosenberg, J.S. Culp, Phosphorylation of serine residue 89 of human adenovirus E1A proteins is responsible for their characteristic electrophoretic mobility shifts, and its mutation affects biological function, *J Virol* 63(4) (1989) 1569-77.
- [315] S.B. Ficarro, M.L. McClelland, P.T. Stukenberg, D.J. Burke, M.M. Ross, J. Shabanowitz, D.F. Hunt, F.M. White, Phosphoproteome analysis by mass spectrometry and its application to *Saccharomyces cerevisiae*, *Nat Biotechnol* 20(3) (2002) 301-5.
- [316] B.A. Garcia, J. Shabanowitz, D.F. Hunt, Analysis of protein phosphorylation by mass spectrometry, *Methods* 35(3) (2005) 256-64.
- [317] A. Pandey, A.V. Podtelejnikov, B. Blagoev, X.R. Bustelo, M. Mann, H.F. Lodish, Analysis of receptor signaling pathways by mass spectrometry: identification of vav-2 as a substrate of the epidermal and platelet-derived growth factor receptors, *Proc Natl Acad Sci U S A* 97(1) (2000) 179-84.
- [318] L. Andersson, J. Porath, Isolation of phosphoproteins by immobilized metal (Fe³⁺) affinity chromatography, *Anal Biochem* 154(1) (1986) 250-4.
- [319] J.A. Bornhorst, J.J. Falke, Purification of proteins using polyhistidine affinity tags, *Methods Enzymol* 326 (2000) 245-54.
- [320] L. Parker, A. Engel-Hall, K. Drew, G. Steinhardt, D.L. Helseth, Jr., D. Jabon, T. McMurphy, D.S. Angulo, S.J. Kron, Investigating quantitation of phosphorylation using MALDI-TOF mass spectrometry, *J Mass Spectrom* 43(4) (2008) 518-27.
- [321] C.D. Cooper, J.L. Solan, M.K. Dolejsi, P.D. Lampe, Analysis of connexin phosphorylation sites, *Methods* 20(2) (2000) 196-204.
- [322] G.Y. Huang, L.J. Xie, K.L. Linask, C. Zhang, X.Q. Zhao, Y. Yang, G.M. Zhou, Y.J. Wu, L. Marquez-Rosado, D.B. McElhinney, E. Goldmuntz, C. Liu, P.D. Lampe, B. Chatterjee, C.W. Lo, Evaluating the role of connexin43 in congenital heart disease: Screening for mutations in patients with outflow tract anomalies and the analysis of knock-in mouse models, *J Cardiovasc Dis Res* 2(4) (2011) 206-12.
- [323] H. Li, G. Spagnol, L. Zheng, K.L. Stauch, P.L. Sorgen, Regulation of Connexin43 function and expression by Tyrosine kinase 2, *The Journal of biological chemistry* (2016).
- [324] P.D. Lampe, C.D. Cooper, T.J. King, J.M. Burt, Analysis of Connexin43 phosphorylated at S325, S328 and S330 in normoxic and ischemic heart, *J Cell Sci* 119(Pt 16) (2006) 3435-42.
- [325] J.L. Solan, P.D. Lampe, Connexin 43 in LA-25 cells with active v-src is phosphorylated on Y247, Y265, S262, S279/282, and S368 via multiple signaling pathways, *Cell communication & adhesion* 15(1) (2008) 75-84.
- [326] L.N. Axelsen, K. Calloe, N.H. Holstein-Rathlou, M.S. Nielsen, Managing the complexity of communication: regulation of gap junctions by post-translational modification, *Frontiers in pharmacology* 4 (2013) 130.
- [327] J.L. Solan, P.D. Lampe, Connexin phosphorylation as a regulatory event linked to gap junction channel assembly, *Biochimica et biophysica acta* 1711(2) (2005) 154-63.
- [328] J.L. Solan, P.D. Lampe, Specific Cx43 phosphorylation events regulate gap junction turnover in vivo, *FEBS Lett* 588(8) (2014) 1423-9.
- [329] J. Li, B. Wilkinson, V.A. Clementel, J. Hou, T.J. O'Dell, M.P. Coba, Long-term potentiation modulates synaptic phosphorylation networks and reshapes the structure of the postsynaptic interactome, *Sci Signal* 9(440) (2016) rs8.
- [330] T. Yi, B. Zhai, Y. Yu, Y. Kiyotsugu, T. Raschle, M. Etzkorn, H.C. Seo, M. Nagiec, R.E. Luna, E.L. Reinherz, J. Blenis, S.P. Gygi, G. Wagner, Quantitative phosphoproteomic analysis reveals system-wide signaling pathways downstream of SDF-1/CXCR4 in breast cancer stem cells, *Proc Natl Acad Sci U S A* 111(21) (2014) E2182-90.
- [331] A. Lundby, M.N. Andersen, A.B. Steffensen, H. Horn, C.D. Kelstrup, C. Francavilla, L.J. Jensen, N. Schmitt, M.B. Thomsen, J.V. Olsen, In vivo phosphoproteomics analysis reveals the cardiac targets of beta-adrenergic receptor signaling, *Sci Signal* 6(278) (2013) rs11.
- [332] J. Schindler, J. Ye, O.N. Jensen, H.G. Nothwang, Monitoring the native phosphorylation state of plasma membrane proteins from a single mouse cerebellum, *J Neurosci Methods* 213(2) (2013) 153-64.
- [333] M. Courcelles, C. Fremin, L. Voisin, S. Lemieux, S. Meloche, P. Thibault, Phosphoproteome dynamics reveal novel ERK1/2 MAP kinase substrates with broad spectrum of functions, *Mol Syst Biol* 9 (2013) 669.

- [334] A. Lundby, A. Secher, K. Lage, N.B. Nordsborg, A. Dmytriiev, C. Lundby, J.V. Olsen, Quantitative maps of protein phosphorylation sites across 14 different rat organs and tissues, *Nat Commun* 3 (2012) 876.
- [335] P.P. Hsu, S.A. Kang, J. Rameseder, Y. Zhang, K.A. Ottina, D. Lim, T.R. Peterson, Y. Choi, N.S. Gray, M.B. Yaffe, J.A. Marto, D.M. Sabatini, The mTOR-regulated phosphoproteome reveals a mechanism of mTORC1-mediated inhibition of growth factor signaling, *Science* 332(6035) (2011) 1317-22.
- [336] M. Klammer, M. Kaminski, A. Zedler, F. Oppermann, S. Blencke, S. Marx, S. Muller, A. Tebbe, K. Godl, C. Schaab, Phosphosignature predicts dasatinib response in non-small cell lung cancer, *Mol Cell Proteomics* 11(9) (2012) 651-68.
- [337] M.M. Shah, A.M. Martinez, W.H. Fletcher, The connexin43 gap junction protein is phosphorylated by protein kinase A and protein kinase C: in vivo and in vitro studies, *Molecular and cellular biochemistry* 238(1-2) (2002) 57-68.
- [338] J.L. Solan, P.D. Lampe, Kinase programs spatiotemporally regulate gap junction assembly and disassembly: Effects on wound repair, *Semin Cell Dev Biol* 50 (2016) 40-8.
- [339] G.T. Cottrell, R. Lin, B.J. Warn-Cramer, A.F. Lau, J.M. Burt, Mechanism of v-Src- and mitogen-activated protein kinase-induced reduction of gap junction communication, *Am J Physiol Cell Physiol* 284(2) (2003) C511-20.
- [340] H. Li, G. Spagnol, N. Naslavsky, S. Caplan, P.L. Sorgen, TC-PTP directly interacts with connexin43 to regulate gap junction intercellular communication, *J Cell Sci* 127(Pt 15) (2014) 3269-79.
- [341] A.F. Thevenin, R.A. Margraf, C.G. Fisher, R.M. Kells-Andrews, M.M. Falk, Phosphorylation regulates connexin43/ZO-1 binding and release, an important step in gap junction turnover, *Mol Biol Cell* 28(25) (2017) 3595-3608.
- [342] M.M. Atkinson, P.D. Lampe, H.H. Lin, R. Kollander, X.R. Li, D.T. Kiang, Cyclic AMP modifies the cellular distribution of connexin43 and induces a persistent increase in the junctional permeability of mouse mammary tumor cells, *J Cell Sci* 108 (Pt 9) (1995) 3079-90.
- [343] A.R. Dukic, P. Gerbaud, J. Guibourdenche, B. Thiede, K. Tasken, G. Pidoux, Ezrin-anchored PKA phosphorylates serine 369 and 373 on connexin 43 to enhance gap junction assembly, communication, and cell fusion, *Biochem J* 475(2) (2018) 455-476.
- [344] J.L. Solan, L. Marquez-Rosado, P.L. Sorgen, P.J. Thornton, P.R. Gafken, P.D. Lampe, Phosphorylation at S365 is a gatekeeper event that changes the structure of Cx43 and prevents down-regulation by PKC, *J Cell Biol* 179(6) (2007) 1301-9.
- [345] W. Nimlamool, R.M. Andrews, M.M. Falk, Connexin43 phosphorylation by PKC and MAPK signals VEGF-mediated gap junction internalization, *Mol Biol Cell* 26(15) (2015) 2755-68.
- [346] R.P. Norris, M. Freudzon, L.M. Mehlmann, A.E. Cowan, A.M. Simon, D.L. Paul, P.D. Lampe, L.A. Jaffe, Luteinizing hormone causes MAP kinase-dependent phosphorylation and closure of connexin 43 gap junctions in mouse ovarian follicles: one of two paths to meiotic resumption, *Development* 135(19) (2008) 3229-38.
- [347] L. Marquez-Rosado, J.L. Solan, C.A. Dunn, R.P. Norris, P.D. Lampe, Connexin43 phosphorylation in brain, cardiac, endothelial and epithelial tissues, *Biochimica et biophysica acta* 1818(8) (2012) 1985-92.
- [348] D. Boassa, J.L. Solan, A. Papas, P. Thornton, P.D. Lampe, G.E. Sosinsky, Trafficking and recycling of the connexin43 gap junction protein during mitosis, *Traffic* 11(11) (2010) 1471-86.
- [349] M.M. Falk, C.L. Bell, R.M. Kells Andrews, S.A. Murray, Molecular mechanisms regulating formation, trafficking and processing of annular gap junctions, *BMC Cell Biol* 17 Suppl 1 (2016) 22.
- [350] J.M. Huibregtse, M. Scheffner, S. Beaudenon, P.M. Howley, A family of proteins structurally and functionally related to the E6-AP ubiquitin-protein ligase, *Proc Natl Acad Sci U S A* 92(11) (1995) 5249.
- [351] J.F. Ek-Vitorin, T.J. King, N.S. Heyman, P.D. Lampe, J.M. Burt, Selectivity of connexin 43 channels is regulated through protein kinase C-dependent phosphorylation, *Circ Res* 98(12) (2006) 1498-505.
- [352] A.C. Cone, G. Cavin, C. Ambrosi, H. Hakozaki, A.X. Wu-Zhang, M.T. Kunkel, A.C. Newton, G.E. Sosinsky, Protein kinase C-mediated phosphorylation of Connexin43 gap junction channels causes movement within gap junctions followed by vesicle internalization and protein degradation, *The Journal of biological chemistry* 289(13) (2014) 8781-98.

- [353] J.T. Fong, W. Nimlamool, M.M. Falk, EGF induces efficient Cx43 gap junction endocytosis in mouse embryonic stem cell colonies via phosphorylation of Ser262, Ser279/282, and Ser368, *FEBS Lett* 588(5) (2014) 836-44.
- [354] K.E. Johnson, S. Mitra, P. Katoch, L.S. Kelsey, K.R. Johnson, P.P. Mehta, Phosphorylation on Ser-279 and Ser-282 of connexin43 regulates endocytosis and gap junction assembly in pancreatic cancer cells, *Mol Biol Cell* 24(6) (2013) 715-33.
- [355] M.Y. Kanemitsu, W. Jiang, W. Eckhart, Cdc2-mediated phosphorylation of the gap junction protein, connexin43, during mitosis, *Cell Growth Differ* 9(1) (1998) 13-21.
- [356] P.D. Lampe, W.E. Kurata, B.J. Warn-Cramer, A.F. Lau, Formation of a distinct connexin43 phosphoisoform in mitotic cells is dependent upon p34cdc2 kinase, *J Cell Sci* 111 (Pt 6) (1998) 833-41.
- [357] R.Y. Huang, J.G. Laing, E.M. Kanter, V.M. Berthoud, M. Bao, H.W. Rohrs, R.R. Townsend, K.A. Yamada, Identification of CaMKII phosphorylation sites in Connexin43 by high-resolution mass spectrometry, *J Proteome Res* 10(3) (2011) 1098-109.
- [358] A.P. Braun, H. Schulman, The multifunctional calcium/calmodulin-dependent protein kinase: from form to function, *Annu Rev Physiol* 57 (1995) 417-45.
- [359] K. Procida, L. Jorgensen, N. Schmitt, M. Delmar, S.M. Taffet, N.H. Holstein-Rathlou, M.S. Nielsen, T.H. Braunstein, Phosphorylation of connexin43 on serine 306 regulates electrical coupling, *Heart Rhythm* 6(11) (2009) 1632-8.
- [360] K. Moore, Z.J. Bryant, G. Ghatnekar, U.P. Singh, R.G. Gourdie, J.D. Potts, A synthetic connexin 43 mimetic peptide augments corneal wound healing, *Exp Eye Res* 115 (2013) 178-88.
- [361] V.C. Chen, A.R. Kristensen, L.J. Foster, C.C. Naus, Association of connexin43 with E3 ubiquitin ligase TRIM21 reveals a mechanism for gap junction phosphodegron control, *J Proteome Res* 11(12) (2012) 6134-46.
- [362] T.S. Richards, C.A. Dunn, W.G. Carter, M.L. Usui, J.E. Olerud, P.D. Lampe, Protein kinase C spatially and temporally regulates gap junctional communication during human wound repair via phosphorylation of connexin43 on serine368, *J Cell Biol* 167(3) (2004) 555-62.
- [363] S.R. Johnstone, B.M. Kroncke, A.C. Straub, A.K. Best, C.A. Dunn, L.A. Mitchell, Y. Peskova, R.K. Nakamoto, M. Koval, C.W. Lo, P.D. Lampe, L. Columbus, B.E. Isakson, MAPK phosphorylation of connexin 43 promotes binding of cyclin E and smooth muscle cell proliferation, *Circ Res* 111(2) (2012) 201-11.
- [364] N.L. Jacobsen, T.K. Pontifex, H. Li, J.L. Solan, P.D. Lampe, P.L. Sorgen, J.M. Burt, Regulation of Cx37 channel and growth-suppressive properties by phosphorylation, *J Cell Sci* 130(19) (2017) 3308-3321.
- [365] J.A. Diez, M. Elvira, A. Villalobo, Phosphorylation of connexin-32 by the epidermal growth factor receptor tyrosine kinase, *Ann N Y Acad Sci* 766 (1995) 477-80.
- [366] A. Davy, J.O. Bush, P. Soriano, Inhibition of gap junction communication at ectopic Eph/ephrin boundaries underlies craniofrontonasal syndrome, *PLoS Biol* 4(10) (2006) e315.
- [367] R. Azarnia, S. Reddy, T.E. Kmiecik, D. Shalloway, W.R. Loewenstein, The cellular src gene product regulates junctional cell-to-cell communication, *Science* 239(4838) (1988) 398-401.
- [368] W.R. Loewenstein, R. Azarnia, Regulation of intercellular communication and growth by the cellular src gene, *Ann N Y Acad Sci* 551 (1988) 337-45; discussion 345-6.
- [369] S.J. Parsons, J.T. Parsons, Src family kinases, key regulators of signal transduction, *Oncogene* 23(48) (2004) 7906-9.
- [370] T.J. Boggon, M.J. Eck, Structure and regulation of Src family kinases, *Oncogene* 23(48) (2004) 7918-27.
- [371] J.E. Smart, H. Oppermann, A.P. Czernilofsky, A.F. Purchio, R.L. Erikson, J.M. Bishop, Characterization of sites for tyrosine phosphorylation in the transforming protein of Rous sarcoma virus (pp60v-src) and its normal cellular homologue (pp60c-src), *Proc Natl Acad Sci U S A* 78(10) (1981) 6013-7.
- [372] M.Y. Kanemitsu, L.W. Loo, S. Simon, A.F. Lau, W. Eckhart, Tyrosine phosphorylation of connexin 43 by v-Src is mediated by SH2 and SH3 domain interactions, *The Journal of biological chemistry* 272(36) (1997) 22824-31.
- [373] R. Lin, B.J. Warn-Cramer, W.E. Kurata, A.F. Lau, v-Src-mediated phosphorylation of connexin43 on tyrosine disrupts gap junctional communication in mammalian cells, *Cell communication & adhesion* 8(4-6) (2001) 265-9.

- [374] R. Lin, B.J. Warn-Cramer, W.E. Kurata, A.F. Lau, v-Src phosphorylation of connexin 43 on Tyr247 and Tyr265 disrupts gap junctional communication, *J Cell Biol* 154(4) (2001) 815-27.
- [375] K.I. Swenson, H. Piwnica-Worms, H. McNamee, D.L. Paul, Tyrosine phosphorylation of the gap junction protein connexin43 is required for the pp60v-src-induced inhibition of communication, *Cell Regul* 1(13) (1990) 989-1002.
- [376] L. Zhou, E.M. Kasperek, B.J. Nicholson, Dissection of the molecular basis of pp60(v-src) induced gating of connexin 43 gap junction channels, *J Cell Biol* 144(5) (1999) 1033-45.
- [377] A. Saidi Brikci-Nigassa, M.J. Clement, T. Ha-Duong, E. Adjadj, L. Ziani, D. Pastre, P.A. Curmi, P. Savarin, Phosphorylation controls the interaction of the connexin43 C-terminal domain with tubulin and microtubules, *Biochemistry* 51(21) (2012) 4331-42.
- [378] C. Ambrosi, C. Ren, G. Spagnol, G. Cavin, A. Cone, E.E. Grintsevich, G.E. Sosinsky, P.L. Sorgen, Connexin43 Forms Supramolecular Complexes through Non-Overlapping Binding Sites for Drebrin, Tubulin, and ZO-1, *PLoS One* 11(6) (2016) e0157073.
- [379] E. Butkevich, S. Hulsmann, D. Wenzel, T. Shirao, R. Duden, I. Majoul, Drebrin is a novel connexin-43 binding partner that links gap junctions to the submembrane cytoskeleton, *Curr Biol* 14(8) (2004) 650-8.
- [380] T. Auth, S. Schluter, S. Urschel, P. Kussmann, S. Sonntag, T. Hoher, M.M. Kreuzberg, R. Dobrowolski, K. Willecke, The TSG101 protein binds to connexins and is involved in connexin degradation, *Experimental cell research* 315(6) (2009) 1053-62.
- [381] J.T. Fong, R.M. Kells, M.M. Falk, Two tyrosine-based sorting signals in the Cx43 C-terminus cooperate to mediate gap junction endocytosis, *Mol Biol Cell* 24(18) (2013) 2834-48.
- [382] M. Schmitt, K. Leykauf, E. Reinz, H. Cheng, A. Alonso, J. Schenkel, Mutation of human connexin43 amino acids s279/s282 increases protein stability upon treatment with epidermal growth factor, *Cell Biochem Biophys* 69(2) (2014) 379-84.
- [383] V.M. Ding, P.J. Boersema, L.Y. Foong, C. Preisinger, G. Koh, S. Natarajan, D.Y. Lee, J. Boekhorst, B. Snel, S. Lemeer, A.J. Heck, A. Choo, Tyrosine phosphorylation profiling in FGF-2 stimulated human embryonic stem cells, *PLoS One* 6(3) (2011) e17538.
- [384] J.T. Kittler, G. Chen, V. Kukhtina, A. Vahedi-Faridi, Z. Gu, V. Tretter, K.R. Smith, K. McAinsh, I.L. Arancibia-Carcamo, W. Saenger, V. Haucke, Z. Yan, S.J. Moss, Regulation of synaptic inhibition by phospho-dependent binding of the AP2 complex to a YECL motif in the GABAA receptor gamma2 subunit, *Proc Natl Acad Sci U S A* 105(9) (2008) 3616-21.
- [385] J.G. Laing, E.M. Westphale, G.L. Engelmann, E.C. Beyer, Characterization of the gap junction protein, connexin45, *The Journal of membrane biology* 139(1) (1994) 31-40.
- [386] A. Oshima, T. Doi, K. Mitsuoka, S. Maeda, Y. Fujiyoshi, Roles of Met-34, Cys-64, and Arg-75 in the assembly of human connexin 26. Implication for key amino acid residues for channel formation and function, *The Journal of biological chemistry* 278(3) (2003) 1807-16.
- [387] T. Thomas, T. Aasen, M. Hodgins, D.W. Laird, Transport and function of cx26 mutants involved in skin and deafness disorders, *Cell communication & adhesion* 10(4-6) (2003) 353-8.
- [388] Y. Chen, Y. Deng, X. Bao, L. Reuss, G.A. Altenberg, Mechanism of the defect in gap-junctional communication by expression of a connexin 26 mutant associated with dominant deafness, *FASEB journal : official publication of the Federation of American Societies for Experimental Biology* 19(11) (2005) 1516-8.
- [389] P.E. Purnick, D.C. Benjamin, V.K. Verselis, T.A. Bargiello, T.L. Dowd, Structure of the amino terminus of a gap junction protein, *Arch Biochem Biophys* 381(2) (2000) 181-90.
- [390] H.L. Wang, W.T. Chang, T.H. Yeh, T. Wu, M.S. Chen, C.Y. Wu, Functional analysis of connexin-32 mutants associated with X-linked dominant Charcot-Marie-Tooth disease, *Neurobiol Dis* 15(2) (2004) 361-70.
- [391] J. Shibayama, R. Lewandowski, F. Kieken, W. Coombs, S. Shah, P.L. Sorgen, S.M. Taffet, M. Delmar, Identification of a novel peptide that interferes with the chemical regulation of connexin43, *Circ Res* 98(11) (2006) 1365-72.
- [392] D. Manthey, K. Banach, T. Desplantez, C.G. Lee, C.A. Kozak, O. Traub, R. Weingart, K. Willecke, Intracellular domains of mouse connexin26 and -30 affect diffusional and electrical properties of gap junction channels, *The Journal of membrane biology* 181(2) (2001) 137-48.
- [393] C. Colussi, J. Rosati, S. Straino, F. Spallotta, R. Berni, D. Stilli, S. Rossi, E. Musso, E. Macchi, A. Mai, G. Sbardella, S. Castellano, C. Chimenti, A. Frustaci, A. Nebbioso, L. Altucci, M.C. Capogrossi, C. Gaetano, Nepsilon-lysine acetylation determines dissociation from GAP junctions

and lateralization of connexin 43 in normal and dystrophic heart, *Proc Natl Acad Sci U S A* 108(7) (2011) 2795-800.

[394] S.M. Wu, W.F. Cheung, D. Frazier, D.W. Stafford, Cloning and expression of the cDNA for human gamma-glutamyl carboxylase, *Science* 254(5038) (1991) 1634-6.

[395] B. Brenner, S. Tavori, A. Zivelin, C.B. Keller, J.W. Suttie, I. Tatarsky, U. Seligsohn, Hereditary deficiency of all vitamin K-dependent procoagulants and anticoagulants, *Br J Haematol* 75(4) (1990) 537-42.

[396] G.L. Nelsestuen, A.M. Shah, S.B. Harvey, Vitamin K-dependent proteins, *Vitam Horm* 58 (2000) 355-89.

[397] J. Stenflo, P. Fernlund, W. Egan, P. Roepstorff, Vitamin K dependent modifications of glutamic acid residues in prothrombin, *Proc Natl Acad Sci U S A* 71(7) (1974) 2730-3.

[398] C.T. Walsh, S. Garneau-Tsodikova, G.J. Gatto, Jr., Protein posttranslational modifications: the chemistry of proteome diversifications, *Angew Chem Int Ed Engl* 44(45) (2005) 7342-72.

[399] V.K. Verselis, M.P. Trelles, C. Rubinos, T.A. Bargiello, M. Srinivas, Loop gating of connexin hemichannels involves movement of pore-lining residues in the first extracellular loop domain, *The Journal of biological chemistry* 284(7) (2009) 4484-93.

[400] Q. Tang, T.L. Dowd, V.K. Verselis, T.A. Bargiello, Conformational changes in a pore-forming region underlie voltage-dependent "loop gating" of an unapposed connexin hemichannel, *The Journal of general physiology* 133(6) (2009) 555-70.

[401] F. Rouan, T.W. White, N. Brown, A.M. Taylor, T.W. Lucke, D.L. Paul, C.S. Munro, J. Uitto, M.B. Hodgins, G. Richard, trans-dominant inhibition of connexin-43 by mutant connexin-26: implications for dominant connexin disorders affecting epidermal differentiation, *J Cell Sci* 114(Pt 11) (2001) 2105-13.

[402] B.C. Stong, Q. Chang, S. Ahmad, X. Lin, A novel mechanism for connexin 26 mutation linked deafness: cell death caused by leaky gap junction hemichannels, *Laryngoscope* 116(12) (2006) 2205-10.

[403] C.M. Pickart, M.J. Eddins, Ubiquitin: structures, functions, mechanisms, *Biochimica et biophysica acta* 1695(1-3) (2004) 55-72.

[404] E. Leithe, E. Rivedal, Ubiquitination and down-regulation of gap junction protein connexin-43 in response to 12-O-tetradecanoylphorbol 13-acetate treatment, *The Journal of biological chemistry* 279(48) (2004) 50089-96.

[405] S.M. Kelly, J.K. Vanslyke, L.S. Musil, Regulation of ubiquitin-proteasome system mediated degradation by cytosolic stress, *Mol Biol Cell* 18(11) (2007) 4279-91.

[406] M.M. Falk, J.T. Fong, R.M. Kells, M.C. O'Laughlin, T.J. Kowal, A.F. Thevenin, Degradation of endocytosed gap junctions by autophagosomal and endo-/lysosomal pathways: a perspective, *The Journal of membrane biology* 245(8) (2012) 465-76.

[407] H. Saitoh, J. Hinchey, Functional heterogeneity of small ubiquitin-related protein modifiers SUMO-1 versus SUMO-2/3, *The Journal of biological chemistry* 275(9) (2000) 6252-8.

[408] M.S. Rodriguez, C. Dargemont, R.T. Hay, SUMO-1 conjugation in vivo requires both a consensus modification motif and nuclear targeting, *The Journal of biological chemistry* 276(16) (2001) 12654-9.

[409] J.R. Gareau, C.D. Lima, The SUMO pathway: emerging mechanisms that shape specificity, conjugation and recognition, *Nat Rev Mol Cell Biol* 11(12) (2010) 861-71.

[410] R. Geiss-Friedlander, F. Melchior, Concepts in sumoylation: a decade on, *Nat Rev Mol Cell Biol* 8(12) (2007) 947-56.

[411] A. Kjenseth, T.A. Fykerud, S. Sirnes, J. Bruun, Z. Yohannes, M. Kolberg, Y. Omori, E. Rivedal, E. Leithe, The gap junction channel protein connexin 43 is covalently modified and regulated by SUMOylation, *The Journal of biological chemistry* 287(19) (2012) 15851-61.

[412] J.K. VanSlyke, L.S. Musil, Analysis of connexin intracellular transport and assembly, *Methods* 20(2) (2000) 156-64.

[413] S. Sirnes, E. Leithe, E. Rivedal, The detergent resistance of Connexin43 is lost upon TPA or EGF treatment and is an early step in gap junction endocytosis, *Biochem Biophys Res Commun* 373(4) (2008) 597-601.

[414] S. Mollerup, J.P. Hofgaard, T.H. Braunstein, A. Kjenseth, E. Leithe, E. Rivedal, N.H. Holstein-Rathlou, M.S. Nielsen, Norepinephrine inhibits intercellular coupling in rat cardiomyocytes by ubiquitination of connexin43 gap junctions, *Cell communication & adhesion* 18(4) (2011) 57-65.

- [415] D.T. Hess, A. Matsumoto, S.O. Kim, H.E. Marshall, J.S. Stamler, Protein S-nitrosylation: purview and parameters, *Nat Rev Mol Cell Biol* 6(2) (2005) 150-66.
- [416] P. Anand, J.S. Stamler, Enzymatic mechanisms regulating protein S-nitrosylation: implications in health and disease, *J Mol Med (Berl)* 90(3) (2012) 233-44.
- [417] D.T. Hess, J.S. Stamler, Regulation by S-nitrosylation of protein post-translational modification, *The Journal of biological chemistry* 287(7) (2012) 4411-8.
- [418] B. Lima, M.T. Forrester, D.T. Hess, J.S. Stamler, S-nitrosylation in cardiovascular signaling, *Circ Res* 106(4) (2010) 633-46.
- [419] A.C. Straub, M. Billaud, S.R. Johnstone, A.K. Best, S. Yemen, S.T. Dwyer, R. Looft-Wilson, J.J. Lysiak, B. Gaston, L. Palmer, B.E. Isakson, Compartmentalized connexin 43 s-nitrosylation/denitrosylation regulates heterocellular communication in the vessel wall, *Arterioscler Thromb Vasc Biol* 31(2) (2011) 399-407.
- [420] P. Kameritsch, N. Khandoga, W. Nagel, C. Hundhausen, D. Lidington, U. Pohl, Nitric oxide specifically reduces the permeability of Cx37-containing gap junctions to small molecules, *J Cell Physiol* 203(1) (2005) 233-42.
- [421] R.L. McKinnon, M.L. Bolon, H.X. Wang, S. Swarbreck, G.M. Kidder, A.M. Simon, K. Tyml, Reduction of electrical coupling between microvascular endothelial cells by NO depends on connexin37, *American journal of physiology. Heart and circulatory physiology* 297(1) (2009) H93-H101.
- [422] M.A. Retamal, C.J. Cortes, L. Reuss, M.V. Bennett, J.C. Saez, S-nitrosylation and permeation through connexin 43 hemichannels in astrocytes: induction by oxidant stress and reversal by reducing agents, *Proc Natl Acad Sci U S A* 103(12) (2006) 4475-80.
- [423] M.A. Retamal, S. Yin, G.A. Altenberg, L. Reuss, Modulation of Cx46 hemichannels by nitric oxide, *Am J Physiol Cell Physiol* 296(6) (2009) C1356-63.
- [424] A.J. Trease, J.M.V. Capuccino, J. Contreras, A.L. Harris, P.L. Sorgen, Intramolecular signaling in a cardiac connexin: Role of cytoplasmic domain dimerization, *J Mol Cell Cardiol* (2017).
- [425] J.A. Palatinus, J.M. Rhett, R.G. Gourdie, The connexin43 carboxyl terminus and cardiac gap junction organization, *Biochimica et biophysica acta* 1818(8) (2012) 1831-43.
- [426] J.M. Anumonwo, S.M. Taffet, H. Gu, M. Chanson, A.P. Moreno, M. Delmar, The carboxyl terminal domain regulates the unitary conductance and voltage dependence of connexin40 gap junction channels, *Circ Res* 88(7) (2001) 666-73.
- [427] A.P. Moreno, M. Chanson, S. Elenes, J. Anumonwo, I. Scerri, H. Gu, S.M. Taffet, M. Delmar, Role of the carboxyl terminal of connexin43 in transjunctional fast voltage gating, *Circ Res* 90(4) (2002) 450-7.
- [428] G.S. Ghatnekar, C.L. Grek, D.G. Armstrong, S.C. Desai, R.G. Gourdie, The effect of a connexin43-based Peptide on the healing of chronic venous leg ulcers: a multicenter, randomized trial, *J Invest Dermatol* 135(1) (2015) 289-98.
- [429] M.P. O'Quinn, J.A. Palatinus, B.S. Harris, K.W. Hewett, R.G. Gourdie, A peptide mimetic of the connexin43 carboxyl terminus reduces gap junction remodeling and induced arrhythmia following ventricular injury, *Circ Res* 108(6) (2011) 704-15.
- [430] V. Verma, B.D. Larsen, W. Coombs, X. Lin, G. Spagnol, P.L. Sorgen, S.M. Taffet, M. Delmar, Novel pharmacophores of connexin43 based on the "RXP" series of Cx43-binding peptides, *Circ Res* 105(2) (2009) 176-84.
- [431] S.R. Coppen, N.J. Severs, R.G. Gourdie, Connexin45 (alpha 6) expression delineates an extended conduction system in the embryonic and mature rodent heart, *Dev Genet* 24(1-2) (1999) 82-90.
- [432] T. Betsuyaku, N.S. Nnebe, R. Sundset, S. Patibandla, C.M. Krueger, K.A. Yamada, Overexpression of cardiac connexin45 increases susceptibility to ventricular tachyarrhythmias in vivo, *American journal of physiology. Heart and circulatory physiology* 290(1) (2006) H163-71.
- [433] R. Veeraghavan, J. Lin, G.S. Hoeker, J.P. Keener, R.G. Gourdie, S. Poelzing, Sodium channels in the Cx43 gap junction perinexus may constitute a cardiac ephapse: an experimental and modeling study, *Pflugers Arch* 467(10) (2015) 2093-105.
- [434] R. Veeraghavan, J. Lin, J.P. Keener, R. Gourdie, S. Poelzing, Potassium channels in the Cx43 gap junction perinexus modulate ephaptic coupling: an experimental and modeling study, *Pflugers Arch* 468(10) (2016) 1651-61.

- [435] S.B. Danik, F. Liu, J. Zhang, H.J. Suk, G.E. Morley, G.I. Fishman, D.E. Gutstein, Modulation of cardiac gap junction expression and arrhythmic susceptibility, *Circ Res* 95(10) (2004) 1035-41.
- [436] D.D. Spragg, C. Leclercq, M. Loghmani, O.P. Faris, R.S. Tunin, D. DiSilvestre, E.R. McVeigh, G.F. Tomaselli, D.A. Kass, Regional alterations in protein expression in the dyssynchronous failing heart, *Circulation* 108(8) (2003) 929-32.
- [437] H.V. van Rijen, D. Eckardt, J. Degen, M. Theis, T. Ott, K. Willecke, H.J. Jongsma, T. Opthof, J.M. de Bakker, Slow conduction and enhanced anisotropy increase the propensity for ventricular tachyarrhythmias in adult mice with induced deletion of connexin43, *Circulation* 109(8) (2004) 1048-55.
- [438] S. Kostin, M. Rieger, S. Dammer, S. Hein, M. Richter, W.P. Klovekorn, E.P. Bauer, J. Schaper, Gap junction remodeling and altered connexin43 expression in the failing human heart, *Molecular and cellular biochemistry* 242(1-2) (2003) 135-44.
- [439] J.L. Kopanic, P.L. Sorgen, Chemical shift assignments of the connexin45 carboxyl terminal domain: monomer and dimer conformations, *Biomol NMR Assign* 7(2) (2013) 293-7.
- [440] I. Bosanac, T. Michikawa, K. Mikoshiba, M. Ikura, Structural insights into the regulatory mechanism of IP3 receptor, *Biochimica et biophysica acta* 1742(1-3) (2004) 89-102.
- [441] I. Wittig, H.P. Braun, H. Schagger, Blue native PAGE, *Nat Protoc* 1(1) (2006) 418-28.
- [442] R.G. Johnson, H.C. Le, K. Evenson, S.W. Loberg, T.M. Myslajek, A. Prabhu, A.M. Manley, C. O'Shea, H. Grunenwald, M. Haddican, P.M. Fitzgerald, T. Robinson, B.A. Cisterna, J.C. Saez, T.F. Liu, D.W. Laird, J.D. Sheridan, Connexin Hemichannels: Methods for Dye Uptake and Leakage, *The Journal of membrane biology* 249(6) (2016) 713-741.
- [443] T.K. Kerppola, Bimolecular fluorescence complementation: visualization of molecular interactions in living cells, *Methods Cell Biol* 85 (2008) 431-70.
- [444] G. Huyer, S. Liu, J. Kelly, J. Moffat, P. Payette, B. Kennedy, G. Tsaprailis, M.J. Gresser, C. Ramachandran, Mechanism of inhibition of protein-tyrosine phosphatases by vanadate and pervanadate, *The Journal of biological chemistry* 272(2) (1997) 843-51.
- [445] R.D. Veenstra, H.Z. Wang, D.A. Beblo, M.G. Chilton, A.L. Harris, E.C. Beyer, P.R. Brink, Selectivity of connexin-specific gap junctions does not correlate with channel conductance, *Circ Res* 77(6) (1995) 1156-65.
- [446] N.L. Jacobsen, T.K. Pontifex, H. Li, J.L. Solan, P.D. Lampe, P.L. Sorgen, J.M. Burt, Regulation of Cx37 channel and growth suppressive properties by phosphorylation, *J Cell Sci* (2017).
- [447] H. Girao, S. Catarino, P. Pereira, Eps15 interacts with ubiquitinated Cx43 and mediates its internalization, *Experimental cell research* 315(20) (2009) 3587-97.
- [448] E. Leithe, A. Kjenseth, S. Sirnes, H. Stenmark, A. Brech, E. Rivedal, Ubiquitylation of the gap junction protein connexin-43 signals its trafficking from early endosomes to lysosomes in a process mediated by Hrs and Tsg101, *J Cell Sci* 122(Pt 21) (2009) 3883-93.
- [449] Q. Wang, B. Shui, M.I. Kotlikoff, H. Sondermann, Structural basis for calcium sensing by GCaMP2, *Structure* 16(12) (2008) 1817-27.
- [450] M. Koval, S.T. Geist, E.M. Westphale, A.E. Kemendy, R. Civitelli, E.C. Beyer, T.H. Steinberg, Transfected connexin45 alters gap junction permeability in cells expressing endogenous connexin43, *J Cell Biol* 130(4) (1995) 987-95.
- [451] J.G. Laing, M. Koval, T.H. Steinberg, Association with ZO-1 correlates with plasma membrane partitioning in truncated connexin45 mutants, *The Journal of membrane biology* 207(1) (2005) 45-53.
- [452] D.F. Hulser, M.L. Rutz, R. Eckert, O. Traub, Functional rescue of defective mutant connexons by pairing with wild-type connexons, *Pflugers Arch* 441(4) (2001) 521-8.
- [453] G. Sahu, A.K. Bera, Contribution of intracellular calcium and pH in ischemic uncoupling of cardiac gap junction channels formed of connexins 43, 40, and 45: a critical function of C-terminal domain, *PLoS One* 8(3) (2013) e60506.
- [454] J.M. Burt, D.C. Spray, Inotropic agents modulate gap junctional conductance between cardiac myocytes, *Am J Physiol* 254(6 Pt 2) (1988) H1206-10.
- [455] S.O. Mikalsen, T. Husoy, G. Vikhamar, T. Sanner, Induction of phosphotyrosine in the gap junction protein, connexin43, *FEBS Lett* 401(2-3) (1997) 271-5.
- [456] B.N. Giepmans, E. Feiken, M.F. Gebbink, W.H. Moolenaar, Association of connexin43 with a receptor protein tyrosine phosphatase, *Cell communication & adhesion* 10(4-6) (2003) 201-5.

- [457] V. Cruciani, S.O. Mikalsen, Stimulated phosphorylation of intracellular connexin43, *Experimental cell research* 251(2) (1999) 285-98.
- [458] J.G. Laing, B.C. Chou, T.H. Steinberg, ZO-1 alters the plasma membrane localization and function of Cx43 in osteoblastic cells, *J Cell Sci* 118(Pt 10) (2005) 2167-76.
- [459] J.M. Rhatt, J. Jourdan, R.G. Gourdie, Connexin 43 connexon to gap junction transition is regulated by zonula occludens-1, *Mol Biol Cell* 22(9) (2011) 1516-28.
- [460] Y. Guo, C. Martinez-Williams, D.E. Rannels, Gap junction-microtubule associations in rat alveolar epithelial cells, *American journal of physiology. Lung cellular and molecular physiology* 285(6) (2003) L1213-21.
- [461] D. Wang, W. Xing, X. Wang, H. Zhu, Taxol stabilizes gap junctions and reduces ischemic ventricular arrhythmias in rats in vivo, *Mol Med Rep* 11(5) (2015) 3243-8.
- [462] P. Beauchamp, C. Choby, T. Desplantez, K. de Peyer, K. Green, K.A. Yamada, R. Weingart, J.E. Saffitz, A.G. Kleber, Electrical propagation in synthetic ventricular myocyte strands from germline connexin43 knockout mice, *Circ Res* 95(2) (2004) 170-8.
- [463] (!!! INVALID CITATION !!! {Bao, 2011 #15;Coppin, 1999 #16;Beauchamp, 2004 #17;Bao, 2011 #15}).
- [464] A.P. Moreno, J.G. Laing, E.C. Beyer, D.C. Spray, Properties of gap junction channels formed of connexin 45 endogenously expressed in human hepatoma (SKHep1) cells, *Am J Physiol* 268(2 Pt 1) (1995) C356-65.
- [465] T.E. Ellenberger, C.J. Brandl, K. Struhl, S.C. Harrison, The GCN4 basic region leucine zipper binds DNA as a dimer of uninterrupted alpha helices: crystal structure of the protein-DNA complex, *Cell* 71(7) (1992) 1223-37.
- [466] X. Zeng, H. Zhu, H.A. Lashuel, J.C. Hu, Oligomerization properties of GCN4 leucine zipper e and g position mutants, *Protein Sci* 6(10) (1997) 2218-26.
- [467] J.S. Davidson, I.M. Baumgarten, E.H. Harley, Reversible inhibition of intercellular junctional communication by glycyrrhetic acid, *Biochem Biophys Res Commun* 134(1) (1986) 29-36.
- [468] D.A. Goodenough, J.A. Goliger, D.L. Paul, Connexins, connexons, and intercellular communication, *Annu Rev Biochem* 65 (1996) 475-502.
- [469] R.D. Veenstra, H.Z. Wang, E.C. Beyer, P.R. Brink, Selective dye and ionic permeability of gap junction channels formed by connexin45, *Circ Res* 75(3) (1994) 483-90.
- [470] A.P. Moreno, Biophysical properties of homomeric and heteromultimeric channels formed by cardiac connexins, *Cardiovasc Res* 62(2) (2004) 276-86.
- [471] D.C. Spray, A.P. Moreno, A.C. Campos-de-Carvalho, Biophysical properties of the human cardiac gap junction channel, *Braz J Med Biol Res* 26(6) (1993) 541-52.
- [472] D.E. Gutstein, G.E. Morley, D. Vaidya, F. Liu, F.L. Chen, H. Stuhlmann, G.I. Fishman, Heterogeneous expression of Gap junction channels in the heart leads to conduction defects and ventricular dysfunction, *Circulation* 104(10) (2001) 1194-9.
- [473] P.L. Sorgen, H.S. Duffy, D.C. Spray, M. Delmar, pH-dependent dimerization of the carboxyl terminal domain of Cx43, *Biophys J* 87(1) (2004) 574-81.
- [474] J.C. Herve, N. Bourmeyster, D. Sarrouilhe, H.S. Duffy, Gap junctional complexes: from partners to functions, *Prog Biophys Mol Biol* 94(1-2) (2007) 29-65.
- [475] D.W. Laird, The gap junction proteome and its relationship to disease, *Trends Cell Biol* 20(2) (2010) 92-101.
- [476] A.D. Martinez, V. Hayrapetyan, A.P. Moreno, E.C. Beyer, A carboxyl terminal domain of connexin43 is critical for gap junction plaque formation but not for homo- or hetero-oligomerization, *Cell communication & adhesion* 10(4-6) (2003) 323-8.
- [477] A.J. Filson, R. Azarnia, E.C. Beyer, W.R. Loewenstein, J.S. Brugge, Tyrosine phosphorylation of a gap junction protein correlates with inhibition of cell-to-cell communication, *Cell Growth Differ* 1(12) (1990) 661-8.
- [478] J.C. Saez, A.C. Nairn, A.J. Czernik, D.C. Spray, E.L. Hertzberg, P. Greengard, M.V. Bennett, Phosphorylation of connexin 32, a hepatocyte gap-junction protein, by cAMP-dependent protein kinase, protein kinase C and Ca²⁺/calmodulin-dependent protein kinase II, *Eur J Biochem* 192(2) (1990) 263-73.
- [479] A.P. Moreno, J.C. Saez, G.I. Fishman, D.C. Spray, Human connexin43 gap junction channels. Regulation of unitary conductances by phosphorylation, *Circ Res* 74(6) (1994) 1050-7.

- [480] B.N. Giepmans, T. Hengeveld, F.R. Postma, W.H. Moolenaar, Interaction of c-Src with gap junction protein connexin-43. Role in the regulation of cell-cell communication, *The Journal of biological chemistry* 276(11) (2001) 8544-9.
- [481] B.N. Giepmans, I. Verlaan, T. Hengeveld, H. Janssen, J. Calafat, M.M. Falk, W.H. Moolenaar, Gap junction protein connexin-43 interacts directly with microtubules, *Curr Biol* 11(17) (2001) 1364-8.
- [482] T. Toyofuku, Y. Akamatsu, H. Zhang, T. Kuzuya, M. Tada, M. Hori, c-Src regulates the interaction between connexin-43 and ZO-1 in cardiac myocytes, *The Journal of biological chemistry* 276(3) (2001) 1780-8.
- [483] T. Toyofuku, M. Yabuki, K. Otsu, T. Kuzuya, M. Tada, M. Hori, Functional role of c-Src in gap junctions of the cardiomyopathic heart, *Circ Res* 85(8) (1999) 672-81.
- [484] S.S. Mitra, J. Xu, B.J. Nicholson, Coregulation of multiple signaling mechanisms in pp60v-Src-induced closure of Cx43 gap junction channels, *The Journal of membrane biology* 245(8) (2012) 495-506.
- [485] J.G. Laing, R.N. Manley-Markowski, M. Koval, R. Civitelli, T.H. Steinberg, Connexin45 interacts with zonula occludens-1 in osteoblastic cells, *Cell communication & adhesion* 8(4-6) (2001) 209-12.
- [486] J.G. Laing, R.N. Manley-Markowski, M. Koval, R. Civitelli, T.H. Steinberg, Connexin45 interacts with zonula occludens-1 and connexin43 in osteoblastic cells, *The Journal of biological chemistry* 276(25) (2001) 23051-5.
- [487] B.R. Kwak, M.M. Hermans, H.R. De Jonge, S.M. Lohmann, H.J. Jongsma, M. Chanson, Differential regulation of distinct types of gap junction channels by similar phosphorylating conditions, *Mol Biol Cell* 6(12) (1995) 1707-19.
- [488] K. Inagaki, Y. Iwanaga, N. Sarai, Y. Onozawa, H. Takenaka, D. Mochly-Rosen, Y. Kihara, Tissue angiotensin II during progression or ventricular hypertrophy to heart failure in hypertensive rats; differential effects on PKC epsilon and PKC beta, *J Mol Cell Cardiol* 34(10) (2002) 1377-85.
- [489] W. Liang, G.Y. Oudit, M.M. Patel, A.M. Shah, J.R. Woodgett, R.G. Tsushima, M.E. Ward, P.H. Backx, Role of phosphoinositide 3-kinase {alpha}, protein kinase C, and L-type Ca²⁺ channels in mediating the complex actions of angiotensin II on mouse cardiac contractility, *Hypertension* 56(3) (2010) 422-9.
- [490] S. Avraham, R. London, Y. Fu, S. Ota, D. Hiregowdara, J. Li, S. Jiang, L.M. Pasztor, R.A. White, J.E. Groopman, et al., Identification and characterization of a novel related adhesion focal tyrosine kinase (RAFTK) from megakaryocytes and brain, *The Journal of biological chemistry* 270(46) (1995) 27742-51.
- [491] P. Rocic, T.M. Griffin, C.N. McRae, P.A. Lucchesi, Altered PYK2 phosphorylation by ANG II in hypertensive vascular smooth muscle, *American journal of physiology. Heart and circulatory physiology* 282(2) (2002) H457-65.
- [492] S. Murasawa, H. Matsubara, Y. Mori, H. Masaki, Y. Tsutsumi, Y. Shibasaki, I. Kitabayashi, Y. Tanaka, S. Fujiyama, Y. Koyama, A. Fujiyama, S. Iba, T. Iwasaka, Angiotensin II initiates tyrosine kinase Pyk2-dependent signalings leading to activation of Rac1-mediated c-Jun NH2-terminal kinase, *The Journal of biological chemistry* 275(35) (2000) 26856-63.
- [493] M. Ishida, M.B. Marrero, B. Schieffer, T. Ishida, K.E. Bernstein, B.C. Berk, Angiotensin II activates pp60c-src in vascular smooth muscle cells, *Circ Res* 77(6) (1995) 1053-9.
- [494] R.M. Touyz, X.H. Wu, G. He, S. Salomon, E.L. Schiffrin, Increased angiotensin II-mediated Src signaling via epidermal growth factor receptor transactivation is associated with decreased C-terminal Src kinase activity in vascular smooth muscle cells from spontaneously hypertensive rats, *Hypertension* 39(2 Pt 2) (2002) 479-85.
- [495] W.G. Paxton, M.B. Marrero, J.D. Klein, P. Delafontaine, B.C. Berk, K.E. Bernstein, The angiotensin II AT1 receptor is tyrosine and serine phosphorylated and can serve as a substrate for the src family of tyrosine kinases, *Biochem Biophys Res Commun* 200(1) (1994) 260-7.
- [496] S. Greco, A. Muscella, M.G. Elia, P. Salvatore, C. Storelli, S. Marsigliante, Activation of angiotensin II type I receptor promotes protein kinase C translocation and cell proliferation in human cultured breast epithelial cells, *J Endocrinol* 174(2) (2002) 205-14.
- [497] Y. Zou, I. Komuro, T. Yamazaki, R. Aikawa, S. Kudoh, I. Shiojima, Y. Hiroi, T. Mizuno, Y. Yazaki, Protein kinase C, but not tyrosine kinases or Ras, plays a critical role in angiotensin II-

induced activation of Raf-1 kinase and extracellular signal-regulated protein kinases in cardiac myocytes, *The Journal of biological chemistry* 271(52) (1996) 33592-7.

[498] S. Eguchi, H. Iwasaki, T. Inagami, K. Numaguchi, T. Yamakawa, E.D. Motley, K.M. Owada, F. Marumo, Y. Hirata, Involvement of PYK2 in angiotensin II signaling of vascular smooth muscle cells, *Hypertension* 33(1 Pt 2) (1999) 201-6.

[499] A. Sabri, G. Govindarajan, T.M. Griffin, K.L. Byron, A.M. Samarel, P.A. Lucchesi, Calcium- and protein kinase C-dependent activation of the tyrosine kinase PYK2 by angiotensin II in vascular smooth muscle, *Circ Res* 83(8) (1998) 841-51.

[500] J. Guo, A. Sabri, H. Elouardighi, V. Rybin, S.F. Steinberg, Alpha1-adrenergic receptors activate AKT via a Pyk2/PDK-1 pathway that is tonically inhibited by novel protein kinase C isoforms in cardiomyocytes, *Circ Res* 99(12) (2006) 1367-75.

[501] A. Blaukat, I. Ivankovic-Dikic, E. Gronroos, F. Dolfi, G. Tokiwa, K. Vuori, I. Dikic, Adaptor proteins Grb2 and Crk couple Pyk2 with activation of specific mitogen-activated protein kinase cascades, *The Journal of biological chemistry* 274(21) (1999) 14893-901.

[502] I. Dikic, G. Tokiwa, S. Lev, S.A. Courtneidge, J. Schlessinger, A role for Pyk2 and Src in linking G-protein-coupled receptors with MAP kinase activation, *Nature* 383(6600) (1996) 547-50.

[503] T.L. Lysechko, S.M. Cheung, H.L. Ostergaard, Regulation of the tyrosine kinase Pyk2 by calcium is through production of reactive oxygen species in cytotoxic T lymphocytes, *The Journal of biological chemistry* 285(41) (2010) 31174-84.

[504] H. Tang, Z.J. Zhao, E.J. Landon, T. Inagami, Regulation of calcium-sensitive tyrosine kinase Pyk2 by angiotensin II in endothelial cells. Roles of Yes tyrosine kinase and tyrosine phosphatase SHP-2, *The Journal of biological chemistry* 275(12) (2000) 8389-96.

[505] M. Zhao, D. Finlay, I. Zharkikh, K. Vuori, Novel Role of Src in Priming Pyk2 Phosphorylation, *PLoS One* 11(2) (2016) e0149231.

[506] A.L. Bayer, M.C. Heidkamp, N. Patel, M.J. Porter, S.J. Engman, A.M. Samarel, PYK2 expression and phosphorylation increases in pressure overload-induced left ventricular hypertrophy, *American journal of physiology. Heart and circulatory physiology* 283(2) (2002) H695-706.

[507] J. Melendez, S. Welch, E. Schaefer, C.S. Moravec, S. Avraham, H. Avraham, M.A. Sussman, Activation of pyk2/related focal adhesion tyrosine kinase and focal adhesion kinase in cardiac remodeling, *The Journal of biological chemistry* 277(47) (2002) 45203-10.

[508] P. Chen, F. Li, Z. Xu, Z. Li, X.P. Yi, Expression and distribution of Src in the nucleus of myocytes in cardiac hypertrophy, *Int J Mol Med* 32(1) (2013) 165-73.

[509] S. Wang, H. Gong, G. Jiang, Y. Ye, J. Wu, J. You, G. Zhang, A. Sun, I. Komuro, J. Ge, Y. Zou, Src is required for mechanical stretch-induced cardiomyocyte hypertrophy through angiotensin II type 1 receptor-dependent beta-arrestin2 pathways, *PLoS One* 9(4) (2014) e92926.

[510] D. Kuppuswamy, C. Kerr, T. Narishige, V.S. Kasi, D.R. Menick, G.t. Cooper, Association of tyrosine-phosphorylated c-Src with the cytoskeleton of hypertrophying myocardium, *The Journal of biological chemistry* 272(7) (1997) 4500-8.

[511] V.O. Rybin, J. Guo, Z. Gertsberg, H. Elouardighi, S.F. Steinberg, Protein kinase Cepsilon (PKCepsilon) and Src control PKCdelta activation loop phosphorylation in cardiomyocytes, *The Journal of biological chemistry* 282(32) (2007) 23631-8.

[512] S.S. Palaniyandi, L. Sun, J.C. Ferreira, D. Mochly-Rosen, Protein kinase C in heart failure: a therapeutic target?, *Cardiovasc Res* 82(2) (2009) 229-39.

[513] Y. Takeishi, T. Jalili, N.A. Ball, R.A. Walsh, Responses of cardiac protein kinase C isoforms to distinct pathological stimuli are differentially regulated, *Circ Res* 85(3) (1999) 264-71.

[514] Y. Koide, K. Tamura, A. Suzuki, K. Kitamura, K. Yokoyama, T. Hashimoto, N. Hirawa, M. Kihara, S. Ohno, S. Umemura, Differential induction of protein kinase C isoforms at the cardiac hypertrophy stage and congestive heart failure stage in Dahl salt-sensitive rats, *Hypertens Res* 26(5) (2003) 421-6.

[515] Y. Takeishi, A. Bhagwat, N.A. Ball, D.L. Kirkpatrick, M. Periasamy, R.A. Walsh, Effect of angiotensin-converting enzyme inhibition on protein kinase C and SR proteins in heart failure, *Am J Physiol* 276(1 Pt 2) (1999) H53-62.

[516] M.U. Braun, P. LaRosee, S. Schon, M.M. Borst, R.H. Strasser, Differential regulation of cardiac protein kinase C isozyme expression after aortic banding in rat, *Cardiovasc Res* 56(1) (2002) 52-63.

- [517] M. Hambleton, A. York, M.A. Sargent, R.A. Kaiser, J.N. Lorenz, J. Robbins, J.D. Molkentin, Inducible and myocyte-specific inhibition of PKC α enhances cardiac contractility and protects against infarction-induced heart failure, *American journal of physiology. Heart and circulatory physiology* 293(6) (2007) H3768-71.
- [518] J.C. Braz, K. Gregory, A. Pathak, W. Zhao, B. Sahin, R. Klevitsky, T.F. Kimball, J.N. Lorenz, A.C. Nairn, S.B. Liggett, I. Bodi, S. Wang, A. Schwartz, E.G. Lakatta, A.A. DePaoli-Roach, J. Robbins, T.E. Hewett, J.A. Bibb, M.V. Westfall, E.G. Kranias, J.D. Molkentin, PKC- α regulates cardiac contractility and propensity toward heart failure, *Nat Med* 10(3) (2004) 248-54.
- [519] S.B. Breitkopf, J.M. Asara, Determining in vivo phosphorylation sites using mass spectrometry, *Curr Protoc Mol Biol Chapter 18* (2012) Unit18 19 1-27.
- [520] T.H. Steinberg, R. Civitelli, S.T. Geist, A.J. Robertson, E. Hick, R.D. Veenstra, H.Z. Wang, P.M. Warlow, E.M. Westphale, J.G. Laing, et al., Connexin43 and connexin45 form gap junctions with different molecular permeabilities in osteoblastic cells, *EMBO J* 13(4) (1994) 744-50.
- [521] O. Destaing, A. Sanjay, C. Itzstein, W.C. Horne, D. Toomre, P. De Camilli, R. Baron, The tyrosine kinase activity of c-Src regulates actin dynamics and organization of podosomes in osteoclasts, *Mol Biol Cell* 19(1) (2008) 394-404.
- [522] N. Osherov, A. Levitzki, Epidermal-growth-factor-dependent activation of the src-family kinases, *Eur J Biochem* 225(3) (1994) 1047-53.
- [523] G.E. Sosinsky, J.L. Solan, G.M. Gaietta, L. Ngan, G.J. Lee, M.R. Mackey, P.D. Lampe, The C-terminus of connexin43 adopts different conformations in the Golgi and gap junction as detected with structure-specific antibodies, *Biochem J* 408(3) (2007) 375-85.
- [524] J.L. Solan, P.D. Lampe, Spatio-temporal regulation of connexin43 phosphorylation and gap junction dynamics, *Biochim Biophys Acta Biomembr* 1860(1) (2018) 83-90.
- [525] A. Moritz, Y. Li, A. Guo, J. Villen, Y. Wang, J. MacNeill, J. Kornhauser, K. Sprott, J. Zhou, A. Possemato, J.M. Ren, P. Hornbeck, L.C. Cantley, S.P. Gygi, J. Rush, M.J. Comb, Akt-RSK-S6 kinase signaling networks activated by oncogenic receptor tyrosine kinases, *Sci Signal* 3(136) (2010) ra64.
- [526] J. Palacios-Moreno, L. Foltz, A. Guo, M.P. Stokes, E.D. Kuehn, L. George, M. Comb, M.L. Grimes, Neuroblastoma tyrosine kinase signaling networks involve FYN and LYN in endosomes and lipid rafts, *PLoS Comput Biol* 11(4) (2015) e1004130.
- [527] A.M.N. Silva, R. Vitorino, M.R.M. Domingues, C.M. Spickett, P. Domingues, Post-translational modifications and mass spectrometry detection, *Free Radic Biol Med* 65 (2013) 925-941.
- [528] R.A. Grucza, K. Futterer, A.C. Chan, G. Waksman, Thermodynamic study of the binding of the tandem-SH2 domain of the Syk kinase to a dually phosphorylated ITAM peptide: evidence for two conformers, *Biochemistry* 38(16) (1999) 5024-33.
- [529] N.J. Anthis, G.M. Clore, Sequence-specific determination of protein and peptide concentrations by absorbance at 205 nm, *Protein Sci* 22(6) (2013) 851-8.
- [530] D. Zablocki, J. Sadoshima, Angiotensin II and oxidative stress in the failing heart, *Antioxid Redox Signal* 19(10) (2013) 1095-109.
- [531] S. Kostin, S. Dammer, S. Hein, W.P. Klovekorn, E.P. Bauer, J. Schaper, Connexin 43 expression and distribution in compensated and decompensated cardiac hypertrophy in patients with aortic stenosis, *Cardiovasc Res* 62(2) (2004) 426-36.
- [532] B.J. Warn-Cramer, G.T. Cottrell, J.M. Burt, A.F. Lau, Regulation of connexin-43 gap junctional intercellular communication by mitogen-activated protein kinase, *The Journal of biological chemistry* 273(15) (1998) 9188-96.
- [533] C.S. Hill, S.Y. Oh, S.A. Schmidt, K.J. Clark, A.W. Murray, Lysophosphatidic acid inhibits gap-junctional communication and stimulates phosphorylation of connexin-43 in WB cells: possible involvement of the mitogen-activated protein kinase cascade, *Biochem J* 303 (Pt 2) (1994) 475-9.
- [534] H.Q. Xie, V.W. Hu, Modulation of gap junctions in senescent endothelial cells, *Experimental cell research* 214(1) (1994) 172-6.
- [535] S.Y. Oh, S.A. Schmidt, A.W. Murray, Epidermal growth factor inhibits gap junctional communication and stimulates serine-phosphorylation of connexin43 in WB cells by a protein kinase C-independent mechanism, *Cell Adhes Commun* 1(2) (1993) 143-9.
- [536] A.F. Lau, M.Y. Kanemitsu, W.E. Kurata, S. Danesh, A.L. Boynton, Epidermal growth factor disrupts gap-junctional communication and induces phosphorylation of connexin43 on serine, *Mol Biol Cell* 3(8) (1992) 865-74.

- [537] B.V. Madhukar, S.Y. Oh, C.C. Chang, M. Wade, J.E. Trosko, Altered regulation of intercellular communication by epidermal growth factor, transforming growth factor-beta and peptide hormones in normal human keratinocytes, *Carcinogenesis* 10(1) (1989) 13-20.
- [538] P.E. Maldonado, B. Rose, W.R. Loewenstein, Growth factors modulate junctional cell-to-cell communication, *The Journal of membrane biology* 106(3) (1988) 203-10.
- [539] G. Vikhamar, E. Rivedal, S. Mollerup, T. Sanner, Role of Cx43 phosphorylation and MAP kinase activation in EGF induced enhancement of cell communication in human kidney epithelial cells, *Cell Adhes Commun* 5(6) (1998) 451-60.
- [540] Y. Zhou, S. Yang, T. Mao, Z. Zhang, MAPanalyzer: a novel online tool for analyzing microtubule-associated proteins, *Database (Oxford)* 2015 (2015).
- [541] S. Sachdev, Y. Bu, I.H. Gelman, Paxillin-Y118 phosphorylation contributes to the control of Src-induced anchorage-independent growth by FAK and adhesion, *BMC Cancer* 9 (2009) 12.
- [542] R. Lin, K.D. Martyn, C.V. Guyette, A.F. Lau, B.J. Warn-Cramer, v-Src tyrosine phosphorylation of connexin43: regulation of gap junction communication and effects on cell transformation, *Cell communication & adhesion* 13(4) (2006) 199-216.
- [543] V.M. Berthoud, E.A. Montegna, N. Atal, N.H. Aithal, P.R. Brink, E.C. Beyer, Heteromeric connexons formed by the lens connexins, connexin43 and connexin56, *Eur J Cell Biol* 80(1) (2001) 11-9.
- [544] D.S. He, J.X. Jiang, S.M. Taffet, J.M. Burt, Formation of heteromeric gap junction channels by connexins 40 and 43 in vascular smooth muscle cells, *Proc Natl Acad Sci U S A* 96(11) (1999) 6495-500.
- [545] D.T. Kurjiaka, T.D. Steele, M.V. Olsen, J.M. Burt, Gap junction permeability is diminished in proliferating vascular smooth muscle cells, *Am J Physiol* 275(6 Pt 1) (1998) C1674-82.
- [546] T. Desplantez, Cardiac Cx43, Cx40 and Cx45 co-assembling: involvement of connexins epitopes in formation of hemichannels and Gap junction channels, *BMC Cell Biol* 18(Suppl 1) (2017) 3.
- [547] G.T. Cottrell, J.M. Burt, Functional consequences of heterogeneous gap junction channel formation and its influence in health and disease, *Biochimica et biophysica acta* 1711(2) (2005) 126-41.
- [548] P.R. Brink, K. Cronin, K. Banach, E. Peterson, E.M. Westphale, K.H. Seul, S.V. Ramanan, E.C. Beyer, Evidence for heteromeric gap junction channels formed from rat connexin43 and human connexin37, *Am J Physiol* 273(4 Pt 1) (1997) C1386-96.
- [549] L. Mendieta, B. Venegas, N. Moreno, A. Patricio, I. Martinez, J. Aguilera, I.D. Limon, The carboxyl-terminal domain of the heavy chain of tetanus toxin prevents dopaminergic degeneration and improves motor behavior in rats with striatal MPP(+)-lesions, *Neurosci Res* 65(1) (2009) 98-106.
- [550] C. Ambrosi, D. Boassa, J. Pranskevich, A. Smock, A. Oshima, J. Xu, B.J. Nicholson, G.E. Sosinsky, Analysis of four connexin26 mutant gap junctions and hemichannels reveals variations in hexamer stability, *Biophys J* 98(9) (2010) 1809-19.
- [551] S. Kyriakoudi, I. Sargiannidou, A. Kagiava, M. Olympiou, K.A. Kleopa, Golgi-retained Cx32 mutants interfere with gene addition therapy for CMT1X, *Hum Mol Genet* 26(9) (2017) 1622-1633.
- [552] A.J. Trease, H. Li, G. Spagnol, L. Zheng, K.L. Stauch, P.L. Sorgen, Regulation of Connexin32 by ephrin receptors and T-cell protein tyrosine phosphatase, *The Journal of biological chemistry* (2018).
- [553] S.L. Fowler, A.C. McLean, S.A. Bennett, Tissue-specific cross-reactivity of connexin32 antibodies: problems and solutions unique to the central nervous system, *Cell communication & adhesion* 16(5-6) (2009) 117-30.
- [554] A. Temme, A. Buchmann, H.D. Gabriel, E. Nelles, M. Schwarz, K. Willecke, High incidence of spontaneous and chemically induced liver tumors in mice deficient for connexin32, *Curr Biol* 7(9) (1997) 713-6.
- [555] T.J. King, P.D. Lampe, Mice deficient for the gap junction protein Connexin32 exhibit increased radiation-induced tumorigenesis associated with elevated mitogen-activated protein kinase (p44/Erk1, p42/Erk2) activation, *Carcinogenesis* 25(5) (2004) 669-80.
- [556] A. Temme, F. Stumpel, G. Sohl, E.P. Rieber, K. Jungermann, K. Willecke, T. Ott, Dilated bile canaliculi and attenuated decrease of nerve-dependent bile secretion in connexin32-deficient mouse liver, *Pflugers Arch* 442(6) (2001) 961-6.

- [557] M. Chanson, M. Fanjul, D. Bosco, E. Nelles, S. Suter, K. Willecke, P. Meda, Enhanced secretion of amylase from exocrine pancreas of connexin32-deficient mice, *J Cell Biol* 141(5) (1998) 1267-75.
- [558] S.S. Scherer, Y.T. Xu, E. Nelles, K. Fischbeck, K. Willecke, L.J. Bone, Connexin32-null mice develop demyelinating peripheral neuropathy, *Glia* 24(1) (1998) 8-20.
- [559] T.J. King, P.D. Lampe, The gap junction protein connexin32 is a mouse lung tumor suppressor, *Cancer Res* 64(20) (2004) 7191-6.
- [560] S.S. Scherer, K.A. Kleopa, X-linked Charcot-Marie-Tooth disease, *J Peripher Nerv Syst* 17 Suppl 3 (2012) 9-13.
- [561] K.A. Kleopa, C.K. Abrams, S.S. Scherer, How do mutations in GJB1 cause X-linked Charcot-Marie-Tooth disease?, *Brain Res* 1487 (2012) 198-205.
- [562] A. Takeda, E. Hashimoto, H. Yamamura, T. Shimazu, Phosphorylation of liver gap junction protein by protein kinase C, *FEBS Lett* 210(2) (1987) 169-72.
- [563] M.S. Seo, J.S. Park, S.R. Yang, K.S. Park, I.S. Hong, E.H. Jo, K.S. Kang, Y.S. Lee, Expression of MAP kinases and connexins in the differentiation of rat mammary epithelial cells, *J Vet Med Sci* 68(6) (2006) 567-71.
- [564] A. Poliakov, M. Cotrina, D.G. Wilkinson, Diverse roles of eph receptors and ephrins in the regulation of cell migration and tissue assembly, *Dev Cell* 7(4) (2004) 465-80.
- [565] E.B. Pasquale, Eph-ephrin bidirectional signaling in physiology and disease, *Cell* 133(1) (2008) 38-52.
- [566] G. Mellitzer, Q. Xu, D.G. Wilkinson, Eph receptors and ephrins restrict cell intermingling and communication, *Nature* 400(6739) (1999) 77-81.
- [567] M. Ishii, I. Mueller, T. Nakajima, E.B. Pasquale, K. Ogawa, EphB signaling inhibits gap junctional intercellular communication and synchronized contraction in cultured cardiomyocytes, *Basic Res Cardiol* 106(6) (2011) 1057-68.
- [568] F. Delaglio, S. Grzesiek, G.W. Vuister, G. Zhu, J. Pfeifer, A. Bax, NMRPipe: a multidimensional spectral processing system based on UNIX pipes, *J Biomol NMR* 6(3) (1995) 277-93.
- [569] B.A. Johnson, R.A. Blevins, NMR View: A computer program for the visualization and analysis of NMR data, *J Biomol NMR* 4(5) (1994) 603-14.
- [570] N.S. Peters, A.L. Wit, Gap junction remodeling in infarction: does it play a role in arrhythmogenesis?, *Journal of cardiovascular electrophysiology* 11(4) (2000) 488-90.
- [571] L. Ren, X. Chen, R. Luechapanichkul, N.G. Selner, T.M. Meyer, A.S. Wavreille, R. Chan, C. Iorio, X. Zhou, B.G. Neel, D. Pei, Substrate specificity of protein tyrosine phosphatases 1B, RPTPalph, SHP-1, and SHP-2, *Biochemistry* 50(12) (2011) 2339-56.
- [572] H. Liu, R.Y. Huang, J. Chen, M.L. Gross, H.B. Pakrasi, Psb27, a transiently associated protein, binds to the chlorophyll binding protein CP43 in photosystem II assembly intermediates, *Proc Natl Acad Sci U S A* 108(45) (2011) 18536-41.
- [573] B.F. Remo, J. Qu, F.M. Volpicelli, S. Giovannone, D. Shin, J. Lader, F.Y. Liu, J. Zhang, D.S. Lent, G.E. Morley, G.I. Fishman, Phosphatase-resistant gap junctions inhibit pathological remodeling and prevent arrhythmias, *Circ Res* 108(12) (2011) 1459-66.
- [574] I. Konstantinova, G. Nikolova, M. Ohara-Imaizumi, P. Meda, T. Kucera, K. Zarbalis, W. Wurst, S. Nagamatsu, E. Lammert, EphA-Ephrin-A-mediated beta cell communication regulates insulin secretion from pancreatic islets, *Cell* 129(2) (2007) 359-70.
- [575] M.M. Atkinson, A.S. Menko, R.G. Johnson, J.R. Sheppard, J.D. Sheridan, Rapid and reversible reduction of junctional permeability in cells infected with a temperature-sensitive mutant of avian sarcoma virus, *J Cell Biol* 91(2 Pt 1) (1981) 573-8.
- [576] M.M. Atkinson, J.D. Sheridan, Altered junctional permeability between cells transformed by v-ras, v-mos, or v-src, *Am J Physiol* 255(5 Pt 1) (1988) C674-83.
- [577] A.F. Lau, W.E. Kurata, M.Y. Kanemitsu, L.W. Loo, B.J. Warn-Cramer, W. Eckhart, P.D. Lampe, Regulation of connexin43 function by activated tyrosine protein kinases, *J Bioenerg Biomembr* 28(4) (1996) 359-68.
- [578] P.J. Thul, C. Lindskog, The human protein atlas: A spatial map of the human proteome, *Protein Sci* 27(1) (2018) 233-244.
- [579] A. Beauchamp, M.O. Lively, A. Mintz, D. Gibo, J. Wykosky, W. Debinski, EphrinA1 is released in three forms from cancer cells by matrix metalloproteases, *Mol Cell Biol* 32(16) (2012) 3253-64.

- [580] S. Alford, A. Watson-Hurthig, N. Scott, A. Carette, H. Lorimer, J. Bazowski, P.L. Howard, Soluble ephrin a1 is necessary for the growth of HeLa and SK-BR3 cells, *Cancer Cell Int* 10 (2010) 41.
- [581] E.M. Lisabeth, G. Falivelli, E.B. Pasquale, Eph receptor signaling and ephrins, *Cold Spring Harb Perspect Biol* 5(9) (2013).
- [582] S.D. Funk, A.W. Orr, Ephs and ephrins resurface in inflammation, immunity, and atherosclerosis, *Pharmacol Res* 67(1) (2013) 42-52.
- [583] M.G. Coulthard, M. Morgan, T.M. Woodruff, T.V. Arumugam, S.M. Taylor, T.C. Carpenter, M. Lackmann, A.W. Boyd, Eph/Ephrin signaling in injury and inflammation, *Am J Pathol* 181(5) (2012) 1493-503.
- [584] M. Riou, D. Stroebel, J.M. Edwardson, P. Paoletti, An alternating GluN1-2-1-2 subunit arrangement in mature NMDA receptors, *PLoS One* 7(4) (2012) e35134.
- [585] E. Leithe, A. Brech, E. Rivedal, Endocytic processing of connexin43 gap junctions: a morphological study, *Biochem J* 393(Pt 1) (2006) 59-67.
- [586] M.A. Lemmon, J. Schlessinger, Cell signaling by receptor tyrosine kinases, *Cell* 141(7) (2010) 1117-34.
- [587] H. Katayama, W.R. Brinkley, S. Sen, The Aurora kinases: role in cell transformation and tumorigenesis, *Cancer Metastasis Rev* 22(4) (2003) 451-64.
- [588] Z. Dong, C. Huang, W.Y. Ma, PI-3 kinase in signal transduction, cell transformation, and as a target for chemoprevention of cancer, *Anticancer Res* 19(5A) (1999) 3743-7.
- [589] M.E. Anderson, Calmodulin kinase signaling in heart: an intriguing candidate target for therapy of myocardial dysfunction and arrhythmias, *Pharmacol Ther* 106(1) (2005) 39-55.
- [590] B.A. Rose, T. Force, Y. Wang, Mitogen-activated protein kinase signaling in the heart: angels versus demons in a heart-breaking tale, *Physiol Rev* 90(4) (2010) 1507-46.
- [591] O. Simsek Papur, A. Sun, J.F.C. Glatz, J. Luiken, M. Nabben, Acute and Chronic Effects of Protein Kinase-D Signaling on Cardiac Energy Metabolism, *Front Cardiovasc Med* 5 (2018) 65.
- [592] L. Zan, H. Wu, J. Jiang, S. Zhao, Y. Song, G. Teng, H. Li, Y. Jia, M. Zhou, X. Zhang, J. Qi, J. Wang, Temporal profile of Src, SSeCKS, and angiogenic factors after focal cerebral ischemia: correlations with angiogenesis and cerebral edema, *Neurochem Int* 58(8) (2011) 872-9.
- [593] L. Zan, X. Zhang, Y. Xi, H. Wu, Y. Song, G. Teng, H. Li, J. Qi, J. Wang, Src regulates angiogenic factors and vascular permeability after focal cerebral ischemia-reperfusion, *Neuroscience* 262 (2014) 118-28.
- [594] B.M. Sefton, T. Hunter, From c-src to v-src, or the case of the missing C terminus, *Cancer Surv* 5(2) (1986) 159-72.
- [595] S.D. Crowley, S.B. Gurley, M.J. Herrera, P. Ruiz, R. Griffiths, A.P. Kumar, H.S. Kim, O. Smithies, T.H. Le, T.M. Coffman, Angiotensin II causes hypertension and cardiac hypertrophy through its receptors in the kidney, *Proc Natl Acad Sci U S A* 103(47) (2006) 17985-90.
- [596] G.D. Frank, S. Saito, E.D. Motley, T. Sasaki, M. Ohba, T. Kuroki, T. Inagami, S. Eguchi, Requirement of Ca(2+) and PKCdelta for Janus kinase 2 activation by angiotensin II: involvement of PYK2, *Mol Endocrinol* 16(2) (2002) 367-77.
- [597] J.F. Ek-Vitorin, T.K. Pontifex, J.M. Burt, Cx43 Channel Gating and Permeation: Multiple Phosphorylation-Dependent Roles of the Carboxyl Terminus, *Int J Mol Sci* 19(6) (2018).
- [598] G.E. Morley, D. Vaidya, F.H. Samie, C. Lo, M. Delmar, J. Jalife, Characterization of conduction in the ventricles of normal and heterozygous Cx43 knockout mice using optical mapping, *Journal of cardiovascular electrophysiology* 10(10) (1999) 1361-75.